



## Utility-Locating Technology Development Using Multisensor Platforms

### DETAILS

---

0 pages | 8.5 x 11 | PAPERBACK

ISBN 978-0-309-43309-9 | DOI 10.17226/22274

### AUTHORS

---

Young, Gary N.; Kennedy, Colin M.; Anspach, Jim; Jones, Ross; Owen, Thomas; Clark, John; Keiswetter, Dean; Allouche, Erez; Simicevic, Neven; and Mark Baker

BUY THIS BOOK

FIND RELATED TITLES

### Visit the National Academies Press at [NAP.edu](http://NAP.edu) and login or register to get:

---

- Access to free PDF downloads of thousands of scientific reports
- 10% off the price of print titles
- Email or social media notifications of new titles related to your interests
- Special offers and discounts



Distribution, posting, or copying of this PDF is strictly prohibited without written permission of the National Academies Press. (Request Permission) Unless otherwise indicated, all materials in this PDF are copyrighted by the National Academy of Sciences.

The Second

STRATEGIC HIGHWAY RESEARCH PROGRAM



SHRP 2 REPORT S2-R01B-RW-1

# Utility-Locating Technology Development Using Multisensor Platforms

GARY N. YOUNG AND COLIN M. KENNEDY  
Underground Imaging Technologies, LLC  
Orlando, Florida

---

**TRANSPORTATION RESEARCH BOARD**

WASHINGTON, D.C.  
2015  
[www.TRB.org](http://www.TRB.org)

## **Subject Areas**

Construction

Highways

## The Second Strategic Highway Research Program

America's highway system is critical to meeting the mobility and economic needs of local communities, regions, and the nation. Developments in research and technology—such as advanced materials, communications technology, new data collection technologies, and human factors science—offer a new opportunity to improve the safety and reliability of this important national resource. Breakthrough resolution of significant transportation problems, however, requires concentrated resources over a short time frame. Reflecting this need, the second Strategic Highway Research Program (SHRP 2) has an intense, large-scale focus, integrates multiple fields of research and technology, and is fundamentally different from the broad, mission-oriented, discipline-based research programs that have been the mainstay of the highway research industry for half a century.

The need for SHRP 2 was identified in *TRB Special Report 260: Strategic Highway Research: Saving Lives, Reducing Congestion, Improving Quality of Life*, published in 2001 and based on a study sponsored by Congress through the Transportation Equity Act for the 21st Century (TEA-21). SHRP 2, modeled after the first Strategic Highway Research Program, is a focused, time-constrained, management-driven program designed to complement existing highway research programs. SHRP 2 focuses on applied research in four areas: Safety, to prevent or reduce the severity of highway crashes by understanding driver behavior; Renewal, to address the aging infrastructure through rapid design and construction methods that cause minimal disruptions and produce lasting facilities; Reliability, to reduce congestion through incident reduction, management, response, and mitigation; and Capacity, to integrate mobility, economic, environmental, and community needs in the planning and designing of new transportation capacity.

SHRP 2 was authorized in August 2005 as part of the Safe, Accountable, Flexible, Efficient Transportation Equity Act: A Legacy for Users (SAFETEA-LU). The program is managed by the Transportation Research Board (TRB) on behalf of the National Research Council (NRC). SHRP 2 is conducted under a memorandum of understanding among the American Association of State Highway and Transportation Officials (AASHTO), the Federal Highway Administration (FHWA), and the National Academy of Sciences, parent organization of TRB and NRC. The program provides for competitive, merit-based selection of research contractors; independent research project oversight; and dissemination of research results.

SHRP 2 Report S2-R01B-RW-1

ISBN: 978-0-309-27434-0

© 2015 National Academy of Sciences. All rights reserved.

### Copyright Information

Authors herein are responsible for the authenticity of their materials and for obtaining written permissions from publishers or persons who own the copyright to any previously published or copyrighted material used herein.

The second Strategic Highway Research Program grants permission to reproduce material in this publication for classroom and not-for-profit purposes. Permission is given with the understanding that none of the material will be used to imply TRB, AASHTO, or FHWA endorsement of a particular product, method, or practice. It is expected that those reproducing material in this document for educational and not-for-profit purposes will give appropriate acknowledgment of the source of any reprinted or reproduced material. For other uses of the material, request permission from SHRP 2.

*Note:* SHRP 2 report numbers convey the program, focus area, project number, and publication format. Report numbers ending in “w” are published as web documents only.

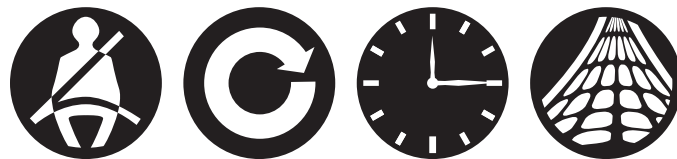
### Notice

The project that is the subject of this report was a part of the second Strategic Highway Research Program, conducted by the Transportation Research Board with the approval of the Governing Board of the National Research Council.

The members of the technical committee selected to monitor this project and to review this report were chosen for their special competencies and with regard for appropriate balance. The report was reviewed by the technical committee and accepted for publication according to procedures established and overseen by the Transportation Research Board and approved by the Governing Board of the National Research Council.

The opinions and conclusions expressed or implied in this report are those of the researchers who performed the research and are not necessarily those of the Transportation Research Board, the National Research Council, or the program sponsors.

The Transportation Research Board of the National Academies, the National Research Council, and the sponsors of the second Strategic Highway Research Program do not endorse products or manufacturers. Trade or manufacturers' names appear herein solely because they are considered essential to the object of the report.



### SHRP 2 Reports

Available by subscription and through the TRB online bookstore:  
[www.mytrb.org/store](http://www.mytrb.org/store)

Contact the TRB Business Office:  
 202-334-3213

More information about SHRP 2:  
[www.TRB.org/SHRP2](http://www.TRB.org/SHRP2)

# THE NATIONAL ACADEMIES

## *Advisers to the Nation on Science, Engineering, and Medicine*

The **National Academy of Sciences** is a private, nonprofit, self-perpetuating society of distinguished scholars engaged in scientific and engineering research, dedicated to the furtherance of science and technology and to their use for the general welfare. On the authority of the charter granted to it by Congress in 1863, the Academy has a mandate that requires it to advise the federal government on scientific and technical matters. Dr. Ralph J. Cicerone is president of the National Academy of Sciences.

The **National Academy of Engineering** was established in 1964, under the charter of the National Academy of Sciences, as a parallel organization of outstanding engineers. It is autonomous in its administration and in the selection of its members, sharing with the National Academy of Sciences the responsibility for advising the federal government. The National Academy of Engineering also sponsors engineering programs aimed at meeting national needs, encourages education and research, and recognizes the superior achievements of engineers. Dr. C. D. (Dan) Mote, Jr., is president of the National Academy of Engineering.

The **Institute of Medicine** was established in 1970 by the National Academy of Sciences to secure the services of eminent members of appropriate professions in the examination of policy matters pertaining to the health of the public. The Institute acts under the responsibility given to the National Academy of Sciences by its congressional charter to be an adviser to the federal government and, on its own initiative, to identify issues of medical care, research, and education. Dr. Victor J. Dzau is president of the Institute of Medicine.

The **National Research Council** was organized by the National Academy of Sciences in 1916 to associate the broad community of science and technology with the Academy's purposes of furthering knowledge and advising the federal government. Functioning in accordance with general policies determined by the Academy, the Council has become the principal operating agency of both the National Academy of Sciences and the National Academy of Engineering in providing services to the government, the public, and the scientific and engineering communities. The Council is administered jointly by both Academies and the Institute of Medicine. Dr. Ralph J. Cicerone and Dr. C. D. (Dan) Mote, Jr., are chair and vice chair, respectively, of the National Research Council.

The **Transportation Research Board** is one of six major divisions of the National Research Council. The mission of the Transportation Research Board is to provide leadership in transportation innovation and progress through research and information exchange, conducted within a setting that is objective, interdisciplinary, and multimodal. The Board's varied activities annually engage about 7,000 engineers, scientists, and other transportation researchers and practitioners from the public and private sectors and academia, all of whom contribute their expertise in the public interest. The program is supported by state transportation departments, federal agencies including the component administrations of the U.S. Department of Transportation, and other organizations and individuals interested in the development of transportation. [www.TRB.org](http://www.TRB.org)

[www.national-academies.org](http://www.national-academies.org)

## SHRP 2 STAFF

**Ann M. Brach**, *Director*  
**Stephen J. Andrie**, *Deputy Director*  
**Cynthia Allen**, *Editor*  
**Kenneth Campbell**, *Chief Program Officer, Safety*  
**Jared Cazel**, *Editorial Assistant*  
**JoAnn Coleman**, *Senior Program Assistant, Capacity and Reliability*  
**Eduardo Cusicanqui**, *Financial Officer*  
**Richard Deering**, *Special Consultant, Safety Data Phase 1 Planning*  
**Shantia Douglas**, *Senior Financial Assistant*  
**Charles Fay**, *Senior Program Officer, Safety*  
**Carol Ford**, *Senior Program Assistant, Renewal and Safety*  
**James Hedlund**, *Special Consultant, Safety Coordination*  
**Alyssa Hernandez**, *Reports Coordinator*  
**Ralph Hessian**, *Special Consultant, Capacity and Reliability*  
**Andy Horosko**, *Special Consultant, Safety Field Data Collection*  
**William Hyman**, *Senior Program Officer, Reliability*  
**Linda Mason**, *Communications Officer*  
**David Plazak**, *Senior Program Officer, Capacity and Reliability*  
**Rachel Taylor**, *Senior Editorial Assistant*  
**Dean Trackman**, *Managing Editor*  
**Connie Woldu**, *Administrative Coordinator*

## ACKNOWLEDGMENTS

This work was sponsored by the Federal Highway Administration in cooperation with the American Association of State Highway and Transportation Officials. It was conducted in the second Strategic Highway Research Program (SHRP 2), which is administered by the Transportation Research Board of the National Academies. The project was managed by Charles Taylor, Special Consultant for SHRP 2 Renewal; James Bryant, Senior Program Officer for SHRP 2 Renewal; and Andy Horosko, Special Consultant for SHRP 2 Renewal. Ralph Hessian, Special Consultant for SHRP 2 Renewal, also contributed to this report.

The research reported on herein was performed by Underground Imaging Technologies, LLC (UIT), and supported by Owen Engineering Services; Psi-G, LLC; Bay Geophysical; J. H. Anspach Consulting; Science Applications International Corporation (SAIC); Sagentia, Ltd.; Louisiana Tech University; Geomedia Research & Development; Benner GeoServices Inc.; and So-Deep, Inc. Gary Young, UIT, was the principal investigator. The other authors of this report are Colin M. Kennedy and Steve DiBenedetto, both with UIT. The authors acknowledge the contributions to this research from Jim Anspach, J. H. Anspach Consulting; Ross Jones, Sagentia; Thomas Owen, Owen Engineering Services; Dean Keiswetter, SAIC; Erez Allouche and Neven Simicevic, Louisiana Tech University; Mark Baker, Geomedia Research & Development; John Clark, Psi-G; Nils Sandin, Bay Geophysical; and Cary Skahn, So-Deep.

## FOREWORD

Andrew T. Horosko, *SHRP 2 Special Consultant, Renewal*

This report documents research and development efforts to improve technologies for detecting, identifying, and mapping buried utilities. The examined technologies were ground-penetrating radar (GPR), time domain electromagnetic induction (TDEMI), and high-frequency seismic imaging. The research and development activities included improving operating, processing, and interpreting software for multisensor GPR; developing and demonstrating an advanced TDEMI prototype system; and conducting a proof of concept of high-frequency seismic imaging. The report will be of interest to engineers and others looking for technologies to enhance traditional utility location and mapping methods.

---

Underground utility installations are common within highway rights-of-way. The location and specific characteristics of many buried utility lines have not been properly documented and thus present a unique challenge for highway renewal projects. The discovery of unexpected utility lines during a project's delivery can pose considerable risk to workers' safety and disrupt the established project schedule. Highway renewal projects depend on the availability of accurate buried utility records and information to support effective planning, design, and delivery of renewal work.

Providing the necessary underground utility information for road renewal projects requires a suite of innovative nondestructive technologies and methods and a decision support framework that can address the complexity of varying utilities, site soil, geology, and environmental conditions. The second Strategic Highway Renewal Program (SHRP 2) Project R01, Encouraging Innovation in Locating and Characterizing Underground Utilities, provided the background and basis for a series of research and development projects that seek to provide products to serve this highway renewal business need.

This research project focused on geophysical tools and accompanying software for locating and mapping buried utilities. Existing GPR equipment and software systems from Underground Imaging Technologies, LLC, were used as a platform for the project. The research built on various features of these systems to construct two functional prototypes: (1) a multichannel GPR system with improved software capabilities and (2) a new TDEMI system. The prototypes included new software capabilities for gathering, processing, fusing, interpreting, and presenting geophysical data sets. Both prototypes were tested at real world project sites to evaluate the quality of the data collection, the software's designed capabilities, and the ability of the prototypes to enhance current data collection capabilities. The development and testing sought to collect utility location data satisfying ASCE 38-02 Quality Level B requirements.

In addition, the project conducted research on a proposed innovative seismic detection technology at an early proof-of-concept level. The research focused on an application using a shear wave imaging system that was intended to provide detection capabilities similar to GPR for soils where GPR is not an effective tool. A series of seismic soil property tests was performed to facilitate model development and to better understand seismic measurements. A practical prototype that incorporates seismic technology was not fully developed.

The R01B project worked closely with the R01C project, Innovations to Locate Stacked or Deep Utilities, to avoid duplication and to provide a complementary set of tools. Some activities of the two projects were conducted together and jointly analyzed.

## CONTENTS

1	<b>Executive Summary</b>
3	<b>CHAPTER 1 Background</b>
3	Problem Statement and Research Objective
4	Scope of Study
4	Research Team
6	<b>CHAPTER 2 Research Approach</b>
6	State-of-the-Art Summary
6	Technologies Explanation
12	<b>CHAPTER 3 Findings and Applications</b>
12	Multichannel GPR System Status, Findings, and Applications
12	Improved Applications for Geophysical Data Analysis Software
20	High-Frequency Seismic Imaging Proof-of-Concept Prototype Status and Findings
42	Seismic Modeling Software
58	Advanced TDEMI System Status and Findings
85	In-Service Testing
90	<b>CHAPTER 4 Conclusions and Suggested Research</b>
90	Conclusions
93	Suggested Research
97	<b>References</b>
98	<b>Appendix A.</b> Standard Operating Procedure for Multichannel GPR Digital Geophysical Mapping Data Collection
106	<b>Appendix B.</b> Standard Operating Procedure for Multichannel GPR Digital Geophysical Mapping Data Processing
110	<b>Appendix C.</b> Standard Operating Procedure for TDEMI Digital Geophysical Mapping Data Collection
116	<b>Appendix D.</b> Standard Operating Procedure for TDEMI Digital Geophysical Mapping Data Processing

# Executive Summary

The purpose of SHRP 2 R01B research is to bring together and develop credible nondestructive geophysical techniques for use on a land-based towed platform capable of detecting and locating underground utilities under all geologic conditions. Varying geologic conditions inhibit the effectiveness of geophysical detection techniques in different ways; therefore, a need exists for a multi-sensor approach that will offer subsurface utility engineers and geophysical service providers the best chance to completely and accurately detect, locate, and characterize subsurface utilities at any location across the United States and the world.

The strategy for developing this multisensor platform technology centered on existing systems of Underground Imaging Technologies, LLC (UIT). UIT's systems consist of a towed geophysical sensor array, capable of digital data acquisition of both detection sensor data and high-precision location data. The research described here builds on several features of UIT's current system. One aspect is the refinement of TerraVision II, a multichannel ground-penetrating radar (GPR) system. Another aspect is the development of a new multisensor advanced time-domain electromagnetic induction (TDEMI) system. Other aspects involve development of and enhancements to software used for the gathering, processing, visualization, fusion, and interpretation of multiple geophysical data sets. The R01B project also researched an innovative seismic detection technology at an early proof-of-concept level. The proposed seismic application called for a shear wave seismic imaging system with an intended detection capability similar to GPR but for use in soils that are not compatible with GPR. As part of the seismic research, the project team conducted a series of seismic soil properties tests at various locations in the United States, and also studied and developed modeling capabilities useful in helping to predict and understand the high-resolution seismic measurements. A practical prototype incorporating the seismic technology was not fully developed under the R01B project; however, a simplified seismic prototype is planned for development as a follow-on to these preliminary research findings.

The R01B project resulted in the development of two functional prototypes: a multichannel GPR system and a new advanced multisensor TDEMI system. The TerraVision II, UIT's multichannel GPR system, was thoroughly tested with refinements applied to the associated software. Based on an array system previously designed collaboratively with SAIC and the U.S. Naval Research Laboratory (NRL), the TDEMI system was developed with the aim of improving our ability to locate and characterize metallic utility targets. Enhancements to Semiautomated Process and Detect (SPADE), UIT's proprietary data analysis software, were also a major focus of the research effort to improve 3-D data visualization and efficiency of data analysis procedures. Several software additions and improvements were developed for incorporation into the geophysical systems. These advancements were designed to assist the software user at all stages of the utility investigation workflow, including geophysical data acquisition, data processing, data analysis, and data interpretation.

To evaluate and validate the hardware and software components of the research prototypes, the project team tested the platform(s) on appropriate live projects with an established Subsurface Utility Engineering (SUE) firm (not associated with UIT or the research) acting as independent evaluators of results. The live-project SUE evaluation was based on comparisons between records and project data gathered using conventional SUE methods versus data collected and analyzed by the project research team using the R01B prototypes. During this in-service testing at project locations in Virginia and Georgia, the project team demonstrated all features of work necessary to execute a subsurface utility investigation, including digital geophysical mapping, field and office quality control procedures, methods for data transfer, initial data processing, advanced data analysis and interpretation, the data fusion process, and the construction of geo-referenced mapping deliverables.

Field testing results of the R01B prototypes were reviewed within the context of the Subsurface Utility Engineering Guidelines ASCE 38-02 Standard, where it is anticipated that these tools will partly contribute to the creation of Quality Level B (QL-B) data. The review process included observing the ease of operations of the new tools, the field data collection activities, and the computer-aided design and drafting (CADD) processing of collected data. Additionally, test holes were selected at one of the testing sites to investigate differences between the UIT and the SUE firm utility plots and to compare depths. Test holes were also selected to investigate potential nonutility anomalies found by the new tools. Ultimately, it was determined that these advanced geophysical tools offer their greatest value if they are used as an enhancement, not a replacement, to traditional utility mapping methods. On certain projects the cost–benefits of using these advanced tools can be significant if used early enough within construction phases. Further testing and verification measures are required to more completely assess these systems' capabilities in providing reliable utility depth estimates; to resolve unknown, small, and deep utility targets; and to accurately identify the cost–benefits directly associated with their use.

## CHAPTER 1

# Background

### Problem Statement and Research Objective

The ASCE 38-02 is the accepted compliance standard for many states and the SUE profession. The standard presents a four-level classification system for the quality of data for existing subsurface utilities. The highest level of quality, known as Quality Level A (QL-A), requires physical exposure of any given buried utility to know and record its exact position in 3-D space. QL-A data on subsurface utilities are not influenced by the surrounding medium. However, the intrusive measures taken to uncover the exact positions of portions of utilities are expensive. They often do not offer a comprehensive understanding of the subsurface, and they can result in unsuccessful locating attempts as well as have unnecessary adverse impact on the community.

Using current appropriate surface geophysical techniques to designate existing subsurface utilities or to trace a particular utility system offers a nondestructive means to identify utility locations in horizontal space. The horizontal positions of geophysical anomaly sources related to underground utilities can be depicted on the ground surface and/or surveyed to produce a computer-aided design and drafting (CADD) or geographic information system (GIS) databases. This is considered the second level of quality of data for existing subsurface utilities and is referred to as Quality Level B (QL-B) information. Typical SUE companies, utility companies, and construction firms use pipe and cable locating geophysical sensor(s) to conduct QL-B subsurface utility investigations. In most cases, this type of geophysical investigation does not allow the detection sensor(s) data to be digitally recorded, positioned, and preserved. Data collected in this manner requires trained data collection operators who are fully experienced in understanding the analog (audio or dial) signals these detection systems produce and how to interpret them correctly. Thus, the data acquired are not often repeatable from one operator to the next. Also for QL-B

utility investigations, the size of utility, the depth to utility from ground surface, the shape and orientation of the utility, the target utility composition, and the material (geologic or anthropogenic) surrounding the buried utility all contribute to whether utilities can be detected with geophysical sensors.

The use of a variety of complementary geophysical methods and sensor configurations offers SUE professionals the best chance to comprehensively investigate and characterize the underground infrastructure. Because site conditions and the subsurface medium are never constant from location to the next, no single geophysical application can be successfully used in all locations. According to the Natural Resources Conservation Service of the U.S. Department of Agriculture, because of attenuation of ground-penetrating radar (GPR) signals in clay or otherwise conductive soils, only a portion of the United States is suitable for effective GPR work. Time-domain electromagnetic induction (TDEMI) can work in highly conductive soils but cannot detect non-metallic utilities without a tracer wire. Oftentimes, a combination of geophysical technologies is best to obtain a more complete and accurate assessment of underground utilities; as shown in Figure 1.1, GPR and electromagnetic induction (EMI) detection sensors locate specific utilities exclusively. These limitations indicate that careful considerations need to be taken in regard to soil type, target(s) of interest, and overall site conditions when determining which technologies of a multisensor system are proper for deployment.

The purpose of the SHRP 2 R01B research was to produce multisensor geophysical systems capable of providing Quality Level B data or better under any site condition and at any site location. The strategy was to develop single-pass digital geophysical mapping systems that knit data together with precision positioning and specialized software, and to develop new sensors to complement existing ones for those geographic areas and conditions continuing to offer detection

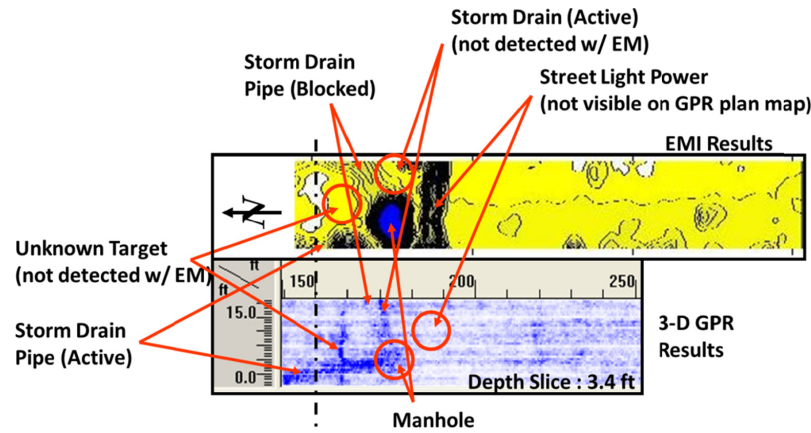


**Figure 1.1. The case for multiple geophysical sensors: comparing TDEMI and GPR data collected at same area.**

challenges. The systems developed through this research were designed to produce a repeatable digital record of precisely positioned sensor detection signals which should provide information on utility locations and characteristics in 3-D space. These data can then be put into engineering context using the ASCE 38 standard while minimizing the use of test holes. These systems may also provide information to project owners, engineers, and constructors on other geotechnical conditions useful to utility design, utility condition, utility relocation, and coordination.

## Scope of Study

The SHRP 2 R01B research focused primarily on the integration of multiple yet distinct geophysical detection and positioning technologies coupled with the development of algorithmic software applications designed to facilitate geophysical data acquisition, processing, and interpretation processes. The overall multisensor system is meant to satisfy specialized requirements which include

1. Detection, identification, and mapping of underground utility pipes and conduits in transportation rights of way where new construction or maintenance is required;
2. Resolution of pipes and conduits as small as 2 in. in diameter at depths of 12 ft below surface, or deeper;
3. Operation on either paved streets or roadways or on soils or backfilled utility trenches;
4. Compact hardware configuration adaptable to efficient mobile operation on streets, roadways, and adjacent terrains;

5. Functional capabilities for providing on-site utility survey maps suitable for direct use by utility system designers and/or construction or maintenance contractors; and
6. Compatibility with other colocated utility detection technologies to implement multisensor surveys.

From the multisensor mobility viewpoint, the various sensor methods should have compatible ground-scanning rates and near-real-time output data displays for use by a trained system operator during the survey data acquisition process. The separate geophysical detection methodologies were to be incorporated on a compatible ruggedized platform. Working prototypes for the TDEMI and the GPR system were tested and refined through this research. The basic concepts and validation behind developing a similar system using seismic reflection technologies was also explored. All multisensor geophysical systems were ultimately to be mounted on and operated from a common transport carriage either self-propelled or towed by a prime mover/data acquisition vehicle.

## Research Team

Much of the work on the project was performed by UIT's subcontractor technical team and consultants. The technical development team for this project consisted of a group of private and university researchers. Each member brought skills specific to a sensor, software, or subsystem included in the development plan. Each group and consultant was involved in the creation of the proposal ideas and the compilation of the final documents. Table 1.1 outlines the SHRP 2 R01B team members and their role in the project.

**Table 1.1. SHRP 2 R01B Research Team**

<b>Team Member</b>	<b>Project Role</b>	<b>Research Area</b>
Underground Imaging Technologies, LLC (UIT)	Lead	Overall project management, system integration, software development, field testing
Owen Engineering Services (OES)	Subcontractor	Seismic system development, vibrator source
Psi-G, LLC	Subcontractor	Seismic system development and deployment
Bay Geophysical	Subcontractor	Seismic system development and deployment
Louisiana Tech University (LTU)	Subcontractor	Computer modeling
SAIC	Subcontractor	Electromagnetic systems
Sagentia, Ltd.	Subcontractor	Software and algorithm development
J. H. Anspach Consulting	Consultant	Outreach, SUE applications, standard EM locators, liaison with user community, coordination of in-service testing
Geomeia Research & Development	Consultant	Seismic system development, receivers

Note: The organizations identified as subcontractors represent those that produced a tangible piece of the research prototypes. Consultants offered advice, helped with field testing, and consulted with SUE companies during the final validation testing phase of work.

## CHAPTER 2

# Research Approach

### State-of-the-Art Summary

This chapter presents the approach used in addressing the challenges faced by utility detection and locating systems across versatile cultural and environmental conditions. The approach focused on the development and advancement of common reliable near-surface geophysical detection technologies coupled with enhancements to data acquisition, data processing, data interpretation, and mapping software. Multichannel GPR, TDEMI, and preliminary high-frequency shear wave seismic applications are the geophysical detection methods studied and designed under this research, along with ongoing software development and improvements to Semiautomated Process and Detect (SPADE) and other commercial geophysical software. Extensive work in the experimentation and development of modeling software was also conducted with an aim to develop finite difference time-domain software capable of simulating propagation of acoustic and elastic waves in realistic soils.

The current UIT system and the improvements implemented under this research are meant to contribute to the determination of utility locations beyond QL-B, which means providing a depth as well as horizontal location. This depth determination is the key feature behind 3-D products designed for mapping subsurface utilities. The GPR and seismic components of this research are to offer a rendering of depth via the data processing used to produce the 3-D images obtained. Accurate depth estimates can also be attained through advanced analysis of TDEMI data. Most other technologies deployed for SUE mapping provide a 2-D product, such as a contour map, from the measurements. The following sections briefly describe each of these elements of the R01B research work aimed at generating accurate 3-D results to subsurface utility investigations.

### Technologies Explanation

The SHRP 2 R01B project can be divided into separate definable features of research work. The technologies addressed under this research include

- Multichannel GPR system (UIT);
- SPADE software enhancements (Sagentia, Ltd.);
- Seismic development (OES, Psi-G, and Bay Geophysical);
- Time-domain electromagnetic development (SAIC); and
- Modeling software development (LTU).

### Multichannel Ground-Penetrating Radar

GPR data gathering processing and interpretation is a preferred method for utility mapping when the depth-to-targets information is important and/or when unknown utilities are suspected to exist on a project. However, clay soils do not allow for the penetration of GPR waves, diminishing their effectiveness on many projects. When GPR waves can sufficiently penetrate the subsurface, they can provide unprecedented 3-D location accuracy on targets, such as pipes, with differing electrical properties from the soil. GPR can detect metal and nonmetallic anomaly sources and provide accurate depth estimates to utilities. The systems work by transmitting a radar signal into the ground and receiving a reflection back at the antenna. An array of GPR antennas widens the detection swath offered by single-channel systems and provides the capability to produce detailed 3-D images of the subsurface; from those images, utilities and other targets of interest may be interpreted and mapped. Multichannel GPR systems have been developed by UIT and others in the past for performing Subsurface Utility Engineering work.

Over the long term, improvements to GPR hardware systems are expected to come from the manufacturing and user communities. Those incremental gains in capabilities resulting from hardware configurations were not the focus of this program,



**Figure 2.1.** *UIT's Multichannel GPR system, the TerraVision II.*

however. SHRP 2 R01B efforts concentrated on improving software functions needed to manage, organize, process, and interpret GPR data from UIT's multichannel GPR system, known as TerraVision II. TerraVision II consists of two banks of seven antennas, each with a fixed spacing of 0.4 ft (12 cm) between each antenna module. (See Figure 2.1.) Data acquired by each of the 14 channels is spaced at 0.08 ft (2.5 cm) in the direction of travel. The central frequency and approximate bandwidth of each GPR antenna element is 400 MHz. Geophysical Survey Systems, Inc. (GSSI), the GPR antenna manufacturer, constructs the TerraVision units with all of the antennas oriented at 45° to the direction of travel of the cart and with each monostatic antenna having relative orthogonal polarization to the one adjacent. (See Figure 2.2.) During the download process,

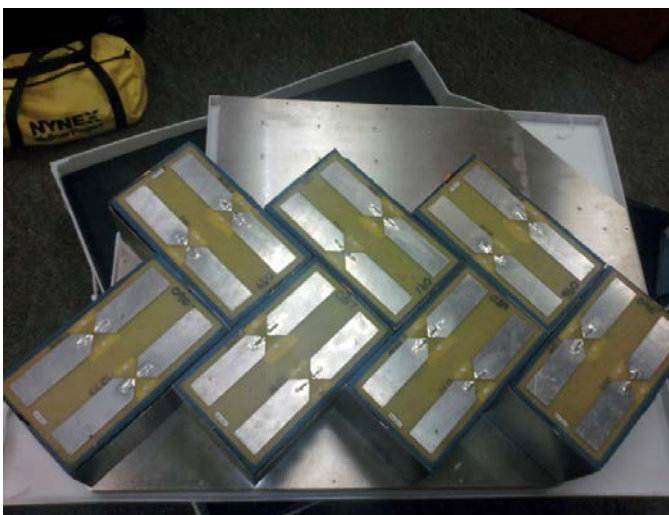


**Figure 2.2.** *Internal arrangement of a single bank of TerraVision II GPR antennas.*

data sets from the 14 channels are sorted and tagged with the appropriate precision survey (surface position) information. Multiple survey swaths, geo-referenced to the desired coordinate system, are assembled into a composite 3-D data block of the project area and subsequently loaded into SPADE for analysis. The data analysis is performed by experienced geoscientists subsequent to field operations, a process which can be time consuming. The new software features developed under SHRP 2 R01B research are aimed at increasing the efficiency of data analysis processes and improving the accuracy of the 3-D interpretation for utility mapping projects. The following section describes improvements to UIT's GPR processing and interpretation software (SPADE) that fulfill this plan.

### **SPADE Software Enhancements (Sagentia, Ltd.)**

SPADE is UIT's primary software package that accepts final interpretation-ready GPR data. The technical approach for the development of algorithms to extract features from GPR, and eventually seismic data, builds on the project team's experience and the existing capabilities of SPADE. The software is designed to automate certain interpretation procedures used in picking utility targets and to make it easier for interpreters to manipulate GPR data for visualization. SPADE also currently has the ability to incorporate geophysical sensor data, imagery data, and geo-referenced feature data within a centralized single software platform. With this capability, interpreters are easily able to correlate geophysical data sets with each other and with as-built drawings and other site data for fast and accurate comparison and verification.

A primary R01B research objective was to improve SPADE's automated feature extraction capability and 3-D migration functions for multichannel GPR data sets, with those advancements ultimately transitioning smoothly to processing of 3-D seismic data sets. In a 3-D graphical environment the data analyst has the ability to view and refine utility-like features that are automatically extracted from the acquired geophysical data. This software-driven "reduction" of geophysical information is applied after field data acquisition and uses a set of parameters defined by the geophysical data analyst. Three-dimensional target picking functions are also incorporated into the SPADE software so that utility information can be interpreted, depicted, and delivered with horizontal and vertical accuracy. Figure 2.3 shows a graphical window example of data analysis in SPADE.

UIT subcontractor Sagentia, Ltd., a technology and product development company in Cambridge, United Kingdom, was the project entity responsible for executing the software development plan and producing SPADE software enhancements. UIT data analysts implemented, reviewed, and tested the

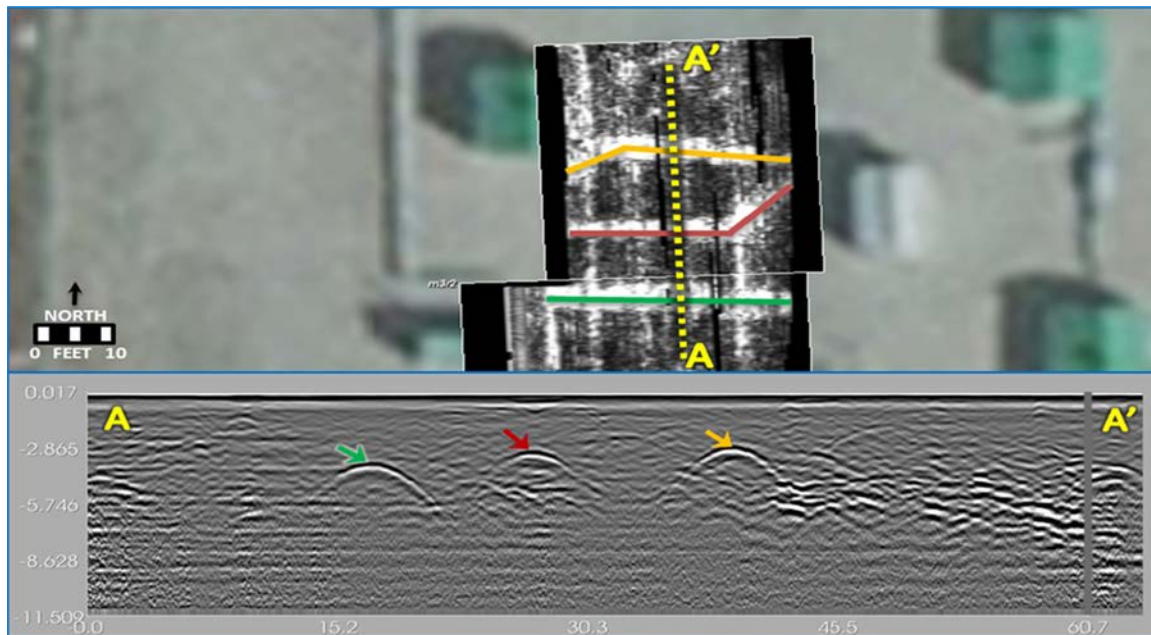


**Figure 2.3. Screen capture of GPR data analysis in SPADE.**

software upgrades and provided user-sustained feedback. The three key technical elements of the Sagentia approach were

- Algorithms for segmenting GPR and seismic data;
- Algorithms for extracting features from segments; and
- A user interface that enables the user to efficiently and flexibly process the whole data set.

Algorithmic elements were developed in a modular fashion; activities included building initial GPR segmentation algorithms, initial user trials, software prototypes, implementation in SPADE, and validation trials. Both project and archive UIT data sets were used in the experimental testing of the software. The range of algorithms developed was specific to GPR data sets. Seismic and TDEMI data sets were managed through separate commercial software. The Sagentia focus of this research was based on a “data segmentation” strategy for handling GPR data sets within a common software interface with capabilities for both data visualization and feature extraction. Other data manipulation features of the software were also studied, such as the effects polarization caused by the arrangement of antennas in the TerraVision multichannel GPR unit. Sagentia has achieved its major deliverable for SHRP 2 R01B, which is the implementation of segments functionality in the VTK version of SPADE.

### **Seismic Development (Owen Engineering Services and Psi-G)**

Given the limitations of GPR in certain soil conditions, an alternate approach that offers 3-D geophysical data sets is

needed to provide information on both the horizontal and depth locations of underground utilities in clay conductive soils. This calls for the development of an acoustic-based geophysical system. The initial idea of the SHRP 2 R01B seismic reflection system—proposed by Owen Engineering Services with support from Psi-G—was an unconventional design comprising a horizontal shear wave sensor array configured to produce zero-offset (monostatic) down-looking target illumination and reflections. This seismic system was envisioned to respond in near-real-time when scanned over utility targets of interest in the same way that, for example, GPR might respond, showing hyperbolic halo-like images of diffractor targets in raw-data displays.

With data-derived migration analysis, the halo images would be processed to present images indicating the approximate localized target depth and position. The advantages important to the success and acceptability of this method were

1. Operation using a proven “pure” horizontally polarized shear (SH)–wave radiating source and matching SH-wave sensor array to use transverse-polarized low-velocity shear waves to best advantage;
2. Vibrator source operation using controlled frequency sweep excitation in the 300–1,500-Hz range and at an appropriate energy level to achieve efficient high-resolution utility target illumination and reflections in soils and backfills without unwanted lower frequency interference;
3. Vertical down-looking directional operation to minimize the detrimental effects of vertical velocity gradients characteristic of near-surface soils and backfills and to avoid interfering lateral reflections;

4. Concomitant transmission and reflection gains in detection signal-to-noise ratio associated with vertically oriented narrow-beam operation;
5. Elimination of the various conventional data processing steps normally applied to seismic measurements, such as ground roll removal, velocity analysis, spatial averaging trace stacking, and removal of interbed multiples, all of which require a relatively large number of source shot points and sensor records together with off-line processing to achieve their results;
6. Ability of seismic waves to penetrate to much greater depths than GPR in practically all types of soils and backfills to provide a more universally applicable utility detection and mapping capability; and
7. Simplified sensor array operation that eliminates the need for multichannel data recording and analysis by directly summing all sensor element signals in the 2-D array to yield a single-output down-looking reflection response.

Figure 2.4 illustrates the envisioned seismic system platform. Testing and equipment requirements were detailed by subcontractor Owen Engineering Services. All of these factors contribute to a prodigious undertaking, so the SHRP 2 R01B project focused primarily on proof of concepts to meet the research objectives behind such prototype development.

To achieve practical mobility of the conceived seismic survey system, proven methods of attenuation compensation and ground coupling must be determined. To that end, the project team conducted a series of preeminent and individualized seismic soil properties tests at various locations across the United States. The results of that testing is discussed further in Chapter 3.

### Time-Domain Electromagnetic Development (SAIC)

Time-domain electromagnetic induction (TDEMI) systems are another geophysical methodology used to support Quality Level B SUE activities. These systems can be operated as single sensor units or as an array of synchronized sensors. They detect subsurface utilities constructed of any type of metal. Detection capabilities depend on the depth to target, composition of target, size and orientation of target, surrounding geology, and the amount of cultural debris or interference from other surface cultural features. TDEMI systems used for digital geophysical mapping (DGM) provide multiple measurements of the decay of the secondary magnetic field associated with any metallic object.

With the current industry standard TDEMI DGM system (Geonics EM61-MK2), data from as many as four monostatic

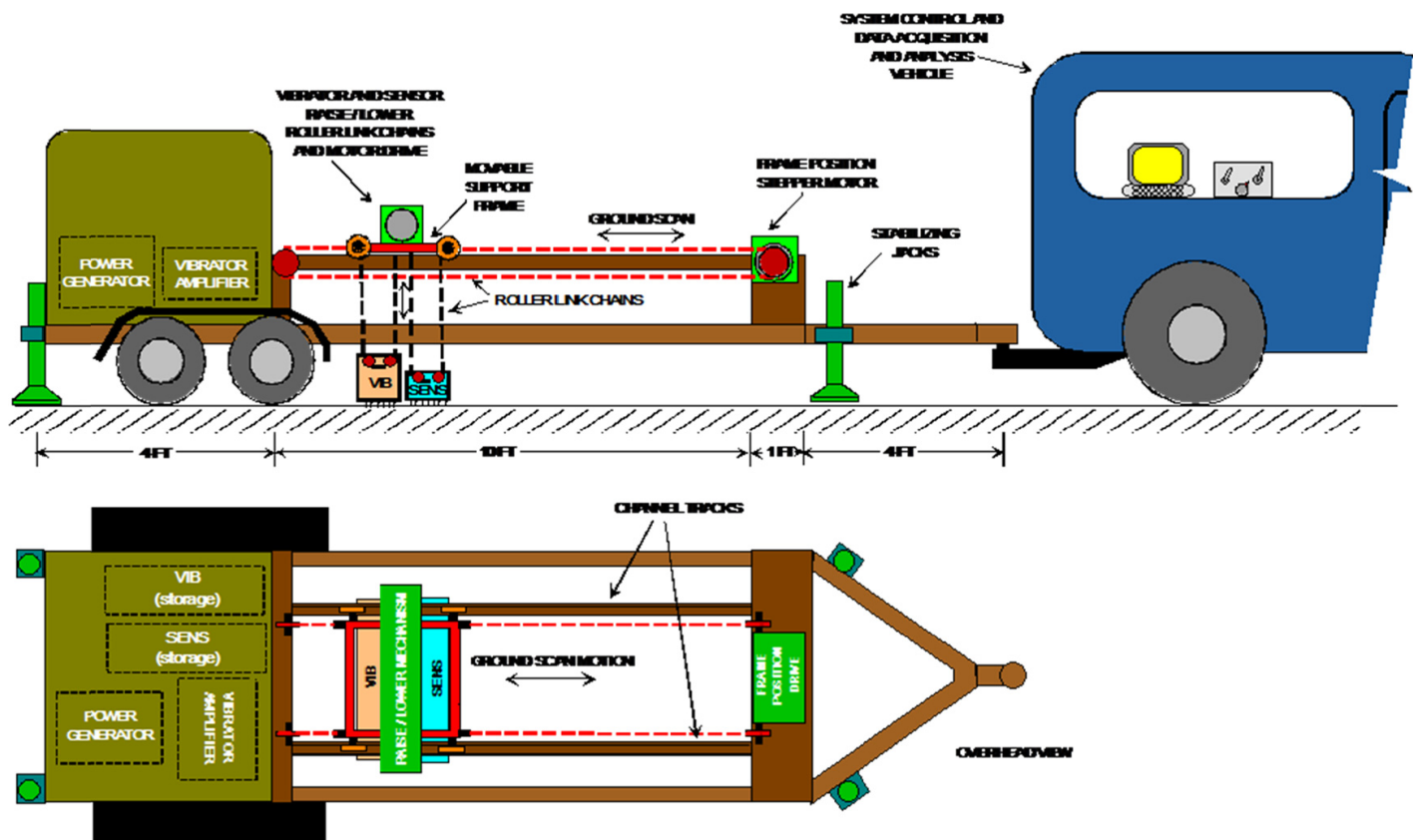


Figure 2.4. Schematic of the production prototype seismic system.

time gates provide geophysical data analysts information on the detection and characterization of utility anomaly sources. The earlier time gates offer improved detection for smaller targets where the decay rate of the secondary field is relatively quick. Additionally, the early gates provide an increase in the response amplitude from any target, regardless of size, compared with later time gate measurements. Later time gate measurements are useful for the description of the time decay associated with any target of interest. Detailed time gate information that is recorded from various sensors at strategic orientations can offer data analysts a basis for constructing software models for specific target discrimination techniques. All data from the detection sensors can be easily integrated with global navigation satellite system (GNSS) and/or robotic total station (RTS) equipment data. With a maximum data collection rate of 15 records (total) per second for current systems, travel speeds up to 3 mph are preferred for optimal detection.

One aspect of the R01B project was to improve on current TDEMI systems by testing and developing a new advanced TDEMI technology for locating and classifying underground utilities. SAIC led the effort, building on the company's work with the U.S. Department of Defense in the development of improved TDEMI technologies for locating and characterizing buried munitions objects. Figure 2.5 shows the TDEMI sensor array that SAIC developed collaboratively with the U.S. Naval Research Laboratory (NRL). The array, which is towed behind a utility vehicle, consists of 25 transmit (Tx) and receive (Rx) coil pairs and is 2 meters square. It has fully programmable Tx and Rx parameters; and because it employs modern digital electronics, it is not subject to the drift problems typically experienced with commercial EMI sensors such as the Geonics EM61 and EM63. As it is usually configured for characterizing buried objects, it measures the EMI decay from



**Figure 2.5. SAIC/NRL TDEMI array for buried-object location and classification.**

0.04 ms to 25 ms. This system has demonstrated near perfect performance in classifying buried targets such as unexploded munitions or metallic clutter at U.S. Army test sites.

The R01B project aimed to develop a prototype transient electromagnetic method (TEM) system consisting of five Tx and Rx coil pairs. The system would use SAIC's current TDEMI processing algorithms that were developed for locating and identifying compact buried objects such as unexploded munitions items. Those algorithms are based on point, rather than line, target models; and the R01B plan involved adapting those TDEMI array data processing and analysis procedures to support classification of underground utility lines, assemble a library of utility signatures, and test the processing and classification procedures using the prototype TDEMI array at a few utility test sites. The full scope of objectives set forth in the plan have yet to be realized; however, a  $5 \times 1$  sensor TDEMI prototype has been developed to operate advanced Tx and Rx coil pairs at variable time gate intervals on a towed instrument platform. The Tx and Rx parameters of the prototype are fully programmable, which is useful in optimizing the detection/location of underground metallic utilities. Data from the TDEMI prototype can be imported into Geosoft Oasis Montaj software for organization, processing, 2-D and 3-D visualization, and interpretation.

### Seismic Modeling Software Development (LTU)

As part of the seismic element of the R01B work, researchers at Louisiana Tech University (LTU) worked to develop modeling capabilities useful in helping to predict and understand high-frequency shear wave seismic measurements and to indicate the amount of computational resources necessary. LTU objectives were to develop finite difference time-domain (FDTD) method software capable of simulating propagation of acoustic and elastic waves in a realistic soil, to study the properties of acoustic and elastic wave propagation through a soil, and to analyze the physical consequences of the obtained results. Based on its results, LTU was to explore the possibilities of developing a virtual testing laboratory for the simulation of the acoustic and elastic methods for the detection of buried pipes and conduits.

During Phase 1 of the project, the 2-D modeling code, already developed by LTU researchers, was expanded to a 3-D model. The code was restricted to run on multiple processors on the Louisiana Optical Network Initiative (LONI) network of supercomputers to achieve a reasonable run time for large models with dimensions similar to some of the proposed field tests. The numerical simulations use the most accurate material properties available, representing the in situ field conditions.

Along with the development of a custom-written code, other commercial software packages, like the Wave Propagation

Program (WPP) from Lawrence Livermore National Laboratory, were used during the simulation exercise. WPP is a finite difference code which solves elastic wave equations in three dimensions. The 3-D elastic wave equations are a 3-by-3 system of second-order hyperbolic equations. The WPP code uses the MPI (Message Passing Interface) library for parallel computations on a Cartesian grid, with variable wave speeds and density throughout the domain. The code was used for simulating both seismic wave propagation and nondestructive testing. WPP was intensively tested in the seismic case to assimilate the scale of application intended for the R01B project.

In the second phase of the project, the results from the numerical models were validated against the data collected

during the field experimentation component of the work. Following validation of the code, multiple simulation runs were performed, with and without attenuation, to cover a wide range of scenarios. Simulations included various soil and source types, along with multiple buried plastic pipe targets and different depths. The goal was to develop a dynamic finite element method to analyze the wave propagation in the nonlinear inelastic soil media. The applications of the FDTD method in numerical simulations started relatively recently; the numerical conditions the FDTD method must satisfy require substantial computer memory and computational power. Therefore, the WPP code and simulations were run and tested on the LONI system of supercomputers.

## CHAPTER 3

# Findings and Applications

### Multichannel GPR System Status, Findings, and Applications

UIT's strategy for part of this project was to build on the multichannel ground-penetrating radar (GPR) system, TerraVision II, already constructed for enhanced utility detection. TerraVision is GSSI's first truly one-pass, 3-D digital geophysical mapping system, and UIT has been using TerraVision II for utility mapping since 2009. TerraVision II collects a 5.12-ft wide ribbon of data at a range of speeds and resolutions that adapt to the desired application. The internal survey wheel keeps track of data spacing while the GNSS or RTS keeps track of the relative sensor positions in project coordinate space. TerraVision II is designed to collect 1,200 ft of data at 3–5 mph, delivering the full resolution of one scan per inch, which allows for detection of smaller utility targets. From these data, 3-D images of the subsurface, along with 2-D map views may be constructed.

Once the data set is collected or a project site has been covered, the data files are transferred to the main system computer and archived to a storage media. The data are then transferred to processing software for analysis. The results of the analysis may be presented, edited, and saved in a 3-D interface that can be output to a CADD file. Appendices A and B are standard operating procedures (SOPs) for multichannel GPR digital geophysical mapping data collection and data processing. This document provides general procedures followed by UIT for geophysical data collection during subsurface utility field investigations with TerraVision II. Similar multichannel GPR systems are commercially available, but UIT has sustained efforts in making TerraVision II the state of the art through hardware improvements and through the development and maintenance of specialized proprietary data acquisition and data processing software.

GPR is an integral part of a multisensor utility detection system. It is an extremely effective tool for mapping utilities 12-ft deep or more in favorable soils, specifically those that

contain a high proportion of sand. With increasing clay content, GPR's penetration depth is decreased because higher soil conductivity values attenuate the imparted radar energy. Because the hardware behind the TerraVision II is well established, the R01B project focused on an approach for dealing with the substantial amount of data that it produces rather than on improvements to the hardware configuration.

Processing and analysis of multichannel GPR data are complex and time-consuming exercises. The R01B project team worked on methods to improve the analysis process through the development of software algorithms designed for GPR feature extraction and user-defined advanced processing parameters. Several algorithms were explored, developed, and tested for use in the system, providing a "toolkit" of methods for the user. The software improvements developed under the R01B project and implemented within SPADE are described in the next section.

### Improved Applications for Geophysical Data Analysis Software

Software is the key to integrated systems. UIT has developed three software packages for operating, processing, and interpreting multiple-sensor data. Data Acquisition Shell (DAS) is the software used to acquire geophysical data. DAS collects all of the field data from the various sensors while allowing the operator to track the system's location and tracks over a site. Data Processing Engine (DPE) performs preprocessing for interpretation of the data, correctly applies position data to each data point, and prepares the data set to go in the visualization and interpretation software. The Semiautomated Process and Detect (SPADE) software package accepts final interpretation-ready data.

The R01B project team and Sagentia, Ltd., have recently enhanced SPADE by making improvements to the semi-automated functions, making it easier for interpreters to

manipulate GPR data for analysis. Other enhancements to SPADE include functions for 3-D migration of GPR data and automated target recognition routines. SPADE was designed to accept any kind of 2-D or 3-D spatial data into the workspace. This feature allows the interpreter to input CADD files of utility data, site photos, field notes, or any other spatially referenced data along with the geophysical data. UIT demonstrated this process to So-Deep, Inc., a subsurface engineering firm, during in-service testing. This process can be considered first-order data fusion and involves getting all data plotted together at the same scale for quick and accurate comparison in 3-D. For in-service testing, data from the R01B prototypes, the associated interpretation layers, and all other relevant geo-referenced data were pulled together and compared against existing SUE records in one graphical and interactive window of SPADE.

The foundational concepts behind SPADE are directly related to the SHRP 2 objectives focused on enhancing utility detection and location using multiple sensors and leveraging the presence of known utilities to enhance detection. Those concepts are

- Integration of data from multiple sensors and existing map data;
- Use of sensor-specific algorithms to process raw data and detect features in a largely automated way; and
- Use of data fusion at the feature level, plus expert human interpretation to produce the best quality output from the available data.

Historically, UIT's workflow for picking features from 3-D GPR images involved working systematically through

2-D slices, a painstaking process that relies on the skill of the interpreter. In Phase 1 of Project R01B, Sagentia developed algorithms for identifying extended structures, referred to as *segments*, in the GPR imagery and presenting them to the user in 3-D views. These segments have the potential to greatly reduce the time taken to reduce an image and to allow the user to focus on interpreting features in the context of other data (aerial photos, TDEMI images, etc.). The R01B research approach was built on the understanding of what works best in practice. The resultant enhancements to SPADE algorithms developed under this research included

- Develop an initial set of segmentation algorithms and create prototype in MATLAB;
- Test algorithms on archived UIT GPR data;
- Create basic user interface for visualization and manipulation of segments and perform validation trials;
- Test segmentation algorithms:
  - Peak finding, and
  - Peak joining;
- Refine algorithms;
- Review raw image quality;
- View images with polarization effects;
- Contribute to GPR migration; and
- Port algorithms to VTK SPADE from MATLAB.

Figure 3.1 illustrates how UIT's approach to feature extraction addresses the main challenges to the requirements when working with multisensor data. This principally relates to

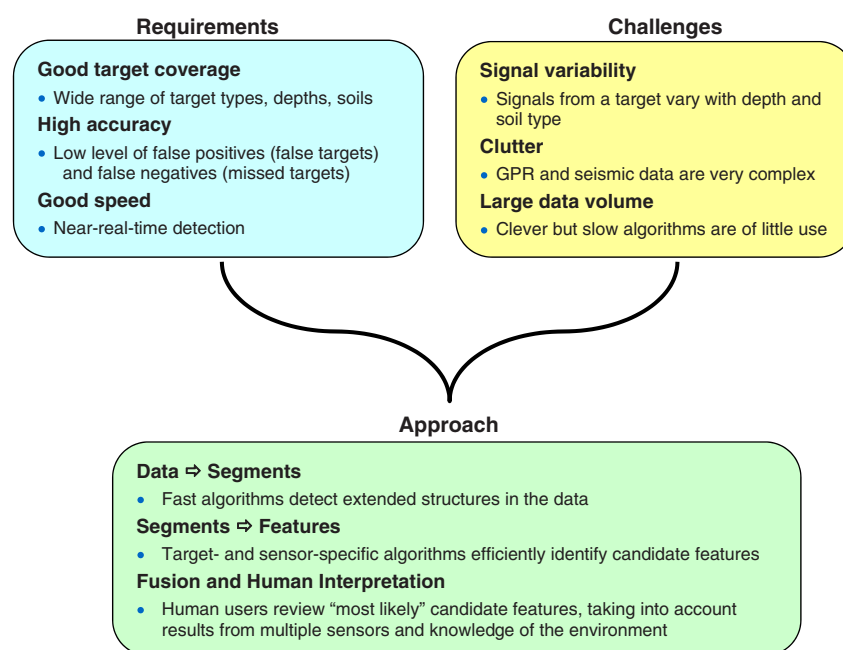


**Figure 3.1. Illustration of UIT's approach to algorithms.**

GPR and potentially to seismic data. The system requires an optimal combination of machine and human intelligence.

UIT's approach involved the following concepts:

1. GPR data can be divided into substantial segments from adjacent data points with similar signal properties. The challenge is in finding which specific signal properties are the results of individual utility target sources when the GPR data sets comprise numerous smaller segments, essentially due to clutter or noise. Furthermore, GPR signals vary with depth and soil type, which increases the challenge in matching adjacent data points of similar properties.
2. Once segments are extracted from the GPR data they can be joined to produce candidate features. Features are analyzed and scored so that the user can be presented with a prioritized list of features for consideration. The algorithms do not determine which features are valid but assist the user in systematically evaluating the whole data set.
3. A human user can assess all of the features and segments identified by the software and decide which features correspond to real targets by making subtle interpretations of visual data, interpreting disparate types of data, and exploiting contextual awareness. This user's task is significantly simplified because the software presents segments and candidate features in order of priority.

## Segments User Interface

This section contains a brief introduction and explanation of the user guide for the segments user interface developed by subcontractor Sagentia, Ltd. The key functions provided by the user interface are as follows:

- A single data object contains all segments, irrespective of their source. This allows segments from multiple images to be viewed together or combined.
- The segments can be sorted by various attributes and organized in folders, to help the user develop a workflow for identifying the segments that correspond to features of interest.
- The segments can be shown in a 3-D view of SPADE, along with other types of image data.
- Segments can be merged to form larger segments or split into smaller pieces. Points can also be picked from segments. (Note: Two SPADE algorithms were developed for creating segments from GPR data: correlation segments and threshold segments. Both algorithms work by finding a small set of peaks in each GPR scan and then connecting neighboring peaks in adjacent scans into segments.)
- The user interface for segmentation in SPADE allows the user to create segments from GPR data by selecting an impulse response width (samples), the minimum segment

size (pixels), and the maximum number of segments (0 for no limit). The user may also view and edit segments.

- The “spdSegments” object contains all the data for the segments, irrespective of how they were created. (This is similar to the “spdFeatures” object). Within spdSegments, all segments are stored in folders. The folders can be used to sort segments into different categories.
- A dialog box enables other SPADE controls to be used at the same time. Segments functionalities include plot controls, folder controls, sort controls, segments listing, and manipulation controls used to select, merge, split, or delete segments. A 3-D picking function also enables picks to be made from segments.
- Segments can be saved as Drawing eXchange Format (DXF) files; however, the export process can be slow because segments can contain many thousands of polygons, and DXF is a verbose format.
- Segments may also be imported into existing or user-created folders in SPADE, and their display properties can be adjusted by the user.

## Segmentation Algorithm Testing—Peak Finding

Much of subcontractor Sagentia, Ltd.'s Phase 1 work focused on the segmentation algorithms testing. The objective of the peak finding algorithm was to identify all of the peaks within the scan that might belong to features. Using this algorithm, it is acceptable to pick an excess of peaks because only those peaks that are adjacent to similar peaks will be used to form segments. However, some simple criteria are required to avoid picking peaks that would confuse the peak joining algorithm. A common approach to identifying peaks that correspond to real features is to use a “spiking filter.” This approach attempts to fit a scan to a set of spikes convolved with the impulse response of the system. Various spiking filters were tested, but with limited success. Wiener filtering attempts to exploit the different spectral characteristics of signal and noise. However, even noise and clutter in GPR scans tends to be bandwidth limited, similar to the signal. Orthogonal matching pursuit uses recently developed methods in compressive sensing; and although its performance was reasonable, the algorithm ran very slowly. Another limitation of these algorithms was that they prioritize large-amplitude peaks over small-amplitude peaks, and the intent of segmentation algorithms was to prioritize peaks based on their connectivity to adjacent peaks, irrespective of their amplitude.

Two simple algorithms were selected for detailed testing. In the first, the GPR scan is initially low-pass filtered to enhance signals in the bandwidth of the system and attenuate noise. All peaks are then selected, except for those closer to their

neighbors than the width of the impulse response, which were assumed to be residual noise. This algorithm method was termed *correlation peaks*. In the second, all peaks with amplitudes above a specified threshold were picked, except for those closer to their neighbors than the width of the impulse response, which were assumed to be residual noise. This provided the equivalent of an “isosurface” function, which is common in other image processing packages. This algorithm method was termed *threshold peaks*. Both algorithms were fast and they avoided picking noisy peaks, which was the most important criteria for the peak finding algorithm. The correlation peaks method, in particular, facilitated picking small-amplitude peaks.

The correlation peaks algorithm involves three steps:

1. Filtering the scan with a broadband, low-pass filter;
2. Picking one peak from each assemblage (or train) of local extrema; and
3. Converting peak heights to impulse amplitudes.

Step 1 was achieved by convolving the data with a narrow Gaussian, with half the width of the Ricker impulse response of the antenna. It conditions the scan by reducing noise, and it turns saturated parts of the scan back into proper local extrema.

In Step 2, illustrated in Figure 3.2, the purpose was to ignore small local minima and maxima that result from noise. Rather than apply an amplitude threshold, which would risk rejecting small but genuine peaks, it uses a spatial criterion. If two peaks are closer together than the width of the Ricker impulse response, then they are unlikely to be due to separate peaks. The algorithm gathers assemblages of local minima and maxima that are closely spaced. If an assemblage has an odd number of extrema—as shown in Figure 3.2a—then the train is ripple on a genuine local maximum or minimum. The most extreme peak within the train is taken to be the real peak, and the others peaks are ignored. If a train has an even number of extrema as shown in Figure 3.2b, then the train is ripple on a monotonic section of signal and can be ignored altogether.

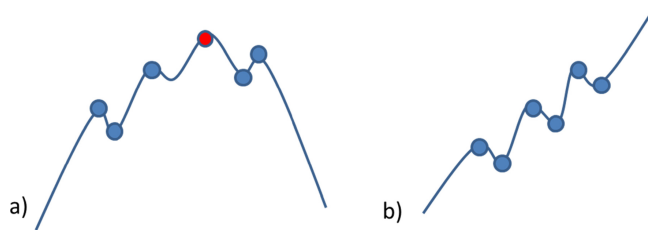


**Figure 3.2. Step 2 in the correlation peaks algorithm: (a) odd number of extrema, with the red dot as the most extreme, and (b) even number of extrema.**

After Step 2, suppose that  $n$  peaks have been identified, with the  $i$ th peak at position  $z_i$  and having amplitude  $A_i$ . Step 3 is a deconvolution step. It assumes that the original set of impulses had the same locations but had amplitudes  $C_i$ . Then

$$A_i = \sum_{j=1}^n I(z_i - z_j) C_j$$

where  $I(z)$  is the impulse response of the antenna.  $C_j$  is the final impulse coefficient of the sequence. This linear set of equations can be inverted to give the original impulse coefficients,  $C_i$ .

Step 3 is optional and omitting it also makes the peak finding step run more quickly.

The threshold peaks algorithm involves a simple modification to the correlation peaks algorithms. Rather than starting with all local extrema in the GPR scan, it starts with only those that exceed a threshold,  $T$ . The data analyst can specify whether to consider only local maxima (with amplitude  $>T$ ), local minima (with amplitude  $<-T$ ), or both. This provides a crude method for ignoring small peaks due to noise.

### Segmentation Algorithm Testing—Peak Joining

The peak finding algorithm developed by Sagentia in Phase 1 reduces each scan to a set of peaks, each with a certain depth location and amplitude. The algorithm connects peaks in adjacent scans to form segments. The peak joining algorithm connects peaks in adjacent scans to form segments.

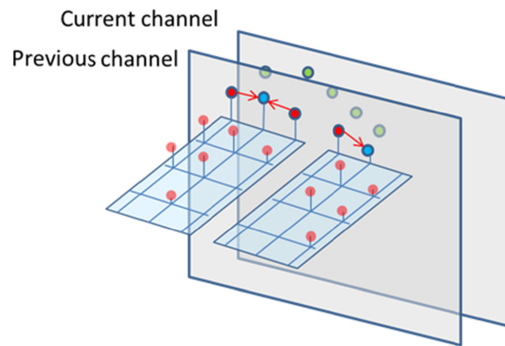
Suppose two peaks occur at depths  $z_1, z_2$  and have amplitudes  $A_1, A_2$ . These are only considered adjacent if  $|z_1 - z_2|$  is not large compared with the width of the antenna’s impulse, and  $A_1, A_2$  have the same sign. These are moderately weak criteria and enable segments to be followed from scan to scan even if confronted by large changes in signal amplitude. For each peak in the first scan there may be two or three peaks in the second scan that meet these criteria. The connection is then made between the peaks that are closest together (i.e., for which  $|z_1 - z_2|$  is smallest). Some additional topological criteria are applied that govern how segments grow and merge. There are two versions of this part of the algorithm: edge segments algorithm and square segments algorithm. The edge algorithm looks for neighboring peaks within the correlation distance and then joins peaks on a one-to-one basis, preferring to join peaks that are closer together given certain conditions: the adjacent peaks cannot change polarity, nor can a peak be joined to a segment if it would cause the segment to overlap in the time direction. The squares algorithm attempts to link peaks into squares (a mutually connected set of four peaks). Out of potential groupings of points, squares are chosen such that the curvatures of both peak height and signal values are minimized and adjacent squares are joined to form segment sheets.

GPR images are typically too large to be read into memory, so the process of joining peaks into segments was constrained to work with one channel of the image at a time. In SPADE, each channel is a contiguous part of the image file, which enables it to be quickly read from disc. Figure 3.3 illustrates four steps that are used in the process of building segments and the data structures that are used. Figure 3.3a shows the state of the system having just found peaks within the current channel. These are shown as green circles. The peaks found in the previous channel are shown as red and blue circles. The connections between adjacent peaks in the previous channel are shown as red arrows. Every segment in the previous channel is represented by a “tree” of peaks in which the blue circles represent the “root” of each tree. Two peaks are therefore part of the same segment if their connections can be followed to the same root peak. These trees are the first data structure used to keep track of segments. Each node peak also has the job of remembering the peaks from all the channels to date that belong to its segment. This information is stored in a “map” (a rectangular array over a range of scans and channels). The maps for two segments are shown in Figure 3.3a as blue gridded rectangles. Non-zero entries in the array specify the depth location of a peak (shown as pale red circles), and zero values correspond to channel scan locations with no peak. These maps are the second data structure that is used to keep track of segments.

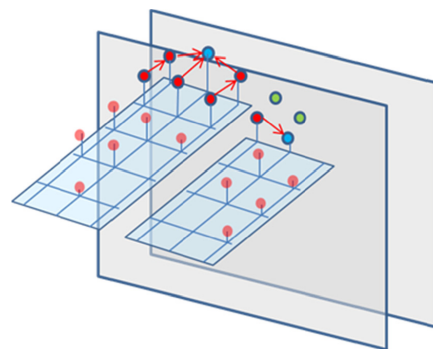
Figure 3.3b shows the state of the system halfway through processing the current channel. Three peaks in the current channel are adjacent to peaks in the segment on the left. New connections have been made between peaks in the previous channel, in the current channel, and between the two. The tree structure for the segment has been reconfigured so that the root peak has moved into the current channel. The map for the segment has also expanded to include the peaks in the current channel.

Figure 3.3c shows the state of the system just at the end of processing the current channel. Not only have the peaks on the right connected to the segment on the right, they have also connected to the peaks on the left in the current channel. This requires merging the two segments. There is now just one root peak (blue circle) and, associated with it, just one map, covering all of the peaks.

Finally, Figure 3.3d shows the system about to advance to the next channel. The peaks in the previous channel are discarded; their existence is recorded in the map. Only the peaks in the current channel remain, with connections between them. If a segment has not connected to any peak in the current channel, it cannot grow any further. It is removed from the set of segments being tracked and is added to the set of segments to be outputted. When the last channel has been processed, all the segments currently being tracked are transferred to the set of segments to be outputted.



**Figure 3.3a. Step 1 of four in peak joining.**



**Figure 3.3b. Step 2 of four in peak joining.**

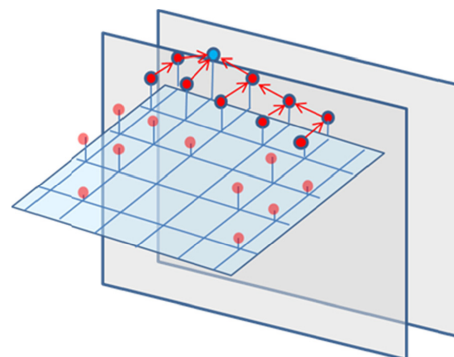


**Figure 3.3c. Step 3 of four in peak joining.**

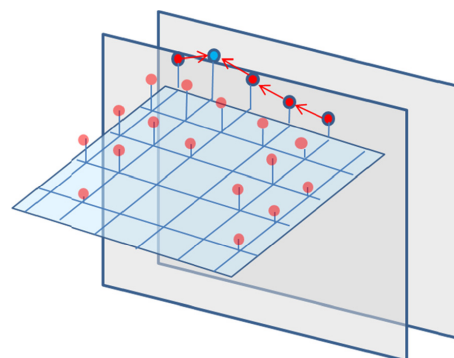


**Figure 3.3d. Step 4 of four in peak joining.**

## Performance and Refinement of the Segmentation Method

Segments offer clear identification of features in data, providing a global view of each structure in a 3-D interface. This can simplify the task of identifying pipe reflections, soil layers, and point objects by providing a more intuitive picture of the signal. In the course of reviewing the segmentation functionality, some improvements were made to the algorithms. It was determined that segmentation finds most of the significant features in an image; however, it can still miss faint features which are disjointed by noise and, therefore, cannot entirely replace visual inspection of 2-D slices.

Analysis of segments is a time-consuming process. A substantial number of segments are produced; and although there are automated ranking systems to filter out the weakest segments, dozens of segments still need to be analyzed by a data analyst for a relatively small image of 300 scans by 14 channels. Furthermore, the algorithm is not completely successful in identifying all features. Examples were discovered in which smaller objects were only partially segmented by the squares algorithm, and neither the edges nor squares algorithms were able to identify all of the pipes on some sample data sets. The majority of features were segmented, in whole or in part. However, the numbers of false negatives are not significantly minimized; thus the effectiveness was determined to be comparable to that of traditional methods of using migrated time slices for GPR analysis and interpretation. On the one hand, the edges algorithm displayed a propensity to connect features to sheets of noise, and to add nonsmooth edges to segment sheets. This made features harder to pick out and identify and increased the analysis time, forcing the user to split and merge segments until a more representative feature became clear. On the other hand, the squares algorithm, which appeared to be only slightly less successful in segmenting features present in the data, did not exhibit such a greedy approach. It provided clearly defined (and more compact) shapes, making it easy to identify features, reducing operator error. This clarity of results made the squares algorithm marginally preferred during testing.

## Raw Image Quality

Sagentia compiled a database of images from UIT TerraVision data sets to aid in the software and algorithms testing. The database identified a set of images, which span a range of features, identifying strength, feature type, feature direction (if linear), number of features, whether features were straight, whether they crossed, and whether they exhibited polarization effects. In all the images compiled, the ground reflection was very well aligned in time across each acquisition swath. The 14 GPR antennas of the TerraVision are array-staggered in the along-channel direction, with the biggest offset occurring between Channels 7 and 8. In most of the images reviewed, the

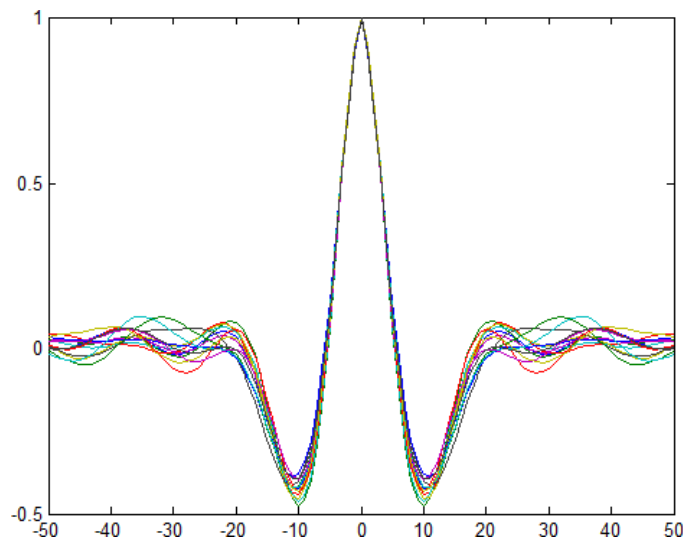


**Figure 3.4. Impulse response for each of 14 channels, derived from raw data by an autocorrelation method.**

channels were very well aligned in along-channel direction, which indicated that the antennas' offsets were being correctly compensated for. However, in rare cases, there were visible misregistrations between adjacent swaths, and it was presumed that such errors could be corrected after-the-fact by adjusting the map files.

Figure 3.4 shows the impulse response of each of the 14 channels in the TerraVision system. These were calculated from an image for which the autocorrelation of the scans was averaged along each channel, and the autocorrelations were converted into impulse responses by assuming a zero-phase signal. The impulse responses were very similar from channel to channel, and they fit well to a Ricker wavelet.

The most imperative issue observed in raw images was the presence of ringing in some channels. "Ringing" involves persistent oscillations that occur in a few specific channels. This is the most serious artifact that occurs in TerraVision data; it can easily obscure features, both in map view and in vertical slices. It is unlikely that this can be addressed by image processing. In many cases, the ringing increases with depth until the data saturates.

## Images Viewed with Polarization Artifacts

Polarization effects in TerraVision data are the occurrence of a strong attenuation of GPR signal at every other channel of the array due to the angled orientation of utility target positions in the subsurface relative to the antennas' direction during acquisition. The effect of splitting channels based on polarization (and analyzing the two sets of images separately) on the ability to identify features from time slices of data was assessed for several pipe situations: diagonal pipes, which show polarization effects; perpendicular

(to the swath) pipes; and longitudinal pipes (in the same direction as the swath).

Most pipes that cut a swath at an angle around  $45^\circ$  exhibit polarization effects. Viewed from a time slice, the pipe appears banded, reducing its visibility. Splitting the image into separate polarizations produces one image in which diagonal pipes are clear and one in which such pipes have a highly attenuated response. (See Figure 3.5.) Splitting an image into two separate polarizations does, therefore, appear to aid pipe detection when using time slices; however, both polarizations must be checked so that pipes in orthogonal directions are not missed.

Perpendicular pipes often show up clearly in time slices. For pipes that give strong signals, viewing only one polarization can give a smoother image. However, the advantages of trying to pick out pipes with weak signals were less clear. When viewed in time slices, longitudinal pipes can be difficult to distinguish from channel imbalances. Splitting polarizations did not seem to reduce the visibility of longitudinal pipes in time slices, and in some cases resulted in a more clearly defined target. Polarization effects are also apparent in the detection of localized objects as well with the target disappearing every other channel in time-slice view. Separation of the data into separate polarizations reduced the ease of identification of these point-source signals in time-slice view, which was not a problem for linear target identification. In general, it was determined that polarization-sensitive methods of viewing the raw multichannel GPR data do not necessarily provide the data analyst with an easy method to detect and identify features, particularly faint features.

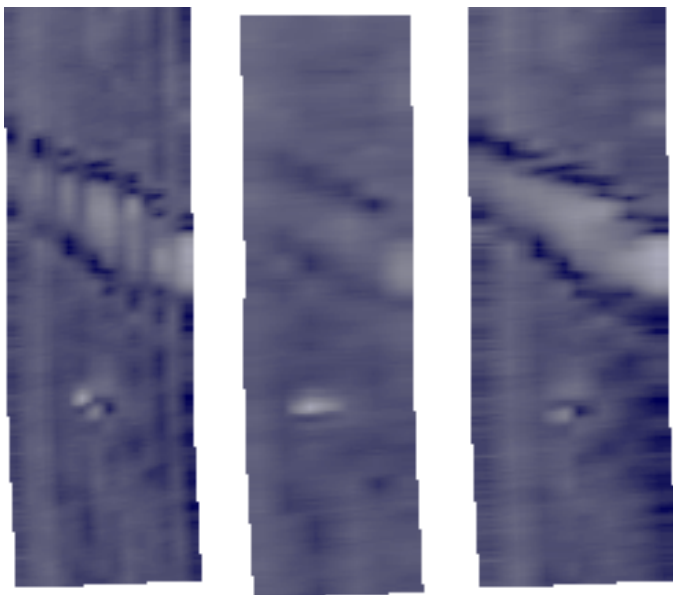


**Figure 3.5. GPR time slice from diagonal pipe: (left) all channels, with polarization effects visible; (middle) Channel B, poor pipe visibility; (right) Channel A, clear pipe definition.**

## Contributions to GPR Migration

Point features in the ground generate hyperbolic cones in raw GPR images; linear features generate hyperbolic sheets. Migration algorithms stack images along hyperboloids, concentrating the energy from hyperbolic cones and sheets back to points and lines respectively. This is not a mathematically perfect inversion, but it serves to increase contrast and sharpen features. UIT has historically had limited success in getting quality migrated images with multichannel GPR data. During the SHRP 2 R01B project, Sagentia released a bug fix for SPADE that addressed this, as well as a migration preview function that makes it easier for the data analyst to set the algorithm parameters.

Three algorithms using a constant soil dielectric were studied: the Witten stack, Stolt migration, and Kirchoff migration. Each algorithm is mathematically similar and displayed similar image quality during testing. The Witten algorithm is simple and intuitive. It does not correspond to any mathematical model of wave propagation, unlike Stolt and Kirchoff migrations. However, it is also slow. The Witten 2-D code explicitly creates the weight image (as illustrated in Figure 3.6) and applies it to the whole raw image, ignoring the fact that the vast majority of weight values are zero.

Stolt and Kirchoff migrations are based on a mathematical model of wave propagation in a medium with a constant speed of light (i.e., constant soil dielectric). Nonetheless, they can both be described in terms of image weights, as with the Witten algorithm. The Stolt algorithm decomposes the raw image into plane waves. The migration step involves altering the wave vector for each mode and recombining the modes to get the migrated image. The conversion to Fourier modes and back again is accomplished by fast Fourier transform (FFT),

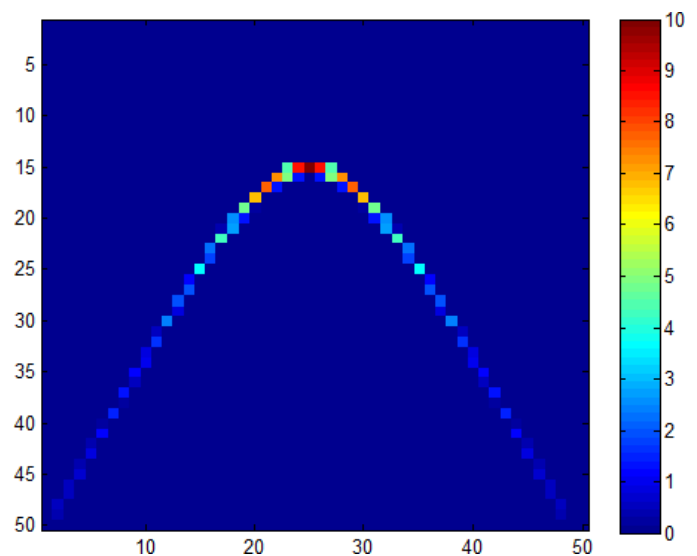


**Figure 3.6. Image weights for Witten migration.**

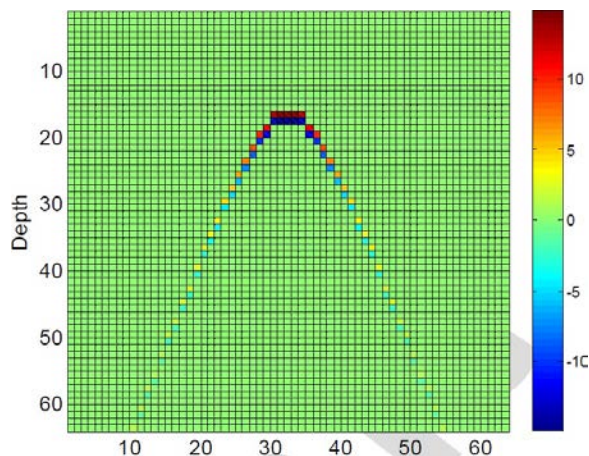


**Figure 3.7. Weights applied to the raw image under Kirchhoff migration (to 1 pixel at apex of hyperbola).**

which makes the algorithm relatively fast. The Kirchhoff algorithm is a reverse time migration in which the raw image represents energy collected at the surface as a function of time, and this is propagated backward to find the distribution of energy in the ground at time zero. The weight image of the Kirchhoff migration (Figure 3.7) appeared less noisy than for the Stolt migration, resulting in a cleaner migrated image; but Kirchhoff migration ran slower than Stolt migration because there is no FFT-style shortcut for its implementation.

The effectiveness of the Stolt migration in SPADE was studied by migrating a small section of GPR data and tuning the “z-scale factor” until the migration was optimized. This factor was then used to migrate larger sets of data from the same site. These studies resulted in a new version of SPADE (delivered to UIT in March 2012) that included bug fixes for the migration algorithm contained.

### GPR Migration and Time Slices

Comparisons of GPR time slices were made with and without migration applied. Linear features associated with subsurface utilities were identified in the migrated GPR slice images and occasionally displayed slightly sharper definition than the unmigrated slices. Figure 3.8 shows a section of GPR data collected along three acquisition passes on a road with two subsurface pipes: one straight, one bent. The center swath is an unprocessed time slice; the outer swaths show the results of migration. It should be noted that although the migrated time slices offer tighter target resolution for several linear targets, some of the weak detection responses from subsurface utility sources were clearer without migration applied.

Near the surface, features in migrated images stand out over a low noise background; but with deeper images, the

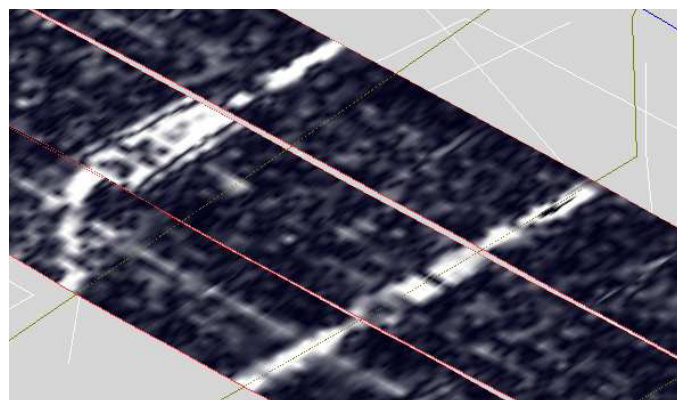


**Figure 3.8. Migrated-unmigrated time-slice comparison.**

noise proved more prominent, even for the migrated image. Weaker signals can align in deep time slices and be mistaken for linear features and potentially targets of interest. For this reason, it is important that the data analysts view both the migrated and unmigrated time slices images during data interpretation. Near-surface targets can be more precisely depicted on migrated GPR time slices, but deeper migrated time slices can display false targets of aligned noise.

### GPR Migration and Polarization

Migration performance with polarization effects was also studied. In theory, the migration algorithm should be unaffected by polarization effects. Summing along a hyperbola in which every second channel has low signal strength will still result in a concentration of energy at the peak, albeit with a reduced signal strength compared with that from an image without polarization effects. To demonstrate this point, a series of synthetic images were constructed for analysis. Each image contained a simulated hyperbolic response from a pipe. Hyperbolic responses were constructed first with all channels responding and second with alternate channels highly attenuated (simulated polarization effects). Both hyperbolae images displayed a bright point after migration, although the image without polarization effects showed a sharper and stronger response, as expected. Indeed, migrated images of diagonal pipes, viewed in time slices, also showed pipes clearly, even when simulated polarization effects were present.

When used on real project GPR data, the migration performed well in coping with images showing polarization effects. Pipes running diagonally across a swath (which do not always show polarization effects) were clearly imaged with no striping observed in the migrated image (Figure 3.9). The contrast between noise and migrated pipe was not as good as for straight pipes without polarization effects (Figure 3.10).

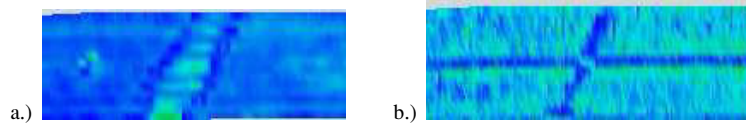


**Figure 3.9. GPR time slices of diagonal pipe: (a) unmodified image, (b) migrated image in which pipe is most visible in negative component of reflected signal.**

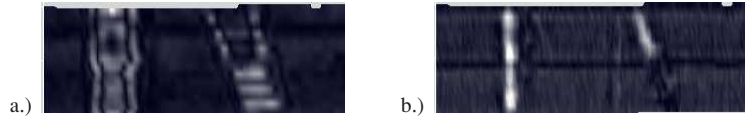


**Figure 3.10. GPR time slices of perpendicular pipe (showing one perpendicular pipe and one pipe at an angle, with polarization effects): (a) unmodified image, (b) migrated image, with migration scaling factor tuned for perpendicular pipe.**

For images which show polarization effects, splitting the polarizations would be expected to increase the performance of the migration process, by removing channels with negligible response to maximize the signal in the mapped hyperbolic sheet. Sagentia used a three-step process to split channels: (1) separate the channels into A and B polarizations, (2) interpolate between the remaining channels in each image, and (3) perform migration on both images separately. Using synthetic images, it was seen that migrating individual polarizations does offer some improvement in the strength and continuity of signal, over migrating both polarizations together. The migrated result from the polarization showing the strongest response was marginally stronger than the result without splitting polarizations. However, the added clarity is probably not worth the time cost of doubling the number of images to view.

### GPR Migration Assessment

GPR migration within SPADE has the potential to be a powerful tool for feature identification from GPR data. Migration collapses the pipe signal to a localized line, and this provides a quicker (and potentially more accurate) estimation of the depth of an object than achievable from the raw signal response. Furthermore, the localized signal could allow tracing algorithms to track the extent of a feature, after one point is identified.

A comparison of migrated and unmigrated images reveals that, in general, pipes which show up in migrated images are also visible in unmigrated time slices. Migrated images tend to have lower noise, which can give sharper pipe definition. While some pipes are clearer after migration, others, particularly those with weak signals, are not. The visibility of the thin signal line in migrated features, particularly when large swaths are viewed as a whole, is often poor when

compared with the broad “bloom” of pipe features in unmigrated time slices.

Successful migration depends on an accurate choice for the z-scale factor (which takes account of the signal speed in local soil type). A number of methods are provided in SPADE for testing this scaling to include hyperbola fitting and migration parameter selection preview options. The benefits of using migration over assessing unmigrated time slices are not readily perceived; the improvements to workflow consist of a transition to assessing time slices of large images (over vertical images of small subsections) and an opportunity for increased automation in feature tracing.

### High-Frequency Seismic Imaging Proof-of-Concept Prototype Status and Findings

The seismic component of the R01B research was a first of its kind endeavor riddled with unknowns, highly technical concepts, and limitations posed to feasible configurations and computational electronics. So the project team focused on proof of concepts (specifically, shallow in situ soil seismic properties) in support of research objectives to design and construct the proposed high-frequency seismic imaging prototype system. This moderate approach to development was due to several factors, including the slow process of finalizing project contracts and subcontracts, unforeseeable manufacturing and vendor equipment delivery delays, limited experience with and knowledge about new system electronics, and the lack of general support documentation. The seismic element of SHRP 2 R01B research work was performed by Owen Engineering Services with support from Psi-G, LLC and Bay Geophysical, Inc.

Knowledge of seismic wave propagation in near-surface soil materials is critical to the design and optimization of an effective seismic method for detecting and mapping underground utilities. Because of regional variability in soils and localized variations in utility backfills, in situ field measurements are essential to gaining a full understanding of underground utility environments for realistic high-resolution seismic system performance. Therefore, actual field testing and site-by-site characterizations of the various utility host media are mandatory for accurate definition of the seismic properties. A regional survey of soil seismic properties was conducted emphasizing measurement of horizontally polarized shear (SH) wave propagation parameters along with similar measurements of compressional (P) waves. The primary seismic parameters were the frequency-dependent viscoelastic attenuation versus depth and the propagation velocity versus depth—both measured along a common down-transmission vertical path. The methodology used in this task was specialized to high-resolution seismic attenuation and velocity measurements using a push-type soil probe system equipped with a three-component seismic CPT (cone-penetration test) toolhead attachment. The information gathered as a result of this testing aided in defining the general ranges of velocity and attenuation in near-surface materials and served to indicate the possibility of following through on the technical approach to develop an effective high-resolution seismic system for underground utility detection and mapping.

### Soil Seismic Properties Background

Only a limited amount of quantitative information was available on in situ seismic properties of shallow soils leading up to the SHRP 2 R01B research work. A noticeable limitation in nearly all of the documentation on seismic velocities in shallow soils was the relatively low frequency range for which practical measurements have been reported. Underground utility environments require defined seismic soils properties up to about 1,600 Hz. The available background of reported work at low frequencies has justifiably neglected the frequency dependence of velocity caused by dispersion effects inherent in viscoelastic attenuation; new measurements would require that velocity dispersion be accounted for in the soil seismic properties. Another characteristic of seismic propagation in shallow surface soils is the velocity gradient versus depth caused by compaction in granular materials. Other factors such as grain size and shape and grain cementation also affect the elastic moduli, giving rise to differences between natural undisturbed soils and trench backfill soils.

The soil modulus factors affect the P-wave and shear wave (S-wave) velocities; in general, soil materials having high moduli have higher seismic velocities and lower internal friction and, therefore, have lower attenuation (and higher attenuation

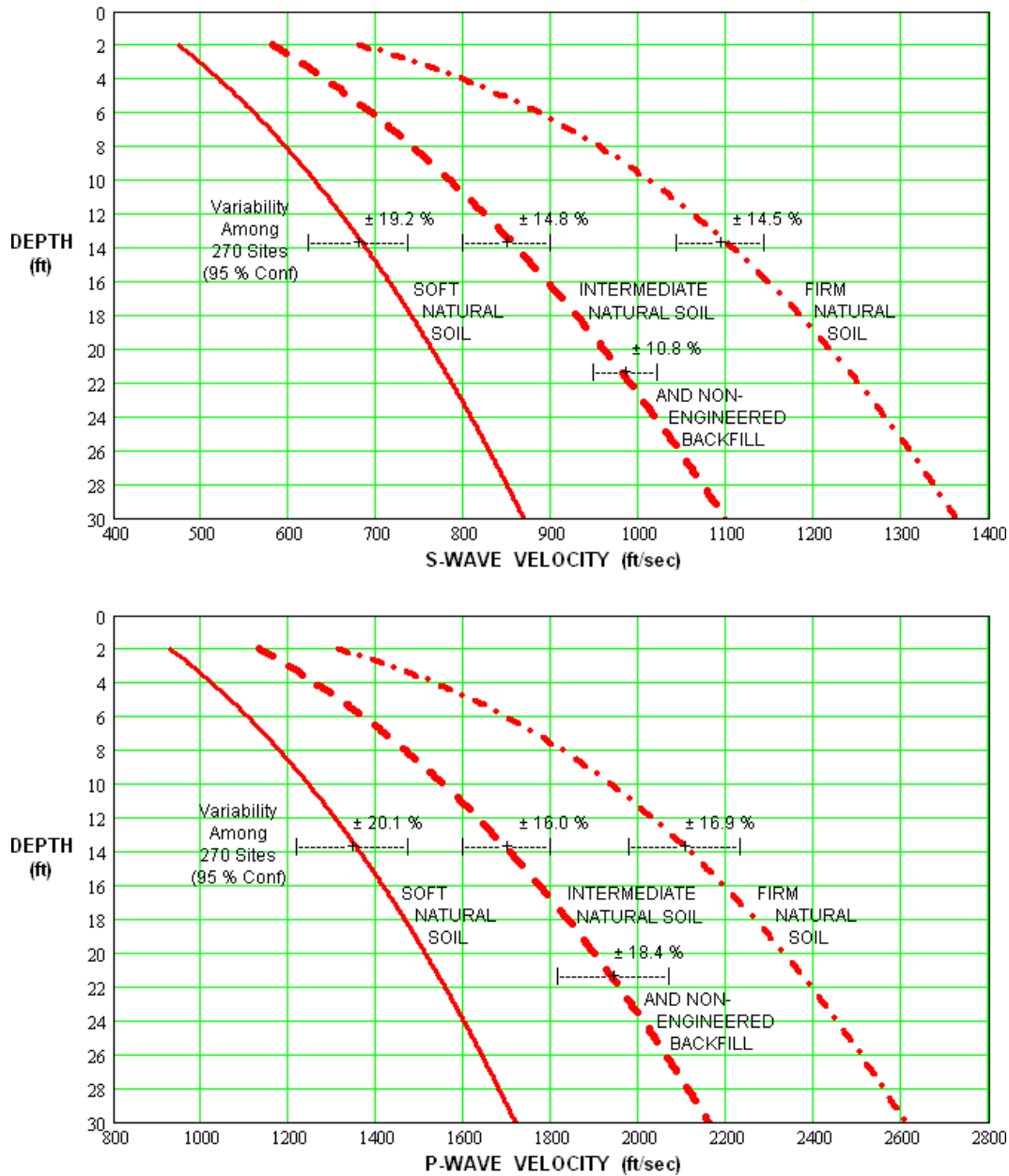
coefficient, Q). Based on limited data researched, typical seismic interval velocities within the top 20–30 ft increase by about a factor of two relative to the velocity at the surface, depending on the soil type and compaction. Sedimentary layer variations in soil type may occur, but lateral variations in velocity are not significant at given localized test sites unless distinct areal changes in soil type are present. A seismic medium of this type is referred to as a transverse isotropic medium, characterized by only a vertical velocity gradient.

In regard to R01B seismic soil properties testing, principal pertinent information was derived from documentation research and is revealed in a paper by Lew and Campbell (1985), which is illustrated in Figure 3.11. That information is as follows:

1. S-wave velocities at all of the test sites exhibited a significant increase versus depth in the top 30 ft of the ground;
2. Compressional wave velocities at all of the test sites exhibited a significant increase versus depth in the top 30 ft of the ground;
3. Statistical variations in S-wave velocity among the 270 test sites (95% confidence), for depths of 2–15 ft, are typically about  $\pm 17\%$  for undisturbed soils and about  $\pm 11\%$  for nonengineered backfills;
4. The highest velocity gradients occur in the top 10 ft compared with gradients in the underlying 10–30 ft, with firm soils and backfill materials having the greatest differences between these depth zones; and
5. The P-wave velocity to S-wave ratio ranged from 1.91 to 1.97 for all of the soil types in the top 30 ft, with the slightly greater effect in the soft natural soil.

Although all of the test sites reported by Lew and Campbell were located in California, their specialized engineering soil classifications are directly relevant to similar soil conditions in other geographic regions. Equally important is that a large number of test sites were used in characterizing the velocities and vertical gradients, resulting in well-represented regression-analyzed nominal in situ velocity profiles for each soil-type classification.

Shear wave velocity measurements versus depth in shallow soils were of direct interest in the planned R01B soil seismic properties survey, so several contributing factors were carefully considered during test planning. Those factors centered on the implications of vertical velocity gradients and the implications of seismic attenuation in shallow soils. All of these considerations provided a clear rationale for conducting new field tests to characterize soil seismic properties relevant to high-resolution underground utility detection and mapping. The scarcity of prior work in measuring attenuation and velocity dispersion in unconsolidated shallow soils indicated that many aspects of the new measurements would



Source: Adapted from Lew and Campbell (1985).

**Figure 3.11. Shear wave and compressional wave velocity versus depth in soft, intermediate, firm natural soils, and nonengineered backfills.**

demand close attention to devising proper field procedures. Thus, proven equipment technology capable of assuring acquisition of high-quality field data was used. In addition, the data processing techniques were expanded to include extracting velocity profiles in the transverse isotropic soils of interest when affected by frequency-dependent dispersion as well as extracting the amplitude attenuation coefficient, or  $Q$ , of the medium as a function of frequency over a range of high seismic frequencies not previously investigated. For accurate and consistent results, these tests required a dedicated mobile field system capable of measuring and recording seismic

velocity and viscoelastic attenuation versus depth for both S-waves and P-waves at depths to 15–20 ft as functions of frequency over the range 50–1,600 Hz.

A primary consideration in performing this study was to determine whether the transmission of high-frequency shear (S) waves or compressional (P) waves is practical given the attenuation that is likely to occur. To that end, the project team selected three separate regional sites to conduct the seismic soil properties testing: Manteno, Illinois; Houston, Texas; and Manassas Park, Virginia. Testing was performed during the fall of 2011. Before actual field testing, significant efforts

were made in preparing and configuring both the software and hardware components of the seismic data acquisition system for a full dry-run soil properties testing procedure. During this trial testing, in Traverse City, Michigan, the team determined the proper procedures for equipment setup, data acquisition, and initial data processing. A coordination plan was also developed to establish responsibilities, schedule sufficient time in obtaining one-call tickets, provide accurate locations of the testing sites, and allow sufficient up-front time to the host installations.

### Soil Seismic Properties Preparation, Equipment, and Data Acquisition

The methodology of measuring soil seismic velocities and attenuation at high frequencies was given detailed consideration by subcontractor Owen Engineering Services. The in situ approach was selected because only such realistic tests could provide meaningful results relevant to actual field conditions. This fundamental criterion determined the planned equipment and measurement methodology.

The system frequency response requirements were calculated on the basis of the project goal of detecting a 3-in.-diameter pipe at a depth of 12 ft. Assuming that the detection threshold occurs when the pipe radius is one-quarter wavelength at the pipe burial depth, the incident seismic wave must have a wavelength of

$$\lambda = 2D_p$$

and a frequency of

$$f = \frac{v}{\lambda} = \frac{v}{2D_p}$$

where

- $v$  = speed of wave,
- $\lambda$  = wavelength,
- $f$  = frequency, and
- $D_p$  = pipe diameter.

Using this relationship, the lowest incident wave frequency for which a 3-in.-diameter pipe is detectable in soils having  $v_s = 500$  ft/s is 1,000 Hz. Larger-diameter pipes are detectable at proportionately lower frequencies.

To produce the desired high-frequency seismic signals required for small-diameter pipe detection, vibrator sources generating continuous linear frequency sweeps were considered, but separating independent frequencies for velocity and attenuation analysis would be difficult from a data processing perspective. Therefore, it was determined that the best way to measure attenuation of signals was to use monochromatic tonebursts with center frequencies of 100, 200, 300, 400, 500,

600, 700, 800, 900, 1,000, 1,100, 1,200, 1,300, 1,400, 1,500, and 1,600 Hz. Figure 3.12 shows the design features of these tonebursts, each having a time duration of 60 ms and separated in time by 120 ms. The amplitude envelopes of the tonebursts are cosine-squared in shape to confine the frequency spectrum to 100-Hz bandwidth at each toneburst frequency.

The seismic microvibrator, MicroVib, was selected as the source for these tests, since it is capable of generating vibrations at the frequencies required. This proprietary source was designed by Owen Engineering Services and constructed under license by Bay Geophysical in the late 1990s. It has been used on numerous seismic surveys for generating SH-waves and P-waves at frequencies up to about 400–500 Hz. The MicroVib was fitted with a fabricated point-source ground-coupling base plate as shown in Figure 3.13. A new power amplifier was chosen as the device to provide current to the vibrator. This device must be capable of delivering constant current at the wide range of frequencies specified for the tonebursts.

Accelerometers were chosen as the transducers to use for the measurements because of their uniform frequency response over the range of frequencies required. In particular, the selected seismic-grade accelerometers have exceptionally low self-noise in the frequency range of interest. A special tri-axial accelerometer probe housing was designed by Owen Engineering Services: the accelerometers were mounted as a set of three orthogonal transducers and pushed into a bore-hole for placement at various depths below surface from the source to measure the travel time and attenuation of the transmitted tonebursts (see Figure 3.14).

Finally, to record the transmitted signals and generate control signals for the vibrator, it was necessary to select a data logging and control system such as the Dewetron Model DEWE-3210 with high sensitivity, high sampling frequency, a wide digital dynamic range, a signal generator, and computer control capabilities. The selected equipment included the Dewetron data acquisition system, Wilcoxon Model 731-207 accelerometer, and the AE Techron Model LVC 5050 excitation power amplifier.

After procurement of the equipment listed above, the components were laboratory tested to verify that the various components functioned correctly. During this shop check, several problems were encountered. Serious ground-loop interference was encountered with the power amplifier—whenever power to the data acquisition system was turned on or whenever a triggered toneburst sequence was originated by the data acquisition system and power amplifier. The cause of this interference was found to be a configuration problem in the power amplifier and was later resolved through conversations with the manufacturer. Also, the Dewetron software was not set up to generate and record causal measurements. That

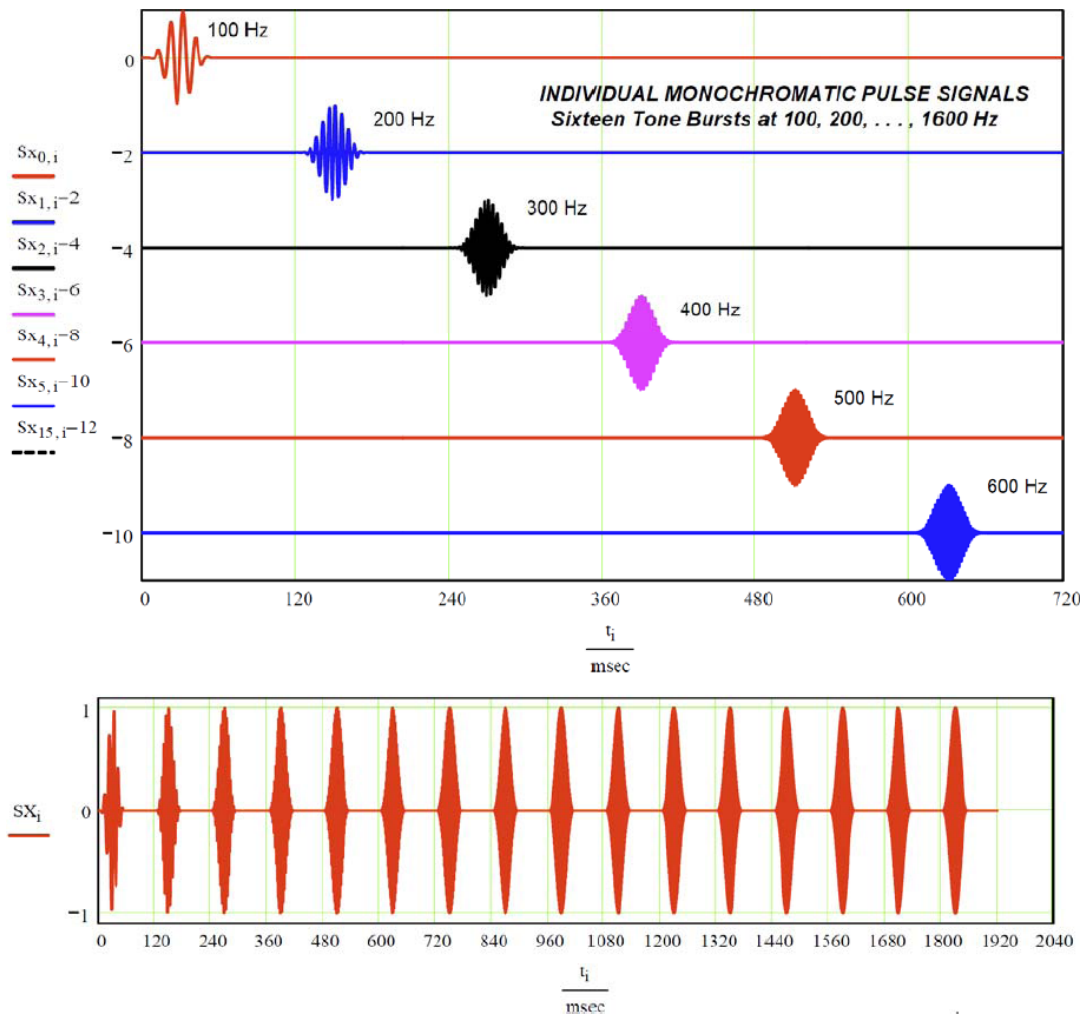


**Figure 3.12.** Design features of tonebursts: (upper graph) first six pulses of 16-toneburst sequence; (lower graph) 16 tonebursts, 60 ms in duration, separated at 120-ms time intervals.



**Figure 3.13.** Ground coupler base late for MicroVib.



**Figure 3.14.** Housing probe and triaxial accelerometers.

is, the software did not allow for synchronized generation of the toneburst excitation signal and the initiation of A-to-D sampling of the accelerometer signals. After some time, Dewetron software engineers were able to generate revisions to the software which allowed the synchronized seismic measurements to be made. Finally, several spurious resonance responses were observed in the operation of the MicroVib during shop testing. As the vibrator generated the stepped-frequency tonebursts, the vibration amplitudes were stronger at some frequencies than at others.

Following the laboratory check of the system and resolution of all non-vibrator-related problems, the system was set up at a soil probing site in Traverse City, Michigan, where the entire system could be tested in a mockup of the actual field measurements. A Model 540UD Geoprobe push-technology ground probe system was used to push the downhole accelerometer probe into a pilot hole previously pushed or cored by the Geoprobe system. The selected location had a soil profile that was entirely sand, at least in the upper 15 ft; and the Geoprobe system was unable to push the downhole accelerometer probe deeper than approximately 8 ft. Other difficulties were encountered during trial testing and lessons learned. Of significance was that the variable amplitude output of the vibrator versus frequency was confirmed to exist in the downhole accelerometer signals. This required additional shop testing and recalibration of the MicroVib before performing the soils properties testing at the regional U.S. locations.

The purpose of the field measurements was to determine the S-wave and P-wave velocity and attenuation (or Q) depth profiles versus frequency for different types of soil. To make the desired velocity and attenuation measurements at discrete frequencies, the MicroVib source was used to generate a sequence of 16 monochromatic toneburst pulses that start at 100 Hz and step up in frequency at 100-Hz intervals to 1,600 Hz at the upper frequency limit. Each toneburst was shaped to have a cosine-squared envelope to minimize the spectral overlap at adjacent toneburst pulses when analyzing the data. The 16 tonebursts were spaced 120 ms apart to produce a total sequence duration of 1.92 s. This toneburst sequence was triggered by the Dewetron data acquisition system at a short time delay of 10 ms after initiating the A-to-D sampling and recording of the six accelerometer sensor channels. The excitation sequence was fed to the Techron power amplifier and MicroVib to produce the ground vibrations.

To measure attenuation of the propagated seismic signals, a reference accelerometer probe was used to record the radiated source waveforms (see Figure 3.15). This reference probe was placed at a depth of 18 in. in a shallow borehole located about 2–3 ft from the downhole accelerometer probe. Triaxial accelerometer signals from these probes were recorded as the downhole probe was pushed downward at 1-ft depth intervals. Simplistically, the ratio of the individual toneburst signal amplitudes

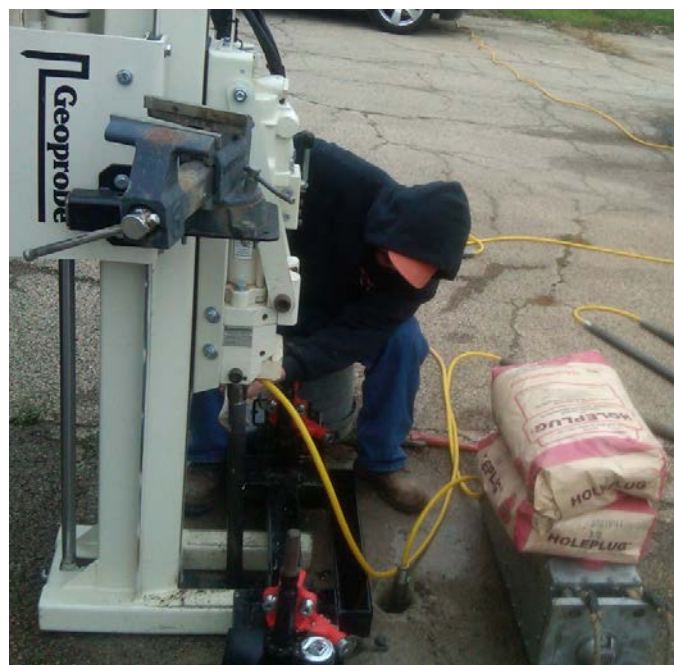


**Figure 3.15. Placement of downhole and reference probes during field testing.**

measured at the downhole probe divided by those measured at the reference probe can be used to derive the net seismic wave attenuation over the distance between the probes. At each borehole location where attenuation was to be measured, both reference and downhole transducer probes were calibrated simultaneously to ensure accuracy of measured amplitudes.

The downhole probe was pushed into the ground at increments of 1 ft. At each increase in depth, a toneburst signal was sent to the MicroVib, and accelerometer responses were recorded from the two sensor probes. This procedure was repeated until the downhole probe was unable to advance to further depths or until a maximum depth of 16 ft was reached. The downhole accelerometer probe was not rotated during the pushing procedures. During each such measurement, the MicroVib was maintained at a specific orientation: vertical for P-waves or horizontal for SH-waves, with SH-wave polarization either in line with the direction of the line between the reference and downhole probe boreholes (radial orientation) or perpendicular to the line between the reference and downhole probes (transverse orientation). These data acquisition procedures were applied in three separate nearby boreholes to permit downward-push measurements for the three vibrator source orientations.

### **Soil Seismic Properties Data Analysis and Results from Houston Testing Site**

Seismic field data collected at the three regional locations was of mixed quality, resulting in usable data from potentially only five of the 11 total number of test boreholes. The quality

of the field data acquired in all of the test boreholes was relatively low because of apparent spurious response effects in the measurement apparatus, variations in coupling of the seismic vibrator source and sensor probes at the ground surface and downhole, and possible anomalous propagation effects and seismic reflection interference from subsurface soil layering. These factors produced amplitude and phase variations in the recorded seismic waveforms, making both velocity and attenuation analyses difficult, or impossible. Additionally, several of the test boreholes were at locations where the Geoprobe push system was unable to drive the downhole sensor probe below depths of about 9–10 ft and/or were in close proximity to 60-Hz power lines that caused excessive inductive interference.

### **Velocity Analysis**

A velocity analysis was performed by reviewing time-series records of S-wave or P-wave toneburst sequences traveling along near-vertical slant paths from the surface vibrator source to the downhole triaxial accelerometer probe. With the vibrator oriented horizontally and transverse to the borehole axis, SH-waves were generated at the base plate point coupler and transmitted downward to be detected by the *y*-axis accelerometer sensor in the downhole probe. With the vibrator oriented vertically, P-waves were generated at the base plate and transmitted downward to be detected by the *z*-axis acceleration sensor in the downhole probe. Separate boreholes located near one another in essentially the same soil structure were used for the S-wave and P-wave measurements. At each borehole location, the vibrator source was placed at an offset distance, typically 24–36 in., away from the borehole. The propagation paths are slant distances from the center of the vibrator source at the ground surface to the sensor location in the downhole probe, as determined by the measured depth and the source offset distance. The seismic wave velocity in near-surface soils increases significantly with depth, causing diverging refraction effects and curved-ray paths in the down-going wavefront. However, since the propagation paths were relatively short and nearly vertical, the curved-ray paths could be accurately approximated by the geometrical slant-path distance associated with each measurement.

The field procedures used to record the slant-path signals included the use of a second triaxial accelerometer probe placed at a fixed depth of 18 in. at a measured location between the source contact point and the borehole. The purpose of this second probe is to provide a reference seismic signal representing the radiated source wave. Detailed analysis techniques were developed to use this reference signal in the velocity analysis. Unfortunately, the spurious responses and interference effects in the recorded downhole

and reference probes caused significant errors in the derived slant-path velocities. To avoid these errors, the excitation current waveform applied to the vibrator source was used in place of the reference probe signal to determine the S-wave and P-wave travel times.

### **Mean Slant-Path Velocity**

Preliminary analyses showed that phase distortions caused by anomalous interference effects yielded different travel times for each of the toneburst signals traveling along a given slant-path distance. This distortion precluded using the toneburst signals to measure the frequency-dependent velocity effects as planned as part of the soil attenuation analysis and made the velocity analysis ambiguous. As an alternative, the single toneburst signal at 200 Hz was selected for use in the velocity analysis. By using this relatively low-frequency waveform, the likelihood of encountering phase errors large enough to cause cycle skipping in the travel time analysis was avoided.

### **Interval Velocity**

The velocity in each soil depth interval between successive downhole probe measurement positions was derived from the experimentally determined mean slant-path velocities. This was based on the assumptions that the downhole depth stations were uniformly spaced at 1-ft intervals and the propagation paths were accurately approximated as straight lines from the surface source to the downhole probe. The uniformly spaced measurement depths allowed the slant-path distances to be divided into an equal number of uniform interval slant-length segments in which the interval velocity was assumed to be constant.

### **Attenuation Analysis**

Seismic wave attenuation is caused by a combination of imperfect elastic properties and scattering by inhomogeneities in the propagation medium. The predominant attenuation factor is viscous friction, which leads to a frequency-dependent exponential decay in amplitude, a factor that surpasses attenuation caused by geometric spreading (as when waves propagate through the distance of a particular medium). A practical method of determining the excess attenuation is to measure the amplitude at one position along a known propagation path and to compare it with the amplitude measured at a second position, usually closer to the source, along the same propagation path. By first compensating the measured amplitudes for the distance-dependent geometric spreading loss, the ratio of the amplitudes can be used to derive the exponential parameters of the attenuation factor. For this method to be effective, the

amplitudes must be free of any differing anomalous variations at the two measurement locations, and the measurements must be made at several frequencies to provide sufficient data for evaluating the frequency-dependent attenuation coefficient.

The vibrator excitation signal used in these measurements was designed to generate toneburst signals having equal amplitudes and bandwidths to facilitate the measurements. However, in practice, the signals transmitted to the downhole and reference probes were found to be distorted by spurious frequency response and interference effects that caused amplitude variations in the signals detected at the two sensor probes. In many cases, the detected signals were sufficiently different to cause large errors when comparing the amplitudes of the separate toneburst signals. As a result, only certain toneburst signals were of suitable quality for attenuation analysis, but these could not be selected in advance. Instead, all of the toneburst signals were processed under the assumption that they could be of use and any extreme outlier values would be identified and removed later. This turned out to be an extensive and time-consuming process.

### **Effective Slant-Path $Q$**

The analysis objective was to determine the effective attenuation at as many toneburst frequencies as practical along the slant path between the surface source and the downhole probe. For this purpose, all of the toneburst signals (100–1,600 Hz) were processed in the frequency domain using spectral magnitudes only to obtain the effective  $Q$  of the medium along the same slant paths used in the mean slant-path velocity analysis. The effective  $Q$  is inversely proportional to attenuation per wavelength in the medium. To minimize the variations in signal amplitude, the downhole and reference signal frequency spectra were reduced to their mean values over the toneburst bandwidth before being normalized for further analysis.

### **Interval $Q$**

Interval  $Q$  values were derived from the derived effective slant-path  $Q$  values. The assumptions and methodology used to determine the interval  $Q$  values were similar to those applied in deriving the interval velocities, with the exception that the cumulative attenuation along the slant path was the product of partial attenuation factors in each interval. The partial attenuation factors in each interval involve both the effective slant-path  $Q$  and the mean slant-path velocity and, thus, were subject to combined error effects. In general, the  $Q$  of the soil medium tends to increase with depth, as with interval velocities. The increasing compaction and shear rigidity of the soil column tends to reduce the anelastic losses and, thus, increase the  $Q$  of the soil with depth.

## **Analysis Results**

The data acquired at the three regional field locations were of mixed quality, requiring special attention to data processing methodology and procedures. The following illustrations are selected examples that show the typical nature of the recorded signals, the irregular responses, and the noise interference affecting the data quality.

The vibrator excitation current waveform was described and illustrated earlier in Figure 3.12. Figure 3.16 shows the detailed SH-wave signals at depths of 1–8 ft at a Houston borehole location. Each trace contains toneburst pulses 100, 200, . . . , 1,600 Hz at 120-ms time intervals. These traces show the combined anomalous effects of vibrator response, ground coupling at the source and at the downhole probe, possible reflections from deeper soil layers, possible guided waves along the borehole, 60-Hz power generator interference, and noise.

Figure 3.17 shows the amplitude frequency spectrum of the toneburst trace detected at 4-ft depth at the Houston borehole. The detected toneburst spectrum is scaled by a factor of 2,000 for convenient comparison. The 60-Hz power generator interference and its harmonics and fractional harmonics are evident. The relatively strong toneburst at 100 Hz followed by the weak toneburst at 200 Hz is a counterintuitive effect since the wavelengths are large compared with the borehole and downhole probe dimensions. Other higher-frequency toneburst spectra also showed strong or weak amplitudes and their spectral content was broadened or reduced in comparison with that of the source excitation current toneburst spectra. Insufficient experimental data are available to identify the reasons for these differences.

Each downhole-detected toneburst could be filtered and analyzed in comparison with the vibrator excitation current and/or reference probe signals. By comparing the quality of the filtered tonebursts at the three regional field sites, the 200-Hz toneburst was selected for use as the reference signal for analyzing the travel time delays and propagation velocities along the near-vertical depth paths. Figure 3.18 shows the 200-Hz time-domain tonebursts overlaid for propagation time-delay analysis at the Houston borehole. The clarity of the overlay match is evident in this 4-ft depth case. The time-lag shift required for this alignment was 7.92 ms, corresponding to a mean slant-path velocity of 543 ft/s.

Although the amplitude envelope of the downhole-detected signal was idealized to overcome much of the distortion in the detected waveform, the phase of the downhole signal was not changed. This phase function contains both the propagation time-lag phase shift and any other phase distortions caused, for example, by variations in ground coupling. As shown in Figure 3.18, the envelope stretching caused by phase distortion of the 200-Hz time-domain toneburst signal is significant, making time-lag matching adjustments imperfect and/or ambiguous as to which cycle in the overlay is correct

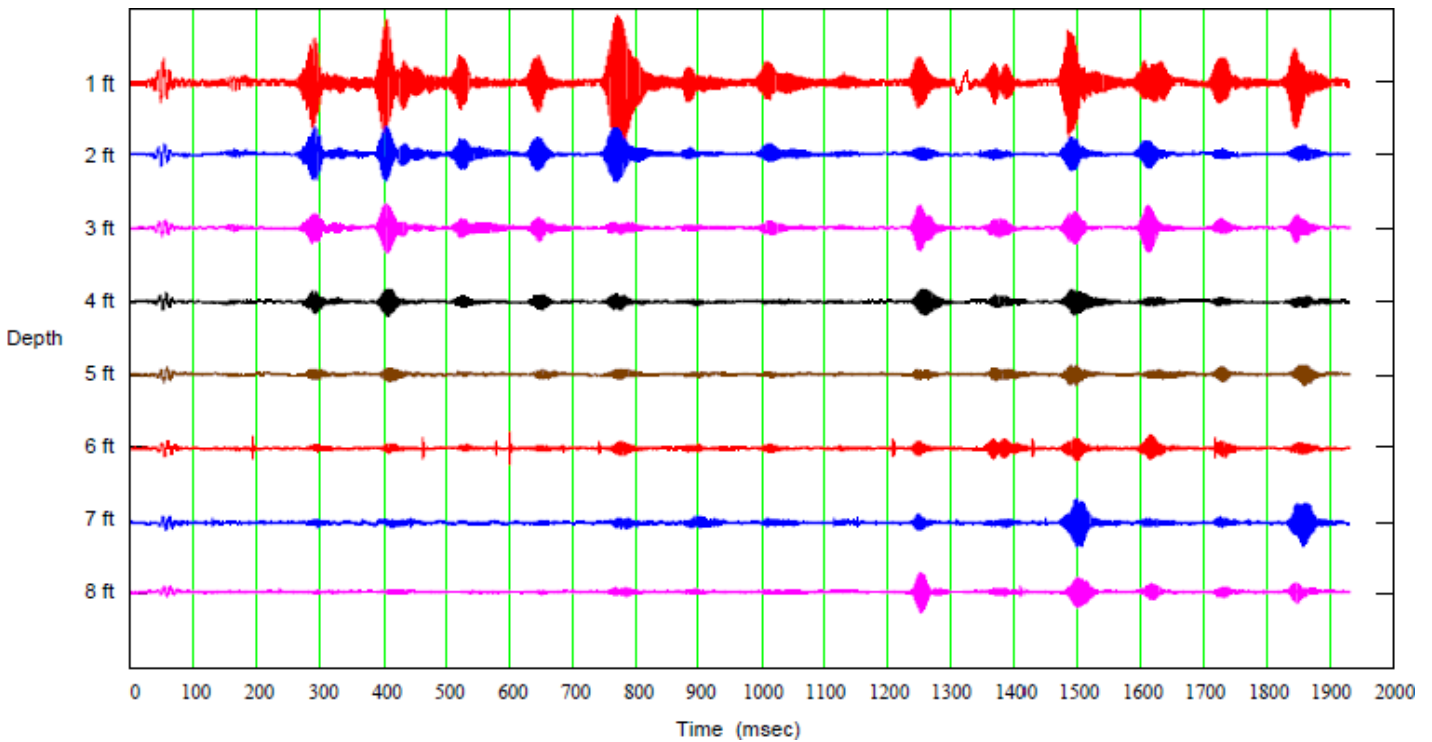


Figure 3.16. Downhole-detected signals at Houston borehole.

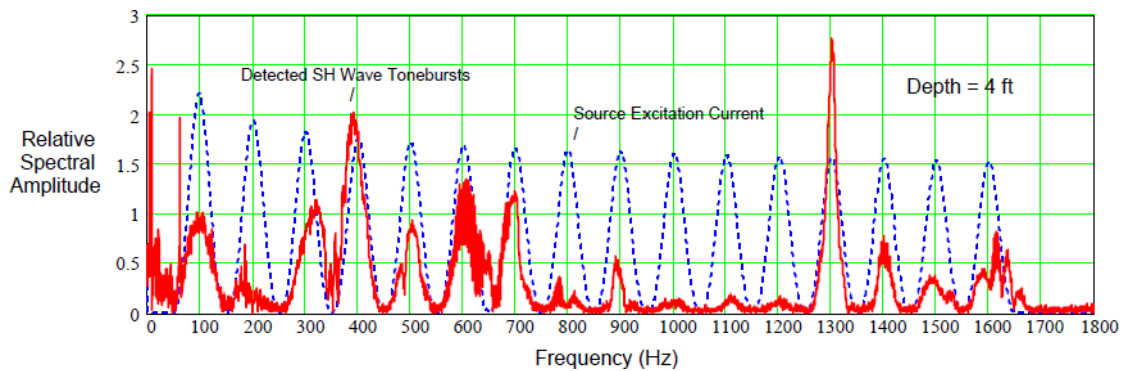


Figure 3.17. Frequency spectrum of the toneburst trace at Houston borehole.

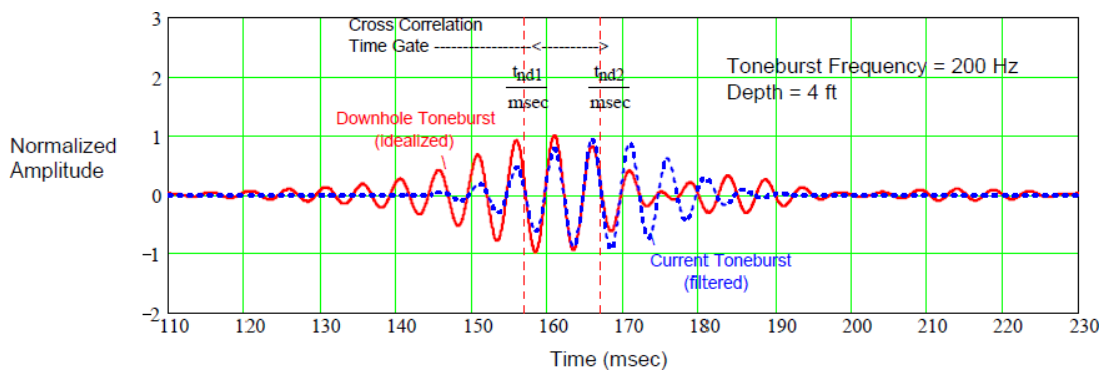


Figure 3.18. Overlay of the idealized 200-Hz downhole toneburst and the 200-Hz current excitation toneburst for Houston borehole.

(introducing a possible cycle-skip error). In several cases, the interference and noise in the weaker signals detected at the greater depths could not be reliably analyzed in this manner to obtain accurate overlay time lag. In other cases, overlay cycle skipping was tested to determine the reasonable bounds for the derived velocity.

Amplitude comparisons of downhole and reference probe toneburst signals were necessary to determine the excess attenuation caused by anelastic absorption and scattering in the soil medium. These comparisons were not productive when using the extracted time-domain toneburst waveforms, but they were improved when their spectral amplitudes were compared in the frequency domain. The spectral envelope displayed a common form of asymmetrical and bimodal distortion caused by interference effects and resulting in inaccurate amplitude ratios. These variations were further suppressed by using only the ratio of the mean spectral amplitudes averaged over the toneburst filter bandwidth. Using this formulation, a useful number of toneburst signals could be compared to yield approximate exponential decay parameters defining the effective  $Q$  of the soil medium.

### Soil Seismic Properties at Regional Testing Sites

The in situ experimental measurements of propagation velocity and attenuation are the descriptive soil seismic parameters of interest in estimating the detectability of underground utility pipes. The analysis methods were determined adequate

to yield useful approximate values of velocity and effective  $Q$  versus depth at the three regional sites. The soil seismic properties differed for the three regions and were also different for multiple test locations at each regional site. For the sake of brevity, the detailed results presented here are only from data acquired at the Houston, Texas, test site location.

Because of data quality limitations, the results show only approximate values of velocities and  $Q$ s but, more clearly, show their trends versus depth. The depth limits were caused either by probe-push penetration refusal or by excessive data analysis errors. Accuracy estimates of all the results are approximately 10% to 15%. Approximate values of velocity and effective  $Q$  versus depth at the Houston testing site are offered below.

### Mean Slant-Path S-Wave Velocity Versus Depth (Houston, Texas)

Figure 3.19 shows the mean slant-path S-wave velocities obtained from measurements in natural soils at three borehole locations (D2, E1, and F2) in the Houston area. The measurements at Borehole D2 were physically limited in depth by the inability of the Geoprobe system to push the downhole accelerometer probe deeper than 9 ft. Similar limitations were encountered in Borehole E1 but with a maximum push depth of 14 ft. In all cases, unlike at Manteno, the quality of the recorded signals was sufficient to allow the mean slant-path S-wave velocity analysis to be productive at all depth positions down to maximum push penetration.

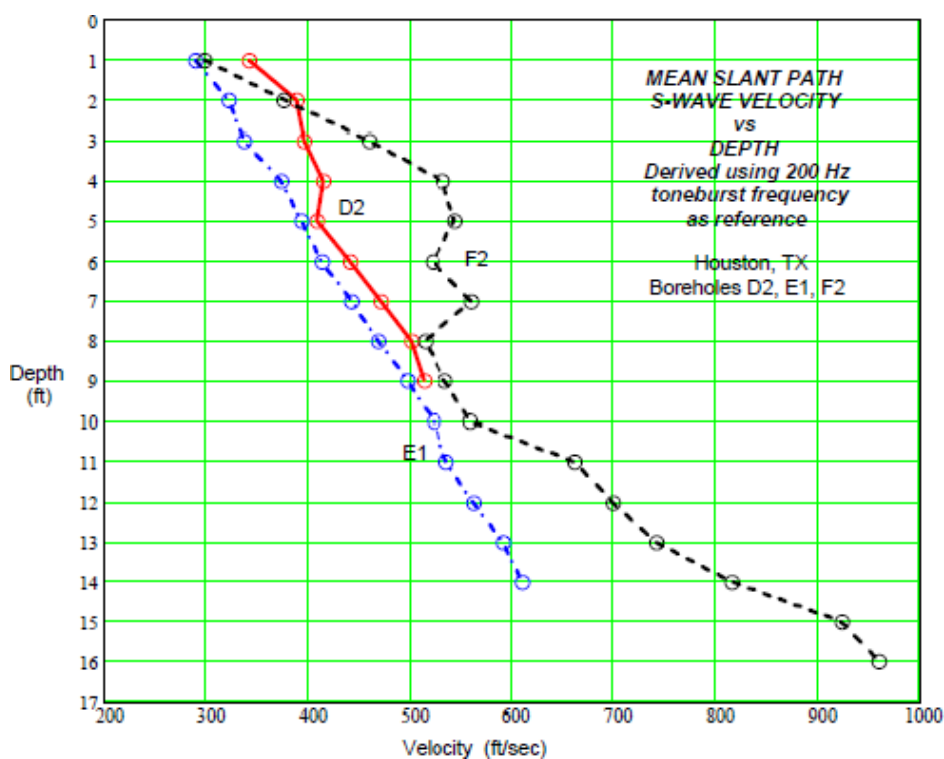


**Figure 3.19. Mean slant-path S-wave velocity, Houston Boreholes D2, E1, and F2.**

The higher velocities in Borehole F2 indicate a change in the soil seismic properties, characterized by an increase in shear modulus, at depths below about 10 ft. The uniform increase in slant-path S-wave velocity below 9 ft in Borehole E1 is indicative of a uniform soil exhibiting only the effects of soil column compaction.

### *Interval S-Wave Velocity Profile (Houston, Texas)*

Figure 3.20a–c shows the derived interval S-wave velocity profiles in natural soil at Houston Boreholes D2, E1, and F2.

The power-law regression curves fitted to these interval velocity profiles tend to smooth the numerical scatter in the derived values. Since interval velocity calculations were not productive at depths deeper than 10 ft in Borehole F2, the regression curve for that borehole does not show a higher velocity gradient at the deeper depths.

### *Mean Slant-Path P-Wave Velocity Versus Depth (Houston, Texas)*

Figure 3.21 shows the mean slant-path P-wave velocities obtained from measurements in natural soil at three test boreholes (D2, E1, and F2) very near the boreholes used for S-wave measurements in the Houston area. The maximum Geoprobe system push depths in these boreholes were 8 ft, 13 ft, and 16 ft, respectively.

The slant-path P-wave velocities in Borehole D2, although limited to a depth of 8 ft, are uniform and consistent with the S-wave velocities in the same soil column. The slant-path P-wave velocities in Boreholes E1 and F2 show wide variations at several depth points below about 4 ft that are inconsistent with the S-wave velocities. These variations are attributed to possible differences in the separate borehole measuring conditions (ground coupling, etc.) or artifacts in the data analysis.

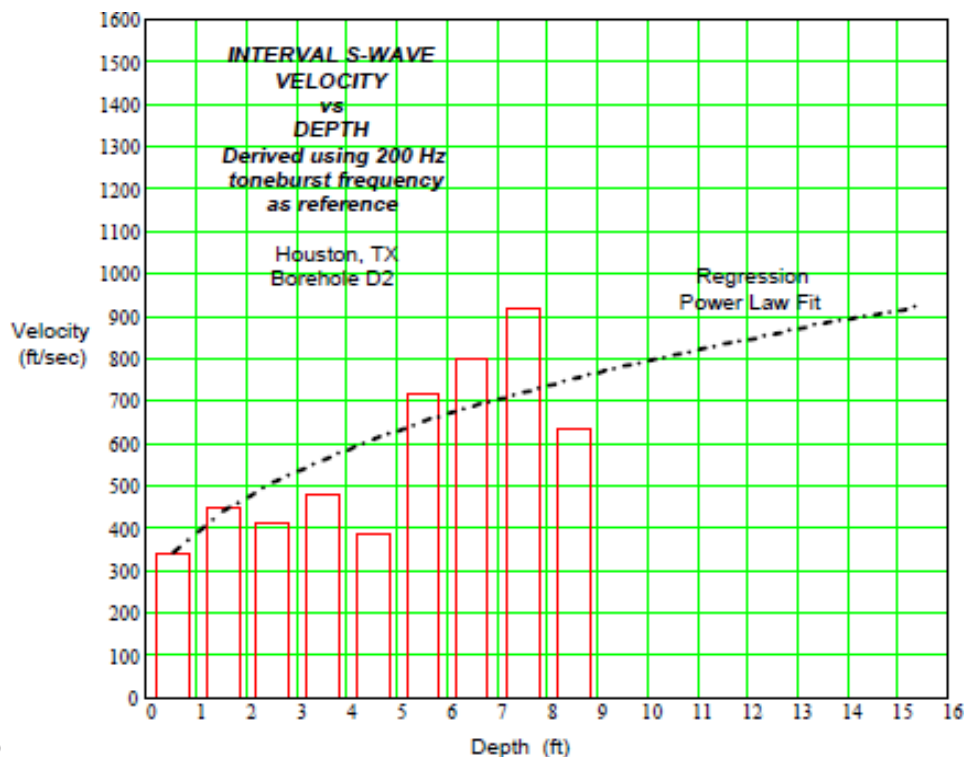
### *Interval P-Wave Velocity Profile (Houston, Texas)*

Figure 3.22a–c shows the derived interval P-wave velocity profiles in natural soils at the three Houston Boreholes D2, E1, and F2.

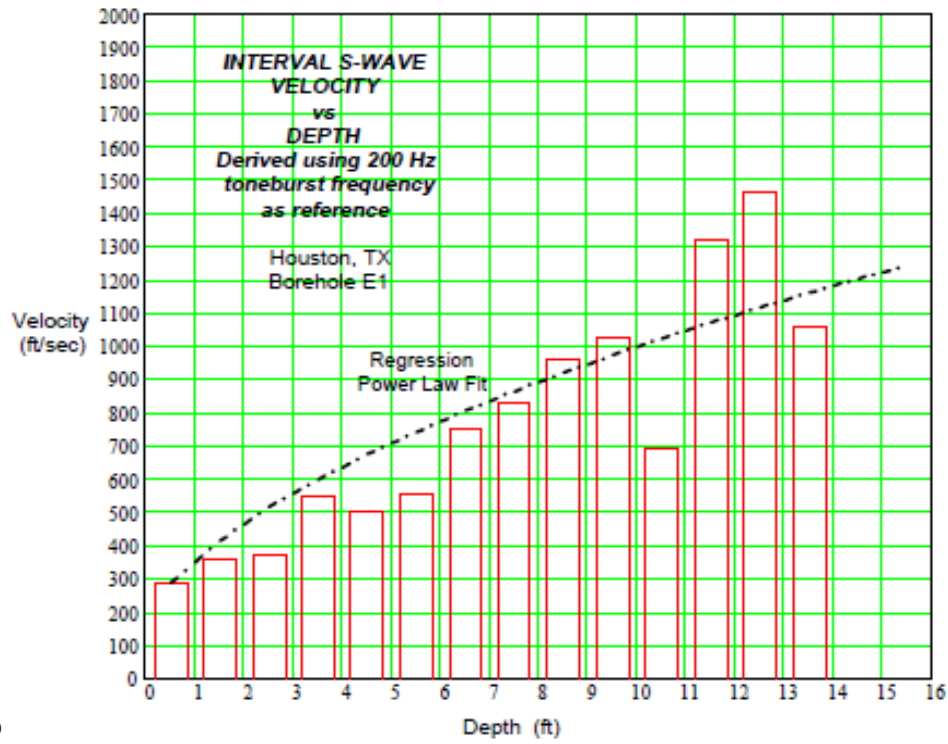
The power-law regression curves fitted to the derived interval velocities bring the scattered values into better agreement with the S-wave velocities and, lacking better information, at these P-wave test boreholes, provide reasonable characterizations of P-wave velocity profiles at these sites.

### *Effective Slant-Path S-Wave Q Versus Depth (Houston, Texas)*

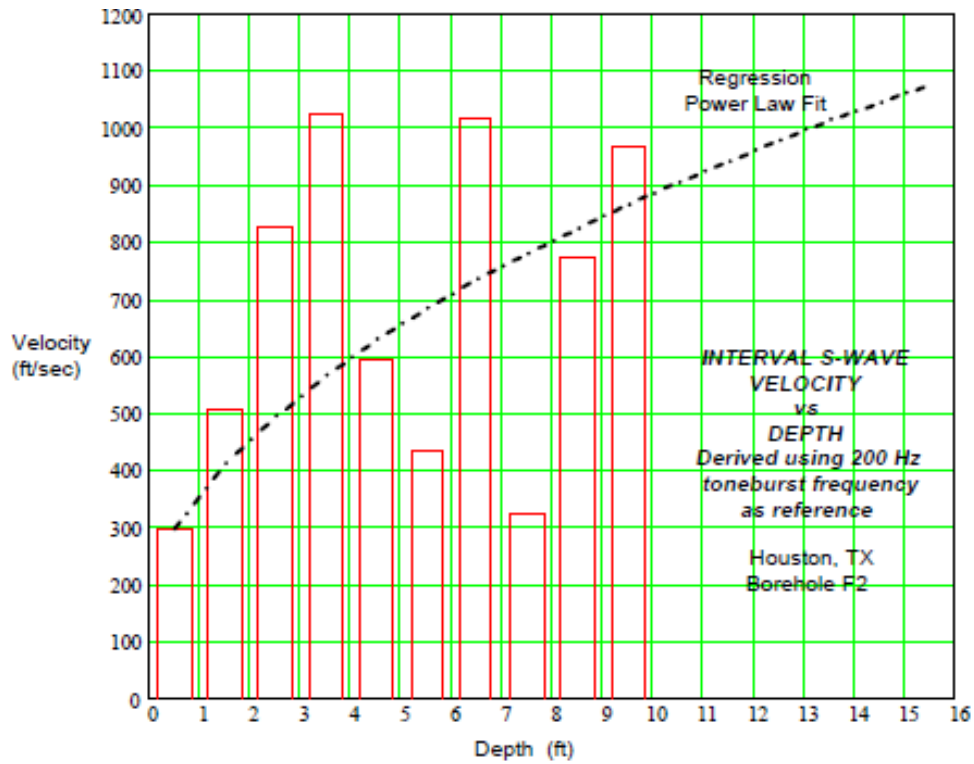
Figure 3.23a–c shows the effective slant-path S-wave Q and related attenuation rate in natural soils at three boreholes (D2, E1, and F2) in the Houston area.



**Figure 3.20. Interval S-wave velocity, Houston boreholes: (a) D2, (b) E1, and (c) F2. (Continued on next page.)**



b.)



c.)

**Figure 3.20. Interval S-wave velocity, Houston boreholes: (a) D2, (b) E1, and (c) F2. (Continued from previous page.)**

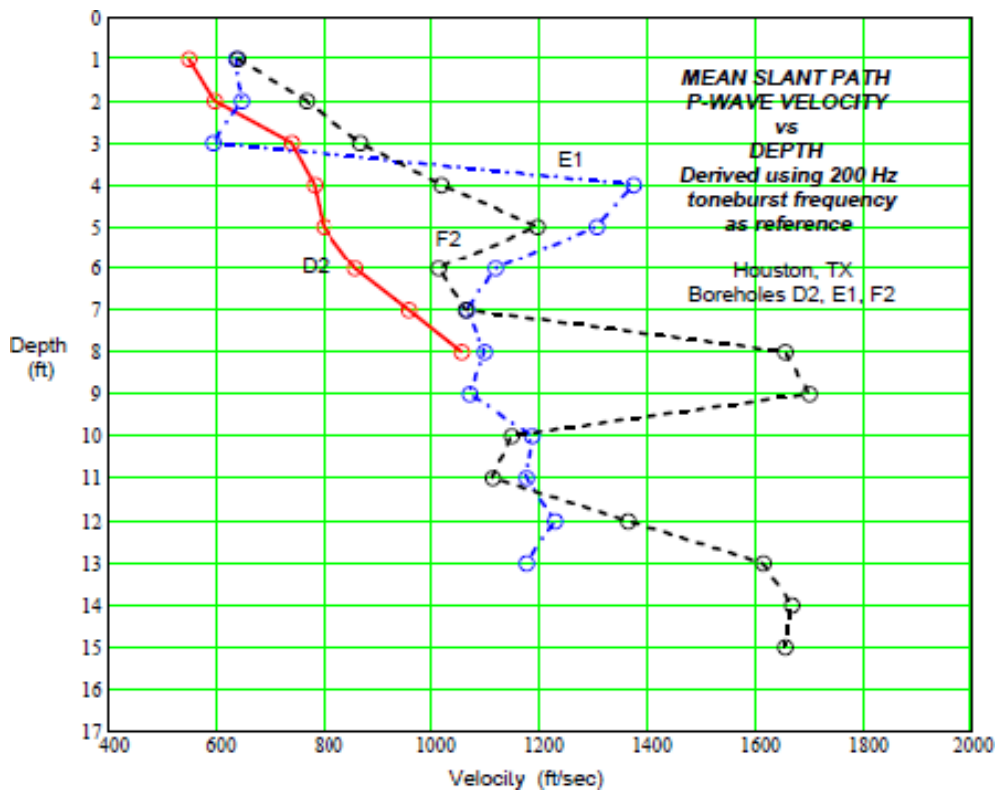
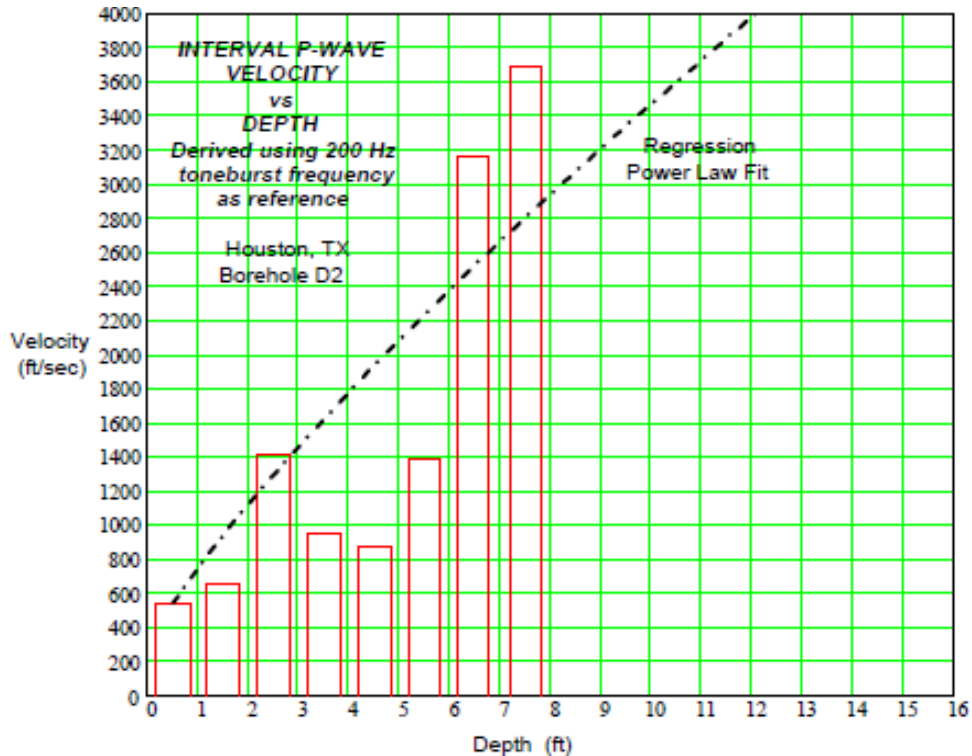


Figure 3.21. Mean slant-path P-wave velocity, Houston Boreholes D2, E1, and F2.



a.)

Figure 3.22. Interval P-wave velocity, Houston boreholes: (a) D2, (b) E1, and (c) F2. (Continued on next page.)

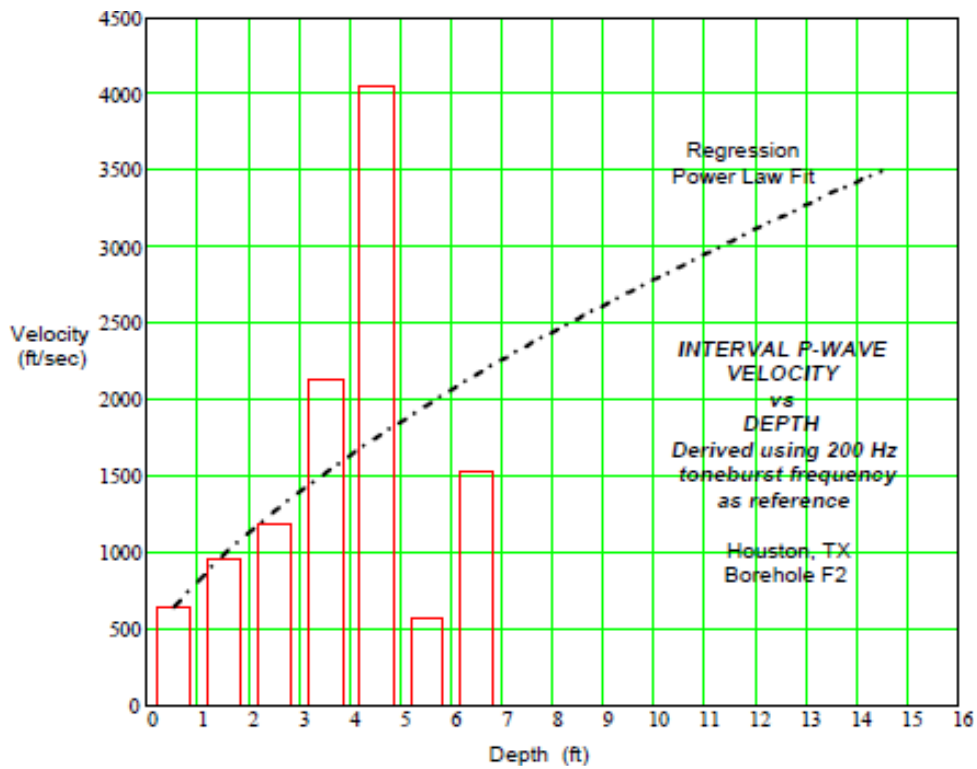
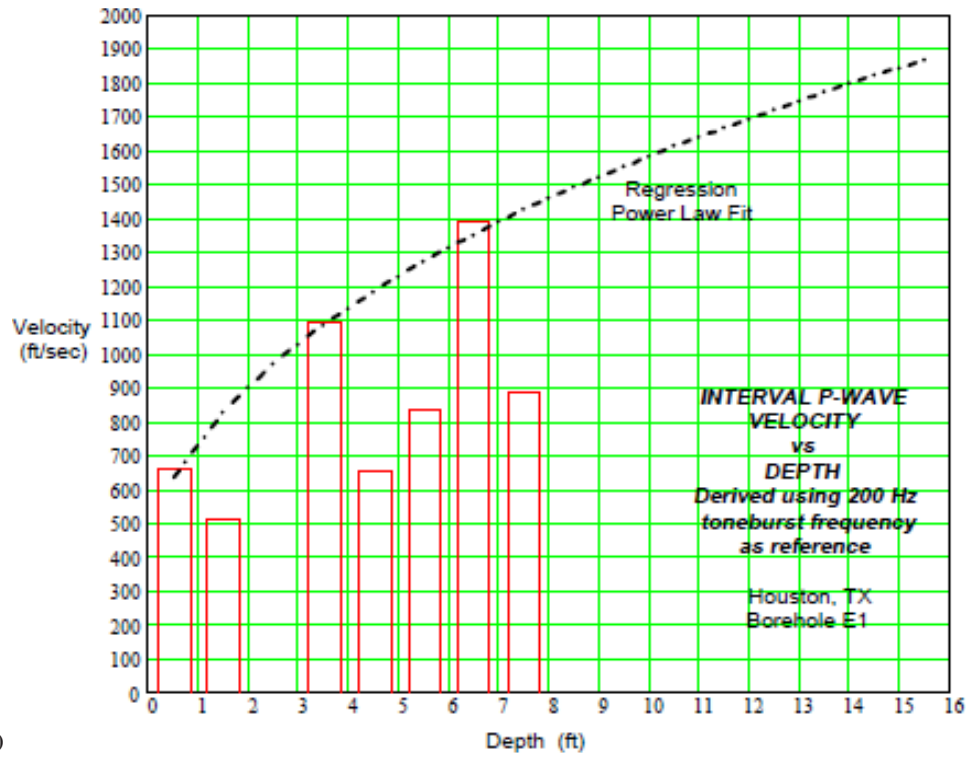
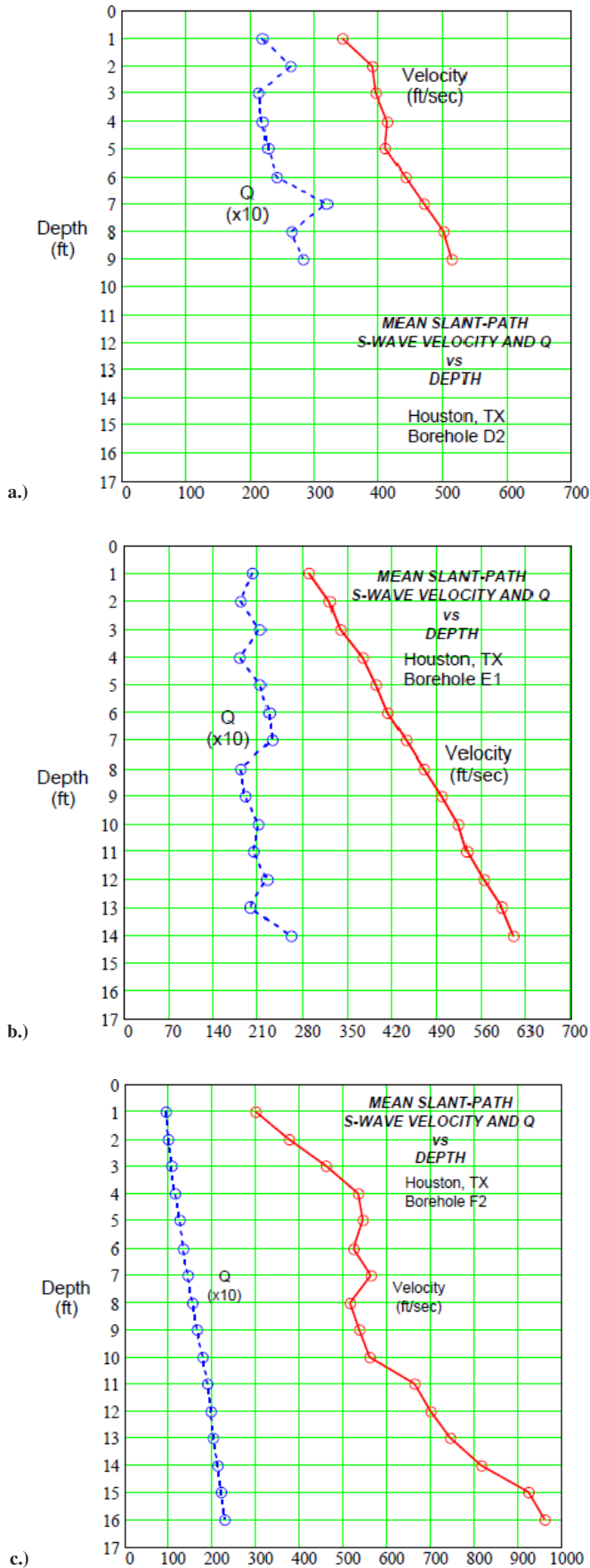


Figure 3.22. Interval P-wave velocity, Houston boreholes: (a) D2, (b) E1, and (c) F2. (Continued from previous page.)



**Figure 3.23. Effective slant-path S-wave Q, Houston boreholes: (a) D2, (b) E1, and (c) F2.**

Sufficient data obtained at depths to 9 ft in Borehole D2 and deeper in Boreholes E1 and F2 allowed reasonable determination of the effective Q values of soils at the three locations. The calculated values for Boreholes D2 and E1 are shown to illustrate the variations in the data. However, the data in Borehole F2 were widely scattered and the effective slant-path S-wave Q values are shown represented by a smoothed curve. The resulting Q values are in the ranges 22–32 for Borehole D2, 20–26 for Borehole E1, and 9–22 for Borehole F2.

### Interval S-Wave Q Profile (Houston, TX)

Figure 3.24a–c shows the derived interval S-wave Q and related attenuation rate profiles in natural soils at the three boreholes (D2, E1, and F2) in the Houston area.

Variations in the interval S-wave Q values at Boreholes E1 and F2 were widely scattered and are shown only by their smoothed values. The interval Q values in Borehole D2 are acceptable within the top 5 ft of the ground and are represented at deeper depths by the mean value of 28.6 in the top 5 ft. The interval Q values in Boreholes D2 and E1 are consistent with the effective slant-path S-wave Q values. However, the interval Q values in Borehole F2 exhibit a much wider range with increasing depth, largely because of the apparently higher S-wave velocity at depths below 10 ft and the data smoothing process.

### Effective Slant-Path P-Wave Q Versus Depth (Houston, Texas)

Figure 3.25a–c shows the effective slant-path P-wave Q and related attenuation rate derived in natural soils at the three boreholes (D2, E1, and F2) in the Houston area.

The effective slant-path P-wave Q values showed more scatter than the corresponding S-wave Q values. These variations were smoothed to avoid extreme values, resulting in slightly increasing Q values versus depth. The calculated P-wave Q values are in the range 13–21 in Borehole D2, 15–27 in Borehole E1, and 31–47 in Borehole F2.

### Interval P-Wave Q Profile (Houston, Texas)

Figure 3.26a–c shows the derived interval P-wave Q and related attenuation rate profiles in natural soils at the three boreholes (D2, E1, and F2) in the Houston area.

The derived interval Q values are widely variable in the three boreholes. The interval P-wave Q values in Boreholes D2 and E1 are represented by their mean values of 13 and 18, respectively. The values in Borehole F2 increase with depth, represented by a fractional power-law curve over the range 31–85.

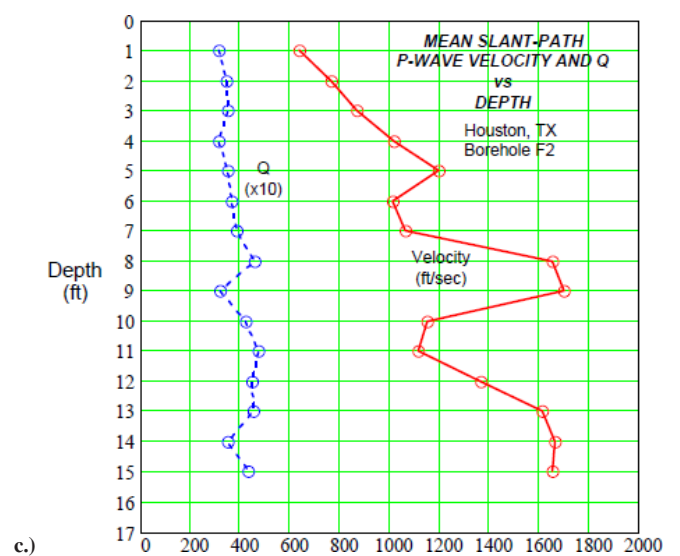
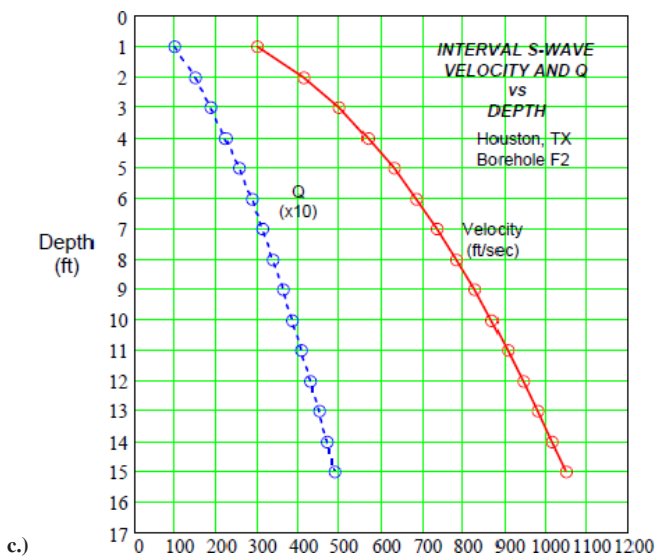
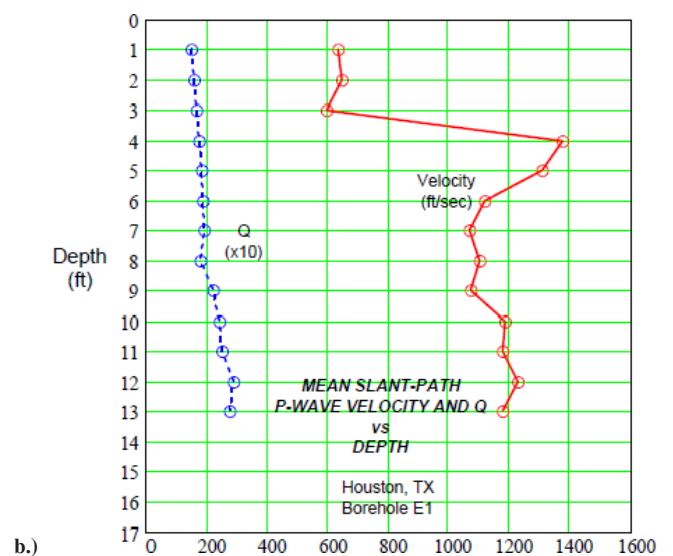
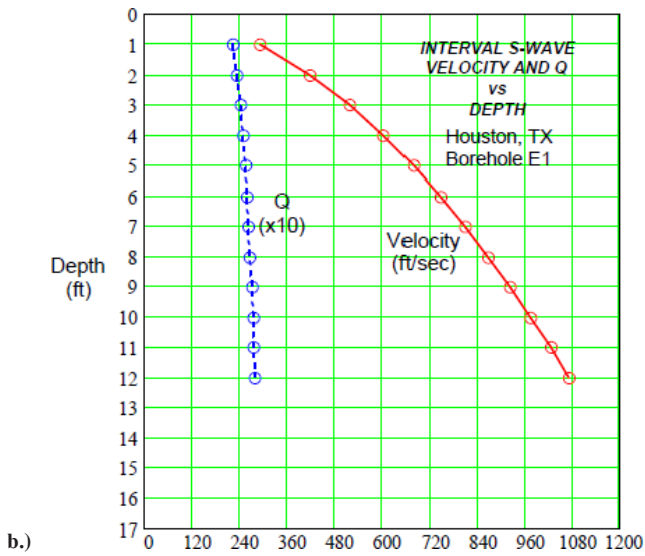
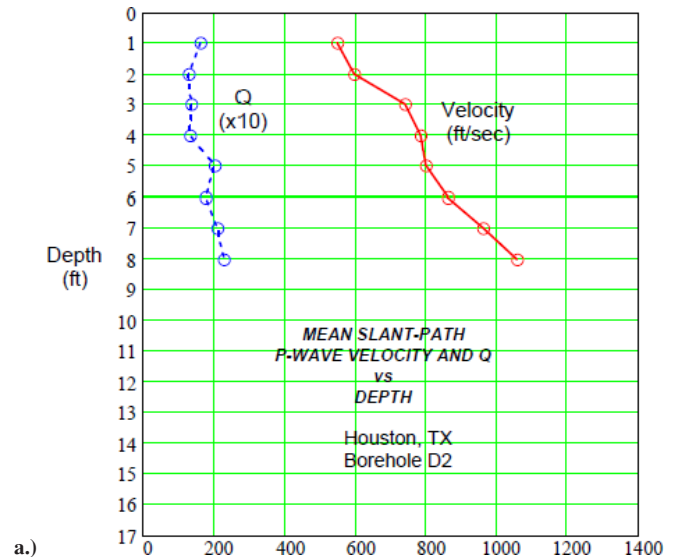
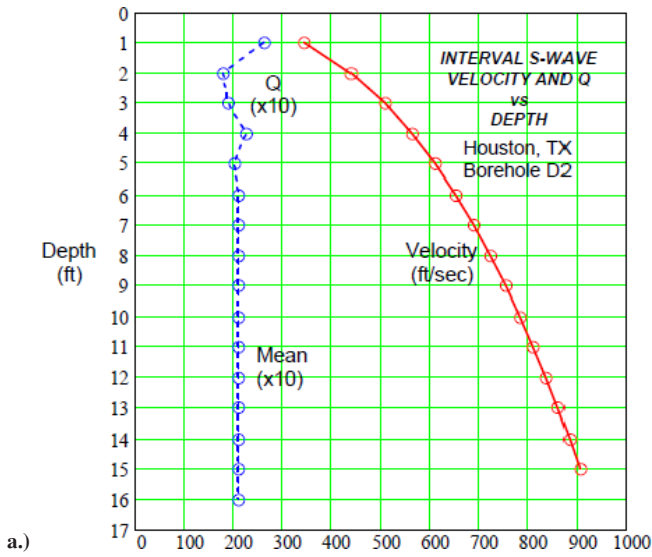
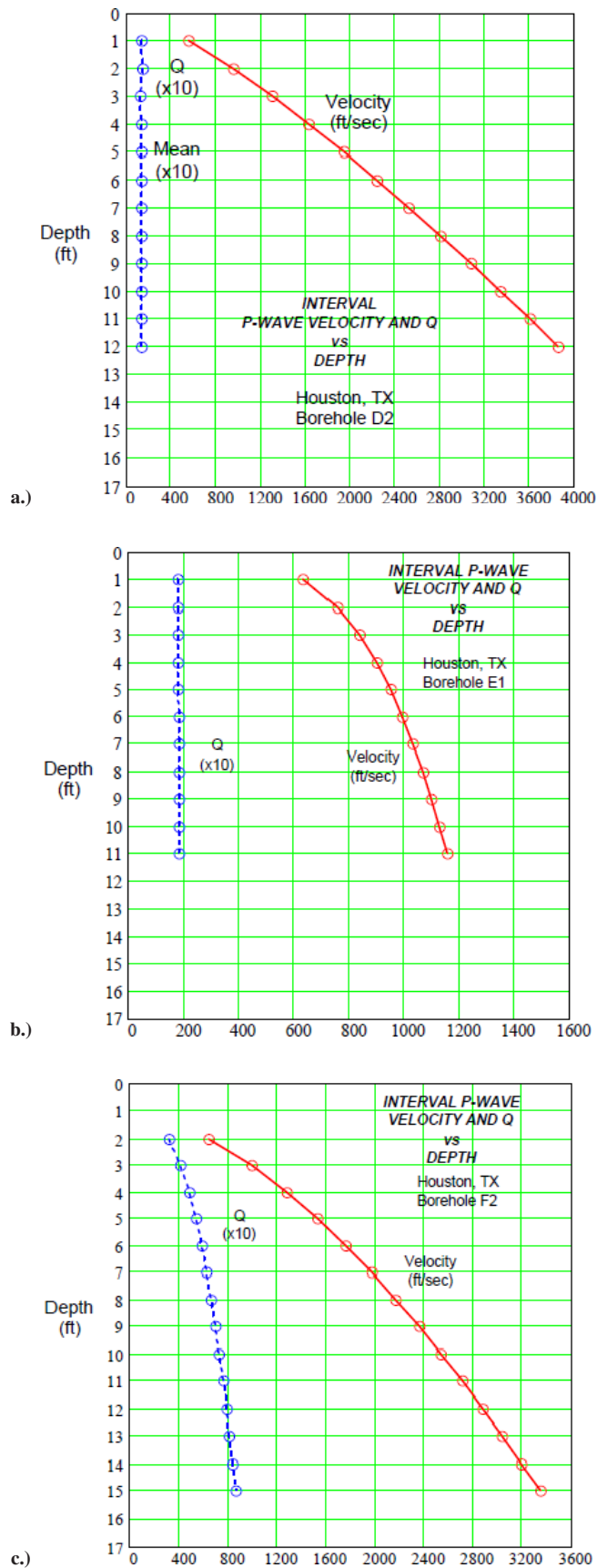


Figure 3.24. Interval S-wave Q profile, Houston boreholes: (a) D2, (b) E1, and (c) F2.

Figure 3.25. Effective slant-path P-wave Q, Houston boreholes: (a) D2, (b) E1, and (c) F2.



**Figure 3.26. Interval P-wave Q profile, Houston boreholes: (a) D2, (b) E1, and (c) F2.**

## Soil Seismic Properties Collective Results

The soil seismic properties measurements were a qualified success in determining S-wave and P-wave velocities and attenuation rates at the three regional field sites. These results are considered to be representative of the seismic parameters of interest and are empirically estimated to have an accuracy tolerance of approximately 10% to 15%.

The measurement objectives were demanding in that new custom-designed downhole instrumentation was required for depth-profile S-wave and P-wave measurements at seismic frequencies up to 1,600 Hz in soils typical of locations where underground utilities are installed. Programming, assembly, and checkout of the Dewetron digital data acquisition system required several revisions and adjustments in both software and hardware to implement the required toneburst excitation and data recording process. The surface seismic vibrator (OES MicroVib) was equipped with a custom-designed ground-coupling device for the purpose of achieving point-source S-wave and P-wave radiation. This small-contact-area ground-coupling technique was successful for S-wave operation but ineffectual for P-wave operation, resulting in a larger ground-coupling base plate being used for the P-wave measurements.

Soil conditions at the Traverse City, Michigan, trial testing location selected for system assembly and checkout were unsuitable (because of their loose and unconsolidated granular nature) for use in quantitative tests at downhole depths greater than just a few feet below surface. This condition limited the full-scale testing and perfection of the planned Geoprobe system push-probe method and, therefore, limited the seismic measurement checkout tests to basic equipment operability. As a result, only minimal seismic measurements were possible, and they were not sufficient to provide preliminary downhole response measurements and sample data for evaluating the complete system performance.

At the first regional field test site at Manteno, Illinois, the combination of vibrator source frequency response, ground-coupling effects related to field conditions, and possible anomalous propagation responses associated with the intended high-frequency downhole sensor measurements was observed to cause significant interference effects in the recorded data. In particular, the borehole diameter and downhole probe dimensions are comparable with the seismic wavelengths at frequencies of about 1,200 Hz and higher. Therefore, operating the system at these higher frequencies may potentially excite guided waves along the borehole and spurious responses in the downhole sensor, resulting in accelerometer interference effects. These effects were noticeable in the recorded data, although not separable into their individual causes as related to the surface and downhole conditions. In general, the interference effects limited the data analysis to toneburst frequencies in the range of 100–1,100 Hz.

Irregular system responses at 1,100 Hz and lower caused amplitude and phase variations that introduced errors in the derived propagation velocity and attenuation. Unconventional analysis methods were devised and adapted to minimize these errors, with trade-offs between obtaining approximate values of S-wave and P-wave velocity and Q and their depth trends in the tested soils and not obtaining any useful information from the data.

The measured S-wave and P-wave velocities and Qs for the three regional field sites are plotted in Figure 3.27, Figure 3.28, Figure 3.29, and Figure 3.30 for comparison. These comparisons show that the S-waves and P-waves at the three regional field sites have the same general trends in soil seismic properties versus depth. The mean combined velocity and Q profiles for S-waves and P-waves at the three Houston borehole sites are shown as bold dash-dot lines.

The respective velocity and Q magnitudes at the three sites are also relatively close in comparison, suggesting that the

seismic properties of near-surface natural soils are governed, in a first-order sense, by their shallow depth and natural compaction in combination with moisture content. Their similarities, as illustrated above, suggest that they may be merged to provide useful composite profiles relevant to these particular sites and perhaps other similar sites. These curves follow a fraction power-law depth dependence with exponents of 0.521 and 0.586 for S-waves and P-waves, respectively.

### Estimated Seismic Reflection System Performance

A cross section of near-surface seismic propagation and reflection applicable to subsurface pipe detection is shown in Figure 3.31. The seismic source and sensor units generate and receive horizontally polarized shear (SH) waves and are located relatively close together to provide near-vertical transmission and reflection paths in a soil medium having a

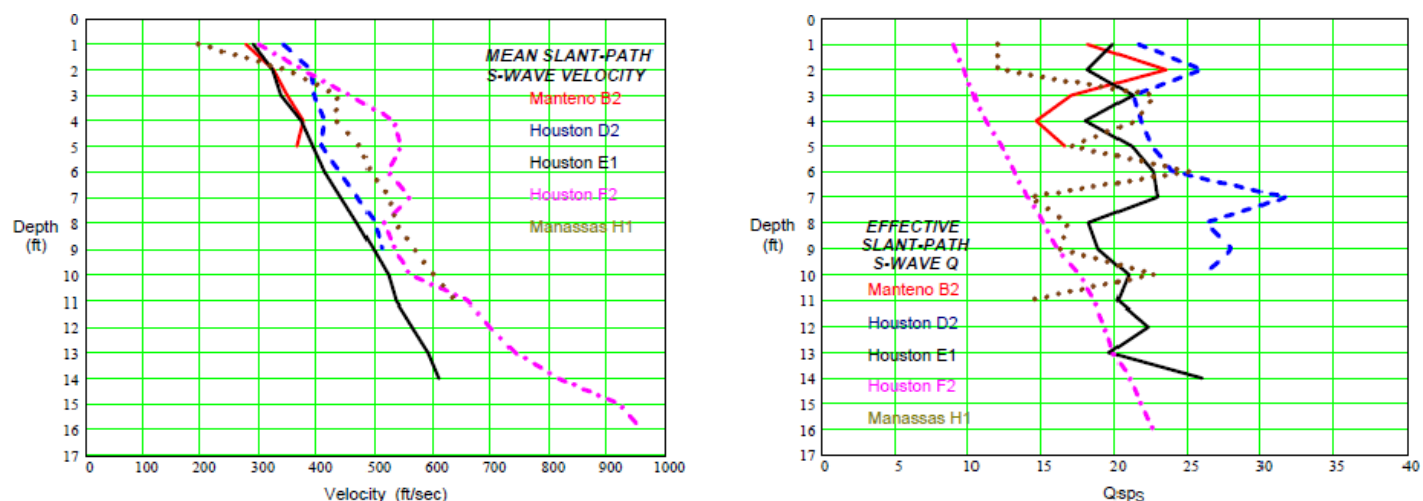


Figure 3.27. Mean slant-path velocity and Q profiles at three regional sites, S-waves.

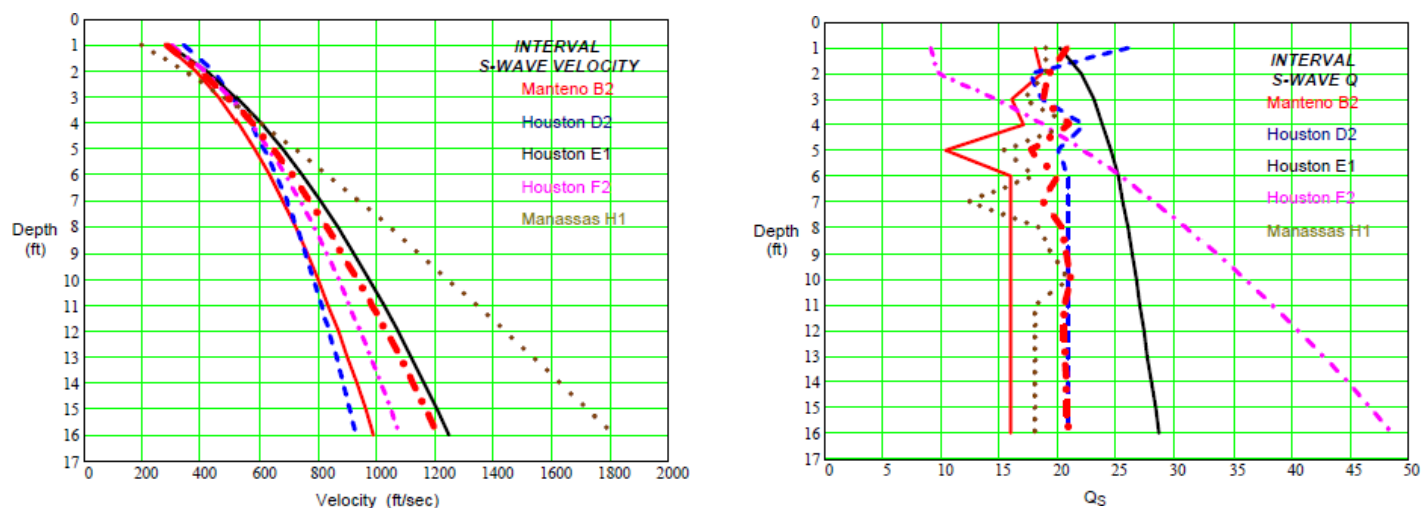


Figure 3.28. Interval velocity and Q profiles at three regional sites, S-waves.

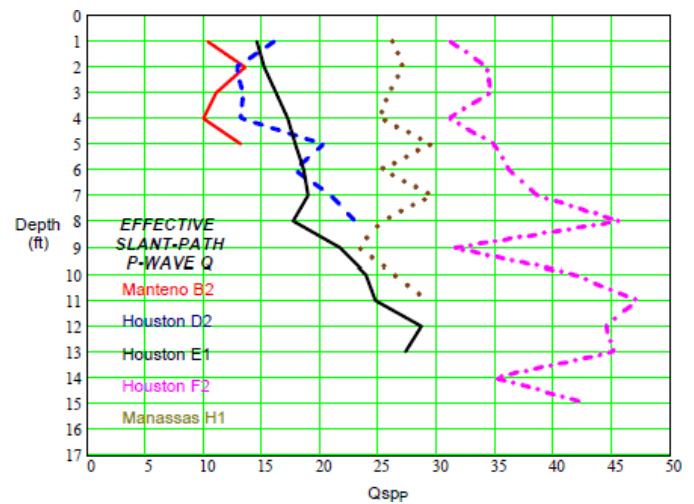
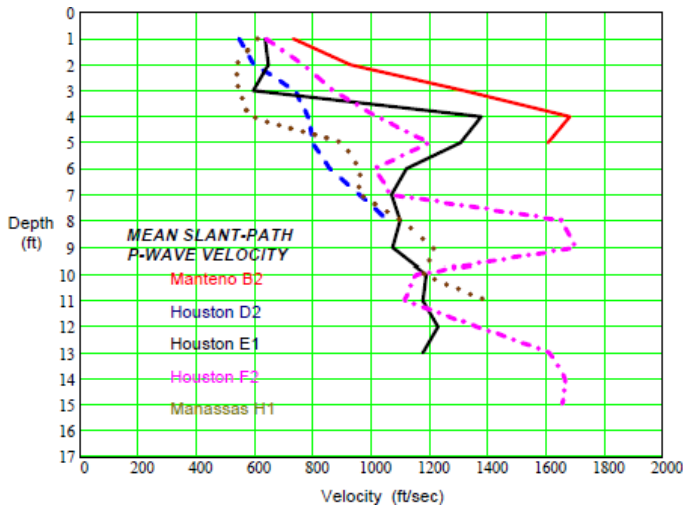


Figure 3.29. Mean slant-path velocity and  $Q$  at three regional sites,  $P$ -waves.

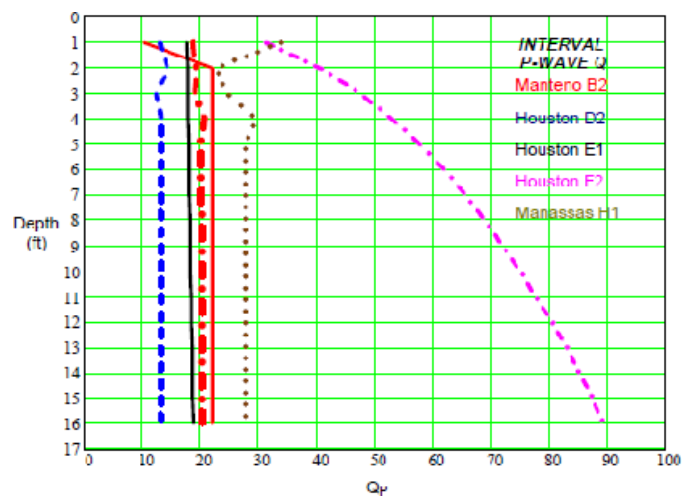
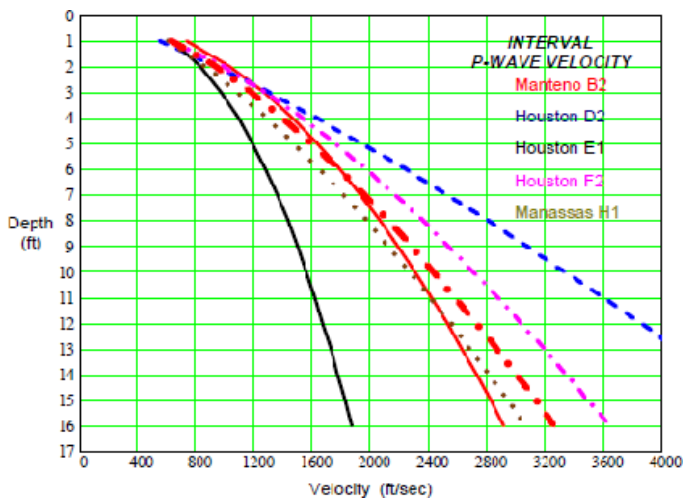


Figure 3.30. Interval velocity and  $Q$  profiles at three regional sites,  $P$ -waves.

positive velocity gradient versus depth. The features indicated in the cross section were divided into categories used to formulate the two-way transmission-reflection loss based on (1) the noise threshold established by the proposed seismic sensor array, and (2) the practical detection limit established by the dynamic range of the seismic data recording system. Those categories, which were characterized completely by the subcontractor Owen Engineering Services, include

- Seismic transmission and reflection paths dependent on the soil velocity and attenuation depth profiles;
- Pipe target reflection; and
- Seismic operating system, including ground coupling.

#### Pipe Detection Performance (Houston, Texas)

Figure 3.32 shows the detection depth of different size pipes using an SH-wave seismic reflection system at the Houston

Borehole D2 test site. SH-wave pipe detection versus depth studies were completed for all borehole locations of the seismic soils properties testing sites where data quality was sufficient to do so. Those results show trends similar to the Houston boreholes represented here. The graphs shown here represent three distinct locations within the Houston metro area separated by several miles. The practical detection threshold indicates the probable maximum detection depth for pipes with diameters in the range of 3–6 in. Larger-diameter pipes are detectable at deeper depths. The slopes of the curves for each pipe size are governed primarily by the shear wave attenuation in the Houston D2 soil column and the target pipe diameter.

The measurements at Borehole D2 were limited to the indicated depth of 9 ft by the Geoprobe system push refusal. The starting sweep frequency is high in this case because of the higher S-wave velocity; and the upper frequency limit is arbitrarily selected as being adequate for resolving the detection depth of the pipes. Conservative estimates of the pipe detection

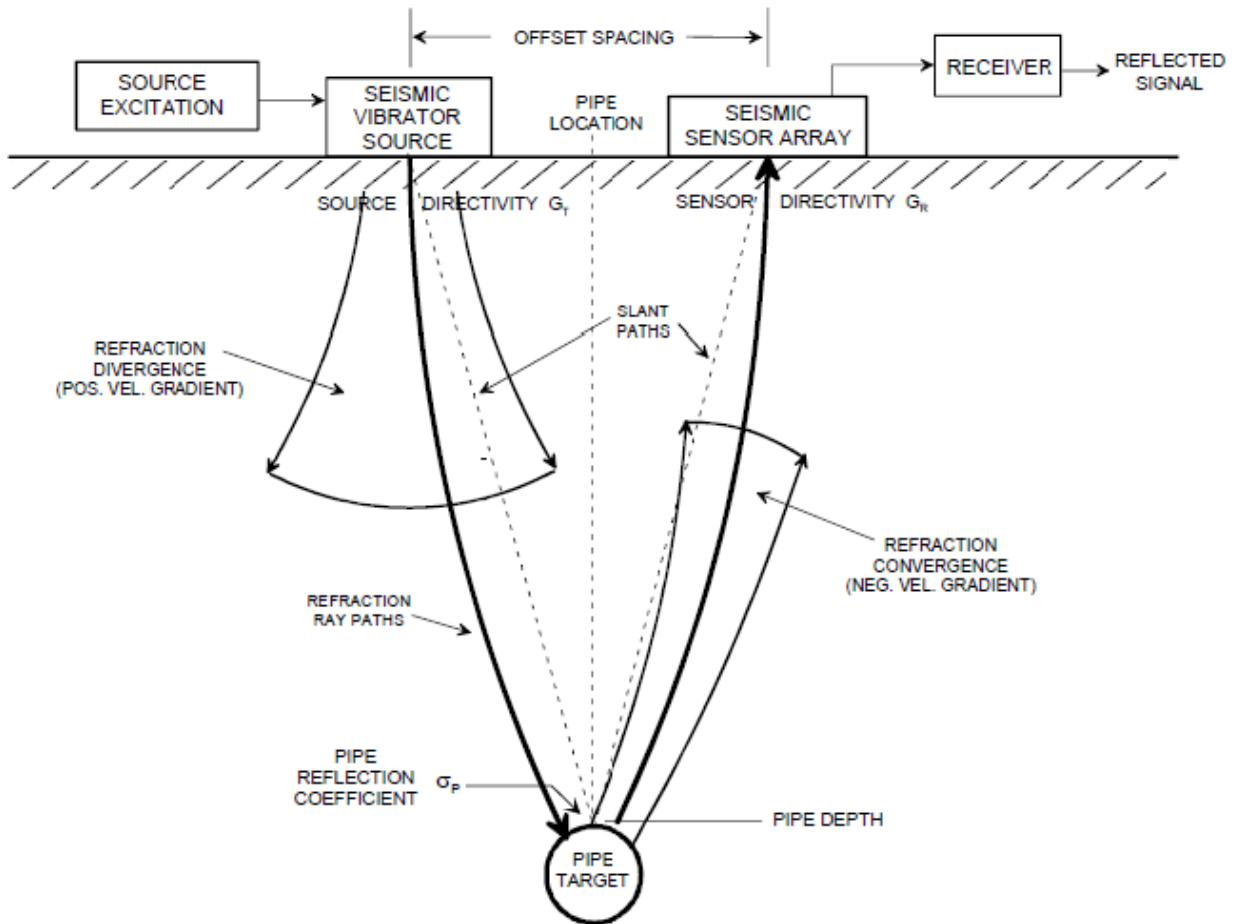


Figure 3.31. Pipe reflection cross section in near-surface soil medium.

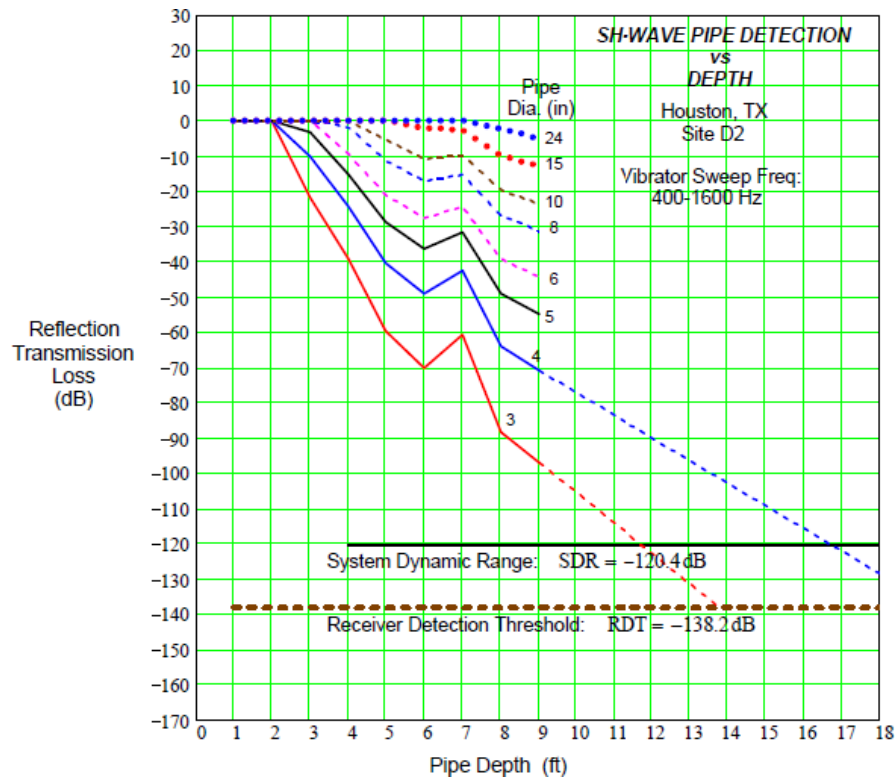


Figure 3.32. SH-wave reflection system performance, Houston Borehole D2.

depths for the different size pipes are indicated by extending the slopes of the curves down to the practical threshold limit (dashed lines). Pipes having a diameter of 3 in. are detectable at a depth of about 10.5 ft, and larger pipes are detectable at deeper depths. Pipes 6 in. in diameter are detectable at depths of about 17 ft. Because of the dominant effects of the soil properties, as long as the system source excitation frequency sweep signal starts at a time when a low frequency limit equals the frequency range for which distinct pipe reflections occur [or ( $f_L = f_r$ )], the indicated pipe detection depths (based on the 120-dB practical system dynamic range threshold) will not change significantly when modest changes are introduced in the other operating system parameters. However, as a cautionary note, because the velocity and Q values were not measured at depths greater than 9 ft, the soil conditions at greater depths are actually unknown.

Figure 3.33 shows the detection depth of different size pipes using an SH-wave seismic reflection system at the Houston Borehole E1 test site. The practical detection threshold indicates the probable maximum detection depth for pipes in the 3-in.-to-6-in.-diameter range. Larger-diameter pipes are detectable at deeper depths. The slopes of the curves for each pipe size are governed primarily by the shear wave attenuation in the Houston E1 soil column and the pipe diameter.

The velocity and attenuation analyses for Borehole E1 were not practical at depths below 14 ft because of Geoprobe system push refusal. The shear wave velocity and Q at this borehole site were lower than at the Borehole D2 site. The selected sweep frequency range of 400–1,600 Hz is a nominal range compatible with detecting pipes in the 3-in.-to-24-in.-diameter range

in Houston E1 soil. Conservative estimates of the pipe detection depths for the different size pipes are indicated by extending the slopes of the curves down to the practical threshold limit (dashed lines). Pipes having a diameter of 3 in. are detectable at a depth of about 5.5 ft, and shallower. Pipes 6 in. in diameter are detectable at depths of about 11.5 ft. Because of the dominant effects of the soil properties, as long as the system source excitation frequency sweep signal starts at  $f_L = f_r$ , the indicated pipe detection depths (based on the 120-dB practical system dynamic range threshold) will not change significantly when modest changes are introduced in the other operating system parameters.

Figure 3.34 shows the detection depth of different size pipes using an SH-wave seismic reflection system having the design and operating parameters (described above) at the Houston Borehole F2 test site. The practical detection threshold indicates the probable maximum detection depth for pipes in the 3-in.-to-6-in.-diameter range. Larger-diameter pipes are detectable at deeper depths. The slopes of the curves for each pipe size are governed primarily by the shear wave attenuation in the Houston F2 soil column and the target pipe diameter.

The velocity and attenuation analyses for Borehole F2 were not practical at depths below 9 ft because of limited data quality. The shear wave velocity and Q at this borehole site were approximately the same as those at Borehole E1 but lower than at Borehole D2. The selected sweep frequency range of 400–1,600 Hz is a nominal range compatible with detecting pipes in the 3-in.-to-24-in.-diameter range in Houston F2 soil. Conservative estimates of the pipe detection

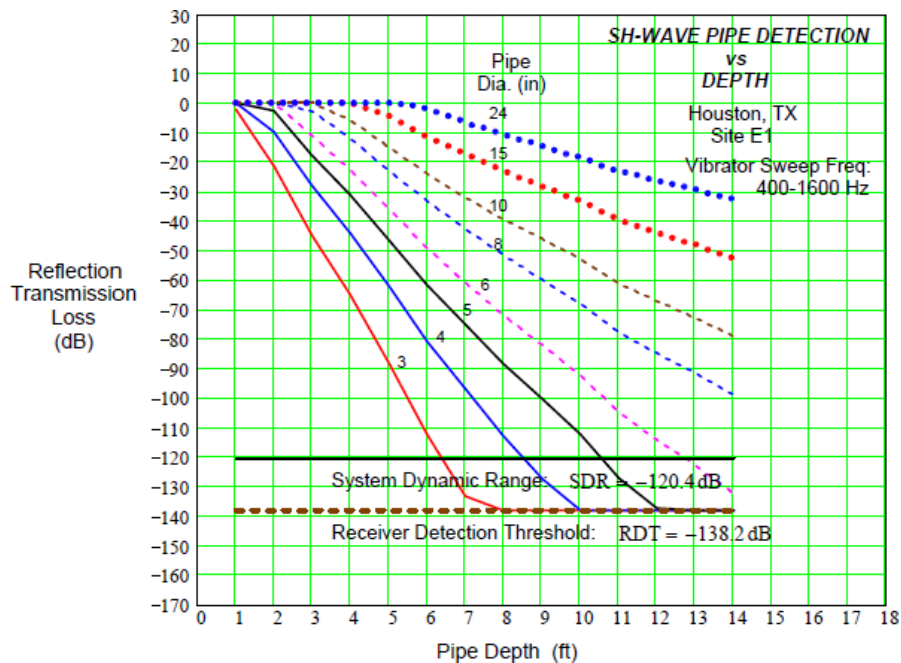


**Figure 3.33. SH-wave reflection system performance, Houston Borehole E1.**

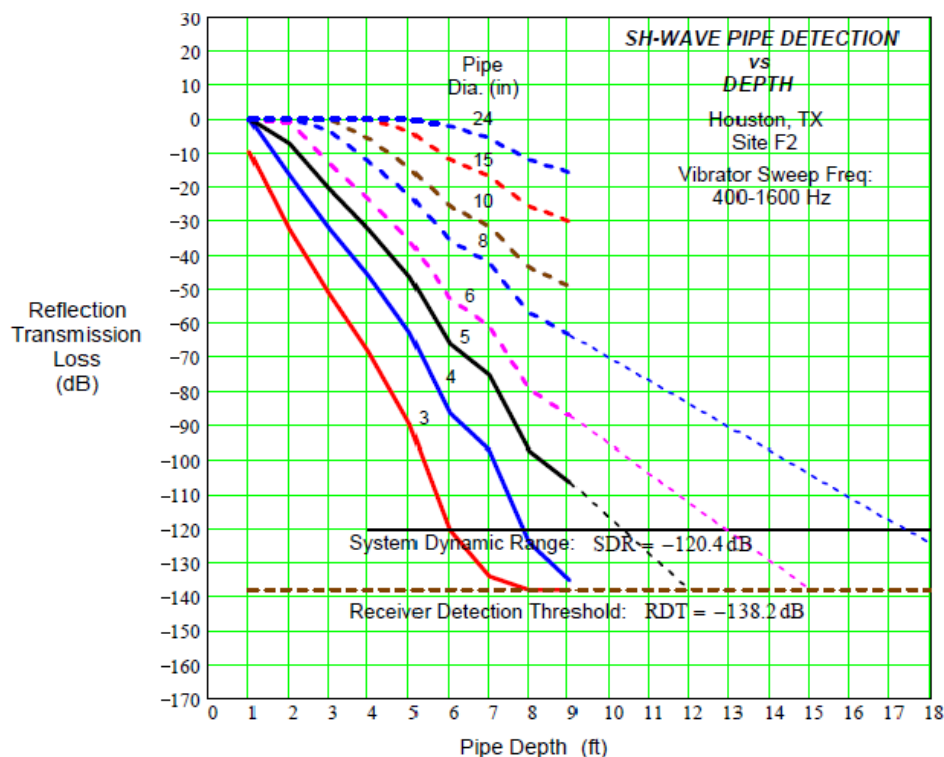


Figure 3.34. SH-wave reflection system performance, Houston Borehole F2.

depths for the different size pipes are indicated by extending the slopes of the curves down to the practical threshold limit (dashed lines). Pipes having a diameter of 3 in. are detectable at a depth of about 5.5 ft and shallower. Pipes 6 in. in diameter are detectable at depths of about 11.5 ft. Pipes larger than 8-in. diameter are detectable at depths of about 15 ft and deeper. Because of the dominant effects of the soil properties, as long as the system source excitation frequency sweep signal starts at  $f_L = f_n$ , the indicated pipe detection depths (based on the 120-dB practical system dynamic range threshold) will not change significantly when modest changes are introduced in the other operating system parameters.

### Seismic Soils Properties Testing Assessment

The project team performed the soil testing analysis on the data gathered by pushing an instrumented cone into the ground and measuring seismic parameters at 1-ft intervals on the way down. The testing was conducted at four regional sites: Traverse City, Michigan; Manteno, Illinois; Houston, Texas; and Manassas, Virginia. The Geoprobe with instrumented cone was not always in perfect contact with the soil surrounding the tip during the tests, leading to gaps in the data coverage in many of the test holes. Owen Engineering Services and Psi-G struggled to find at least one completely satisfactory data set from the multiple tests that were done at each site. This difficulty was predictable given past experience in making in situ

measurements; several test holes were made at each site to attempt to make up for the predicted ground-coupling problems. The seismic team felt that enough good data were obtained at each site for the planned analysis to be done.

The research that has been done so far has been largely aimed at determining the basic physical properties (seismic velocity and wave attenuation) of shear waves in soils when using frequencies in the range of 100–1,600 Hz. This work was performed because no literature exists in this area of study; without knowing these parameters, the project team could not establish the specifications for seismic measurement and imaging systems. Three basic results came out of this work. First, velocity and attenuation of shear waves in a wide range of soils are within ranges that make it possible to specify a measurement system that can be operated within the capabilities of modern electronic components, such as analog-to-digital converters and amplifiers. Second, the tests demonstrated that shear waves could be generated and propagated in the subsurface soils within the frequency range of interest, most of the time. In some cases the linearity of soil behavior is in question and further testing to track down this variable will be done in the final work phase as described below. Third, subsurface soil environments are even more complex and heterogeneous than the R01B team expected. The last point has the effect of requiring more work than expected in structuring and operating sources, constructing receiver arrays, and performing data processing.

## Seismic Source Evaluation

A major issue in evaluating the soil testing data was that many data sets contained data that didn't meet quality criteria for processing and computing of the desired parameters. With further study, the project team determined that many of the data sets were experiencing nonlinear results because larger than necessary signals were being generated by the microvibrator source. The MicroVib was developed for study of deeper geologic targets, perhaps greater than 500 ft. The source energy necessary to do that is so large as to affect the structure of the surface soils on which the source sits and through which signals must pass. While the MicroVib's operating system was more than capable of reproducing the high-frequency signals required for this work, its output could not be "dialed down" to levels that would not drive the soils nonlinearly. That resulted in higher source levels than were appropriate for shallower depths and unconsolidated soils. A number of issues surrounding the source operations needed to be altered to solve this problem. By the time the project team figured out the issues with this system, the project was almost complete. As a way to move as far forward as allowed by the time and money available, the team decided to design a completely new source generator that would account for the issues discovered in the soil testing.

The prototype new shear wave seismic source is shown in Figure 3.34A. It is over-engineered to solve a range of problems and suspected problems and is clearly not ready for more than very rudimentary prototype testing. As the prototype goes through further development, it will be refined to get to a commercially workable system.

This prototype and a receiver prototype have now been developed. They work well enough on the bench to say that

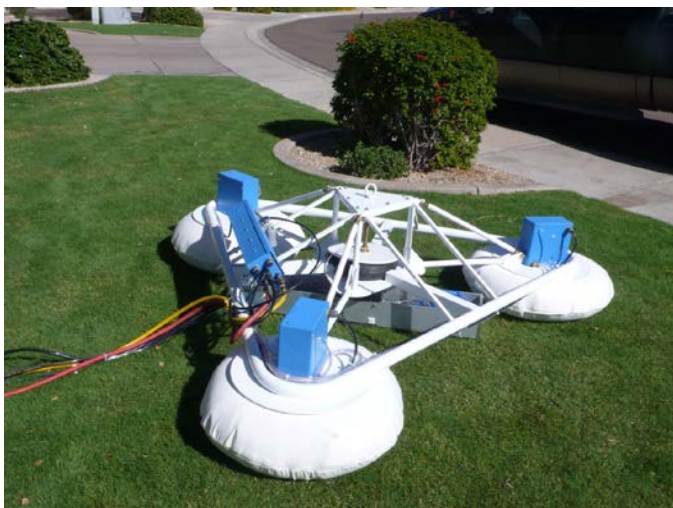


**Figure 3.34A.** Newly designed seismic source preprototype.

the team is very close to proving feasibility, but the system has not yet been tested in the field.

## Seismic Modeling Software

Dr. Nevin Simicevic and the team at Louisiana Tech University (LTU) have produced the basic code for 3-D modeling of seismic signals. Models were created using soil parameters derived from the seismic field testing. This work progression has been significant and will become increasingly valuable in the interpretation of test results moving forward toward a seismic prototype system. Dr. Mark Baker of Geomedia Research & Development is already beginning to use the results for his seismic prototype development work on SHRP 2 Renewal Project R01C, Innovations to Improve the Extent of Locatable Zone.

## Wave Propagation Program Modeling

### WPP Modeling—Soil Properties

Soil densities, the velocities of the waves in the soil, and the coefficients needed to describe the wave attenuation are the soil properties needed to describe the elastic and acoustic wave propagation using the finite difference time-domain (FDTD) method. Depending on the type of the soil used in the simulation, they should be measured or, if the data exist, taken from the literature. An example of the parameters used by LTU is taken from the work of Michael L. Oelze, William D. O'Brien, and Robert G. Darmody—Measurement of Attenuation and Speed of Sound in Soils (Oelze et al. 2002). Table 3.1 describes the type of soil used, and Table 3.2 describes the soil mean bulk densities. Table 3.3 describes the mean acoustic propagation speed in the soil, and Table 3.4 shows the mean attenuation coefficients valid in the frequency range between 2 kHz and 6 kHz.

The attenuation coefficients in Table 3.4 are obtained from the relation

$$\alpha x = -20 \log \frac{p(x)}{p_0}$$

where  $p(x)$  is the measured pressure as a function of the thickness,  $x$ , traveled by the acoustic wave. The measured pressure is normalized to the pressure at the sound source. The WPP code uses quality factors,  $Q$ , instead of the attenuation coefficients. The relation between the  $Q$  factors and the attenuation coefficient is

$$Q = \frac{\pi \cdot f}{\alpha \cdot v}$$

where  $v$  is the speed of the wave, and  $f$  is the frequency.

**Table 3.1. Chemical Composition of a Soil Material (Oelze et al. 2002)**

Soil code <sup>‡</sup>	Sand	Silt	Clay	Organic matter	Soil texture class	Liquid limit	Plastic limit	Plasticity index	COLE
									%
ADA	72	18	10	11.7	fine sandy loam	NP <sup>‡</sup>	NP	NP	NP
CAB	11	53	36	0.5	silty clay loam	43	24	19	14
DRA	12	50	38	9.8	silty clay loam	43	28	15	13
MEA	38	38	24	2.3	loam	28	19	9	7
PLA	97	1	2	0.4	sand	NP	NP	NP	NP
SAC	2	82	16	0.1	silt loam	29	24	5	4

<sup>‡</sup> ADA, Adrian soil, A-horizon; CAB, Catlin soil, Bt-horizon; DRA, Drummer soil, Ap-horizon; MEA, Medway soil, Ap-horizon; PLA, Plainfield soil, Ap-horizon; SAC, Sable soil, Cg-horizon.

<sup>‡</sup> NP, non-plastic.

Reprinted by permission, ASA, CSSA, SSSA.

**Table 3.2. Mean Bulk Densities of a Soil Material (Oelze et al. 2002)**

Treatment code <sup>‡</sup>	Soil type <sup>‡</sup>					
	ADA	CAB	DRA	MEA	PLA	SAC
	Bulk density, g cm <sup>-3</sup>					
11	0.92	1.27	1.32	1.13	1.51	1.36
14	1.03	1.44	1.40	1.37	nd <sup>§</sup>	1.41
21	0.83	1.16	1.00	1.11	1.45	0.98
24	1.00	1.36	1.19	1.30	1.62	1.36
31	0.79	0.90	0.88	0.97	1.46	1.24
34	0.92	1.14	1.26	1.35	1.57	1.62
51	0.92	1.11	1.27	1.23	1.57	1.35

<sup>‡</sup> The first digit of the code designates soil moisture; 1, air dry, to 5, saturated. The second digit designates soil compaction, 1 is loose and 4 is dense.

<sup>‡</sup> ADA, Adrian soil, A-horizon; CAB, Catlin soil, Bt-horizon; DRA, Drummer soil, Ap-horizon; MEA, Medway soil, Ap-horizon; PLA, Plainfield soil, Ap-horizon; SAC, Sable soil, Cg-horizon.

<sup>§</sup> nd, not determined.

Reprinted by permission, ASA, CSSA, SSSA.

**Table 3.3. Mean Propagation Speed of Acoustic Waves in Soil (Oelze et al. 2002)**

Treatment code <sup>‡</sup>	Soil type <sup>‡</sup>					
	ADA	CAB	DRA	MEA	PLA	SAC
	Propagation speed, m s <sup>-1</sup>					
11	153	190	177	154	260	140
14	121	150	159	126	nd <sup>§</sup>	139
21	89	114	118	151	138	117
24	147	102	136	93	103	122
31	87	150	107	161	122	121
34	86	105	245	105	253	176
51	102	102	118	139	189	207

<sup>‡</sup> The first digit of the code designates soil moisture; 1, air dry, to 5, saturated. The second digit designates soil compaction, 1 is loose and 4 is dense.

<sup>‡</sup> ADA, Adrian soil, A-horizon; CAB, Catlin soil, Bt-horizon; DRA, Drummer-soil, Ap-horizon; MEA, Medway soil, Ap-horizon; PLA, Plainfield soil, Ap-horizon; SAC, Sable soil, Cg-horizon.

<sup>§</sup> nd, not determined.

Reprinted by permission, ASA, CSSA, SSSA.

While some of the soil properties described in this report apply only to the propagation of acoustic or P-waves, the same formalism applies to S-wave propagation, which will be studied in the rest of this report. The parameters for S-wave propagation in soils are less available in the literature than those for the propagation of P-waves.

### WPP Modeling—Sources

In the WPP code, the soil can be deformed by a time-dependent force inducing the propagation of elastic or viscoelastic waves. Several shapes of time-dependent sources are possible; but, generally, they can be separated into three groups: a unipolar pulse with a power spectrum in the frequency domain peaking at 0 Hz (Figure 3.35), a multipolar pulse for which the power density at 0 Hz is zero (Figure 3.36), and the Gaussian window function used to represent a quasi-monochromatic wave (Figure 3.37). For the pulsed sources, the time durations of the source were chosen to conform to the frequency range requirement of the R01B project, 30–4,000 Hz. In addition,

**Table 3.4. Mean Attenuation Coefficients of Acoustic Waves in Soil (Oelze et al. 2002)**

Treatment code <sup>‡</sup>	Soil type <sup>‡</sup>					
	ADA	CAB	DRA	MEA	PLA	SAC
	Attenuation coefficient, dB cm <sup>-1</sup> kHz <sup>-1</sup>					
11	0.31	0.14	0.21	0.12	0.23	0.39
14	0.20	0.59	0.53	0.63	nd <sup>§</sup>	0.36
21	0.68	0.36	0.38	0.39	0.35	0.46
24	0.58	0.91	0.56	0.62	0.50	0.69
31	0.39	0.45	0.51	0.28	0.81	0.50
34	0.71	0.90	0.71	0.90	0.16	0.96
51	0.49	0.58	0.58	0.31	0.75	0.38

<sup>‡</sup> The first digit of the code designates soil moisture; 1, air dry, to 5, saturated. The second digit designates soil compaction, 1 is loose and 4 is dense.

<sup>‡</sup> ADA, Adrian soil, A-horizon; CAB, Catlin soil, Bt-horizon; DRA, Drummer-soil, Ap-horizon; MEA, Medway soil, Ap-horizon; PLA, Plainfield soil, Ap-horizon; SAC, Sable soil, Cg-horizon.

<sup>§</sup> nd, not determined.

Reprinted by permission, ASA, CSSA, SSSA.

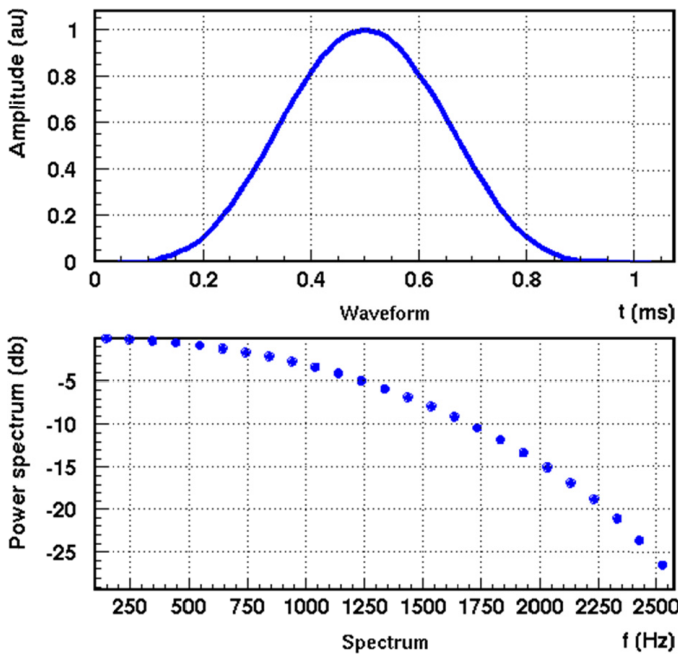


**Figure 3.35.** Unipolar pulse example (in the shape of a very smooth bump and its power spectrum; the frequency parameter for this pulse was 1,000 Hz).

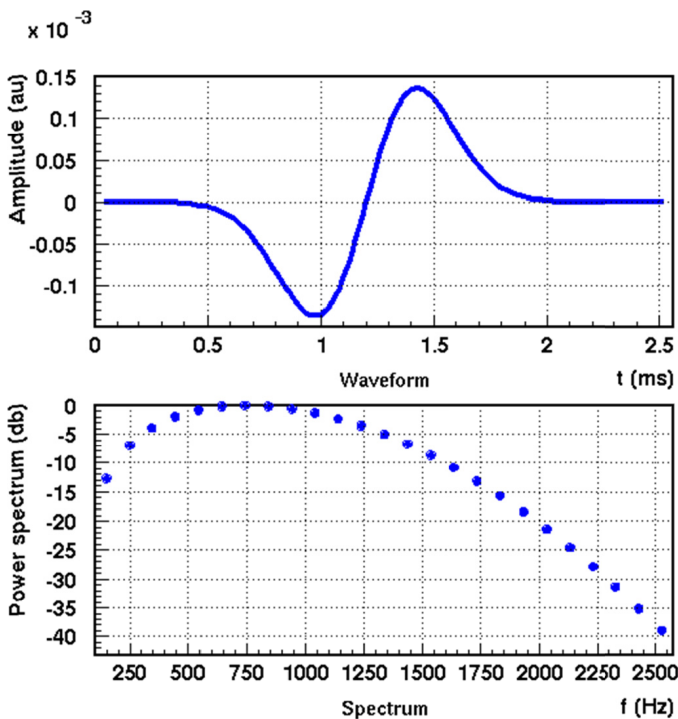


**Figure 3.36.** Bipolar pulse example (in the shape of the time integral of the Ricker function, proportional to the time derivative of the Gaussian function; the frequency parameter for this pulse was 1,000 Hz).

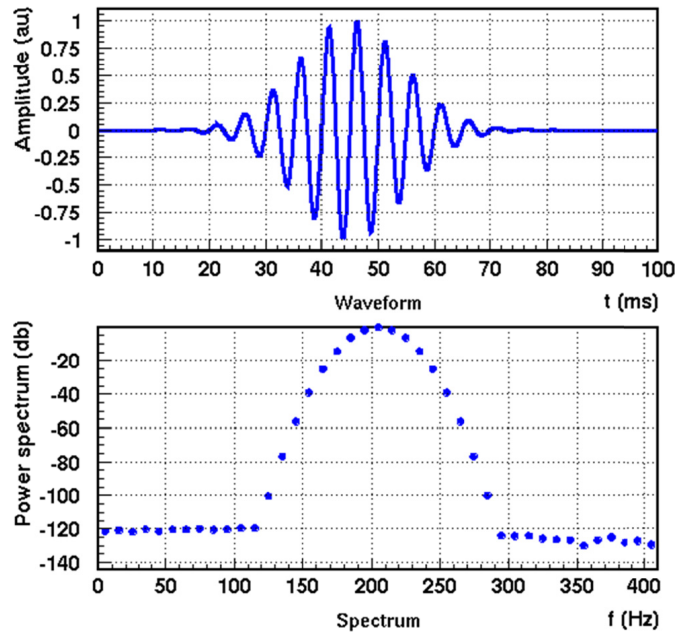


**Figure 3.37.** Gaussian window of monochromatic wave example (with central frequency of 200 Hz; the number of windowed cycles was 12).

because of the increase of wave attenuation with the increase in wave frequency, the selected frequency range was as low as possible, as long as it satisfied imposed requirements on the resolution.

### WPP Modeling—Attenuation

To calculate the attenuation of the waves in the material instead of the attenuation coefficients, the WPP code uses the Q factors of the material. The relation between the Q factors and the attenuation coefficient is

$$Q = \frac{\pi \cdot f}{\alpha \cdot v}$$

where  $v$  is the speed of wave, and  $f$  is the frequency.

WPP uses the linear viscoelastic material model to simulate the wave attenuation. Using this model results in a requirement for more computer memory and more processing time. In a compromise between the computational requirements and physical accuracy, the number of relaxation mechanisms was set to three, resulting in solving 12 differential equations simultaneously. In this case, the modeling was restricted to the frequency band of  $[\omega, 100\omega]$ ; in that range, the quality factors (Q) for both P- and S-waves are assumed to be constant for a particular material.

Quality factors used in the simulations were provided by the subcontractor Owen Engineering Services. An example

of provided parameters used in the simulation is shown in Figures 3.24 through 3.26.

### WPP Modeling—Computational Requirements

The factors contributing to the computational requirements (RAM and number of CPUs) depend on the size of the physical volume, the frequencies and velocities of waves, and the attenuation parameters. For a realistic and useful simulation, an ideal computational volume would be of the size  $400\text{ cm} \times 400\text{ cm} \times 300\text{ cm}$ . The computation volume of  $400\text{ cm} \times 400\text{ cm} \times 300\text{ cm}$ , if required to be discretized by cells of the size  $5\text{ mm} \times 5\text{ mm} \times 5\text{ mm}$ , results in a total of  $3.84 \times 10^8$  computational cells, requiring large RAM and a large number of CPUs. Imposing attenuation may result in even smaller discretization cells, more memory, and more CPUs. Such a computation can only take place in a high-performance computing (HPC) environment. The WPP code is written to take advantage of the parallelization in a HPC environment; and Louisiana Tech University has access to the Louisiana Optical Network Initiative (LONI), providing a powerful system of high-performance computers.

Testing of the speed of WPP was performed at the LONI system of supercomputers; the speed of computation was measured as a function of the number of CPUs involved. Using the same volume size and discretization, the model was run for a total of 9,468 time steps. Identical calculations were carried out on 8, 20, 40, 80, and 100 processors separately. Figure 3.38 shows the time in minutes it took the computation to finish, as a function of the number of processors used. Calculation that takes 309 minutes using 8 processors takes only 24 minutes using 100 processors (~13 times faster). It can also be observed in Figure 3.38 that the increase of

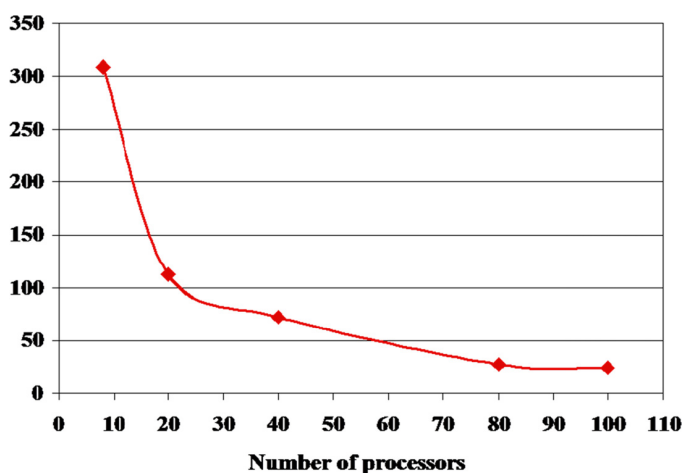


**Figure 3.38.** Total computation time to complete as function of the number of processors, in minutes.

computation speed is not linearly proportional to the number of processors.

### WPP Modeling—Monitoring of Quantitative Values

Many physical situations were simulated using the WPP computer code, including the propagation of S- and P-waves through a soil with or without a reflecting target, with or without attenuation, and using pulsed or quasi-continuous waves. The output from the simulation consisted of physical quantities in the form of a time series of the values of the displacement at specific points in space—underground or on the ground. Particularly, to estimate possible measured values, a network of imaginary motion sensors was positioned on the ground. They were used to study the difference in the strength and the time of arrival of the reflected signal. The schematic of the sensor positions is shown in Figure 3.39. The amplitude of the displacement and the time of arrival of the reflected pulse were recorded at those positions throughout the entire simulation run. The results from the simulation of pulse propagation and the reflection from buried pipes were then used to test possible signal processing, analysis methods, and target recognition. The goal was to determine the positions of buried pipes from the time series of the values of the displacement, or its time derivatives, recorded at the position of sensors.

### WPP Modeling—Simulation of Propagation of Shear Waves Without Attenuation

A series of simulations of the signal propagation was performed assuming no physical attenuation of the waves. Quantitative values of the displacement were recorded as a time series at

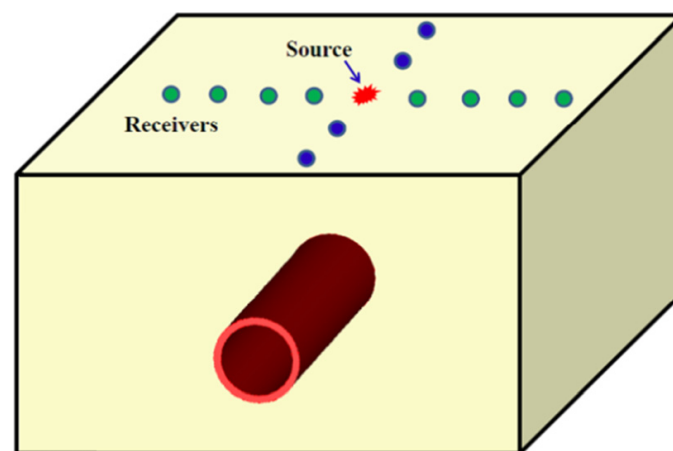


**Figure 3.39.** Schematic of the position of a source and motion sensors at the top of the soil.

chosen points under or on the ground. The unipolar case was represented by the shear pulse excitation in the form of the very smooth bump along the  $x$ -axis on the surface of the ground. The frequency parameter,  $\omega$ , was the same as in the case of the bipolar excitation—1,000 Hz. The shape of this pulse and its power spectrum are shown in Figure 3.35. The pulse was reflected from a plastic pipe with the diameter

of 1 ft, positioned 115 cm under the surface of the soil. The soil and the plastic pipe were modeled in the same way as in the case of the bipolar excitation. The size of the computational volume was also the same. For the case of unipolar excitation, the change in the shape of the  $x$ -component of the S-wave displacement in the  $x$ - $z$  plane as the pulse propagates through the soil and reflects from the plastic pipe is shown in Figure 3.40.

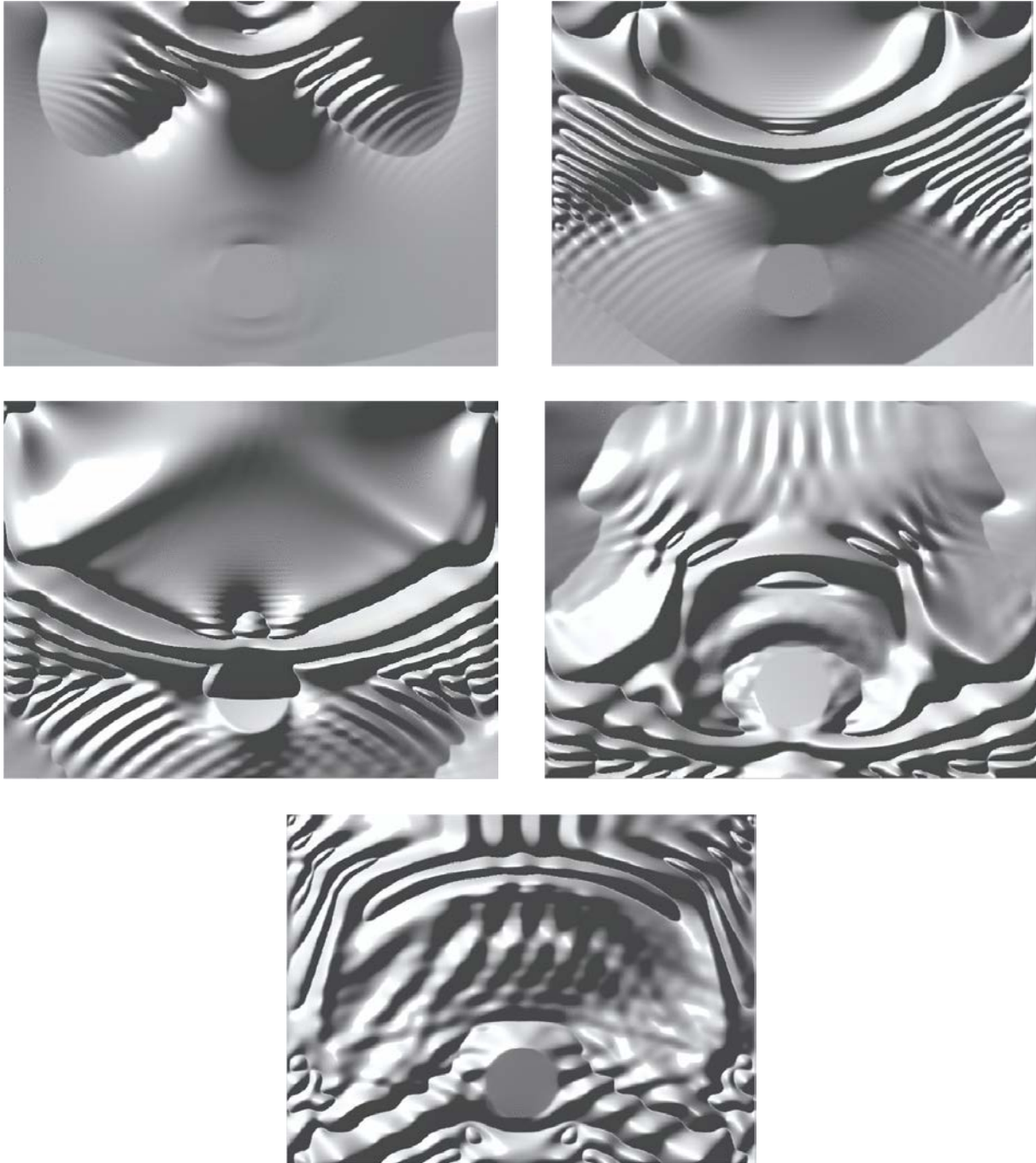


**Figure 3.40.** The propagation and reflection of the  $x$ -component of the unipolar shear pulse displacement in the  $x$ - $z$  plane. (The animation is at <http://www.phys.latech.edu/~neven/uit/final>.)

The  $y$ -component of the same S-wave displacement is small in the  $x$ - $z$  plane. The propagation of the  $z$ -component is shown in Figure 3.41.

Also in this case, the quantitative values of the displacement were shown at chosen points under or on the ground. The values of the  $x$ -component of the S-pulse displacement for each time step of the computation are shown in Figure 3.42 at

positions of 25, 50, and 75 cm under the ground, between the source of the pulse and the plastic pipe. The same study was done by replacing the plastic pipe with water. Furthermore, to test the target recognition software, simulations were performed in which the pulse propagated through the soil and was reflected off multiple plastic pipes, each with diameters of 1 ft and positioned at different depths.

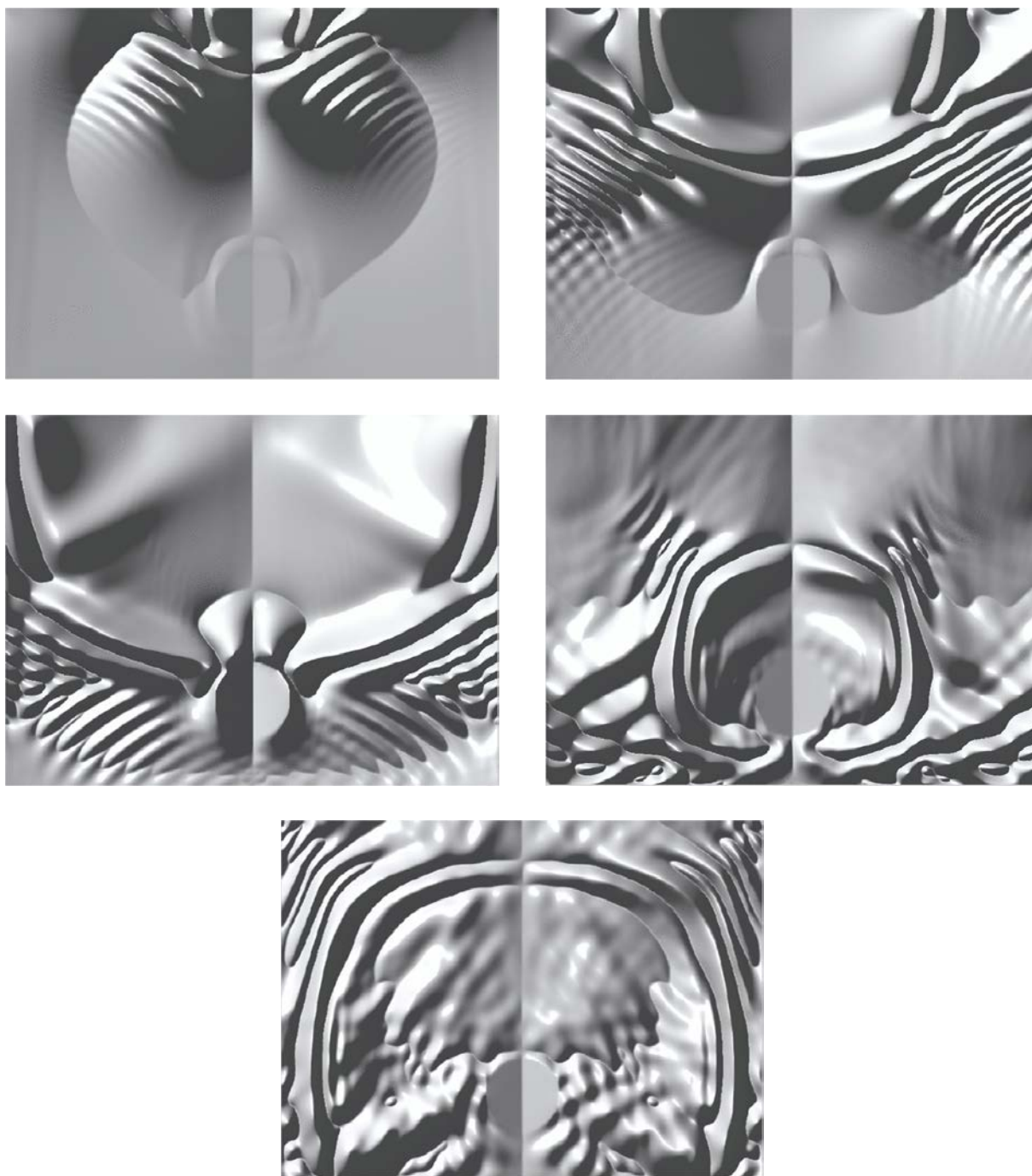


**Figure 3.41.** The propagation and reflection of the  $z$ -component of the unipolar shear pulse displacement in the  $x$ - $z$  plane. (The animation is at <http://www.phys.latech.edu/~neven/uit/final>.)

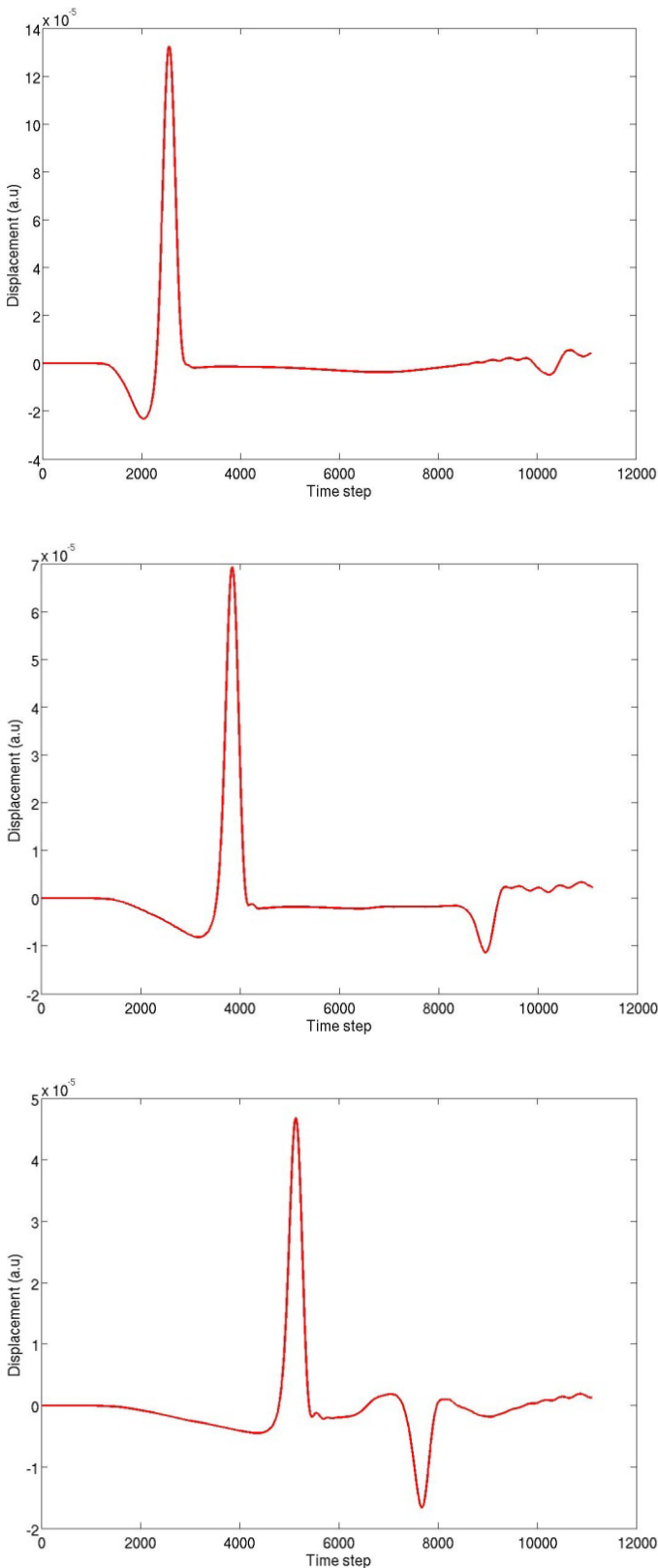


**Figure 3.42.** Values of the  $x$ -component of the unipolar  $S$ -wave displacement for each time step, at positions of 25 (top), 50 (middle), and 75 (bottom) cm underground (the form of excitation was a smooth bump; the transmitted and reflected pulses are shown).

While still not introducing the attenuation, LTU attempted to simulate the propagation using the pulse as measured in the trial seismic soil test in Traverse City, Michigan. LTU downloaded the vibrator data and performed the Fourier analysis. The shape of the pulse and its Fourier spectrum are shown in Figure 3.43. The Fourier analysis shows that the power spectrum peaks at a frequency of  $\sim 10$  kHz, much higher than the frequency used in previous simulations. In the simulation, an experimentally obtained pulse shape was modified into the pulse shape compatible with one of the input modes of the Wave Propagation Program (WPP). The physical properties of such a pulse differ very little from the physical properties of an experimental pulse. The shape of the inputted pulse is shown in Figure 3.44.

The simulation of the propagation of the Traverse City shear wave was performed in a volume equaling  $200 \text{ cm} \times 200 \text{ cm} \times 170 \text{ cm}$ , which was due to the power spectrum peaking at a frequency of  $\sim 10$  kHz, discretized into  $1,001 \text{ cubes} \times 1,001 \text{ cubes} \times 851 \text{ cubes}$  for an overall total of  $8.53 \times 10^8$  grid points. The length of a cell side was 2 mm, and the velocity of the shear wave was 214 m/s, resulting in  $\sim 10$  samples per wave length at a frequency of 10 kHz. The stepping time was  $5.41 \times 10^{-7}$  s. The pulse propagated through the soil and was reflected by a plastic pipe that was the diameter of 1 ft, positioned at a depth of  $\sim 140$  cm vertically under the position of the source. The  $P$ -wave velocity of the soil was 432 m/s, and the  $S$ -wave velocity was 214 m/s. For the plastic pipe, the  $P$ -wave velocity was

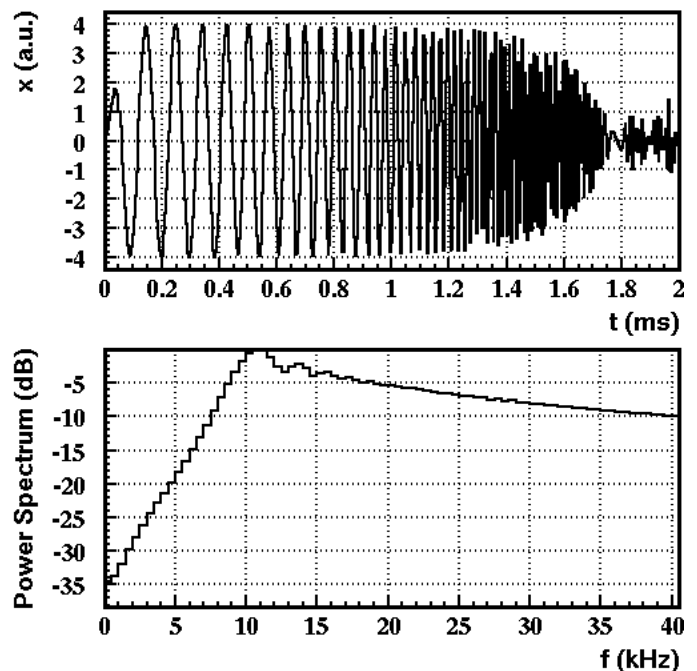


**Figure 3.43.** The experimental vibrator pulse and its Fourier power spectrum.

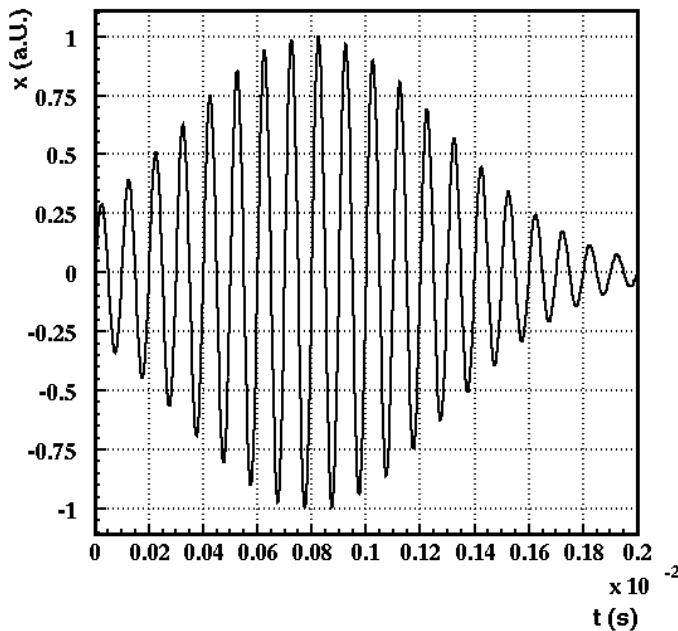


**Figure 3.44.** The shape of the vibrator pulse as input to WPP.

2,458 m/s and the S-wave velocity was 1,164 m/s. The program ran on more than 120 processors over a time period of 30 hours, making 30,000 time steps. The execution of such a program is at the limit of LONI capabilities, assuming that the resources are shared with other users. At this stage, no physical pulse attenuation was computed.

Assuming geometrical, but not physical attenuation, it was shown that such pulse can detect a buried pipe; but due to the frequency content and width of the pulse, the detection was not as straight forward as with simple pulses used in previous simulations. To facilitate the use of time-of-flight techniques to reconstruct targets positions, the Hilbert transformation was used.

### **WPP Modeling—Simulation of Propagation of Shear Waves with Attenuation**

Simulations that include physical attenuation require more computational resources than simulations without attenuation. Still, several simulations, which included physical attenuation of the propagation of shear waves, were performed. Depending on the frequency of the wave and the allowed time of the execution, the conditions of the simulations, including the size of the physical volume and the time of propagation, varied.

In the first set of examples, signals from the vibrator's monochromatic tonebursts, as shown in Figure 3.12, were used. Since the time duration of a toneburst was 60 ms, larger computational volumes were required. In the first simulation, a shear wave in the form of a toneburst of 200 Hz was used.

The pulse shape and its frequency power spectrum are shown in Figure 3.37.

Because of its low-frequency content, the computation could be performed relatively fast in a larger volume. The shear wave was excited along the  $x$ -axis on the surface of the ground. The propagation was simulated in the physical volume equaling  $400\text{ cm} \times 400\text{ cm} \times 366\text{ cm}$ . The parameters of the soil—including its density, P-wave and S-wave velocities, and the Q factors—varied with the depth of the soil. They are shown in Table 3.5.

The simulated pulse propagation is shown in Figure 3.45. The attenuation of the pulse is shown in Figure 3.46.

While the simulation of the propagation of a shear wave in the form of a toneburst of 200 Hz produced results when the attenuation was incorporated in the computation, several steps were necessary to fully understand the physical meaning of those results. The contribution to the attenuation also comes from the dependence of the amplitude on the distance from the source; for spherical waves, this dependence is  $1/r$ , on numerical precision, on reflection from different type of soils, and so on. To fully understand the physical meaning of the simulation results and to properly incorporate the attenuation, a systematic study of the propagation of a shear wave in different conditions was done. In the process, the sizes of the amplitudes were determined using the Hilbert transformation.

To test the geometrical  $1/r$  amplitude attenuation, a shear wave isotropic point source of the 200-Hz toneburst was excited along the  $x$ -axis on the surface of the ground. The propagation was simulated in the physical volume

**Table 3.5.** Input Parameters for WPP Modeling Simulation

<i>Block vp</i>	<i>vs</i>	<i>rho</i>	<i>z1</i>	<i>z2</i>	<i>qp</i>	<i>qs</i>
193	88	1155	0.000	0.305	17.4	14.5
253	127	1236	0.305	0.610	17.5	15.2
296	157	1286	0.610	0.914	17.6	16.2
331	183	1322	0.914	1.219	17.6	17.2
362	206	1352	1.219	1.524	17.7	17.8
388	226	1375	1.524	1.829	17.7	18.5
412	245	1396	1.829	2.134	17.8	18.9
434	255	1415	2.134	2.438	17.9	17.6
454	280	1430	2.438	2.743	18	21.7
474	296	1446	2.743	3.048	18.1	23.9
492	311	1460	3.048	3.35	18.2	24.7
508	326	1472	3.35	3.66	18.2	28.6

Note: *vp* and *vs* are depth-dependent P-wave and S-wave velocities, in m/s; *rho* is depth-dependent density, in  $\text{kg/m}^3$ , and *z1* and *z2* are the limits of the soil depth, in m; *qp* and *qs* are depth-dependent Q factors.

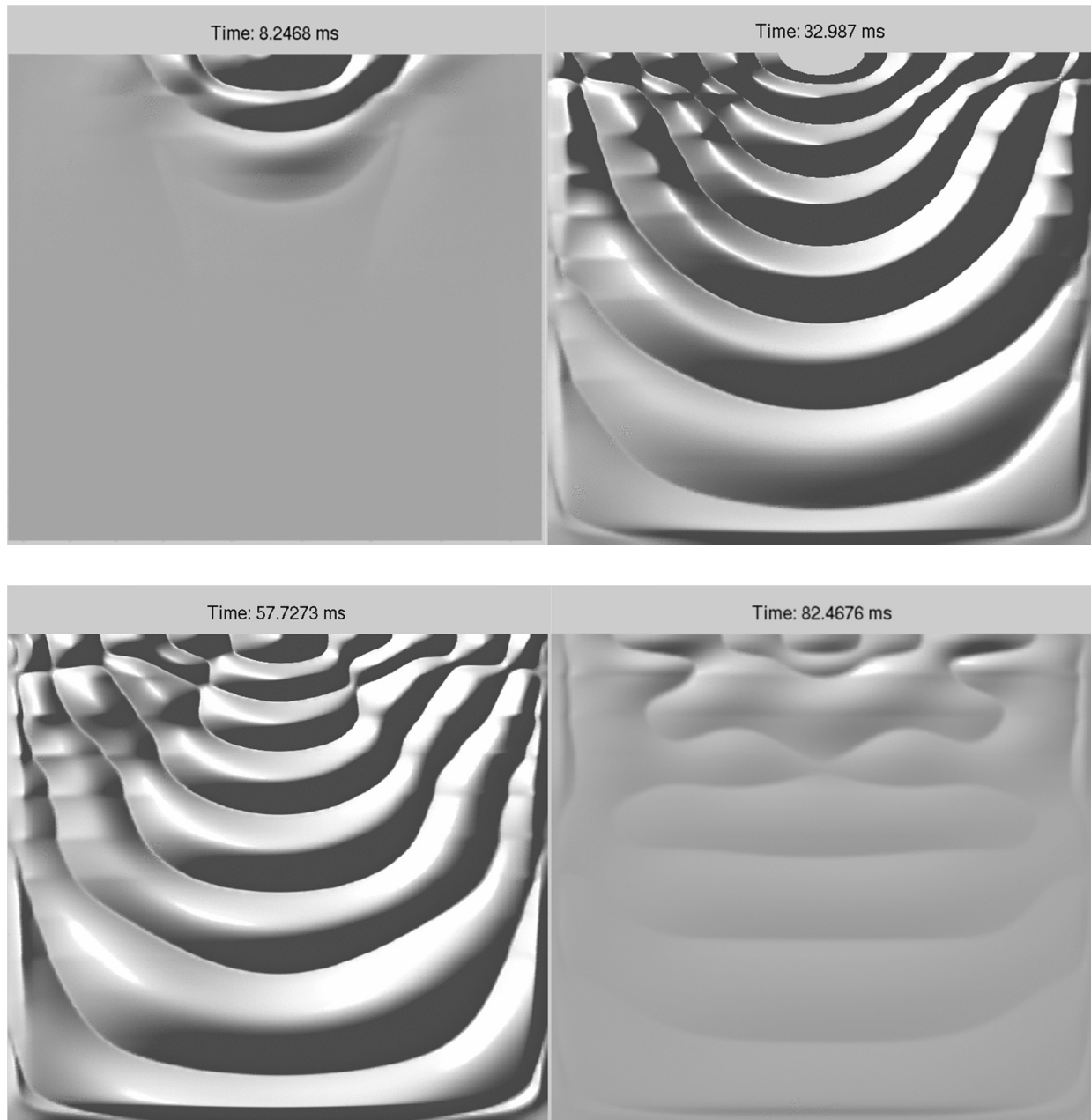


**Figure 3.45.** The propagation of the simulated pulse in the  $x$ - $z$  plane. (The animation is at <http://www.phys.latech.edu/~neven/uit/final>.)

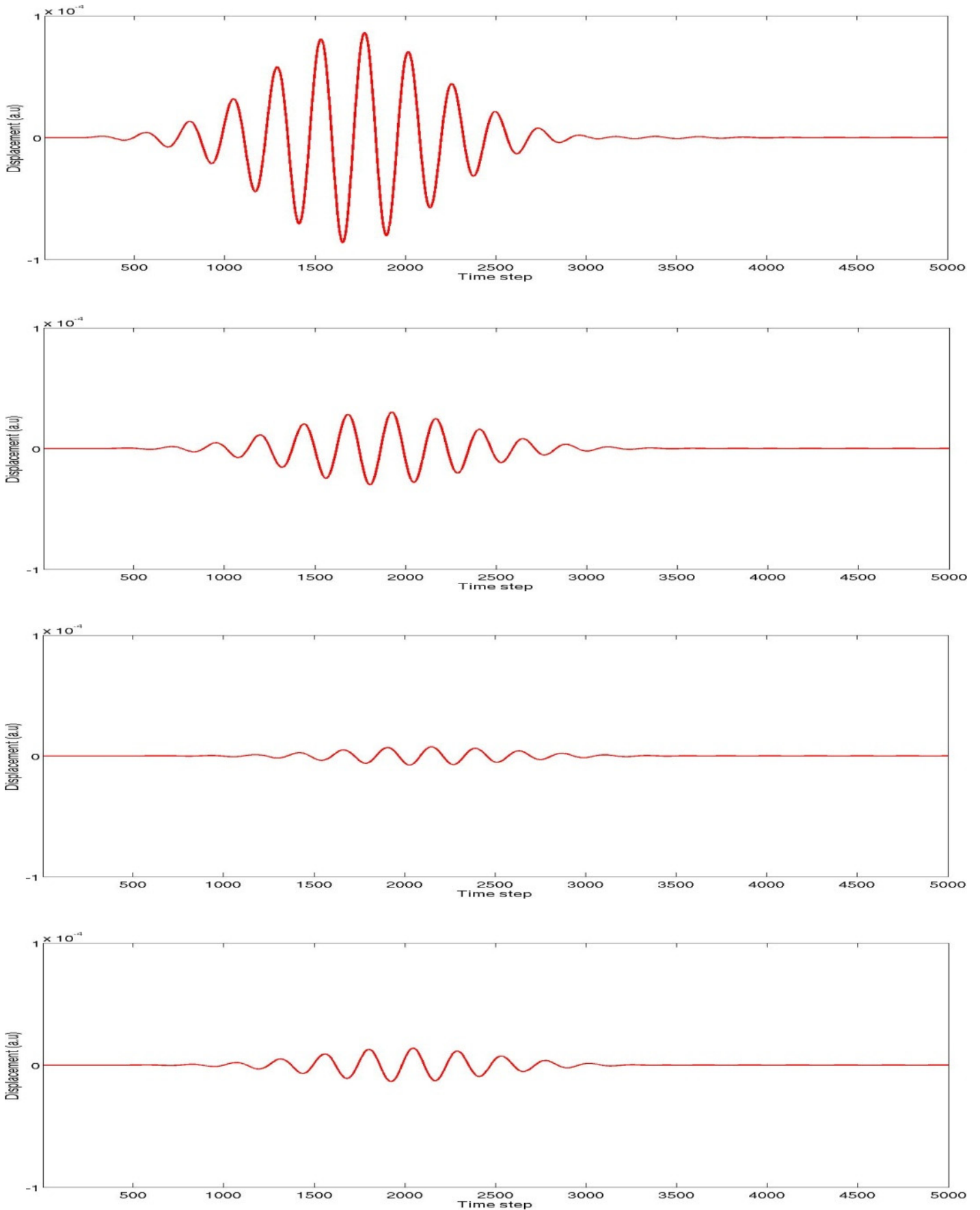


**Figure 3.46.** Time series of the strength of the x-component of displacement at depths of, from top to bottom, 50, 100, 150, and 200 cm, showing the signal attenuation (the source was at a depth of 6 cm).

equaling  $400\text{ cm} \times 400\text{ cm} \times 366\text{ cm}$ . The parameters of the soil included the density of  $1,155\text{ kg/m}^3$  and P-wave and S-wave velocities of  $193\text{ m/s}$  and  $88\text{ m/s}$ , respectively. The amplitudes of the wave were measured at depths incremented by  $50\text{ cm}$ . The results of the values of the amplitudes at different depths, normalized to the amplitude at the source, and their agreement with the predicted  $1/r$  attenuation, is shown in Figure 3.47. The perfect agreement between the values of the amplitudes in the simulated wave propagation and the theoretical prediction was also used as a test of the simulation software.

In the second test, to test the effects of the soil properties, the same shear wave isotropic point source of the  $200\text{-Hz}$  toneburst was excited along the  $x$ -axis on the surface of the ground. Again, the propagation was simulated in the physical volume equaling  $400\text{ cm} \times 400\text{ cm} \times 366\text{ cm}$ , but the parameters of the soil were taken from Table 3.5. The amplitudes of the wave were measured at the depths incremented by  $50\text{ cm}$ . The results of the values of the amplitudes at different depths, normalized to the amplitude at the source, are shown in Figure 3.48. Also shown in Figure 3.48, the attenuation is greater than the  $1/r$  geometrical attenuation. As expected, the transition of the wave from one soil density and propagation velocity to another one increased the attenuation.

In the third test, to test the effects of the nonisotropic source distribution, several isotropic point sources of the

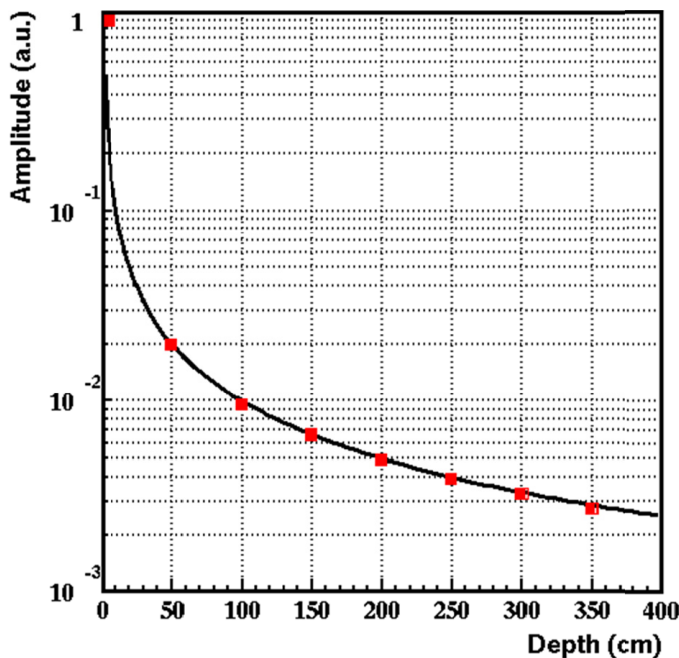


**Figure 3.47.** Values of the  $200\text{-Hz}$  toneburst's amplitudes at different depths (normalized to the amplitude at the source, in agreement with the predicted  $1/r$  attenuation).

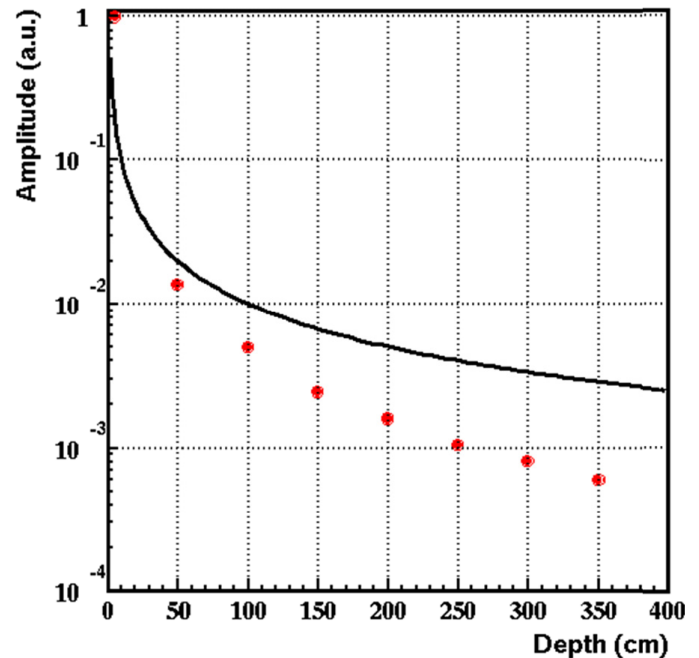


**Figure 3.48.** Values of the  $200\text{-Hz}$  toneburst's amplitudes at different depths with attenuation (normalized to the amplitude at the source, in agreement with the predicted  $1/r$  attenuation).

$200\text{-Hz}$  toneburst were distributed at the surface of the ground and excited along the  $x$ -axis. The array of sources' distribution mimicked the soft-soil vibrator used by subcontractor Owen Engineering Services. The propagation was simulated in the physical volume equaling  $400\text{ cm} \times 400\text{ cm} \times 366\text{ cm}$ , and the parameters of the soil were taken from Table 3.5. The amplitudes of the wave were measured at the depths incremented by  $50\text{ cm}$ . The results of the values of the amplitudes at different depths, normalized to the amplitude at the source, are shown in Figure 3.49. Again, as expected, the attenuation is slower than the  $1/r$  geometrical attenuation since the shape of the wave changed from the spherical-type wave to the plane-wave-type wave.

Finally, a full simulation was put together with the physical attenuation. Densities of the soil, velocities, and attenuation  $Q$  factors were taken from Table 3.5. An array of several isotropic point sources of the  $200\text{-Hz}$  toneburst mimicking the soft-soil vibrator used by Owen Engineering Services was positioned at the surface of the ground and excited along the  $x$ -axis. The propagation was simulated in the physical volume of the size  $400\text{ cm} \times 400\text{ cm} \times 366\text{ cm}$ . The amplitudes of the wave were measured at depths incremented by  $50\text{ cm}$ . The results of the values of the amplitudes at different depths, normalized to the amplitude at the source, are shown in Figure 3.50. They are compared, in the same figure, with the results without the physical attenuation. The overall attenuation increased, but

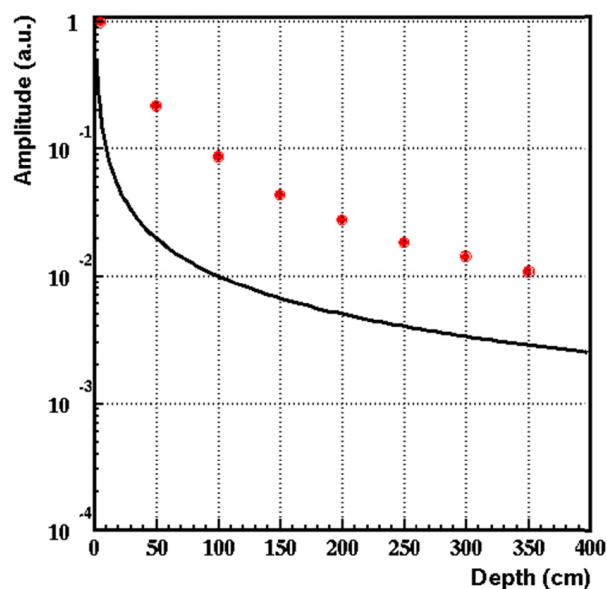


**Figure 3.49.** Values of the 200-Hz toneburst's amplitudes at different depths, MicroVib source (normalized to the amplitude at the source compared with the geometrical  $1/r$  attenuation; the source of the wave was the soft-soil Owen vibrator).

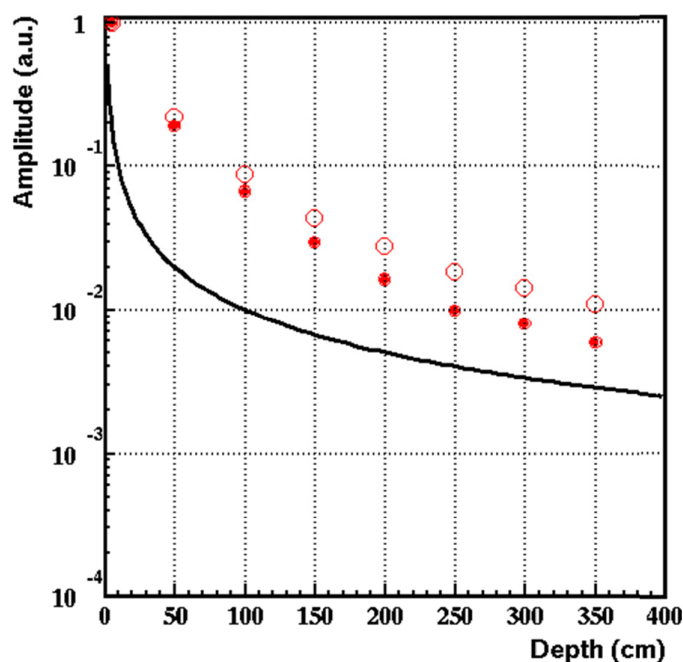


**Figure 3.50.** Values of the 200-Hz toneburst's amplitudes at different depths, MicroVib source and physical attenuation (normalized to the amplitude at the source compared with the geometrical  $1/r$  attenuation; the source of the wave was the soft-soil Owen vibrator).

since the Q values are large, the attenuation did not increase as much as expected.

To test the attenuation dependence on the wave frequency, the propagation of 400-Hz and 800-Hz tonebursts was simulated. As in the case of the propagation of the 200-Hz toneburst, densities of the soil, velocities, and attenuation Q factors were taken from Table 3.5. An array of several isotropic point sources was positioned at the surface of the ground and excited along the  $x$ -axis. The propagation was simulated in the physical volume of the size 400 cm  $\times$  400 cm  $\times$  366 cm. The amplitudes of the wave were measured at depths incremented by 50 cm; and the results of the values of the amplitudes at different depths, normalized to the amplitude at the source, were reviewed for 400-Hz tonebursts and 800-Hz tonebursts.

As expected, since the attenuation of the wave increases with frequency, a significant decrease in the wave amplitudes was observed when the wave frequency increased. The 800-Hz toneburst propagation is shown in Figure 3.51. When compared with the propagation of the 400-Hz toneburst, the attenuation is unexpectedly lower. Since the wave is produced by a source array, this may be attributed to a narrower beam width for higher frequency. In the final test, the attenuation of the 1,200-Hz toneburst was compared with the attenuation of the 800-Hz toneburst; and, as expected, a significant decrease in the wave amplitudes was observed for a higher frequency. It was also observed that the beam width got narrower with higher frequency.

The simulation of the signal attenuation for the pulsed source was done using the shear wave excited in the form of a very smooth bump along the  $x$ -axis on the surface of the ground. All the other parameters were the same as in the simulation of the tonebursts. The pulse shape and power spectrum of this pulse are shown in Figure 3.52. The amplitudes of the pulse in the form of a very smooth bump were measured at depths incremented by 50 cm. The attenuation was comparable to the attenuation of the 200-Hz to 300-Hz tonebursts.

Finally, LTU simulated the signal attenuation after reflection from a target. The soil parameters and the geometry were kept the same as in the case of no target. The full 3-D simulation of the propagation of shear waves was performed in a volume equaling 400 cm  $\times$  400 cm  $\times$  367 cm. The shear wave was excited in the form of the very smooth bump shown in Figure 3.52. The source was the soft-soil vibrator. The pulse was reflected from plastic pipe that had a diameter of 2 ft and was positioned 250 cm under the surface of the soil. For the plastic pipe, the P-wave velocity was 2,458 m/s, and the S-wave velocity was 1,164 m/s, with no signal attenuation inside of the pipe. The propagation of the pulse is shown in Figure 3.53.

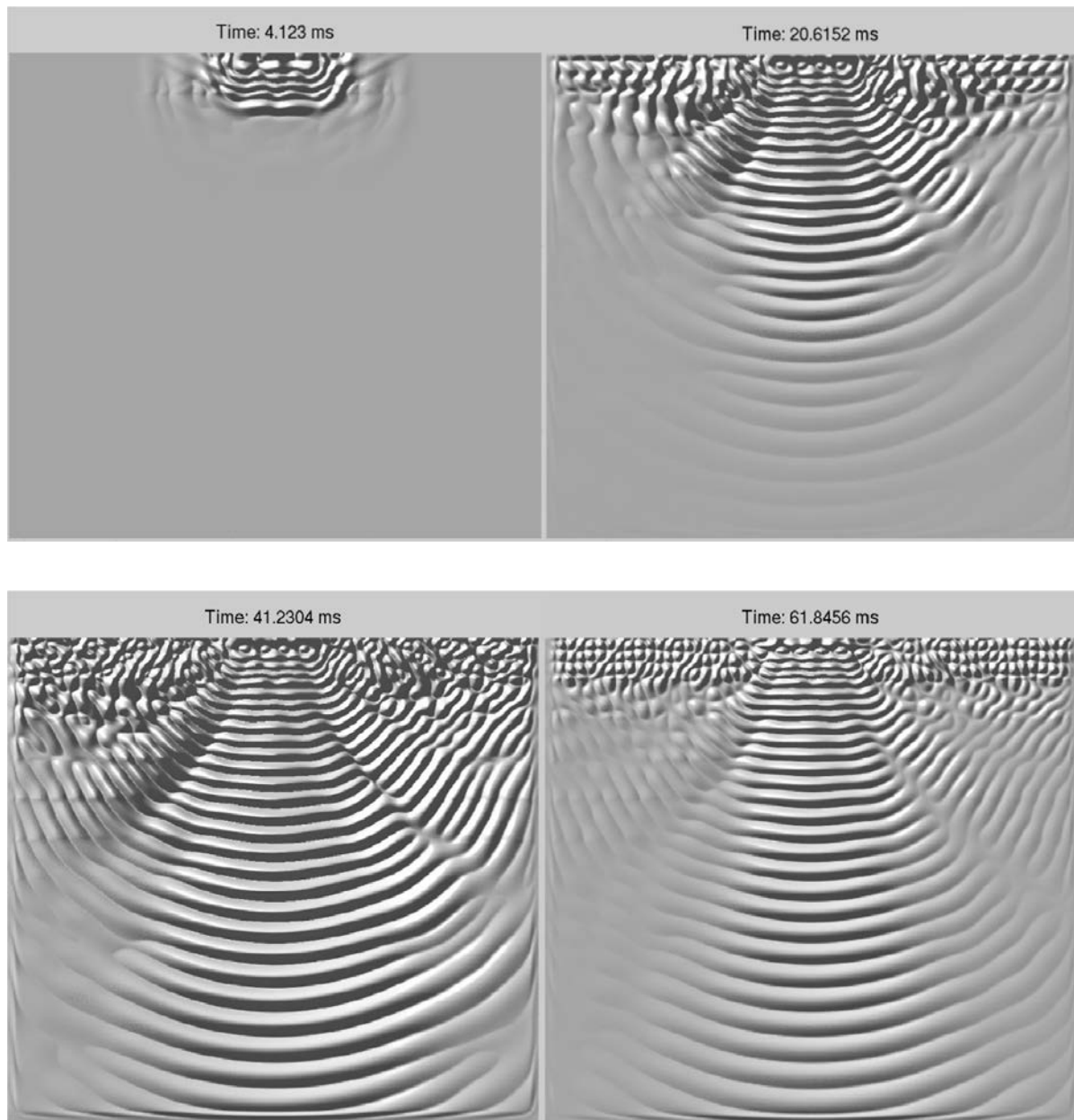


**Figure 3.51.** The propagation, in  $x$ - $z$  plane, of the  $x$ -component of the 800-Hz toneburst. (The animation is at <http://www.phys.latech.edu/~neven/uit/final>.)

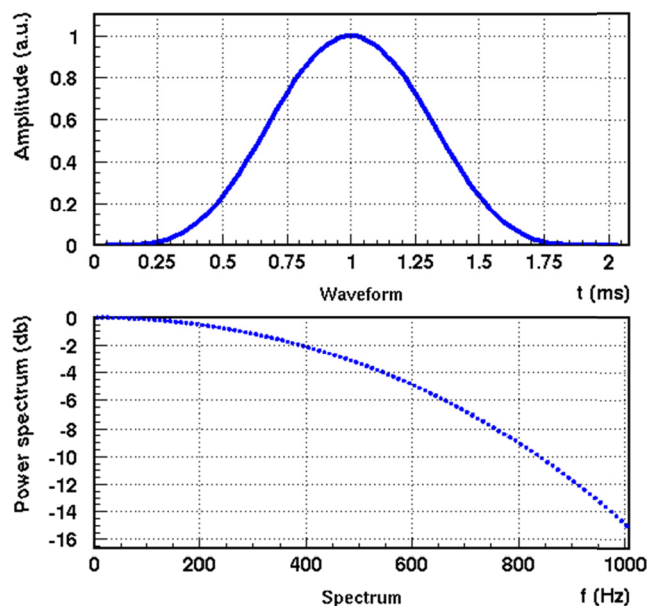


**Figure 3.52. Shape and power spectrum of a very smooth bump (the frequency parameter,  $\omega$ , for this pulse was 500 Hz).**

Figure 3.53 and the accompanying animation show that the reflected signal is clearly visible. They also show that the strength of the reflected signal is on the order of the magnitude of physical and numerical background.

The attenuation of the reflected signal was studied by performing two simulations: with the target and without the

target. The amplitudes of the pulse were recorded at depths incremented by 50 cm. The physical and numerical background was subtracted from the signal. The difference between the amplitudes with no target is shown in Figure 3.54. The reflected amplitude is clearly visible at the depth of 150 cm (at the time 23 ms); its value is comparable to the background at the depth of 100 cm (at the time 26 ms) and becomes less than the background at the depths of 50 cm and 0 cm. While the reflected signal could be resolved with multiple sensors and sophisticated signal processing, the goal here was to estimate signal attenuation.

To avoid complicating signal processing, the attenuation of the reflected signal was estimated in three steps:

1. The attenuation from the surface of the ground to the depth of 150 cm is calculated from the values of the amplitudes of the 500-Hz smooth bump at different depths when physical attenuation was included and found to be **~35 dB**.
2. The attenuation due to the reflection is calculated by comparing amplitudes of the 500-Hz smooth bump at different depths when physical attenuation was included with the information from Figure 3.54 and found to be **~7 dB**.
3. The attenuation from the depth of 150 cm back to the surface of the ground is again **~35 dB**.

The total attenuation of the signal for the reflection of a pulse shown in Figure 3.52 from a 2-ft-diameter plastic pipe

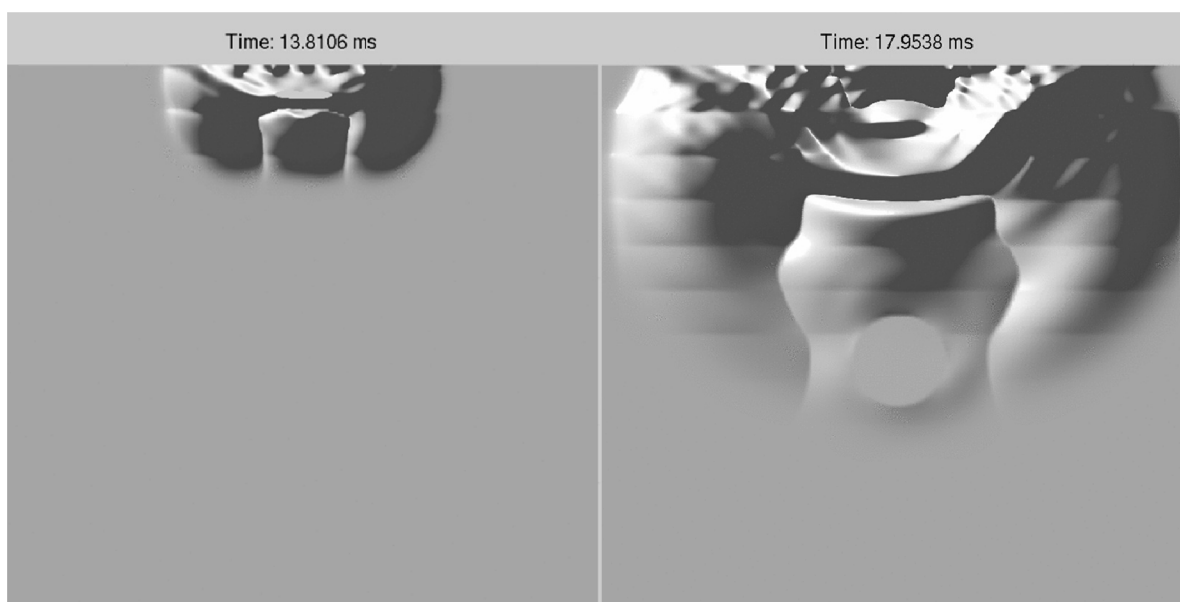


**Figure 3.53. The propagation and reflection of the x-component of the S-wave excited in form of a smooth bump with attenuation. (The animation is at <http://www.phys.latech.edu/~neven/uit/final/>.) (Continued on next page.)**

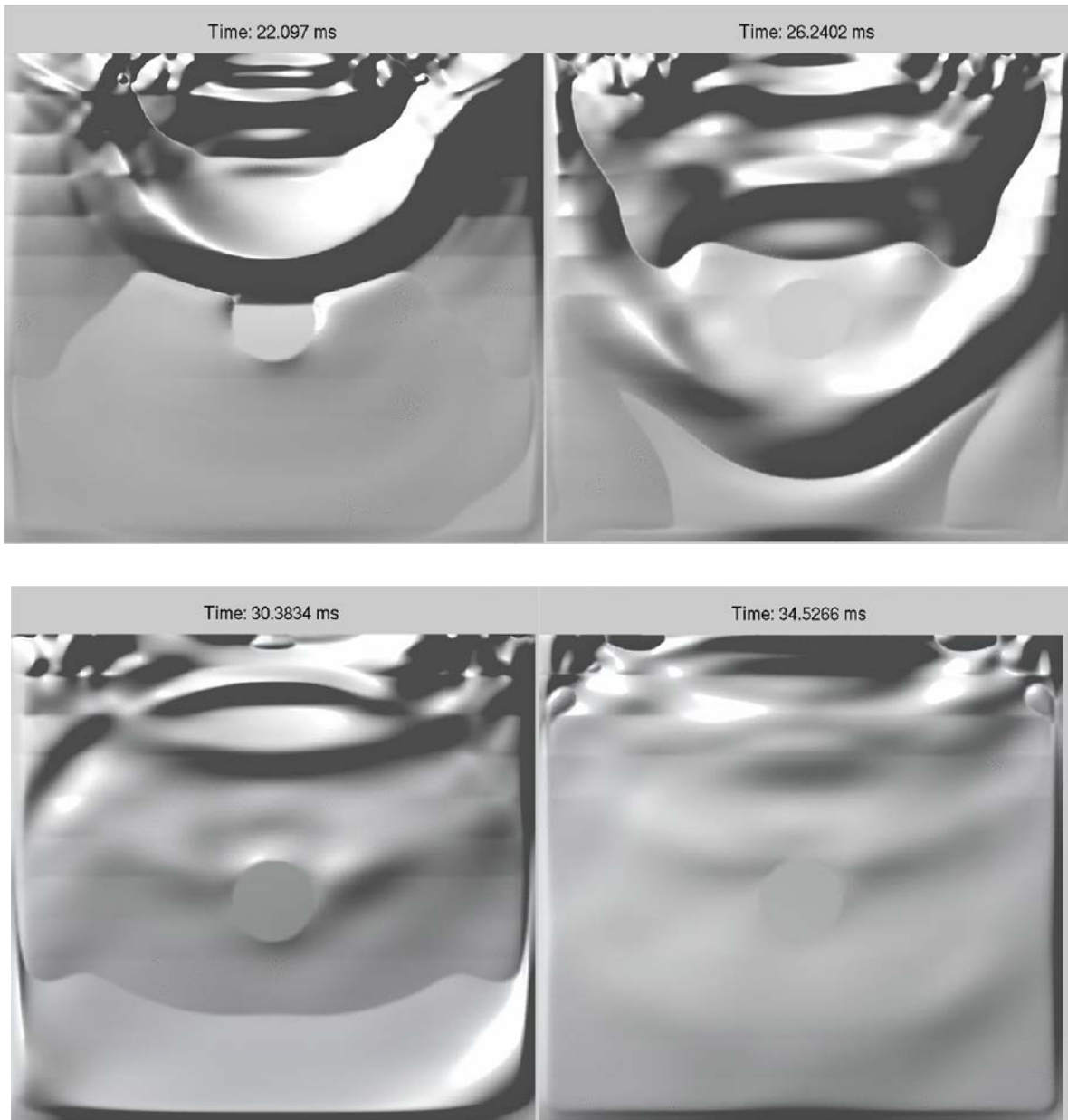


**Figure 3.53.** *The propagation and reflection of the x-component of the S-wave excited in form of a smooth bump with attenuation. (The animation is at <http://www.phys.latech.edu/~neven/uit/final/>.) (Continued from previous page.)*

2 m under the ground is estimated to be  $\sim 77$  dB. The simulation for a 1-ft-diameter plastic pipe 2 m under the ground showed that the total attenuation was  $\sim 87$  dB.

While the simulations of the propagation of the pulses in the form of a very smooth bump and the reflection from 2-ft- or 1-ft-diameter plastic pipes buried 2 m under the ground are only some of the possible cases, they were a testing foundation for all the tools needed in the simulation. The tools required to carry out the simulations include the software, a proper description of the source, a proper description of the properties of the soil and the target, and a proper description of attenuation. This case also showed that the simulation requires

access to state-of-the-art supercomputers, but the computation can be performed in a reasonable amount of time.

### Signal Processing and Analysis Method

The results from the simulation of pulse propagation were also used for testing possible signal processing and analysis and target recognition. The position of the buried pipes could be determined from the time series of the values of the displacement, or its time derivatives, at chosen points in space under or on the ground. In the case tested here, the imaginary motion sensors were positioned on the ground, as shown in

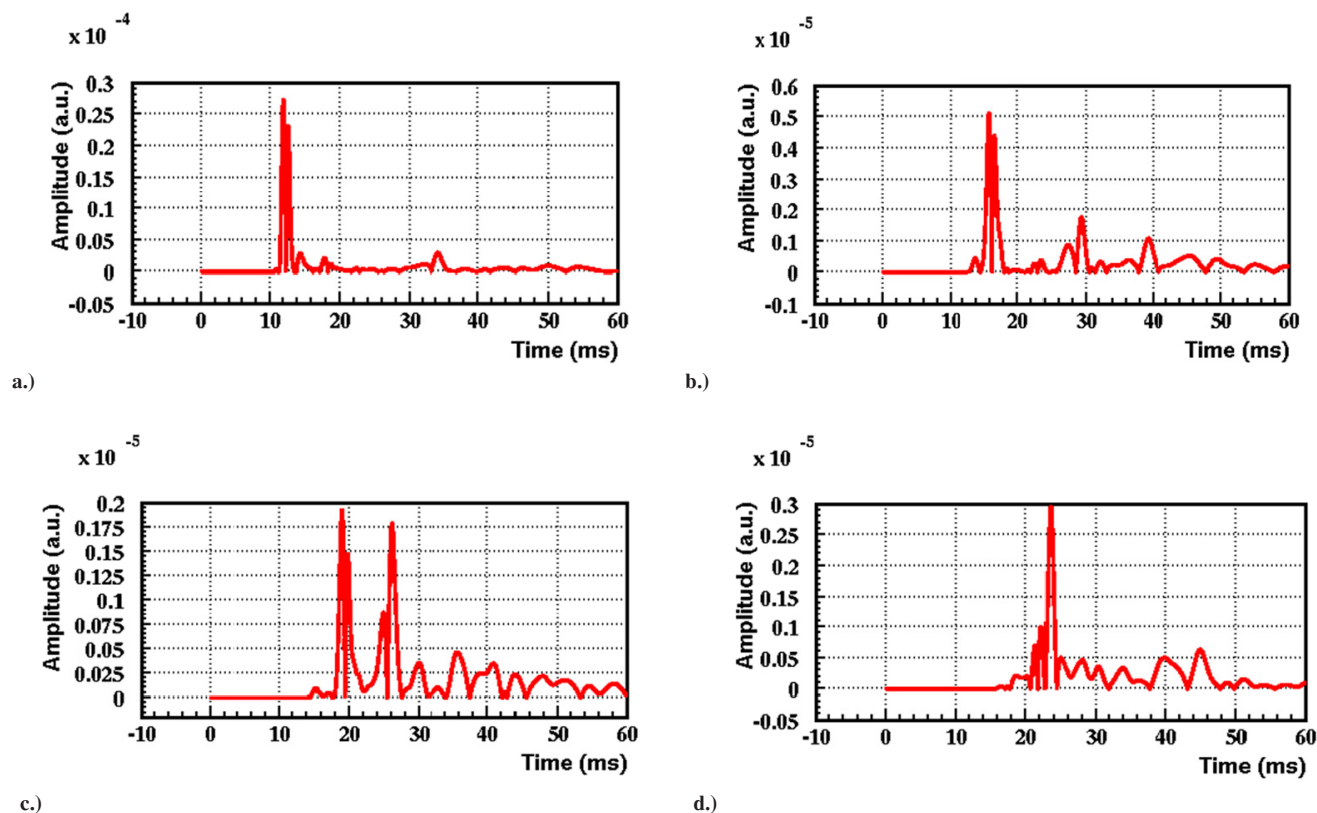


**Figure 3.54.** Values of the background-subtracted amplitudes of the 500-Hz smooth bump reflected from target [target is 2-ft-diameter plastic pipe; depths are (a) 0 cm, (b) 50 cm, (c) 100 cm, and (d) 150 cm; MicroVib source].

Figure 3.39. The amplitude of the displacement and the time of arrival of the reflected pulse were recorded at those positions through the entire simulation run.

In the case of a pulsed source, the position of a pipe could be determined from the values of the displacements and their time of arrival. The possible methods used in electromagnetics to estimate the position of a target, but applied here for the reflection of the elastic pulses, are shown in Figure 3.55. The method used to determine the positions of the buried pipes was based on the difference of the time

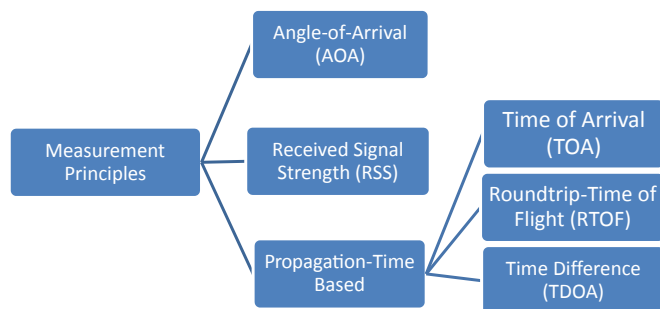


**Figure 3.55.** Localization methods used with ultra-wideband electromagnetic pulses (Vossiek et al. 2003).

propagation of the transmitted and reflected signals from different sensors.

Because the distance between the target and a particular sensor is different, the round-trip time of flight of the signal is also different; as a consequence, the time of signal arrival can be used to locate the target. There are two possibilities: round-trip time of flight (RTOF) or time difference of arrival (TDOA). In the case of RTOF, the position of the target is obtained as a point of the intersection of sphere sizes that are determined from the round-trip time of flight and the speed of propagation of the elastic pulse. In the case of TDOA, the position of the target is obtained by the intersection of hyperboloids; the size of each hyperboloid is determined from the difference of the time of the signal arrival to different receivers.

The method of choice described in this report is the time difference of arrival. The advantage of using the TDOA method instead of RTOF is the less-strict requirements on the transceivers' clock synchronization.

The position of targets using the TDOA method was obtained by determining the time difference in the arrival of the reflected signal between different receivers. The points in space corresponding to the same TDOA between two receivers define a hyperboloid, the size of which is determined by the difference in the time of signal arrival. Different pairs of

receivers define different hyperboloids, and the point of their intersection defines the position of the target.

### Verification of TDOA Method

Many simulations were performed to demonstrate the adequacy of the TDOA method. The results of some of the performed simulations, starting from a simple one-pipe case to a more complicated two-pipes case, are described in this chapter. The simulations were performed without the inclusion of the physical attenuation of the signal in the soil.

The TDOA of the reflected signal between different receivers was found by first calculating the pair-wise cross-correlation of the signals. The TDOAs corresponded to the maxima in the cross-correlation. In a 2-D space constant, TDOA defines a hyperbola. The position of the target is obtained by the intersection of hyperbolas corresponding to different TDOAs between different receivers.

In the first simulation, the pulse propagated through the soil and was reflected from a plastic pipe that had a 1-ft diameter and was positioned at a depth of 125 cm. The P-wave velocity of the soil was 432 m/s, and the S-wave velocity was 214 m/s. For the plastic pipe, the P-wave velocity was 2,458 m/s, and the S-wave velocity was 1,164 m/s. The density of the soil was 1,650 kg/m<sup>3</sup>, and the pipe was 1,400 kg/m<sup>3</sup>. The computed *x*- and *z*-components of the elastic wave displacement propagation for this case are shown in Figures 3.56 and 3.57. The position of the buried pipe was obtained using the TDOA method. It is shown as color contours in Figure 3.58 and is superimposed to the exact pipe position shown as a black circle. To determine the position, the data from five receivers were used. The *x*- and the *z*-components of the elastic wave displacement were tested; and, for this situation, the *z*-component showed a better position determination.

The case of two buried pipes is more complicated. The pipes were positioned at depths of 2.0 m and 1.5 m—1.0 m left and 1.0 m right of the transmitter. The positions of buried pipes, obtained using the TDOA method, are shown as color contours in Figure 3.59 and are superimposed to the exact pipes positions shown as black circles. The simulation described in this report demonstrated that the TDOA method was able to resolve two buried pipes positioned at different depths under the ground.

### Modeling Summary

WPP is written to take advantage of parallelization in a high-performance computing (HPC) environment, and the Louisiana Optical Network Initiative (LONI) provides a powerful HPC environment for using WPP. WPP comes with a repertoire of test scenarios that both demonstrate how the WPP may be used and provide checks as to whether WPP is

running correctly. To date, the WPP scenarios that have run on LONI have been the default Lamb's problem WPP test scenario and an adaptation of a scenario that modeled a pipe.

In the case of the pipe scenario, a large amount of time was devoted to devising tools for the postprocessing of the output files from WPP scenarios. While WPP does supply a collection of basic MATLAB scripts for visualizing its output, these scripts do not form a complete tool by themselves and are weakly documented. In the interests of performance and scalability to large data sets, a C++ program was written to perform the postprocessing tasks.

The postprocessing program addressed two major visualizations of the data generated from a single WPP run. Using WPP's output image files, the program can make movies and images of cross sections of the computational domain in different scenarios. WPP also outputs sac files, which are files that contain the entire history of the simulation from the perspective of a single point in the computational domain. Using these files, the postprocessing program can plot the histories for a given component of the computational domain (*x*, *y*, and *z*) at a particular location in the computational domain, or make movies of a series of such histories sampled along a path (presently a line) in the computational domain.

The postprocessing program depended on two third-party libraries. MathGL was used to perform plotting and graphics, and some of the libraries in the Boost C++ libraries were used on several computational tasks that show up during the postprocessing. The postprocessing program depended on a single third-party software, FFmpeg, which is used via system calls to produce movies.

## Advanced TDEMI System Status and Findings

The SHRP 2 R01B time-domain electromagnetic induction (TDEMI) component of research is also an innovative approach to digital geophysical mapping. The primary objective was to develop a functional, advanced, sensor coil array prototype that continuously and dynamically records accurately positioned TDEMI geophysical data based on user set parameters and multiple coil configuration geometries. As mentioned before, the prototype TDEMI system was modeled after a first prototype version developed with other funding by SAIC and the U.S. Naval Research Laboratory. This 5-by-5 coil sensor array has proven to be very successful for unexploded ordnance (UXO) classification under static data acquisition conditions. These successful contributions to an alternate application increased demand for the technology in the munitions response community, thus limiting the resources available for developing the R01B system during the project life cycle. The plan was to leverage the technology in two ways: (1) by collecting test data using the existing

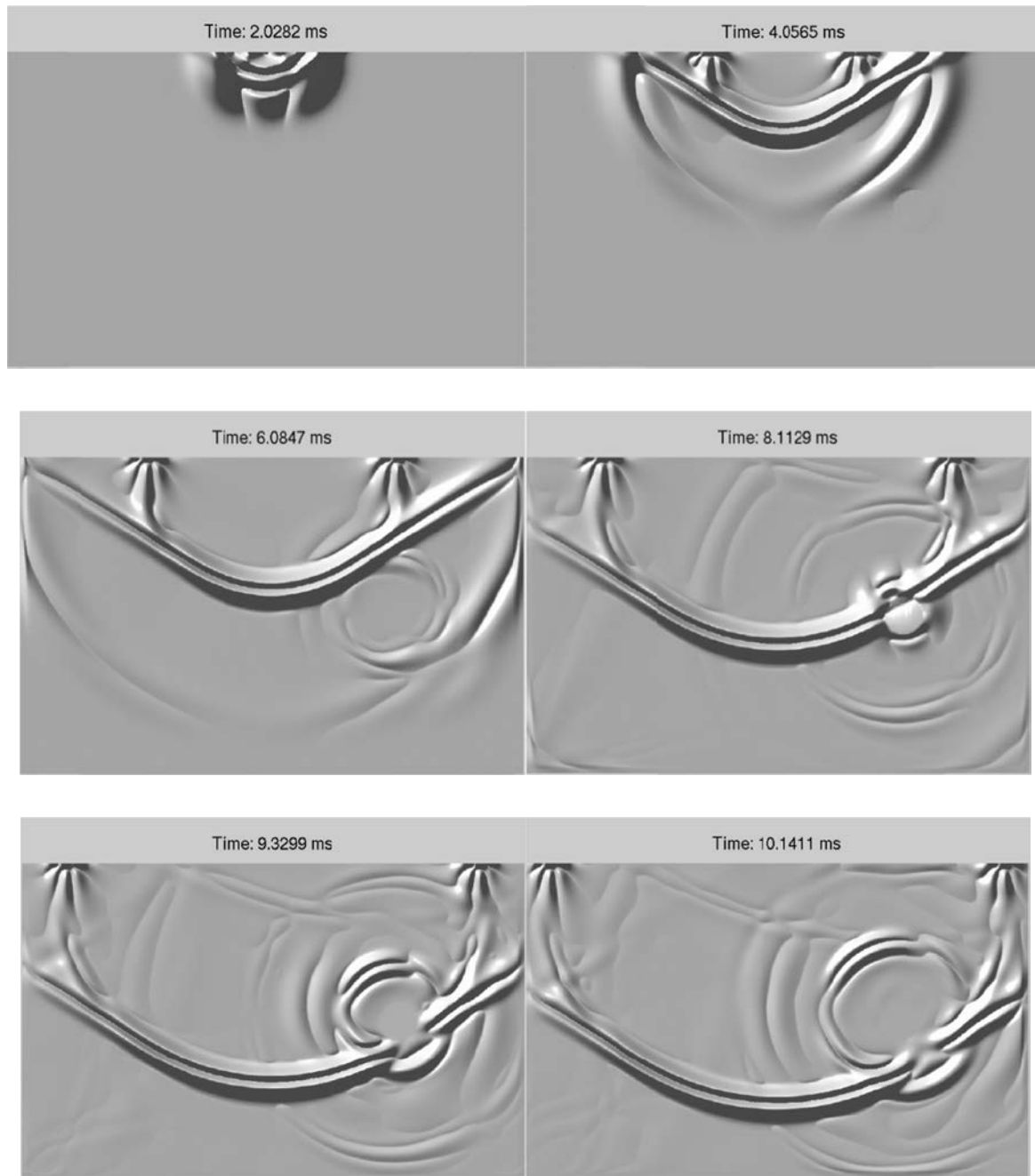


**Figure 3.56.** *The propagation through the soil and reflection from the plastic pipe of the x-component of the shear pulse. (The animation is at <http://www.phys.latech.edu/~neven/uit/final>.)*

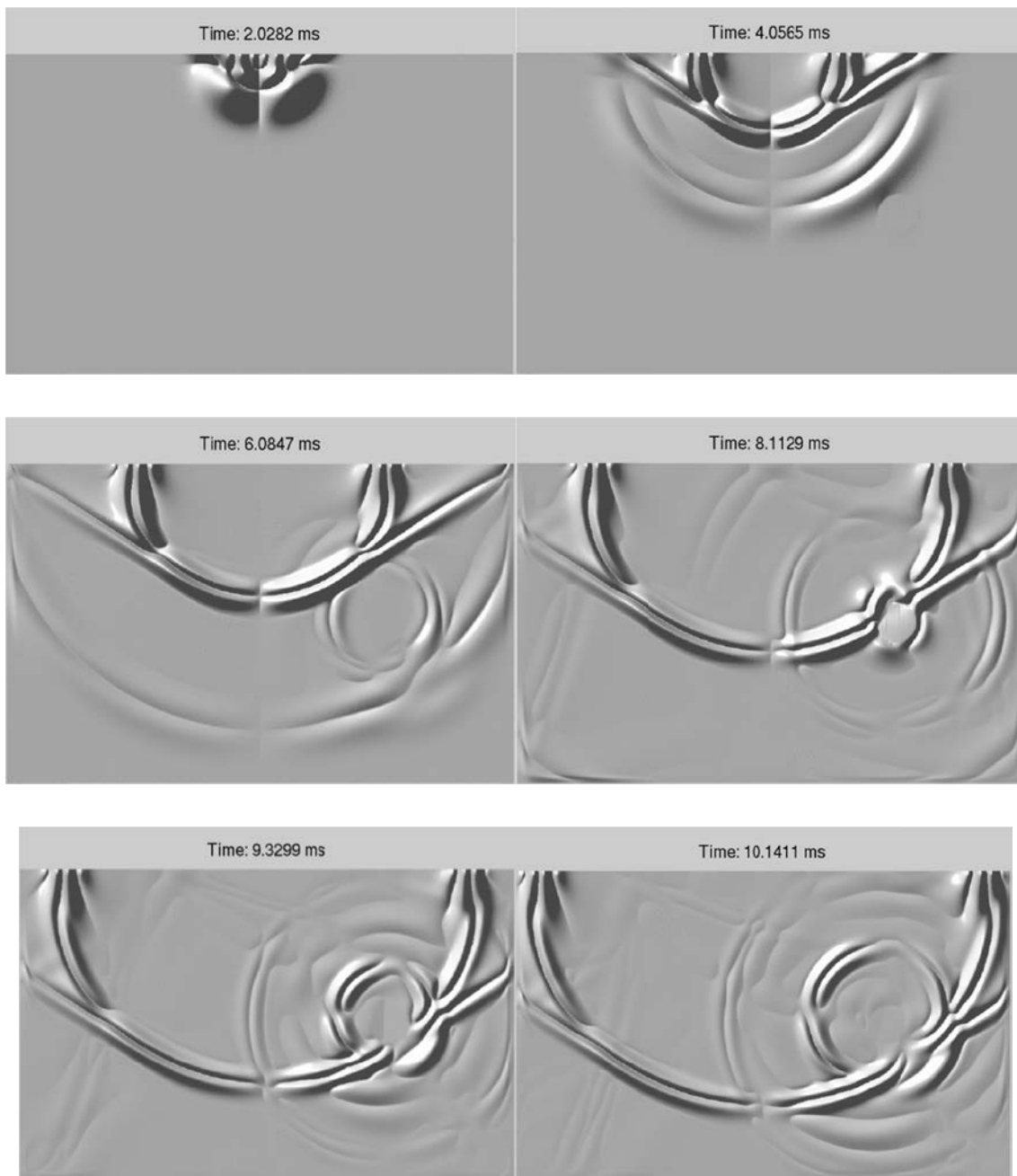


**Figure 3.57.** The propagation through the soil and reflection from the plastic pipe of the z-component of the shear pulse. (The animation is at <http://www.phys.latech.edu/~neven/uit/final>.)

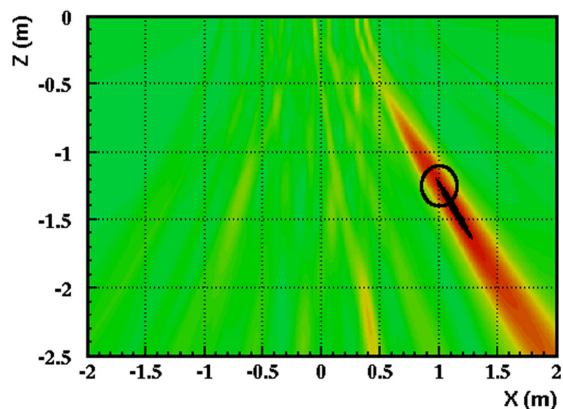


**Figure 3.58. Position of the buried pipe obtained using the TDOA method.**

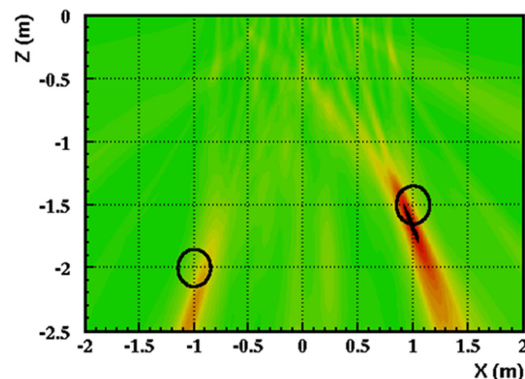


**Figure 3.59. Position of two buried pipes obtained using the TDOA method.**

5-by-5 array in the first prototype, and (2) by asking the developer to build a custom 5-by-1 array for integration for the SHRP 2 R01B EMI prototype. The TDEMI element of the R01B research work was performed by SAIC, G&G Sciences, and UIT, with support from Geosoft.

After some difficulties in construction and testing by the subcontractors, UIT received the system in November 2011, and initial testing has been performed. The instrumentation received is shown in Figure 3.60, including

- Five coils plus a spare;
- Five preamps plus a spare;
- Approximately 20 ft of cabling for five transmit-receive coils;
- National Instruments electronics box with embedded computer and analog-to-digital converter (A/D) card;
- G&G electronics box attached to National Instruments box;
- Power cables for National Instruments box and G&G box; and
- Package of National Instruments software and CDs.

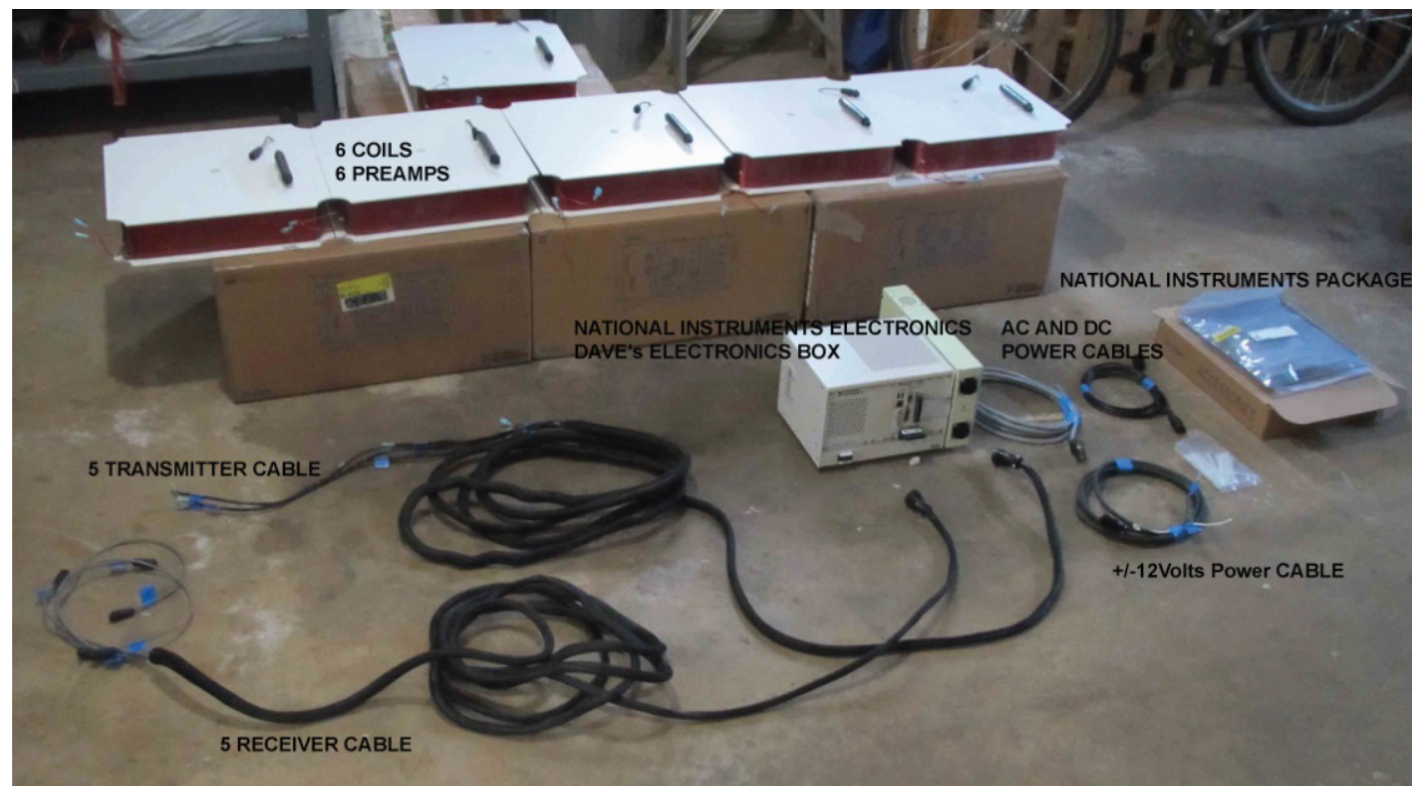


**Figure 3.60. TDEMI system instrumentation.**

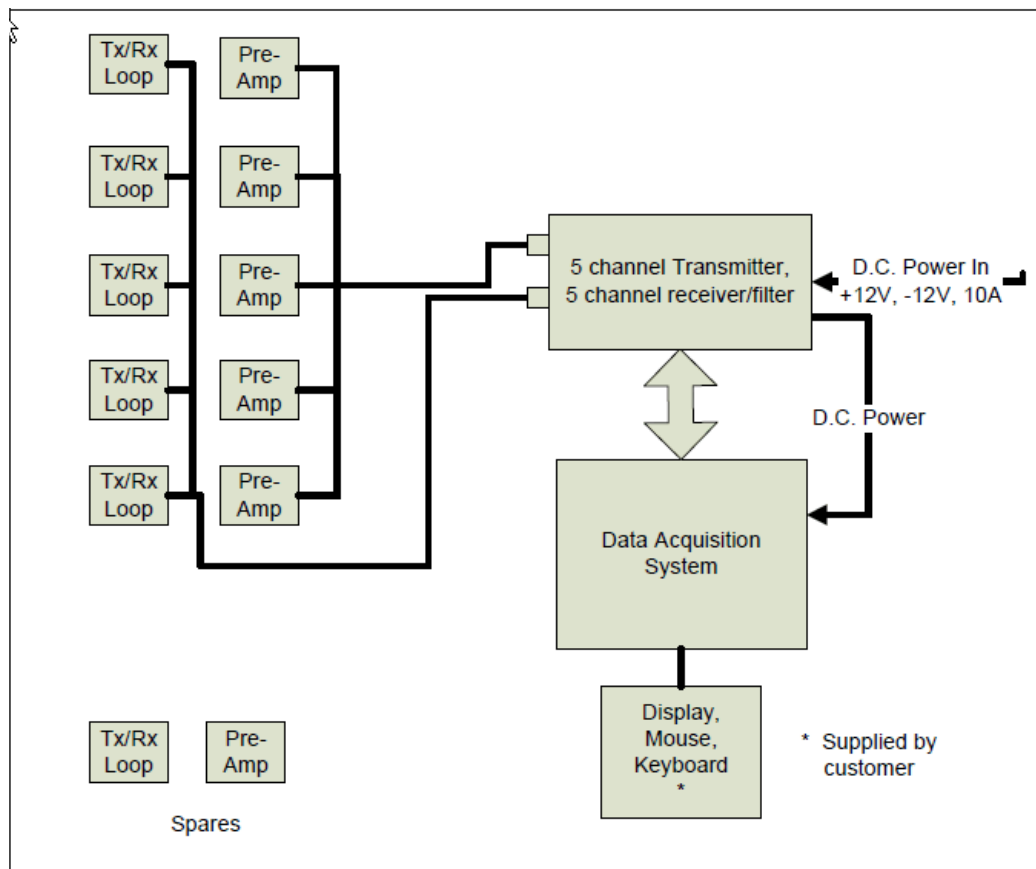


**Figure 3.61. Block diagram of the advanced TDEMI system.**

The system arrangement is shown in Figure 3.61. Equipment needed to run the system included the following:

- AC power or 18-30V DC for the National Instruments box;
- +12 and -12 volts for G&G box;
- Monitor, mouse, and keyboard (These were needed initially to set up networking on the embedded computer. Once the networking is configured, a laptop computer and a network cable can be used to “remote desktop” onto embedded computer.); and
- Data copied from the embedded computer using a USB thumb drive.

EM3D is the software program developed by G&G Sciences for data acquisition. It has the following characteristics:

- Multiple windows for configuration, mapping, and GPS features;
- EM3D window used to configure
  - Base file name;
  - Transmit pulse length, pulse repetition, and pulse stacking;
  - Single-shot or continuous operation; and

- Single transmit coil or all five transmit coils sequentially;
- EM3DPlot window used to plot collected data and to export binary \*.tem files to comma-delimited \*.csv files.

Screenshots of running program are represented in Figure 3.62.

### TDEMI Prototype Bench Testing

Before delivery of the system, G&G Sciences performed static bench testing to ensure system stability and expected functionality. Testing involved the analysis of decay curves, so calibration results are offered here. Plots of test data collected are shown in Figures 3.63 through 3.72.

- Data were collected with only the center transmitter firing and with all five transmitters firing sequentially.
- Data collection was performed as follows:
  - Single-shot with pulse on/off duration of 25 ms, nine repetitions of bipolar pulses, and the data collected and averaged three times. Total collection time for a single transmit coil is 2.7 s ( $0.025 \times 2 \times 2 \times 9 \times 3$ ). For all five transmit coils, the collection time is 13.5 s.

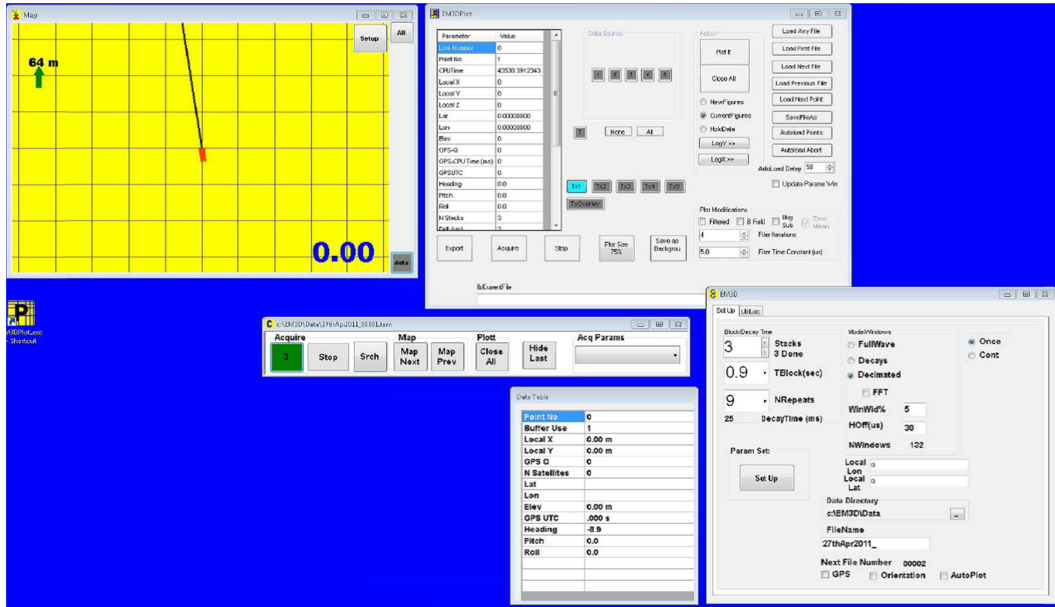


Figure 3.62. Screenshots of EM3D data acquisition software.

- ii. Continuous with pulse on/off duration of 8.33 ms, a single bipolar pulse, and no averaging. The time for a single transmit should be 33.33 ms ( $8.33 \times 2 \times 2$ ). For five transmits sequentially, the collection time is 0.16667 s.
- c. Figure 3.63 plots the single-shot transmit currents measured as coils 0 through 4 (left to right) sequentially fire. The currents vary slightly with coil and peak between 9 and 10 amps.
- d. Figure 3.64 plots the sequentially firing transmit currents as the array fires continuously. The transmit currents change slightly from shot to shot.
- e. To check that the five receivers were responding equally to the same signal, a 2-in.-diameter steel sphere was placed at a fixed distance above the center of each coil. Figure 3.65 plots the current normalized and background-subtracted

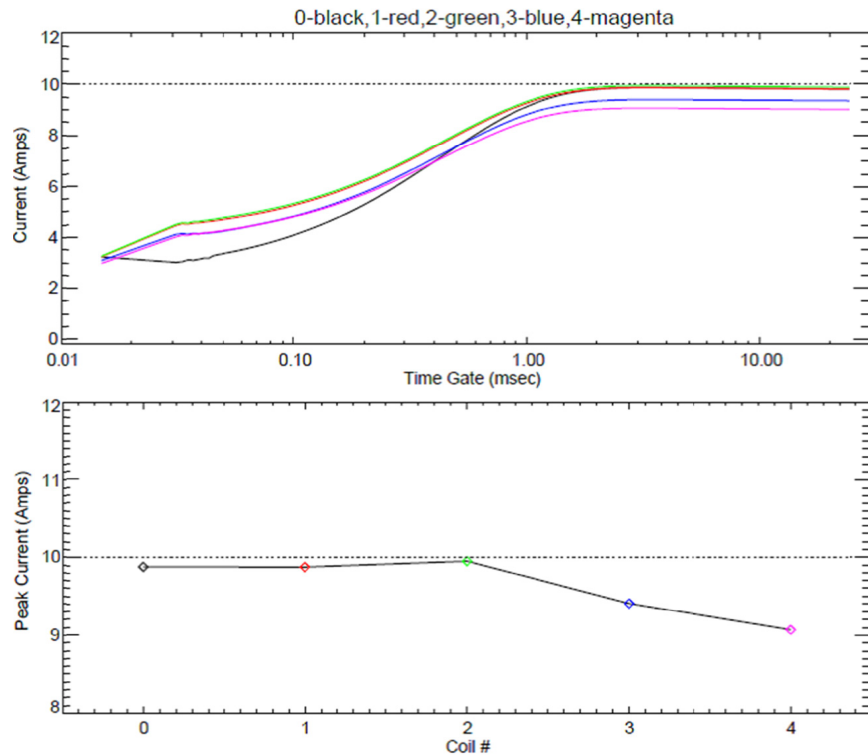
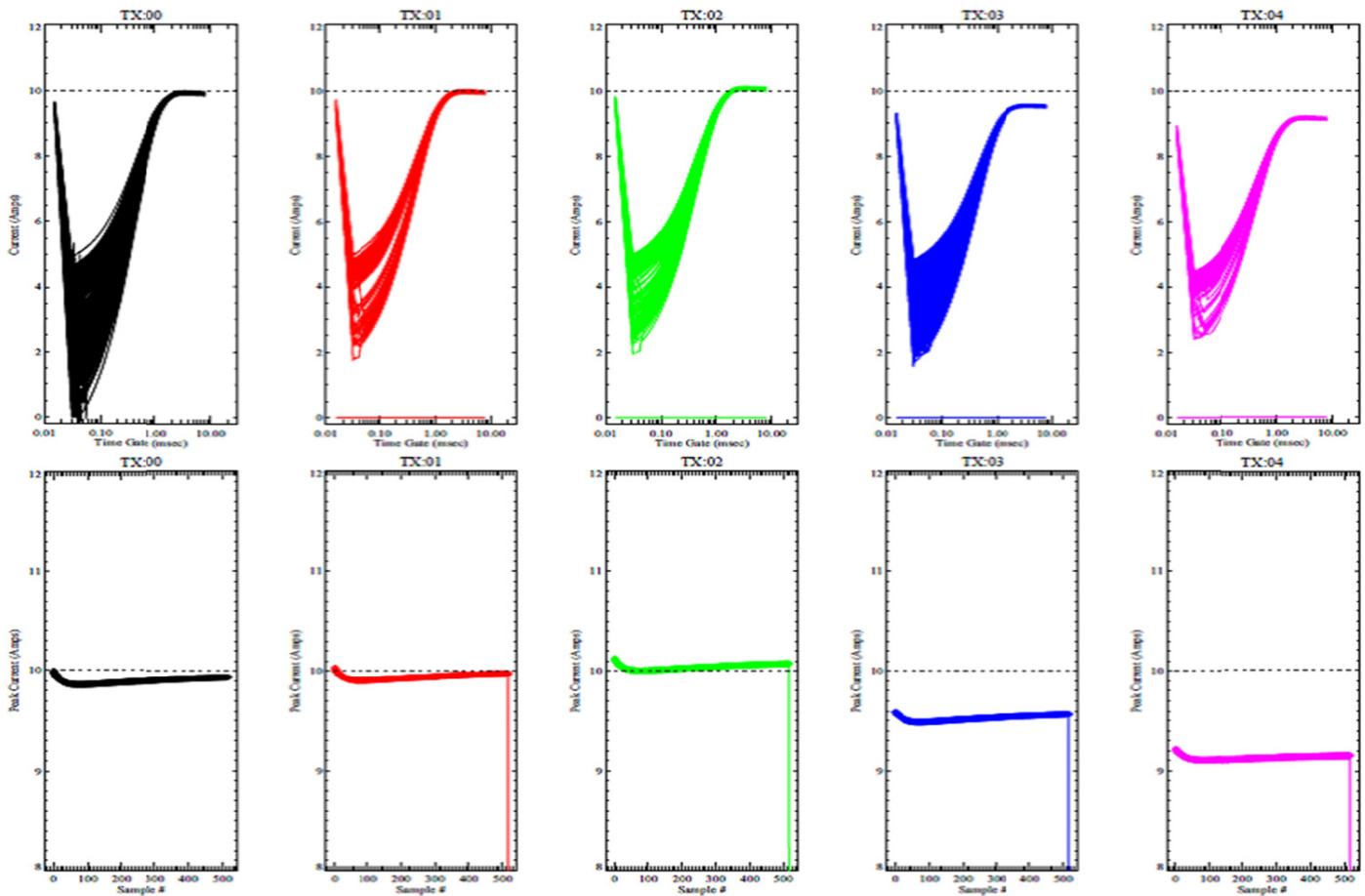


Figure 3.63. Single-shot, measured transmit currents.



**Figure 3.64. Continuous shots, measured transmit currents.**

receive signals for this sphere's data. The top plot shows the monostatic responses (same transmit-receive coil directly under sphere). The bottom plot shows the adjacent bistatic response (transmit under the sphere, receive coil to the left and/or right). The amplitudes are equal, and the array was well calibrated. Figure 3.66 plots the same sphere data in separate plots. The solid lines are positive

signal, and the dotted lines are negative. The consistent polarities indicate that all of the transmit-receive coils are wound in the same direction.

- f. Figure 3.67 plots the background signals measured on all 25 Tx-Rx pairs (array in the air and no metallic objects present). Note that there is significant ringing in the receive coil response to the transmit current turn-off in time gates

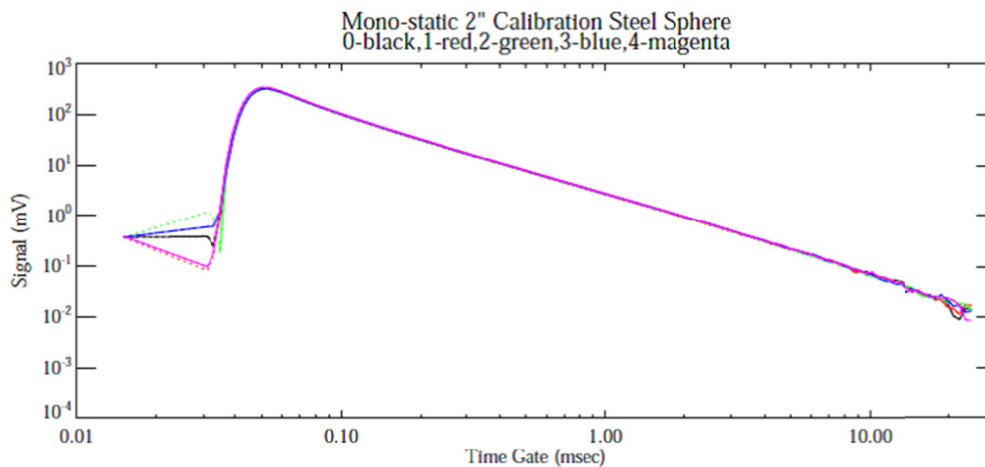


**Figure 3.65. Current normalized and background-subtracted receive signals for 2-in. calibration sphere. (Continued on next page.)**

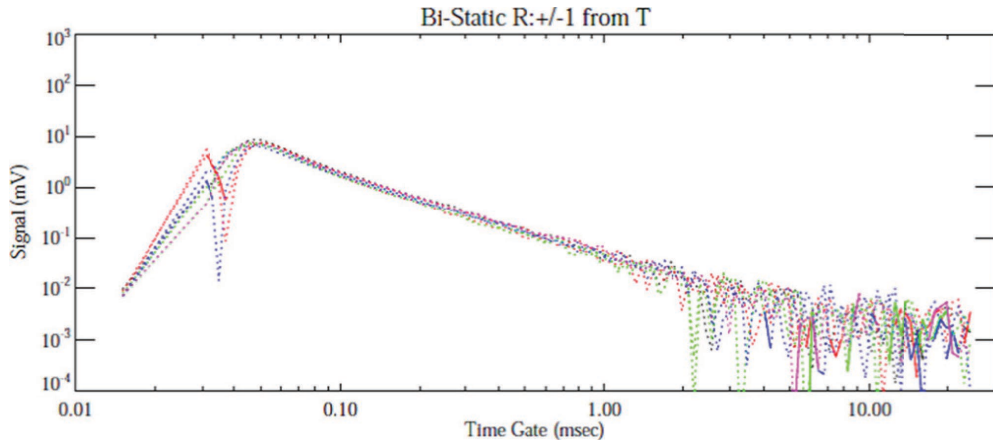


**Figure 3.65.** Current normalized and background-subtracted receive signals for 2-in. calibration sphere. (Continued from previous page.)

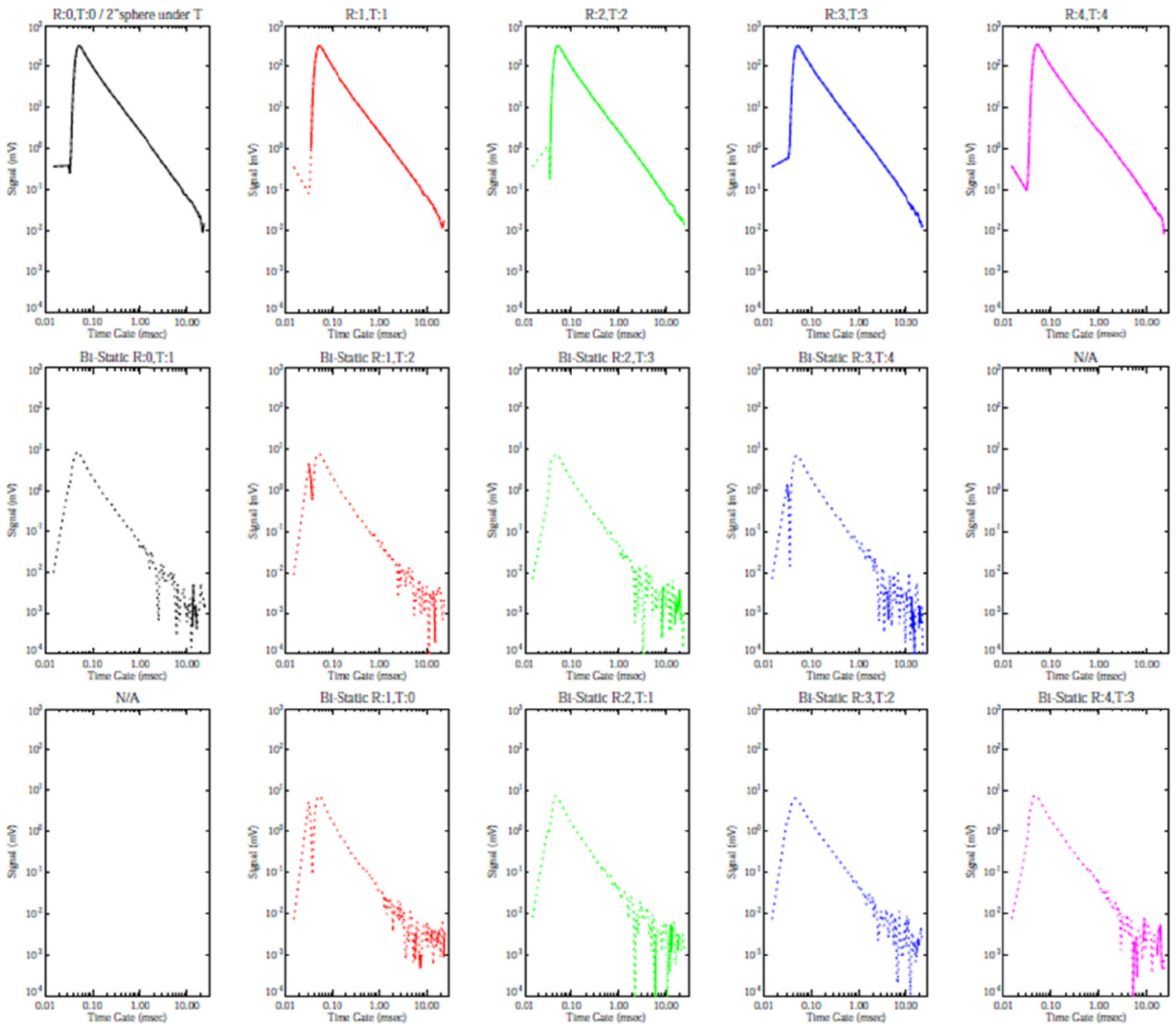


**Figure 3.66.** Two-inch calibration sphere above each transmit coil, mono- and bistatic terms.

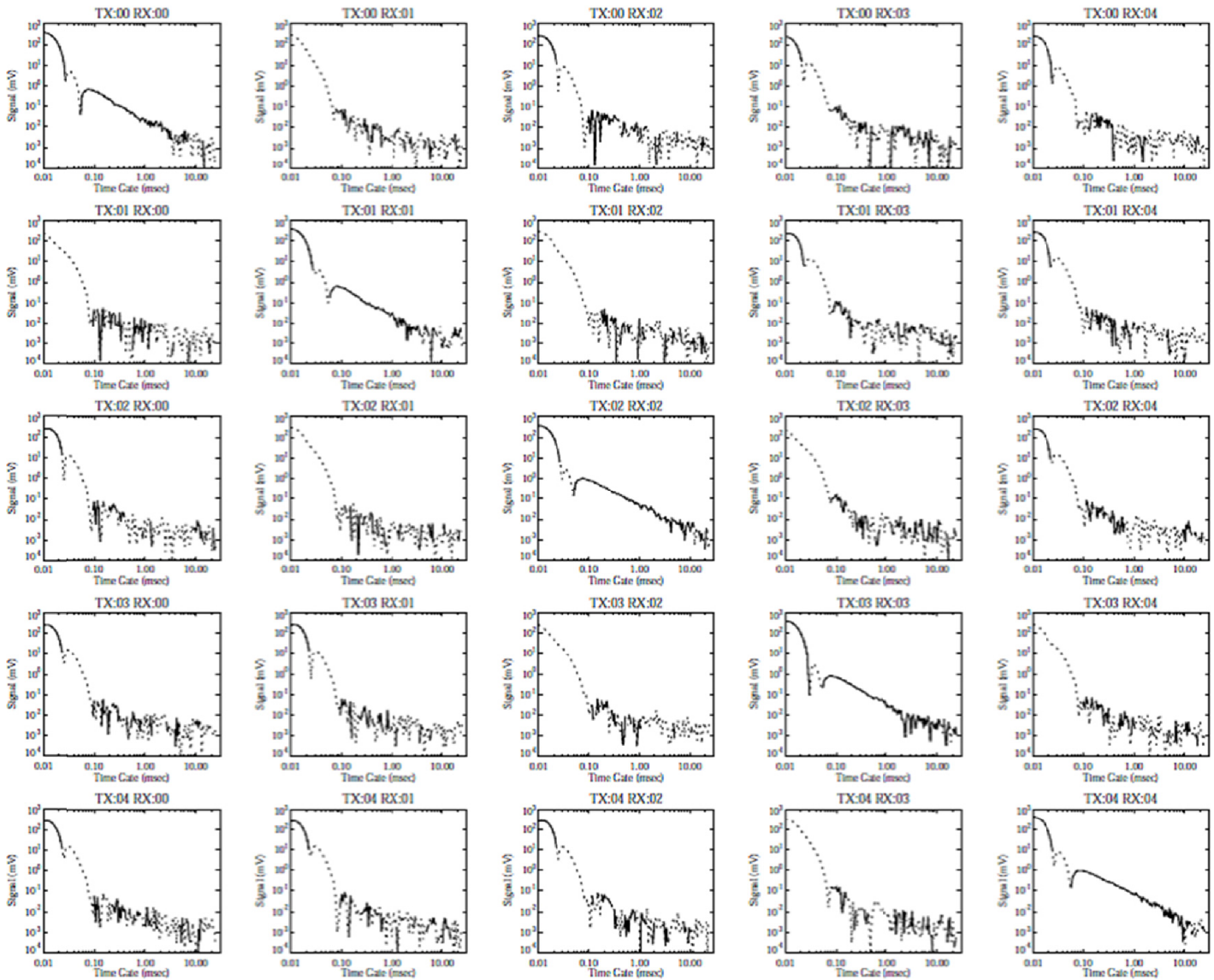


**Figure 3.67. Background signals measured on all 25 Tx-Rx pairs.**

- earlier than 0.100 ms (from millivolts to volts in amplitude). The monostatic pairs have measurable ringing even after this (tenths of a millivolt). The sensor noise levels are on the order of 0.01 millivolts in the later gates.
- g. Figure 3.68 plots the result of subtracting one background from one measured several minutes later. For early gates, the ringing varied slightly, and there was significant spurious signal present. After 0.100 ms, the background differencing process removed most of the sensor ringing and results in sensor noise levels on the order of 0.01 millivolts.
- h. Plots were generated for a collection of continuous background signals over periods of several minutes. The ringing response was the same as the single-shot data; the later noise levels were somewhat higher due to the lack of averaging.

- i. Figure 3.69 plots the result of subtracting the average background from continuous backgrounds. The noise in the later gates was closer to 0.1 millivolts.
- j. Figure 3.70 plots the recorded time between data samples for continuously collected data. The red symbols are for a single transmit coil firing constantly, and the black symbols are for all five transmit coils firing continuously in a sequence. The dotted lines are the expected data rates based on the pulse settings. It appears that there is some delay between each data collection.
- k. Figures 3.71 and 3.72 show the array signals from a 1-in.-diameter black steel pipe centered under coil 2 but orthogonal to the array. The pipe was 30 cm and 60 cm below the array. The data were collected in the single-shot mode with repeated pulses and averaging.

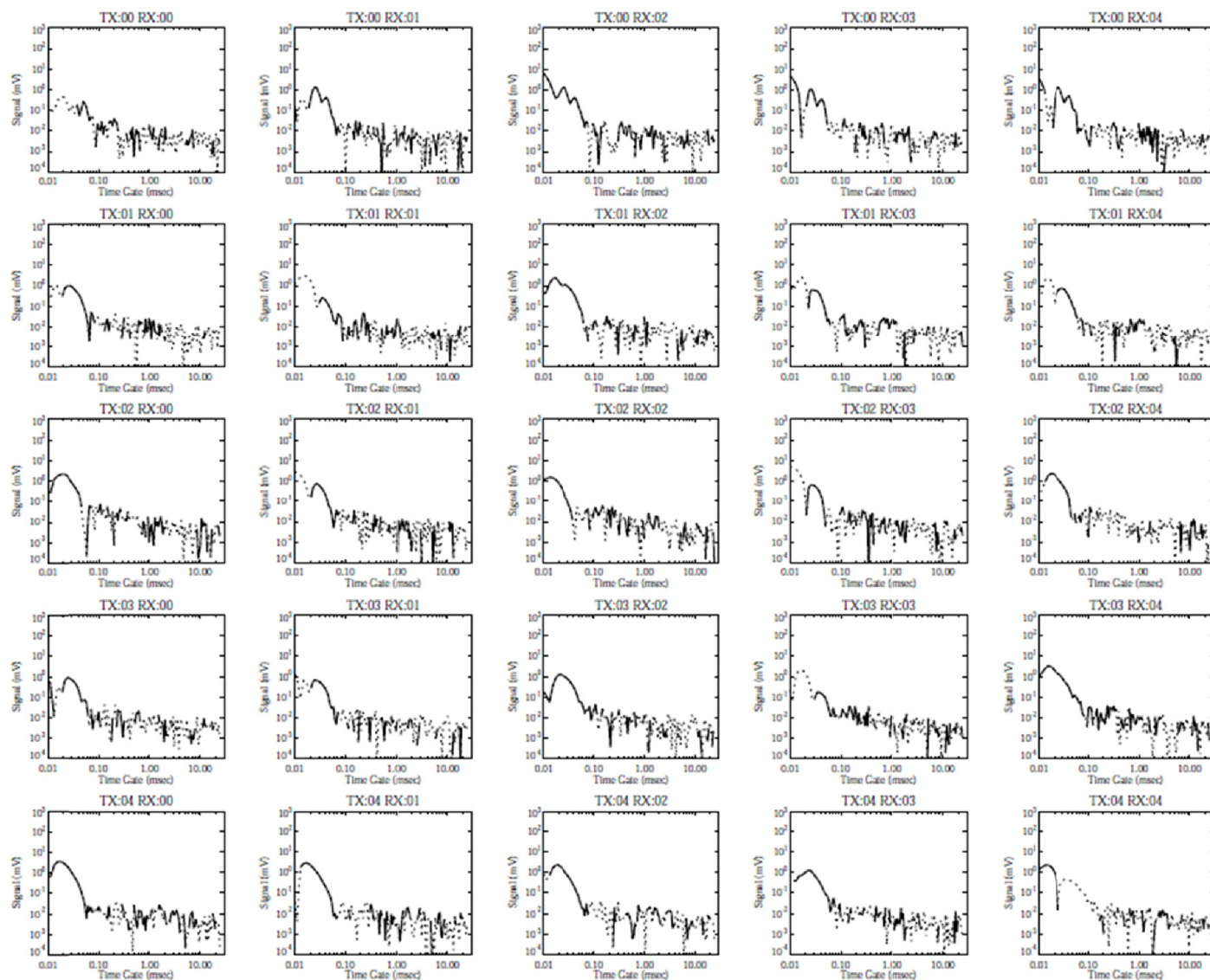


**Figure 3.68.** Signal shot measured on all 25 Tx-Rx pairs with differenced background.

These tests indicated that the system was performing comparably to the original NRL TEMTADS 5-by-5 EMI array. SAIC sent a representative to assist UIT in the setup of the sensor platform and to conduct basic training on the R01B TDEMI system prototype. The sensor array was prepared for data acquisition transport on UIT's existing metal-free trailer, as shown in Figure 3.73. The arrangement of sensors on the trailer offers a detection swath footprint of approximately 190 cm; the coils sit approximately 26 cm from the ground surface; and the GNSS antenna is centered on the sensor array and offset backward from the direction of acquisition travel approximately 35 cm. After assembling the power source and electronic connections, UIT conducted a series of static tests to become more familiar with the data acquisition software, the output data, and the general hardware configuration.

### TDEMI Prototype Data Acquisition Parameters

The parameters selected for initial testing of the TDEMI prototype with the EM3D program are presented in Table 3.6 and offer an explanation of user-defined characteristics of the acquisition software. The list of parameters is copied from the \*.AcqParams file. Delt is the data acquisition sampling rate in seconds. BlockT is the total measurement time in seconds. nRepeats is how many times the transmit cycle is repeated within BlockT. In this case, if one repeats nine times in 0.9 s, the transmit cycle is 0.1 s. Each transmit cycle consists of a bipolar pulse. With the Duty Cycle set at 50% (DtyCyc = 0.5), the transmit cycle consists of ¼th positive pulse, ¼th off, ¼th negative pulse, and ¼th off. So, in this case, the transmit pulse on time is  $0.1/4 = 0.025$  s, and the measurements made

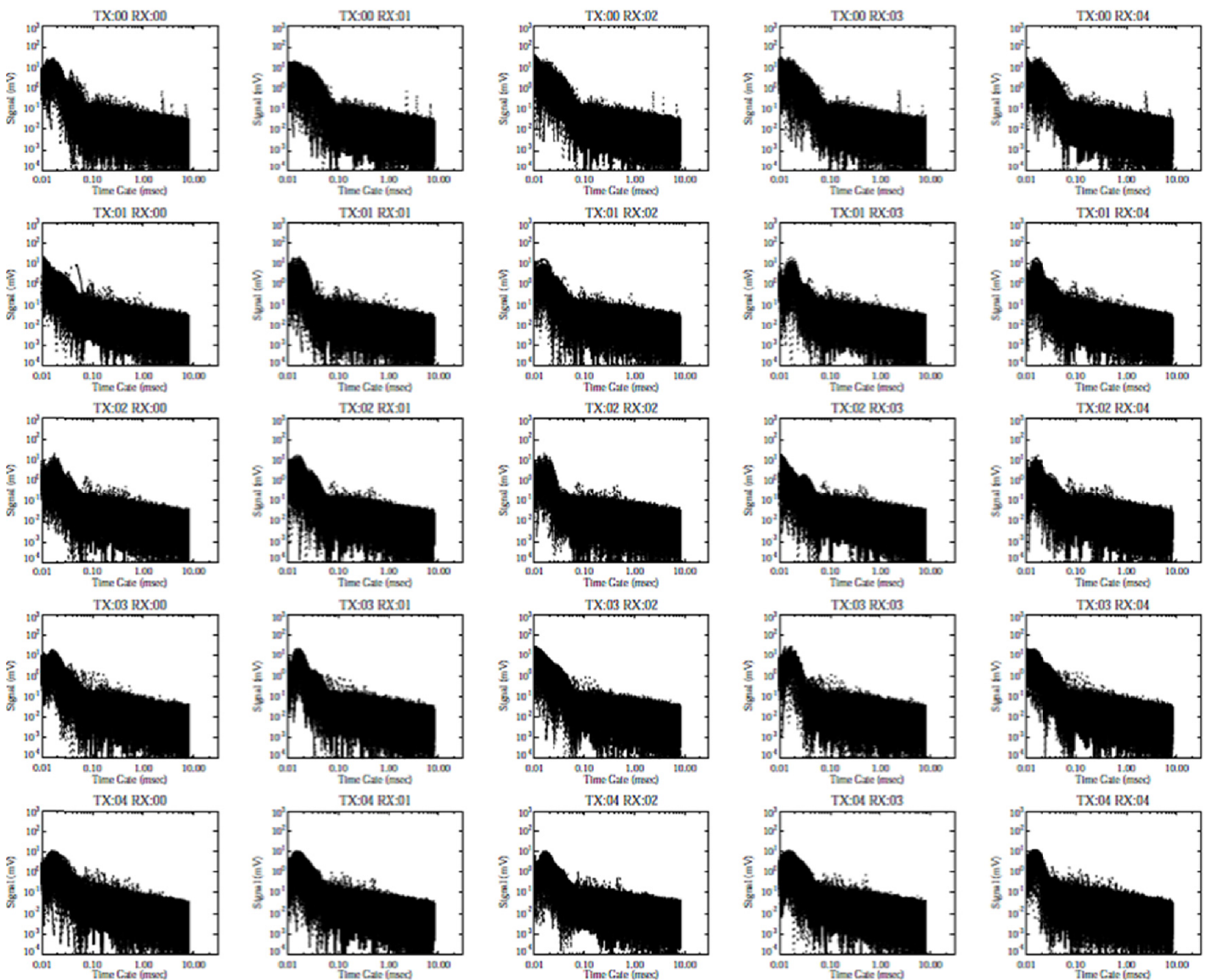


**Figure 3.69. Continuous data collection with background gate averages subtracted.**

while the pulse is off can only go out to 0.025 s. As one changes BlockT and nRepeats, one gets different pulse on/off times, which limits how late the time gates can go. A setting of BlockT = 0.1 and nRepeats = 1 would result in the same 0.025 on/off time and the same number of possible gates. A setting of BlockT = 0.03333 and nRepeats = 1 would only have a 0.00833-s pulse and gates out to 0.00833 s.

The parameter nStk just repeats the measurement that many times and “stacks” the result to provide averaging and reduce general noise. If BlockT is 0.9 s and nStk = 3, the total time to take a measurement is 2.7 s.

The AcqMode determines how the measurements made every 2.00E-06 over the total time block are averaged together. If AcqMode = FullWaveform, the entire set of measurements over BlockT is dumped. This setting is good for diagnosing

problems, but it generates very large data files. In some cases, it may lock up the program. If set to DecaysOnly, the off time period after the negative pulse is subtracted from the off time period after the positive pulse (this cancels 60-Hz noise sources but adds signal). If there are multiple repeats, these are averaged together; but the final averaged data are still dumped at the 2.00E-6 sampling. The files are still quite large. Again, this is good for diagnosing noise sources and equipment problems.

The third AcqMode is the one mostly used: DecaysDecimated. After dealing with the plus/minus pulse data and averaging over the nRepeats, the data are averaged over windows. The width of these windows is determined as a percentage by the parameter GateWid. A setting of 0.15 means the width of the window will be 15% of the time gate. This makes earlier

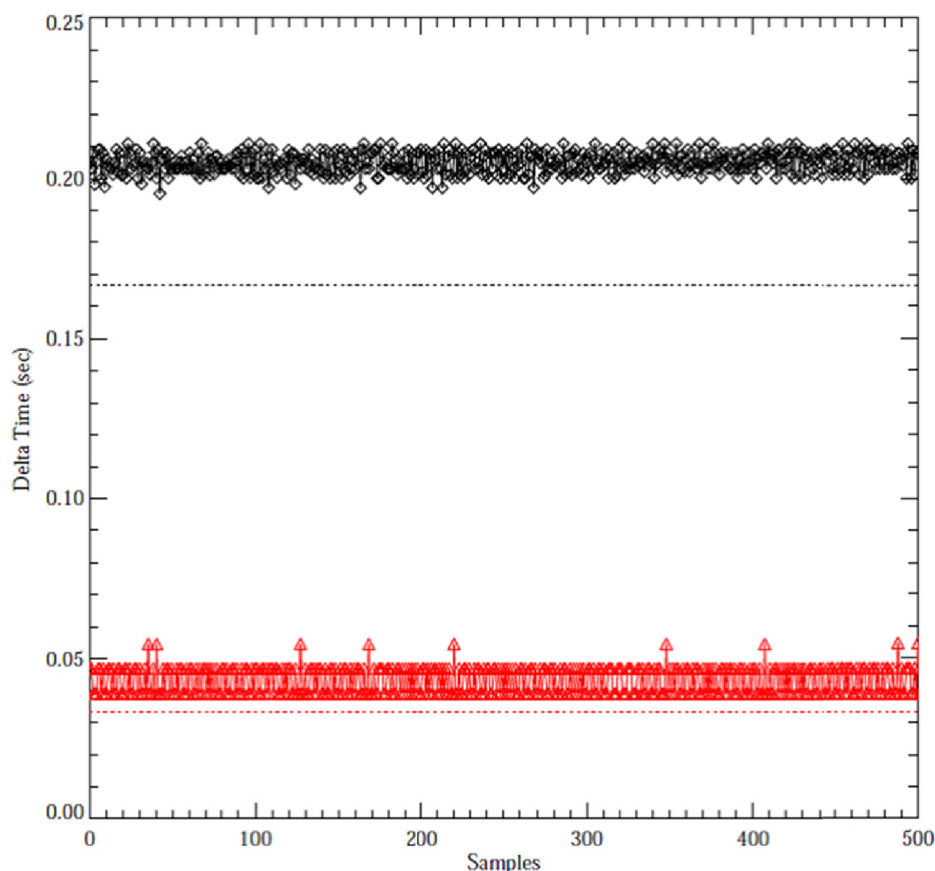


**Figure 3.70. Measured data rate for single transmitter fired (red) and all five fired (black) (dotted line indicates expected rate).**

gates averaged over fewer of the  $2.00 \times 10^{-6}$  samples and later gates averaged over more. The higher the percentage is set, the fewer the time gates will result. Averaging over wider gates reduces high-frequency noise. SAIC has worked with settings from 0.05 (5%) to 0.20 (20%) and is unsure what the limits are.

The last setting is GateHOff, which is the “hold-off time” in seconds after the transmit pulse is off before data are kept. UIT was uncertain on the details of how this feature was supposed to work and so did not try changing it. SAIC suggested keeping it at the manufacturer’s setting—around  $3.0 \times 10^{-5}$  to  $5.0 \times 10^{-5}$ .

SAIC has used several of the G&G TDEMI sensors for the purpose of identifying buried unexploded ordnance and for stationary measurements; in those cases it has used BlockT = 0.9, nRepeats = 9, nStk = 3, and GateWid = 0.05. These settings allow multiple transmits (one system has 25) to be fired and data collected on the minute(s) time scale and seems to beat down noise sufficiently to detect items of interest at depths of interest. For smaller targets, SAIC has tried increasing the stacking to 10–20. The noise goes down with the square root of the stacks. However, at greater numbers of stacks, SAIC was concerned that instrument drift might be a factor.

SAIC studied, and is still studying, the noise issues in collecting continuous, moving data with the TDEMI prototype. The sensor should not be moving very far on the time scale of the measurement. This results in increased noise because one cannot average over repeats and stacks. It was determined that the fastest measurement the TDEMI prototype can make is 1/30th of a second. At a speed of 1 m/s, the sensor moves 3 cm during the measurement. With BlockT = 0.0333, nRepeats = 1, and nStk = 1, the pulse time becomes 0.00833; so, later time gates are not possible. Greater gate widths reduce some of the noise, so SAIC suggested setting GateWid to 0.20 or higher. With BlockT = 0.0333, nRepeat could also be set higher—at the cost of shorter pulses and losing late time gates.

### TDEMI Prototype Dynamic Testing

In preparation for in-service testing, UIT conducted a series of dry-run tests while operating the TDEMI prototype system in continual mode and integrated with GNSS. The objectives were to obtain further familiarity with the system setup, directly compare the TDEMI prototype data and detection capabilities with UIT’s current Geonics EM61 MKII towed sensor array

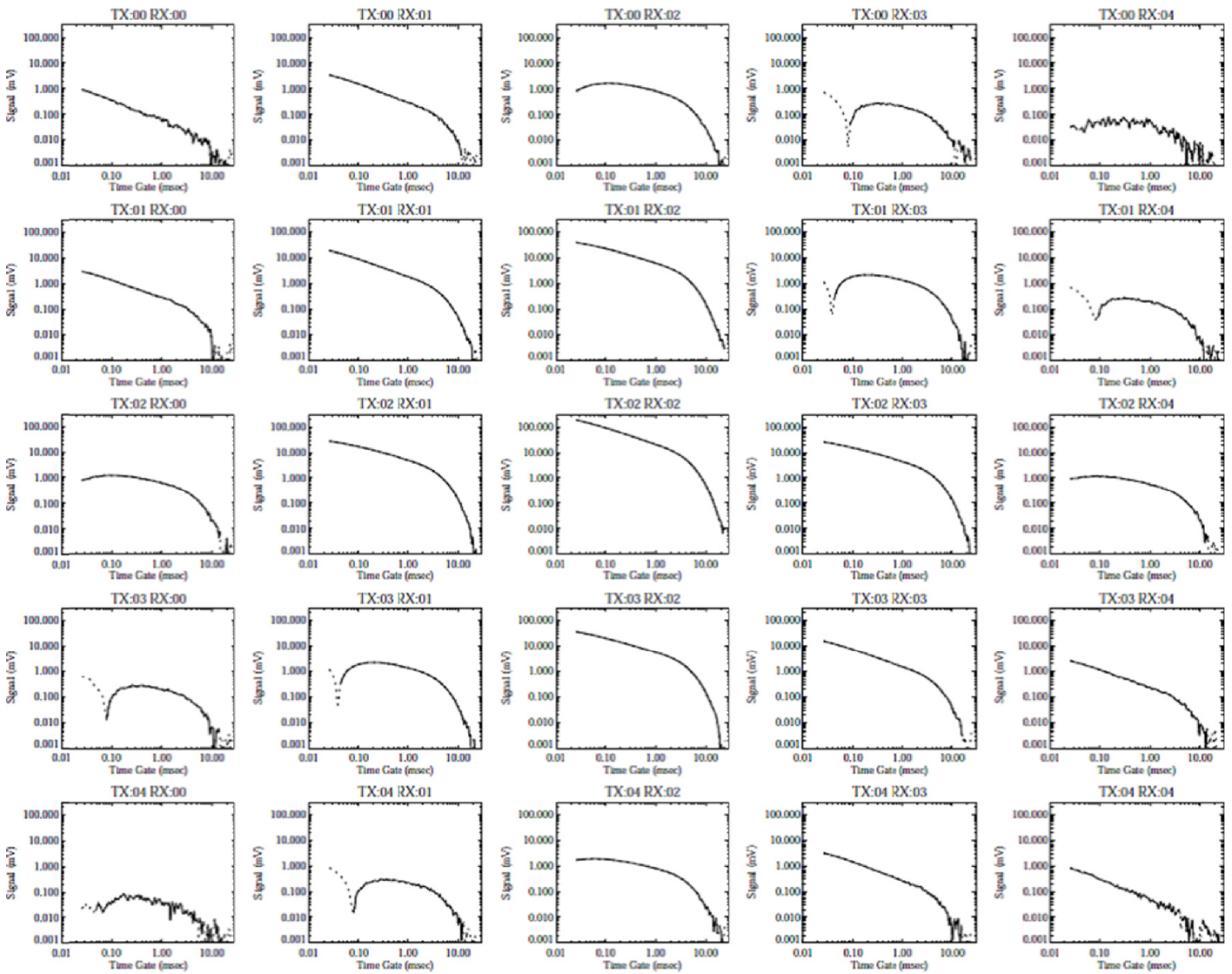


**Figure 3.71. TDEMI measurements with 1-in.-diameter pipe 30 cm below sensor array.**

geophysical system, and gather information on optimal acquisition settings for detecting underground metallic utilities. In addition to static testing, dynamic detection and positioning testing of the prototype TDEMI system was performed by laying out metal chains of various sizes straight across the ground surface at various spacing and orientations. Operators of the system traversed the chains at differing speeds, using different acquisition parameter settings. Figure 3.74 is a general depiction of the type of field tests conducted for the dynamic testing. This initial attempt to view and evaluate the TDEMI data was performed with Geosoft's Oasis Montaj software.

By March 2012, the project team was able to put together a brief outline summary of the data collection methods and preliminary results and observations:

#### 1. Stationary data collection

- a. Sensor array stationary test of metallic objects placed beneath.

- b. Data acquisition set to collect data continuously (including a single-shot mode), with
  - i. Acquisition parameters: nRepeats = 1, BlockT = 0.0333 s.
  - ii. This setting results in bipolar pulse (+on, off, -on, off), with a pulse on time of 8.33 ms and a total bipolar pulse length of  $4 \times 8.33 = 33.33$  ms.
  - iii. Transmitters were fired sequentially. Total time to fire all five was  $5 \times \text{BlockT}$  value plus some extra time gap between firings. Total time recorded in data files was roughly 0.21 s ( $5 \times 0.0333 + 0.043$  extra). This total time and array speed determine data sampling density along track when the array is moving.
  - iv. Time gate width was set to 15%, resulting in 36 logarithmically spaced time gates out to 8.33 ms. Larger gate widths (20% to 40%) would average over more of the time decay and reduce high-frequency noise at the cost of fewer time gates over the same decay

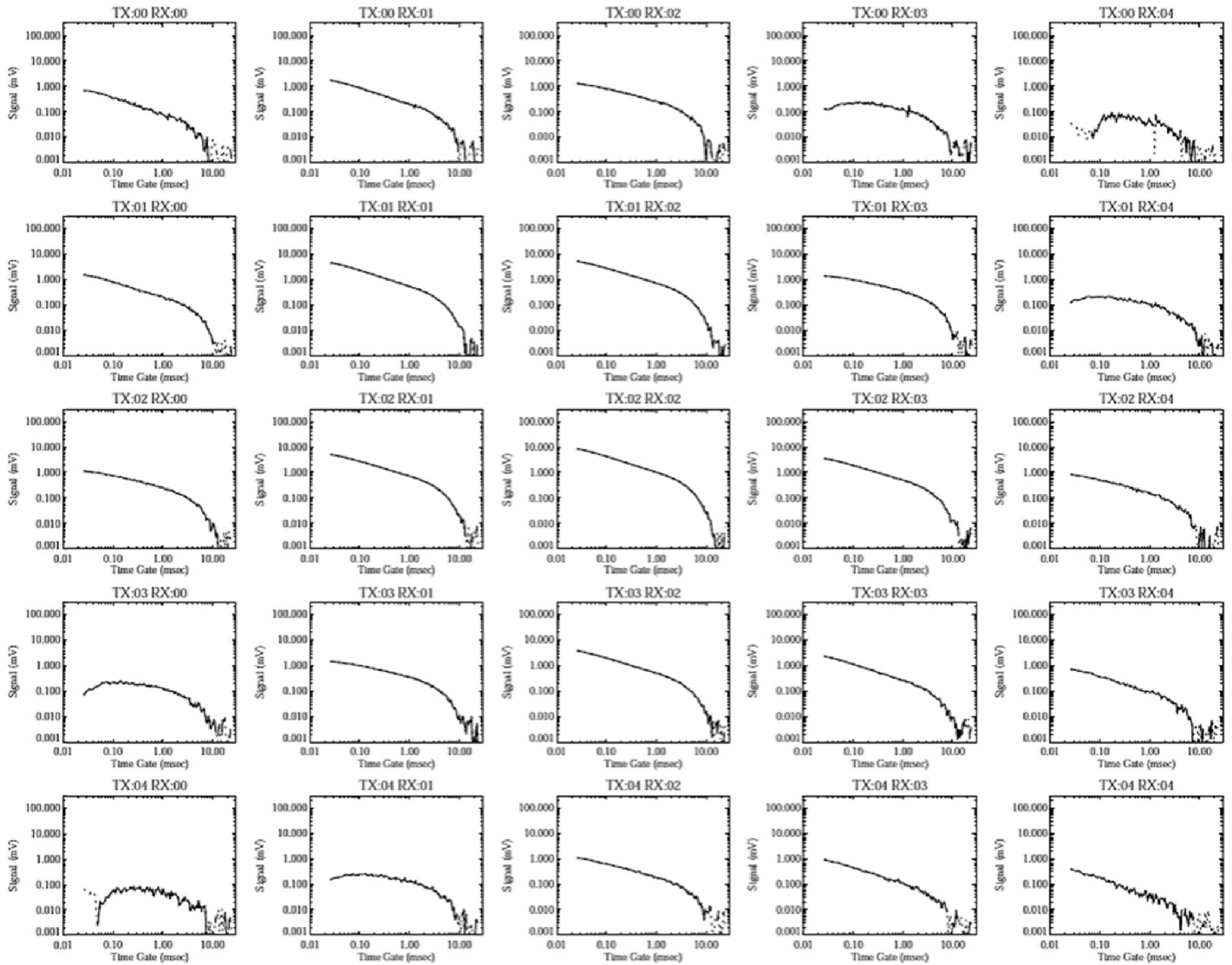


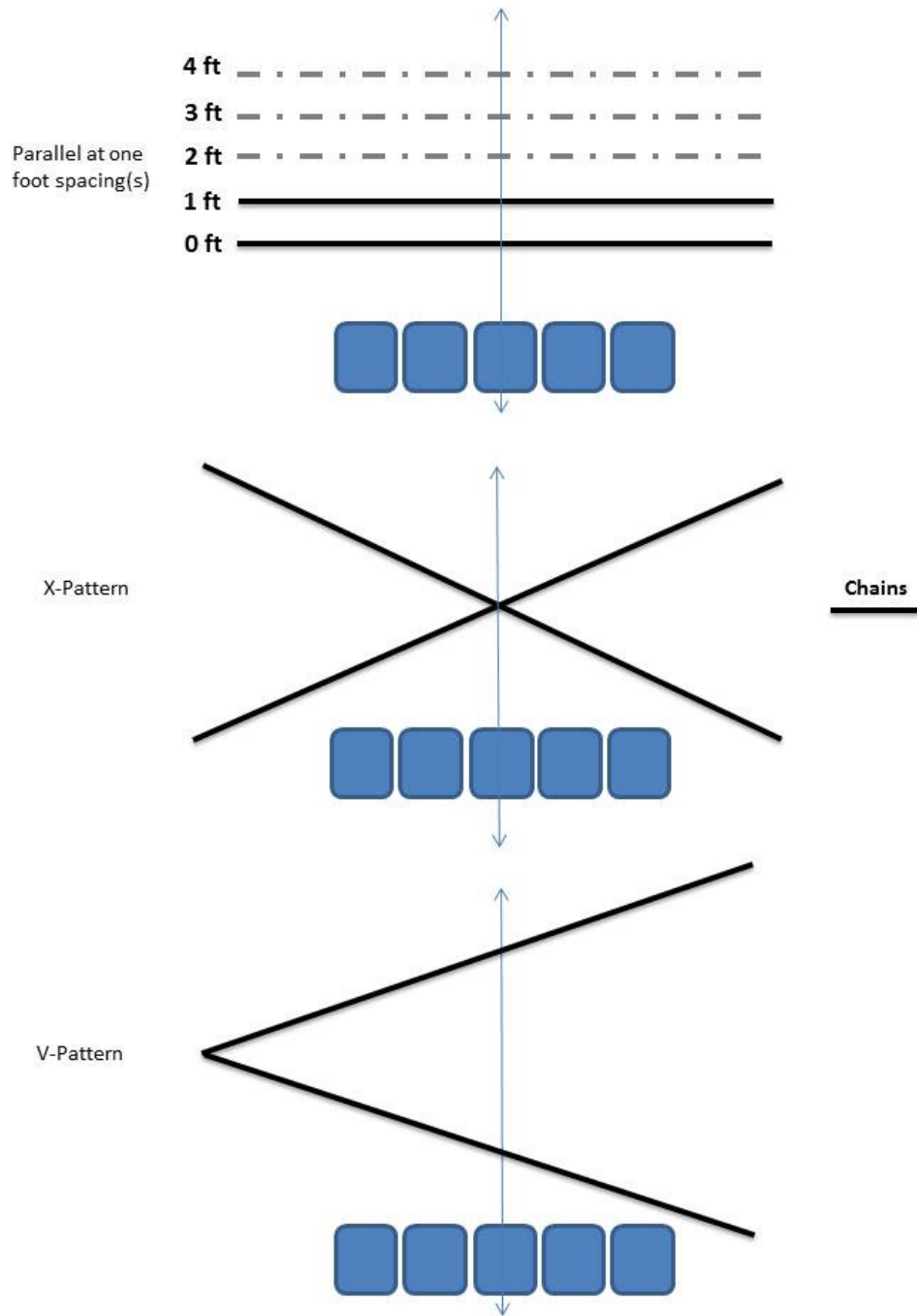
Figure 3.72. TDEMI measurements with 1-in.-diameter pipe 60 cm below sensor array.



Figure 3.73. Configuration and testing of the 5-by-1 TDEMI sensor array on UIT’s metal-free trailer.

Table 3.6. Parameters for the Initial Testing of the TDEMI Prototype with the EM3D Program

Parameter	Setting
Delt (s)	2.00E-06
BlockT (s)	0.9
nRepeats (n)	9
DtyCyc	0.5 (50%)
nStk (n)	3
AcqMode	DecaysDecimated
GateWid	0.15 (15%)
GateHOff (s)	3.00E-05



**Figure 3.74.** TDEMI prototype dynamic field test design.

- range. At a gate width of 30%, there would be 16 time gates.
- c. Three test objects: large metal object (LMO), medium metal object (MMO), and small metal object (SMO). They are all 4-in.-long steel pipe nipples: 1.25-in., 1.0-in., and 0.75-in. diameters, respectively.
  - d. Each object was placed under an array coil, and a data file was collected for 60–70 s with roughly 300 samples collected.
  - e. Data files were collected for all three objects under each of the five coils in two different orientations. The orientations had the pipe lying flat with the long pipe axis pointing along the direction of travel (called *parallel*) and the long pipe axis pointing orthogonal to the direction of travel (called *perpendicular*).
  - f. One background file was collected for each object.
2. Stationary data processing and observations
    - a. All data were normalized by the measured transmit current.
    - b. For each file, the mean and standard deviation were calculated for each data channel (transmit-receive coil combination).
    - c. The mean was also calculated for the background files by channel.
    - d. The signal from a given object is found by subtracting the average background from the average measured signal.
    - e. Figure 3.75 plots the average/background-subtracted array time-decay response as a function of time gate to the LMO in the two orientations directly under the center coil.
      - i. The top five plots are for the LMO perpendicular, and the bottom five parallel.
      - ii. The five plots across are for the five receive coils across the array.
      - iii. Each plot has five colored curves. The color indicates which transmit is firing: 1 = black, 2 = red, 3 = green, 4 = blue, 5 = cyan. For five receives and five transmits, there are 25 data channels total.
      - iv. The largest response is for the center receive coil when the center transmit coil is fired (green curve in center plot), since the object is directly below this transmit-receive pair. Coaxial transmit-receive pairs are termed monostatic.
      - v. Solid curves are positive responses. Dotted curves are negative. Some of the separated transmit-receive pairs have negative responses. The separated pairs are termed bistatic.
      - vi. The vertical black dotted line indicates roughly where the transmit-receive coil response has stabilized from the “ringing” of the transmit current turn off.
      - vii. The slanted dotted line indicates a rough noise floor of the stationary array for the given data acquisition settings (see Figure 3.75).
    - f. Figure 3.76 plots the standard deviation of the measured time-decay responses for two of the stationary data files. This is the stationary root mean square (RMS) noise level of the array for the given continuous data and data acquisition parameters. (Note that Figure 3.75 data are averaged over 300 samples and have a lower noise floor.) The five plots across indicate the receive coil, and the five colors indicate the transmit coil—as in Figure 3.75.
      - i. The noise levels vary by receive coil.
      - ii. The noise levels vary by data file.
      - iii. It is probable that a time varying noise source is close to the array.
      - iv. For later time gates, noise should fall off as  $t^{-1/2}$  as indicated by slanted, dotted lines.
    - g. Figure 3.77 summarizes the response of the three objects (by row) and the two orientations (by column) as the objects are placed under each coil.
      - i. The upper five curves are the monostatic responses with the object directly underneath. The color indicates which coil the object is under.
      - ii. The lower curves are bistatic responses from adjacent coils.
      - iii. For the parallel cases, the monostatic and bistatic responses have the same curve shape. This is because the field from the transmit coils is only directed orthogonally to the long axis of the pipe nipple.
      - iv. For the perpendicular cases, the bistatic response curves have a different shape. This is because some of the transmit field is directed along the long axis of the pipe nipple.
      - v. The array transmit fields never intersect the test objects in three orthogonal directions. Because the objects are axisymmetric, only one or two unique directions are covered by the transmit field.
    - h. Because of the limited “illumination” by the array transmit fields, a complete inversion of all dipole model parameters was not possible with the test object data.
      - i. By constraining the object location to be directly centered under a given coil (in this case the center coil), a limited inversion of the polarization terms is possible.
      - ii. Figure 3.78 plots the decay polarizations terms as a function of time gate for the three objects (LMO = black, MMO = red, and SMO = green).
      - iii. For the parallel cases, the long axis is not illuminated; and only the equal, transverse polarizations are inverted. For the perpendicular cases, the long axis and transverse polarizations are both found.

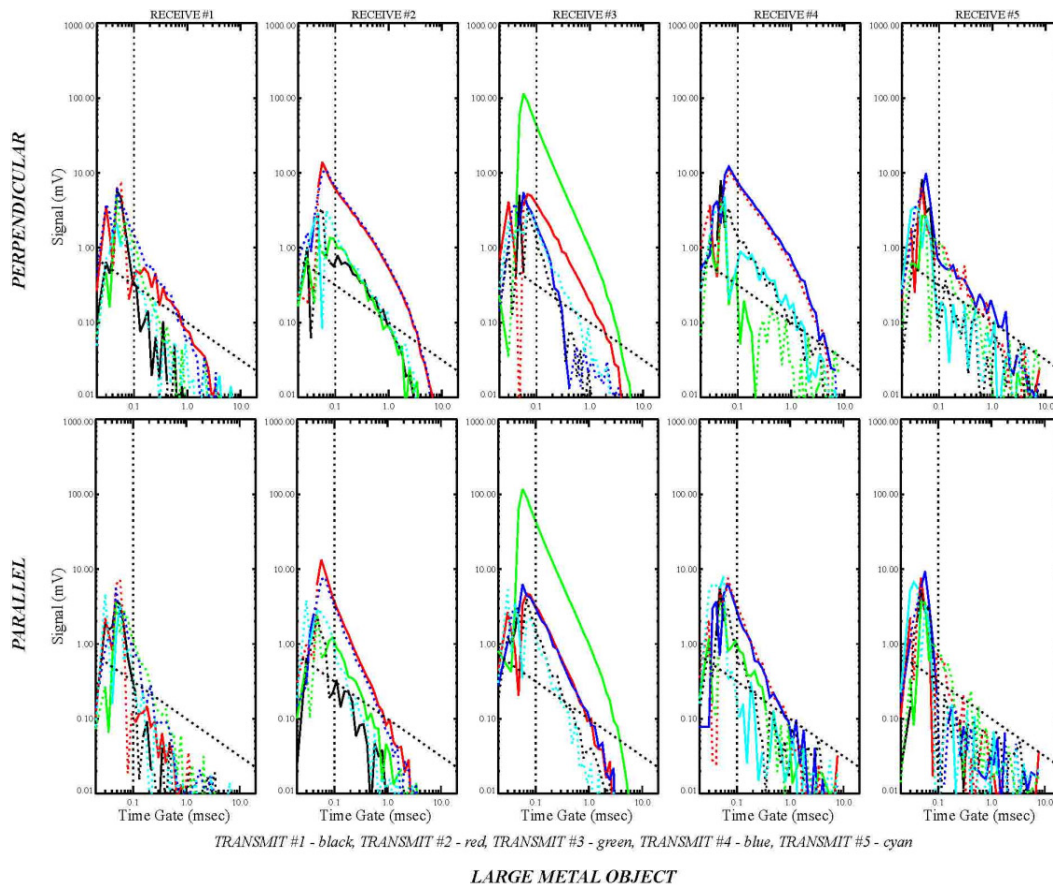


**Figure 3.75.** Plot showing the average/background-subtracted array time-decay response as a function of time gate(s) to the LMO.

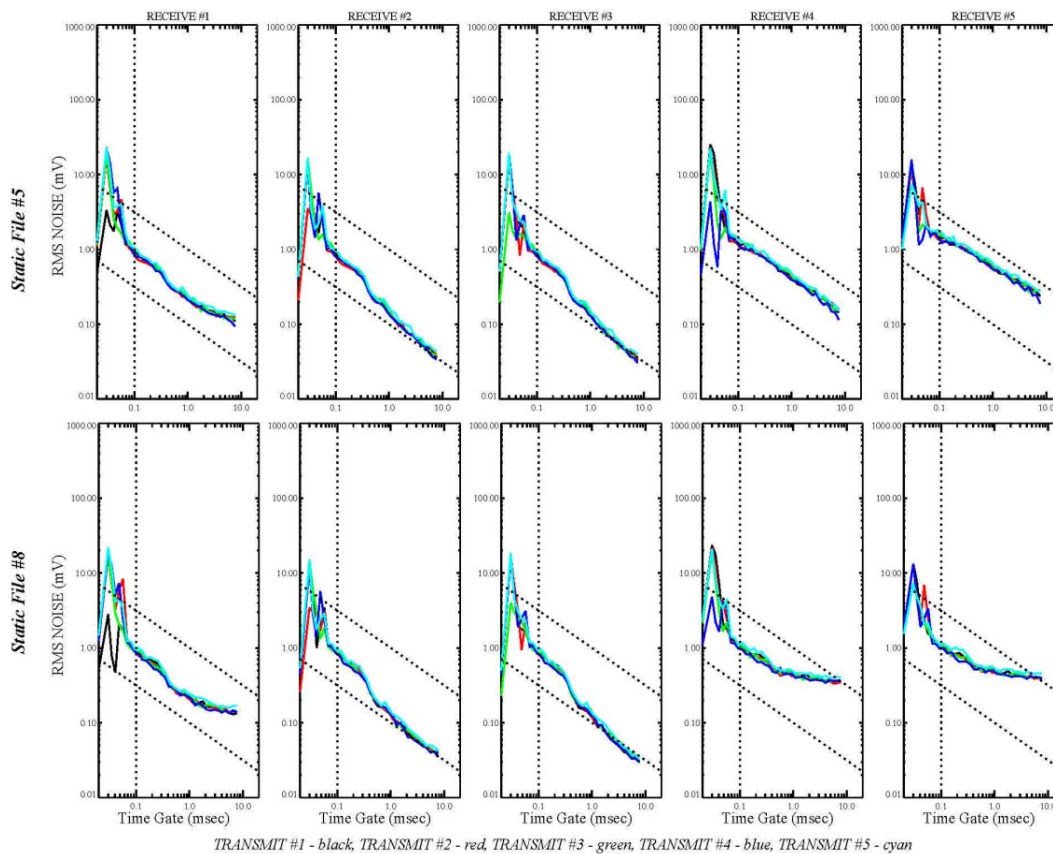


**Figure 3.76.** Plot showing the rough noise floor of the stationary array.

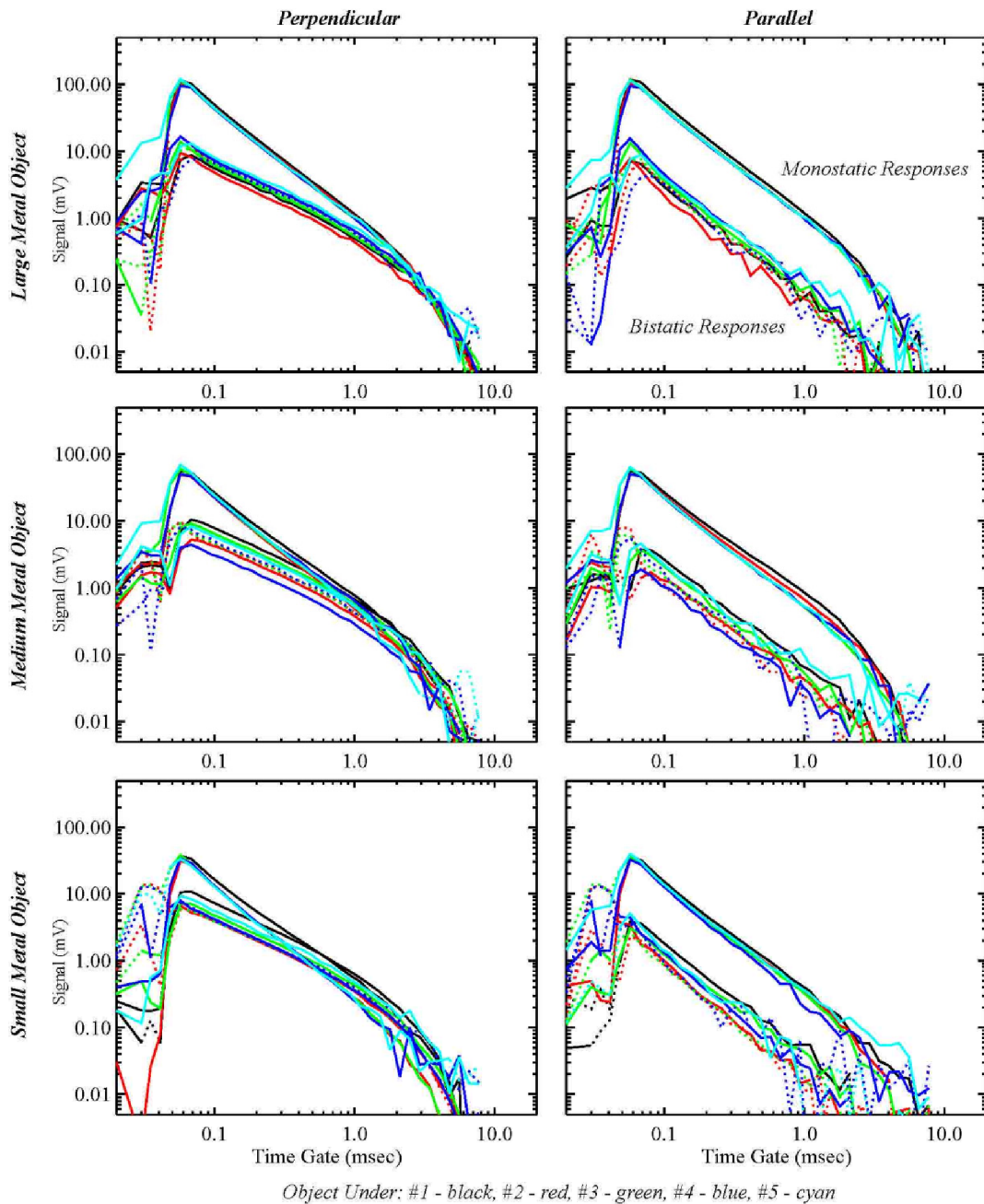


**Figure 3.77.** Plot summing the array response of the three objects (by row) and the two orientations (by column) as the objects are placed under each coil.

- iv. For this relatively high signal-to-noise ratio (SNR), stationary data, the inverted polarizations were sufficient to distinguish the three pipe sizes.
3. Dynamic data processing and observations
  - a. The baseline data were collected with the 8.33-ms pulse, 33.33 ms for the total bipolar pulse, and 0.21 s for all five transmitters to fire sequentially.
  - b. At an array speed of 1 m/s, this means each set of transmit data is sampled roughly every 0.21 m along track.
  - c. There are recorded time stamps only for each set of all five transmitters firing. It is assumed that the data for each transmit is uniformly spaced over this interval.
  - d. The data acquisition program records and averages all of the GNSS data that come in while the five transmitters are firing. Because the GNSS data rate during field testing was slower than this time, many of the “5 transmit” data records are not updated in position at all (i.e., GNSS every 0.5 s and data record every 0.21 s).

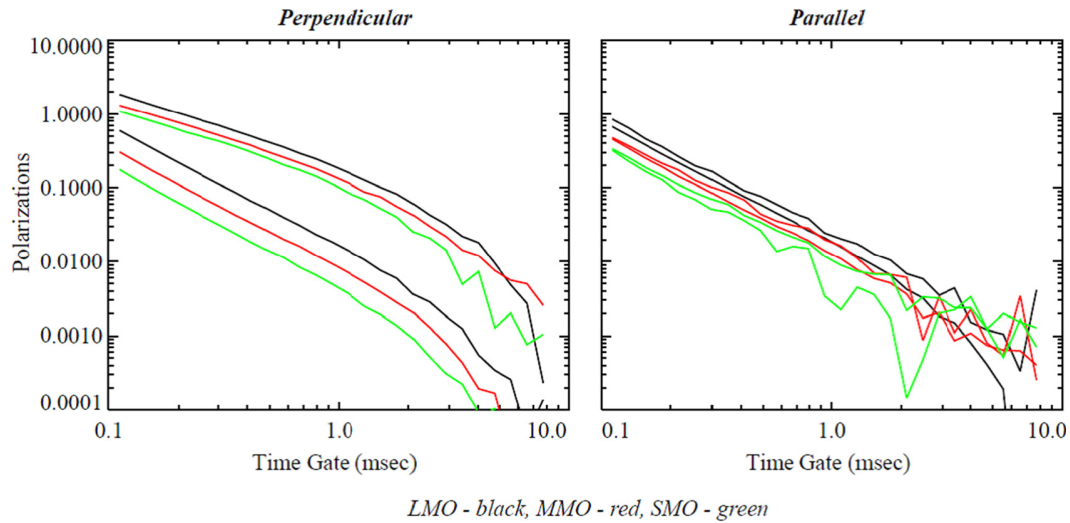


**Figure 3.78.** Plot showing the decay polarizations terms as function of time gate(s) for the three metal objects.

- e. To map the data, only new GNSS updates were kept. The GNSS antenna was centered behind the array. A course-over-ground had to be calculated from the GNSS trajectory and the GNSS position projected forward 0.35 m to the array. The recorded GNSS times with an arbitrary time shift were used to interpolate GNSS positions at GNSS times to transmit firing times. This shift was determined by looking at dynamic data collected in back-and-forth paths over two chains separated at different spatial intervals and positions at a variety of orientations.
- f. Figure 3.79 plots the RMS noise measured with the array moving over a reasonable stretch of ground just before the placed chain. The dynamic noise levels are higher than the stationary levels and are worse on the array edges. The source of this noise has yet to be determined.
- g. Figure 3.80 plots rasters of the monostatic channels as the array drives back and forth over parallel chains laid on the ground surface.
- i. The outer sensors 1, 4, and 5 show the increased noise.

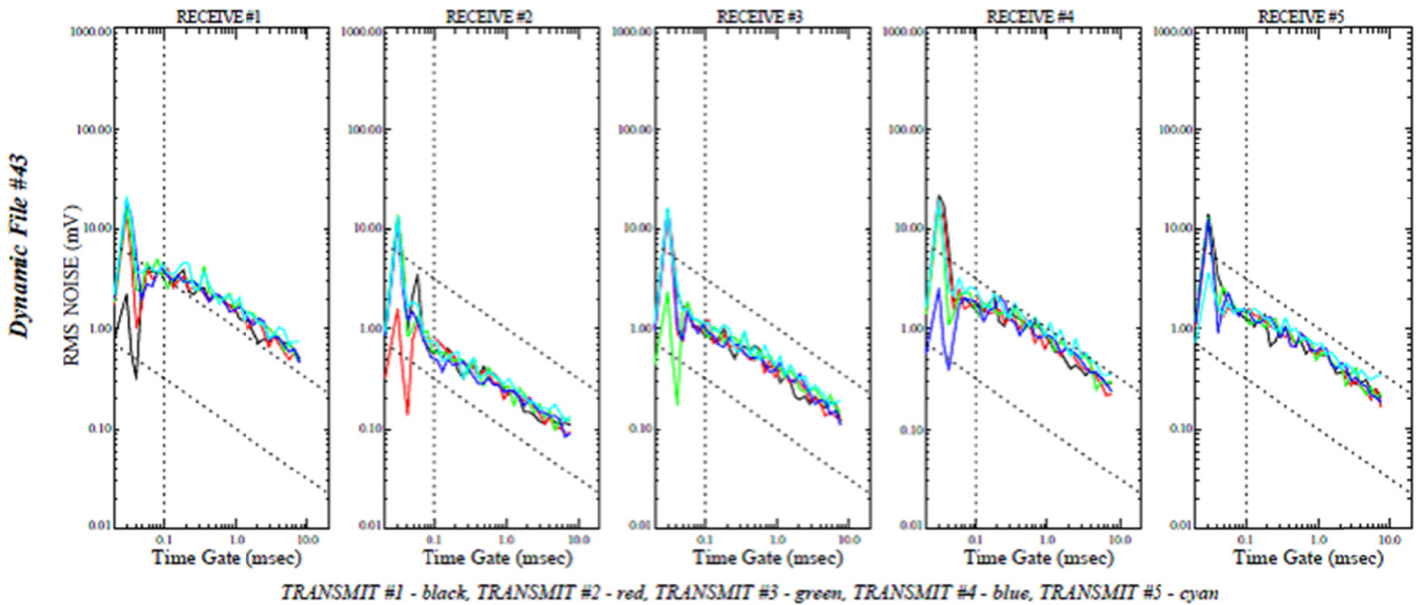


**Figure 3.79.** Plot displaying the RMS noise measured with the array moving over reasonable stretch of ground before chain emplacement.

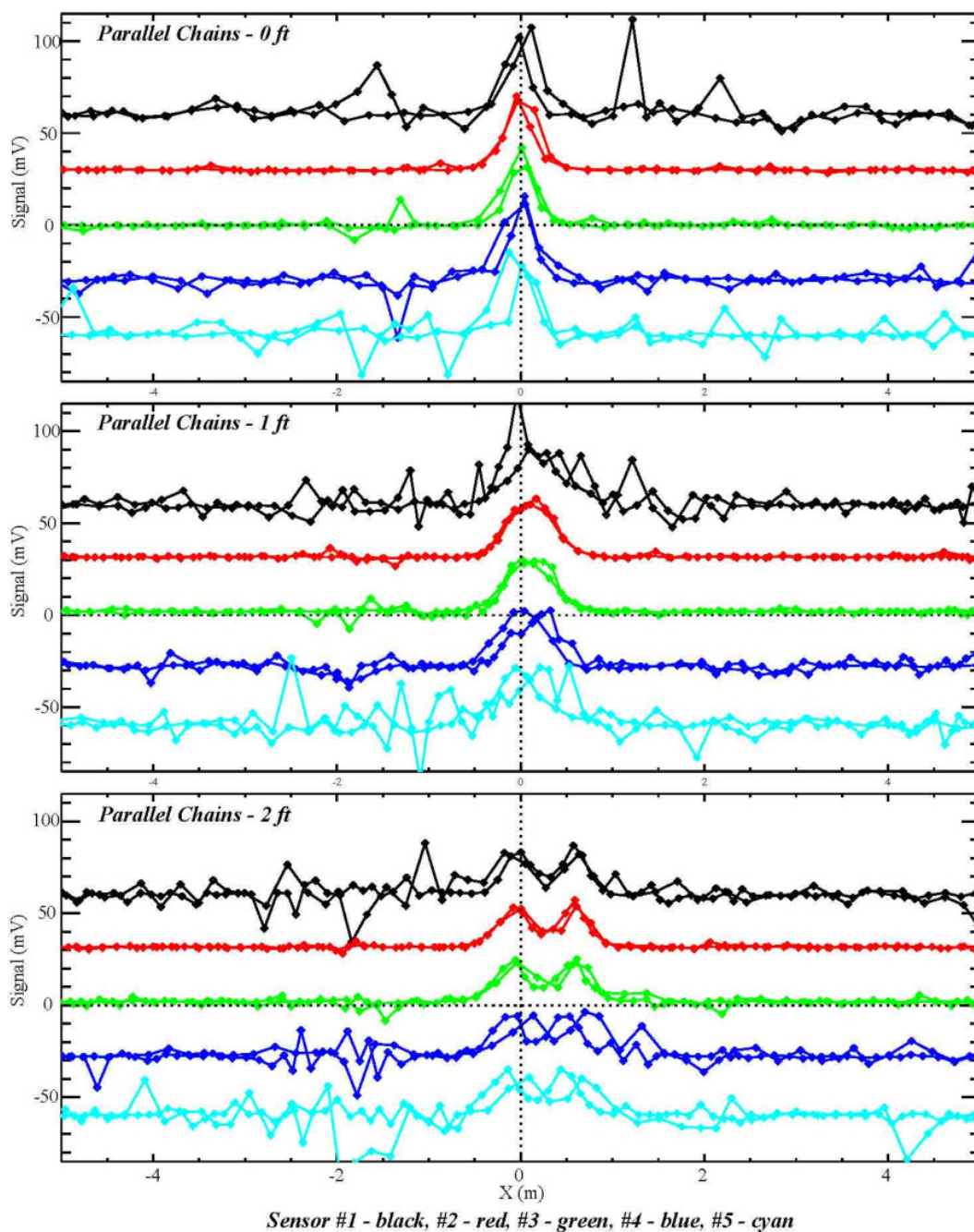


**Figure 3.80.** Plot displaying rasters of the monostatic channels as the array drives back and forth over parallel chains laid on the ground surface at separation distances of 0 ft, 1 ft, and 2 ft.

- ii. From top to bottom, the chains are spaced at 0-ft, 1-ft, and 2-ft apart. The array can resolve two chains at the 2-ft chain separation distance.
- iii. Figure 3.81 shows similar data for the 3-ft and 4-ft separations.
- h. Different array speeds and different acquisition parameters were also tested.
  - i. In addition to the basic fast rate ( $nRepeats = 1$ ,  $BlockT = 0.0333$ ), a medium rate of ( $nRepeats = 3$ ,

$BlockT = 0.1$ ) and a slow rate of ( $nRepeats = 9$  and  $BlockT = 0.3$ ) were used. These settings provide more averaging to reduce noise.

- ii. The medium rate records a new transmit sample every 0.56 s. At a speed of 1 m/s, this means a sample every half meter or so. At the slow rate, there is a sample every 1.6 s with a 1 m/s distance of 1.6 m between samples. The slow data rate is not viable at reasonable acquisition speeds.

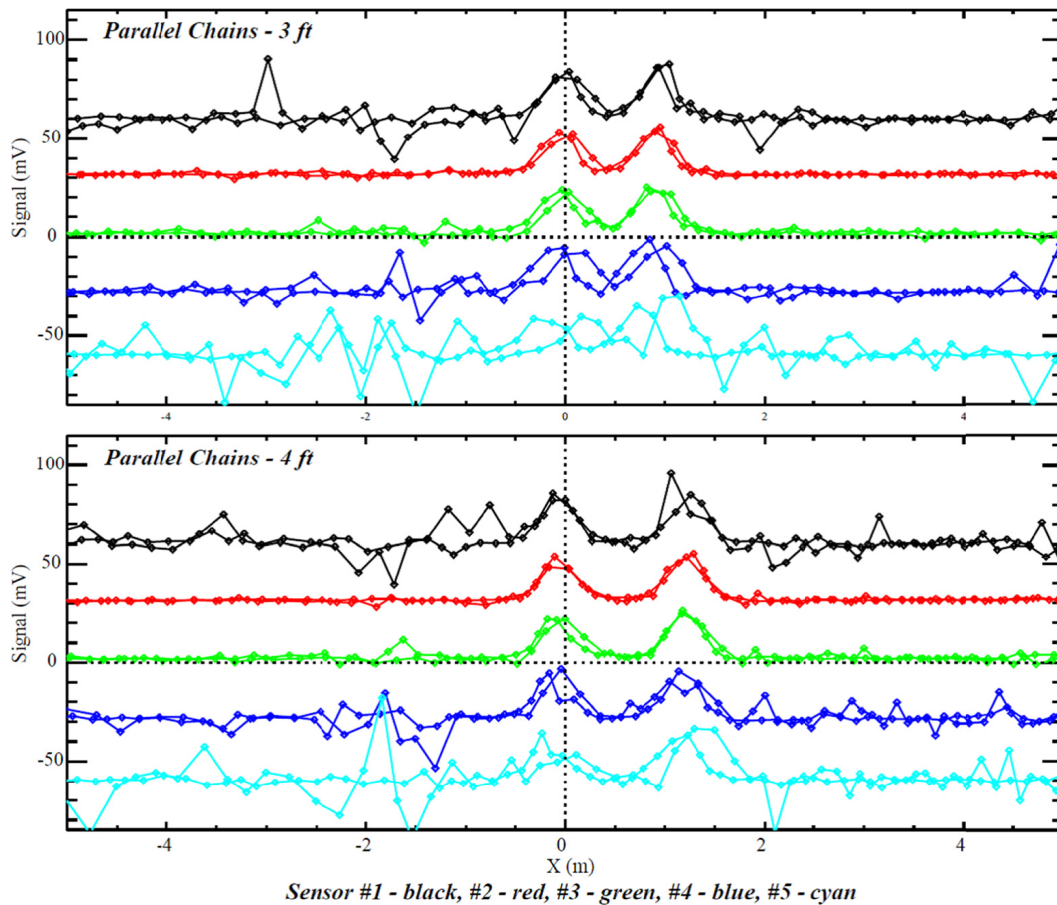


**Figure 3.81.** Plot displaying rasters of the monostatic channels as the array drives back and forth over parallel chains laid on the ground surface at separation distances of 3 ft and 4 ft.

- iii. Speeds were varied from less than 0.5 m/s up to roughly 1.5 m/s. Figure 3.82 plots the responses over chains placed in an X pattern. At the fast data rate, the pattern is well resolved at a slow speed (top plot), but not as well at the fast speed (bottom plot).
- iv. Figure 3.83 plots the same X-pattern data at the medium data rate and the two speeds. At a slow speed, the pattern is still resolved. At the fast speed, the pattern dissipates.
- v. At the slowest data sampling rate, all of the chain patterns were completely washed out.
- vi. At the price of later time gates, two other data acquisition settings were considered to reduce noise:
  - (1) One is  $n\text{Repeats} = 3$  and  $\text{BlockT} = 0.0333$ . This setting produces an “on” pulse of 2.77 ms. The time for all five transmits to fire would still be 0.21 s, and at 1 m/s a sample every 0.21 m.
  - (2) The other is  $n\text{Repeats} = 9$  and  $\text{BlockT} = 0.1$ . Again, this is a 2.77-ms pulse; but with a time of 0.56 s per sample and a slow speed of 0.5 m/s,

there would still be a measurement roughly every 0.25 m.

- (3) In addition, the gate width parameter could be increased to 20–40% at the cost of fewer gates spaced over the same time-decay period.

### TDEMI Prototype Data Manipulation

Although preliminary field testing was performed with the R01B TDEMI system, additional testing was needed before the in-service testing process to determine optimal acquisition parameter settings; to compare against currently used TDEMI systems; and to determine effective ways to organize, view, and process the expansive data sets generated by the prototype. UIT elected to conduct data evaluations with Geosoft Oasis Montaj software. Initial data management included two methods. The first involved viewing the data on a point-sample-by-point-sample basis. Each line of the Geosoft database represents a specific data point, and the array channels of each line represent the various Tx-Rx pairs’ decay curves, as well as the five signal transmit strengths.

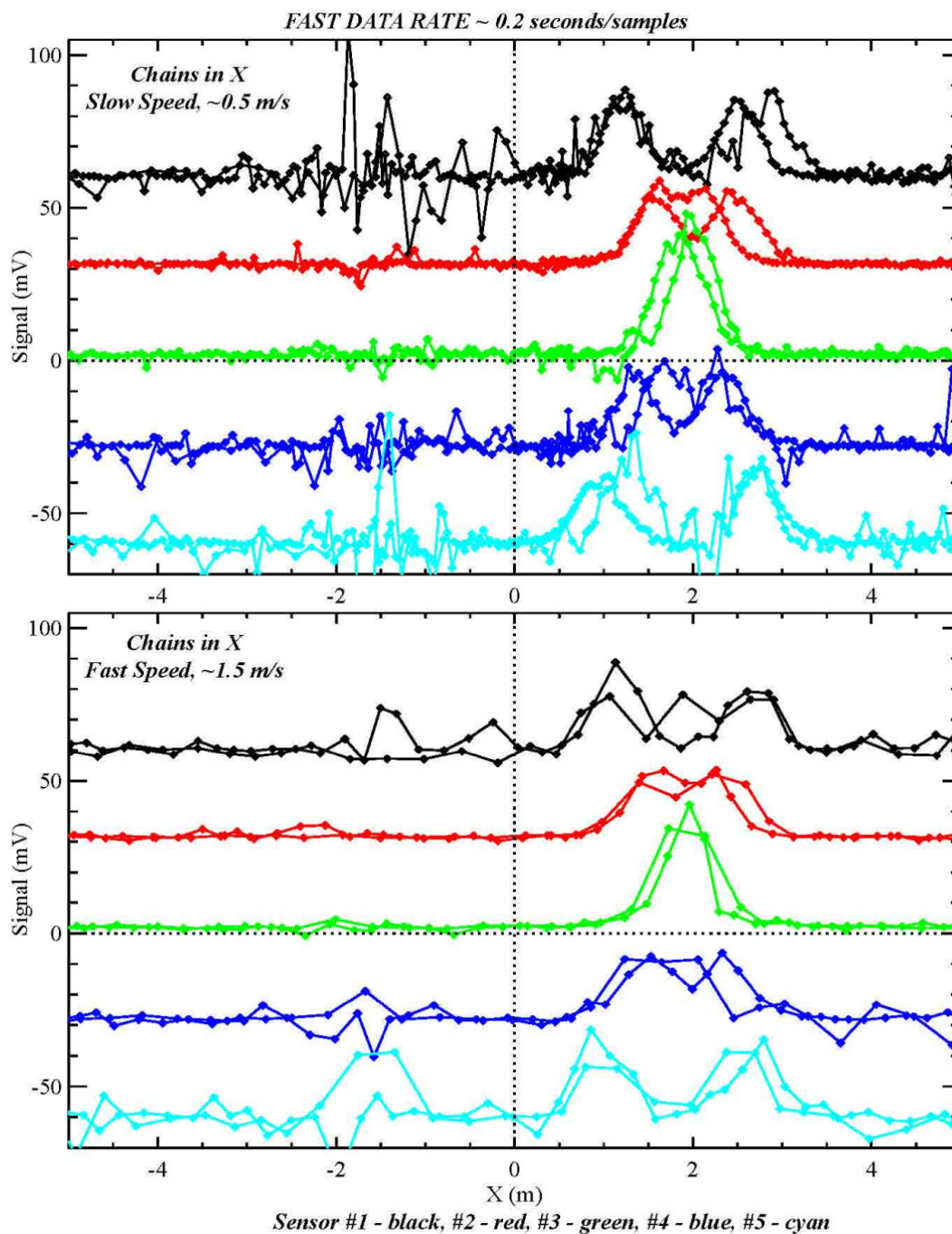


**Figure 3.82.** Plot showing the array responses over chains placed in an X pattern at speeds of  $\sim 0.5$  m/s and  $\sim 1.5$  m/s (fast data sampling rate).

The second involved viewing the data on a sensor-by-sensor basis. Each line of the Geosoft database represents a specific sensor, and the channels of each sensor line represent the exact numerical values for each point of the transmit-decay arrays. Using either method, the process proved to be quite time consuming, so UIT continued searching for optimal data acquisition parameter settings and data workflows to account for the relatively large volume of data being generated.

UIT's collaboration with Geosoft programmers resulted in the development of an import template with which TDEMI prototype data could be imported into a Geosoft database; each line of the database represents a specific sensor of the array. Individual channels of the database can carry values—such as Easting, Northing, Elevation, Heading, Pitch, Roll, Point Number, GPS Coordinated Universal Time (UTC), GateTime, and the various decay curve arrays of the Tx-Rx pairs. UIT data analysts beta-tested these new user-interface

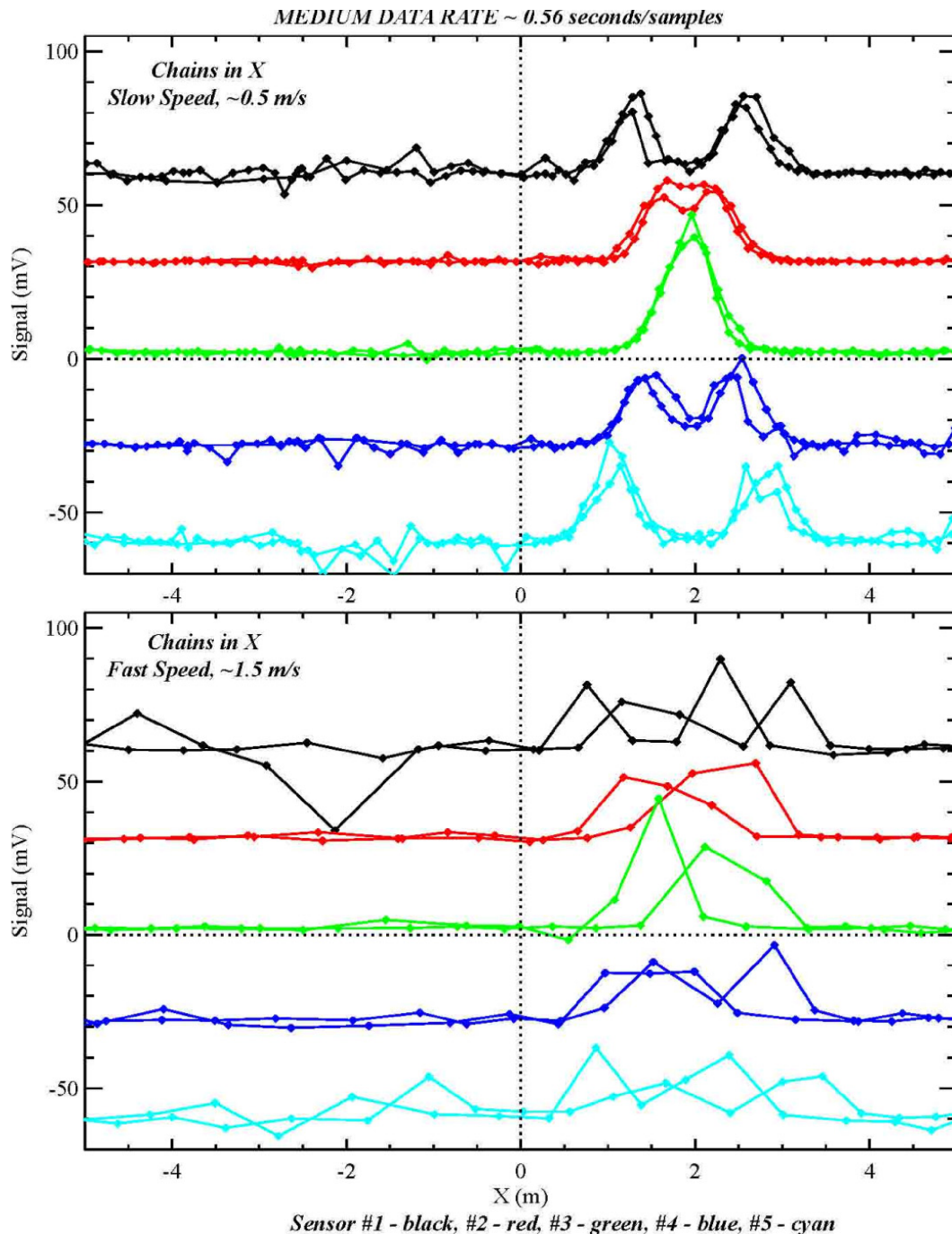


**Figure 3.83.** Plot showing the array responses over chains placed in an X pattern at speeds of  $\sim 0.5$  m/s and  $\sim 1.5$  m/s (medium data sampling rate).

functions and offered feedback to developers on a continual basis. Figure 3.84 illustrates the graphical user interface from this tool development of data import to a geophysical analysis software package. The primary notion was to evaluate the system's performance as a digital geophysical mapping tool with which data are collected in continued and dynamic mode rather than in a static "cued interrogation" mode as is used for munitions response applications with similar TDEMI technologies.

For the R01B TDEMI prototype, the raw TEM data files are recorded and stored on the field acquisition computer. The operator is allowed to set a file name prefix within the setup display window, and the EM3D acquisition software automatically names individual data sets sequentially and numerically thereafter. These raw files are generated in binary format and come with an extension of ".TEM." To change raw files into a usable format, the operator is required to convert the .TEM data files into an ASCII format (.CSV). This procedure

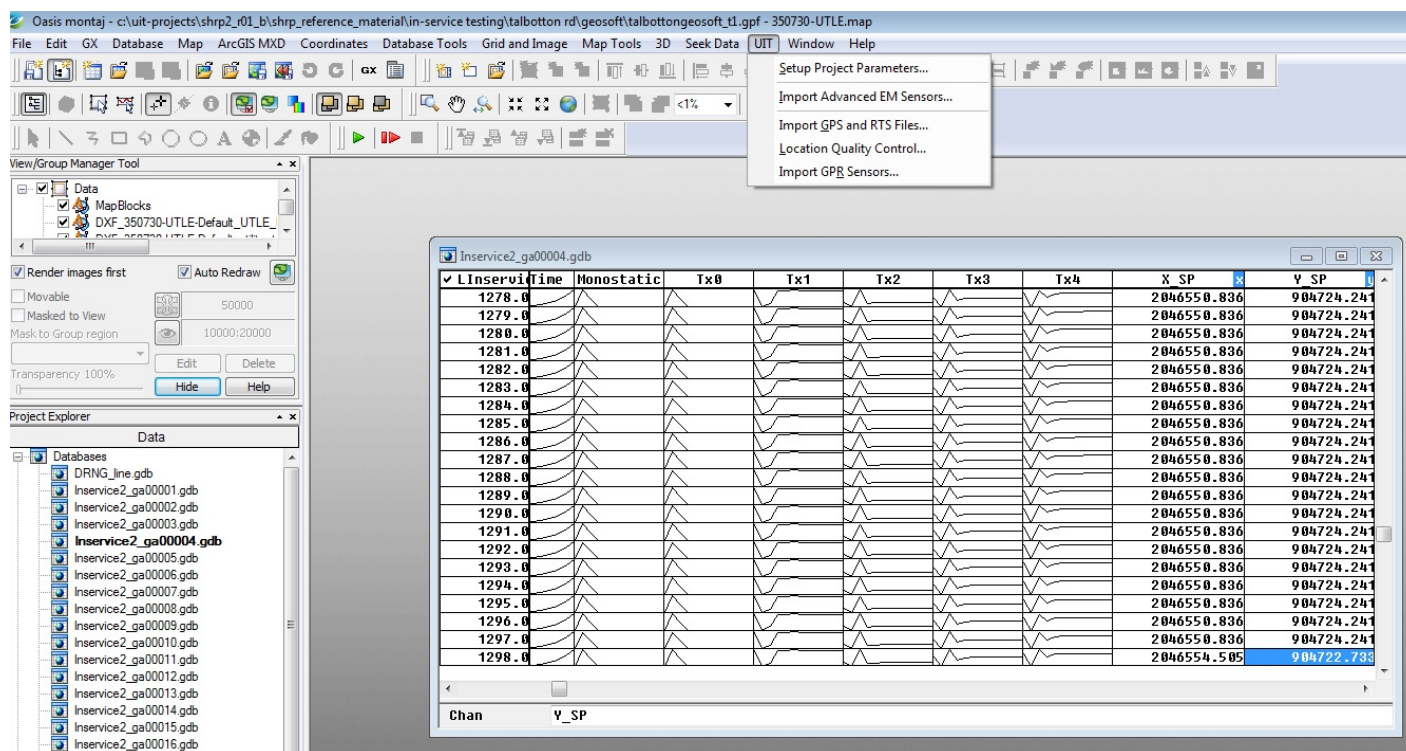


**Figure 3.84. Screenshot of Oasis Montaj, representing customized data import function and resultant Geosoft database array channel for each Tx-Rx coil pair.**

is performed within the EM3D environment and is typically conducted at the end of a production day. This action results in the generation of two distinct files for each data set collected: the actual numerical data file (shown in Figure 3.85), and the user-defined acquisition parameters file (shown in Figure 3.86).

On import of TEM data CSV files, a separate Geosoft database is created for each data session. The geophysical data are split and organized for each data set imported, such that each line of the Geosoft database corresponds to one sensor of the sensor array. A monostatic (Rx coil = Tx coil) data channel is also created within the database so that data can be viewed in a similar fashion to existing TDEMI digital geophysical mapping systems in which transmit coils are the same (and equally positioned) as receiving coils. Given the vast amount of data acquired (compared with current digital geophysical mapping EMI systems), sensor values are stored as arrays within each cell of the Geosoft database as shown in Figure 3.84, rather than individual numerical digits.

Once the TDEMI prototype data are imported to Geosoft Oasis Montaj, data analysts are able to perform all data processing, data interpretation, and mapping procedures. Data points may be translated into the site-specific coordinate system and plotted against existing geo-referenced records to check for accuracy and completeness; data can be corrected for instrument latency and drift; data can be reviewed in profile view for multiple data channels (see Figure 3.87), and/or

single channels can be gridded and color contoured for collective views within map space (see Figure 3.88). The software involves dynamically linked databases, maps, and 3-D views to give the analyst all the spatial and detection factors needed to perform and devise a well-informed subsurface assessment. Figure 3.89 shows a 3-D view in Geosoft Oasis Montaj; each time gate measurement is combined and gridded as a full block of data (voxel). The time gate intervals of the TDEMI prototype act like a pseudo-depth component; the earliest time gate measurements are depicted at the actual ground surface elevations, and later time gate measurements are depicted at deeper intervals. This is done by flipping the gate time about the 0-time axis and essentially making the gate times correspond to equivalent depth values below the ground surface. Although this does not provide any sort of true depth-to-target estimations, it does allow the analyst to view, manipulate, and rotate all of the EMI data within one graphical window. Finally, TDEMI data interpretations of suspect utility locations can be synthesized down, graphically drafted, and exported from the software. Mapping deliverables to engineering firms can be produced in a variety of compatible computer-aided design (CAD) and GIS formats.

### TDEMI Prototype Testing Summary

During the course of SHRP 2 R01B research work, a practical prototype was constructed and tested using advanced TDEMI

GPSUTC	Lat	Lon	Elev	GPScpuTime	GPSFixQ	LocalX	LocalY	LocalZ	CPUms	Heading	Pitch	Roll	PtNo	
55315	38.88148	-77.4071	148.168	41431.875	4	-8616918	4328267	148.168	41432503	0	0	0	1	
Txl_0	Txl_1	Txl_2	Txl_3	Txl_4	Rx0Z_Tx0	Rx0Z_Tx1	Rx0Z_Tx2	Rx0Z_Tx3	Rx0Z_Tx4	Rx1Z_Tx0	Rx1Z_Tx1	Rx1Z_Tx2	Rx1Z_Tx3	Rx1Z_Tx4
6.144998	6.473807	6.368599	6.450402	6.049966177	3.48E-05	-3.13E-05	1.07E-05	3.86E-06	-1.29E-07	-3.38E-05	4.09E-05	-3.00E-05	8.95E-06	3.11E-06
3.779864	4.575777	4.517524	4.599159	4.331476121	0.003857	-0.00227	-0.00038	-0.00031	-0.00038	-0.00242	0.003876	-0.00232	-0.00038	-0.00035
3.913971	4.690043	4.631622	4.715902	4.443725586	0.002005	-0.0026	0.00183	0.00096	0.0006	-0.00277	0.002571	-0.00245	0.001579	0.000889
4.12517	4.848246	4.788452	4.876411	4.59910753	-5.52E-05	-0.00013	-9.87E-05	-0.00015	-0.00021	-0.00017	7.63E-05	-9.29E-05	-7.84E-05	-0.00013
4.419564	5.071246	5.01024	5.101301	4.817157322	6.78E-06	-1.98E-05	-1.97E-05	-2.30E-05	-2.61E-05	-2.02E-05	1.98E-05	-1.68E-05	-1.74E-05	-2.10E-05
4.804355	5.367016	5.302787	5.397919	5.102074425	7.58E-06	2.89E-06	1.86E-06	4.00E-07	-4.58E-07	3.56E-06	1.08E-05	3.05E-06	2.72E-06	8.60E-07
5.253519	5.718046	5.648865	5.746444	5.431227911	4.66E-06	3.16E-06	2.24E-06	1.63E-06	9.15E-07	3.53E-06	6.29E-06	2.97E-06	2.48E-06	1.26E-06
5.714692	6.086181	6.011582	6.102972	5.762025095	2.38E-06	1.79E-06	1.28E-06	5.28E-07	4.65E-07	1.88E-06	3.45E-06	1.62E-06	1.05E-06	5.34E-07
6.097349	6.404874	6.324339	6.400384	6.028731617	1.17E-06	1.26E-06	1.36E-06	7.64E-07	1.99E-07	8.26E-07	1.83E-06	1.66E-06	8.68E-07	3.26E-07
6.322883	6.609399	6.514688	6.584008	6.181481834	9.27E-07	7.00E-07	1.05E-06	3.86E-07	3.43E-07	8.72E-07	7.99E-07	1.15E-06	3.58E-07	3.60E-07
6.408317	6.69513	6.576662	6.657504	6.235670581	5.54E-07	7.23E-07	6.15E-07	7.16E-07	2.06E-07	4.21E-07	6.62E-07	5.83E-07	6.31E-07	2.04E-07
6.421227	6.715922	6.590127	6.67417	6.238065911	4.22E-07	3.01E-07	2.36E-07	2.61E-07	-4.67E-08	4.02E-07	3.59E-07	2.32E-07	1.27E-07	-9.83E-09
Rx2Z_Tx0	Rx2Z_Tx1	Rx2Z_Tx2	Rx2Z_Tx3	Rx2Z_Tx4	Rx3Z_Tx0	Rx3Z_Tx1	Rx3Z_Tx2	Rx3Z_Tx3	Rx3Z_Tx4	Rx4Z_Tx0	Rx4Z_Tx1	Rx4Z_Tx2	Rx4Z_Tx3	Rx4Z_Tx4
9.60E-06	-3.00E-05	3.80E-05	-3.26E-05	7.76E-06	3.78E-06	1.17E-05	-2.98E-05	3.84E-05	-3.26E-05	1.71E-07	5.29E-06	8.47E-06	-3.34E-05	3.32E-05
-0.00048	-0.00239	0.003884	-0.00232	-0.000505084	-0.00031	-0.00035	-0.00234	0.003886	-0.00231	-0.00033	-0.00028	-0.00036	-0.00239	0.003891
0.001763	-0.00244	0.002266	-0.00267	0.001608573	0.000941	0.001863	-0.00231	0.002336	-0.00264	0.000576	0.001071	0.001553	-0.00271	0.001826
-0.00011	-6.47E-05	3.57E-05	-0.00014	-0.000114824	-0.00013	-1.96E-05	-0.00011	2.76E-05	-0.00016	-0.00018	-8.06E-05	-8.35E-05	-0.00015	-8.49E-05
-1.86E-05	-1.50E-05	1.58E-05	-2.48E-05	-2.03E-05	-2.20E-05	-1.69E-05	-2.60E-05	2.12E-05	-2.25E-05	-2.75E-05	-2.28E-05	-2.25E-05	-2.37E-05	2.61E-06
2.22E-06	3.85E-06	7.34E-06	1.77E-06	6.44E-07	9.54E-07	1.98E-06	-7.88E-08	9.26E-06	1.12E-06	-1.78E-06	-6.43E-07	-1.06E-06	5.13E-07	5.95E-06
3.05E-06	3.35E-06	4.46E-06	2.17E-06	1.29E-06	1.76E-06	2.12E-06	2.28E-06	4.28E-06	1.45E-06	3.74E-07	8.87E-07	7.00E-07	1.49E-06	3.77E-06
1.49E-06	1.90E-06	2.37E-06	1.08E-06	6.57E-07	7.33E-07	1.13E-06	1.16E-06	2.31E-06	7.80E-07	5.49E-08	2.74E-07	1.84E-07	6.62E-07	2.56E-06
6.47E-07	1.15E-06	2.05E-06	9.67E-07	4.21E-07	9.84E-08	6.61E-07	1.34E-06	1.62E-06	6.40E-07	1.43E-09	3.05E-07	6.03E-07	6.50E-07	1.46E-06
7.67E-07	7.53E-07	1.35E-06	4.34E-07	3.91E-07	3.40E-07	2.22E-07	9.73E-07	6.28E-07	4.59E-07	1.72E-07	1.26E-07	8.02E-07	3.05E-07	9.84E-07
3.70E-07	5.53E-07	6.17E-07	6.84E-07	1.83E-07	3.19E-07	4.42E-07	4.37E-07	7.46E-07	2.62E-07	9.45E-08	2.75E-07	4.04E-07	6.68E-07	5.84E-07
4.97E-07	3.02E-07	1.13E-07	8.05E-08	-7.28E-09	3.17E-07	1.84E-07	5.02E-08	1.21E-07	9.37E-08	1.90E-07	1.52E-07	7.05E-08	1.40E-07	3.05E-07

Figure 3.85. Sample raw excerpt (one data point) of TDEMI prototype data file.

lineNo	0	OrientSensor_Z	1.5	TxLoop1Vertex3X	-0.225	TxLoop3Vertex2Y	-0.175	RxCube2_Z	0
Delt	2.00E-06	TxLoop0Vertex0X	-0.625	TxLoop1Vertex3Y	-0.175	TxLoop3Vertex2Z	0.04	RxCube3_X	0
BlockT	0.033336	TxLoop0Vertex0Y	0.175	TxLoop1Vertex3Z	0.04	TxLoop3Vertex3X	0.225	RxCube3_Y	0
nRepeats	3	TxLoop0Vertex0Z	0.04	TxLoop2Vertex0X	0.175	TxLoop3Vertex3Y	-0.175	RxCube3_Z	0
DtyCyc	0.5	TxLoop0Vertex1X	-0.975	TxLoop2Vertex0Y	0.175	TxLoop3Vertex3Z	0.04	RxCube4_X	0.4
nStk	1	TxLoop0Vertex1Y	0.175	TxLoop2Vertex0Z	0.04	TxLoop4Vertex0X	0.625	RxCube4_Y	0
AcqMode	DecaysDecimated	TxLoop0Vertex1Z	0.04	TxLoop2Vertex1X	-0.175	TxLoop4Vertex0Y	0.175	RxCube4_Z	0
GateWid	0.35	TxLoop0Vertex2X	-0.975	TxLoop2Vertex1Y	0.175	TxLoop4Vertex0Z	0.04	RxCube5_X	0.8
GateHoff	3.00E-05	TxLoop0Vertex2Y	-0.175	TxLoop2Vertex1Z	0.04	TxLoop4Vertex1X	0.975	RxCube5_Y	0
TxSeq	NRLTx04	TxLoop0Vertex2Z	0.04	TxLoop2Vertex2X	-0.175	TxLoop4Vertex1Y	0.175	RxCube5_Z	0
GPSReceiverID	GPGGA	TxLoop0Vertex3X	-0.625	TxLoop2Vertex2Y	-0.175	TxLoop4Vertex1Z	0.04	TimeGate_0	1.20E-05
GPSTriggered	FALSE	TxLoop0Vertex3Y	-0.175	TxLoop2Vertex2Z	0.04	TxLoop4Vertex2X	0.975	TimeGate_1	3.10E-05
OrientReceiverID	MICROSTRAIN3DMGX1	TxLoop0Vertex3Z	0.04	TxLoop2Vertex3X	0.175	TxLoop4Vertex2Y	-0.175	TimeGate_2	4.80E-05
nChannelsPerCube	1	TxLoop1Vertex0X	-0.225	TxLoop2Vertex3Y	-0.175	TxLoop4Vertex2Z	0.04	TimeGate_3	7.30E-05
MapOrientation	0	TxLoop1Vertex0Y	0.175	TxLoop2Vertex3Z	0.04	TxLoop4Vertex3X	0.625	TimeGate_4	0.000112
MagDeclination	-8.9	TxLoop1Vertex0Z	0.04	TxLoop3Vertex0X	0.225	TxLoop4Vertex3Y	-0.175	TimeGate_5	0.000173
HeightAboveGround	0.2	TxLoop1Vertex1X	-0.575	TxLoop3Vertex0Y	0.175	TxLoop4Vertex3Z	0.04	TimeGate_6	0.000266
GPSAntenna_X	0	TxLoop1Vertex1Y	0.175	TxLoop3Vertex0Z	0.04	RxCube1_X	-0.8	TimeGate_7	0.000409
GPSAntenna_Y	0	TxLoop1Vertex1Z	0.04	TxLoop3Vertex1X	0.575	RxCube1_Y	0	TimeGate_8	0.00063
GPSAntenna_Z	1.52	TxLoop1Vertex2X	-0.575	TxLoop3Vertex1Y	0.175	RxCube1_Z	0	TimeGate_9	0.000969
OrientSensor_X	0	TxLoop1Vertex2Y	-0.175	TxLoop3Vertex1Z	0.04	RxCube2_X	-0.4	TimeGate_10	0.00149
OrientSensor_Y	-0.1	TxLoop1Vertex2Z	0.04	TxLoop3Vertex2X	0.575	RxCube2_Y	0	TimeGate_11	0.002292

Figure 3.86. Sample raw TDEMI prototype acquisition parameters file.

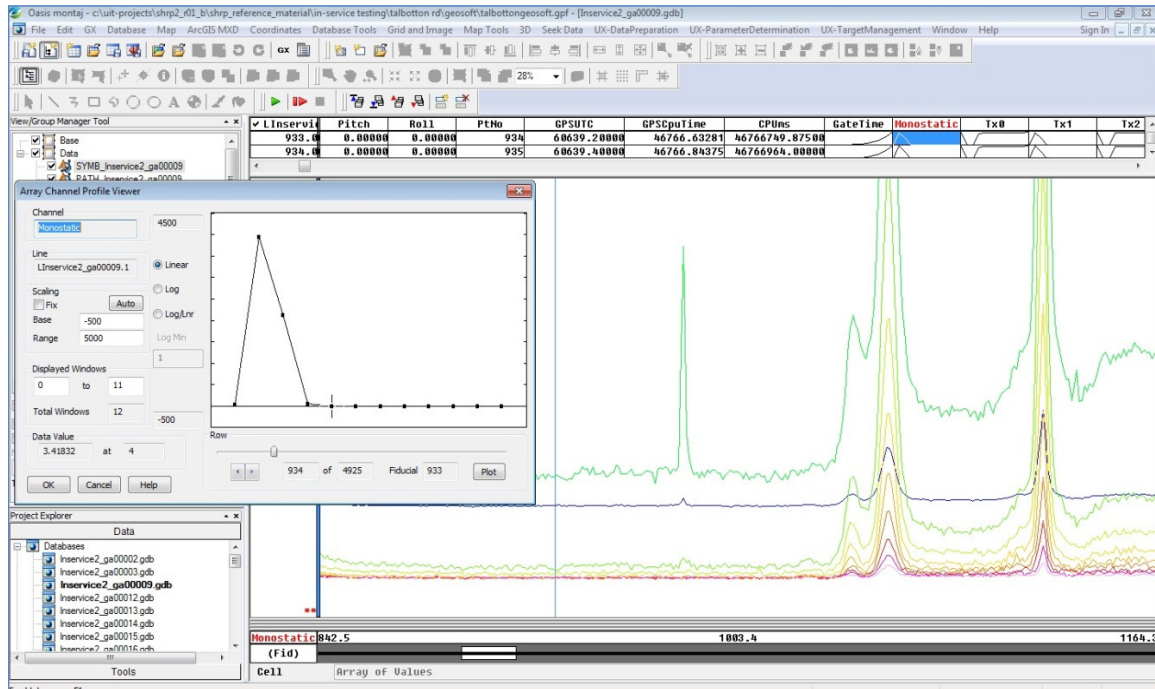


**Figure 3.87.** Screenshot of Oasis Montaj profile view of monostatic channel for Sensor 1 (colored profile) and individual array view (smaller window) of one individual data point.

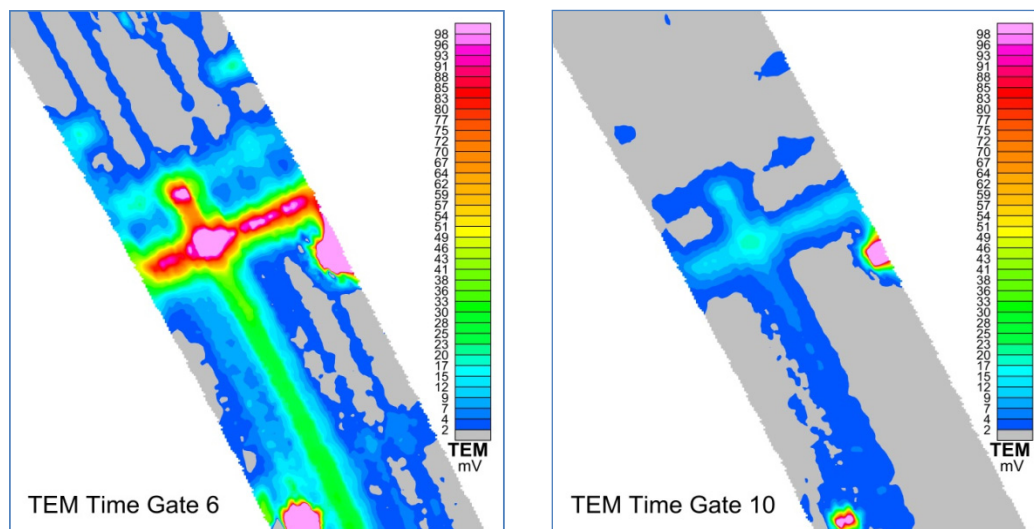


**Figure 3.88.** Screenshots of various TDEMI prototype grids in Oasis Montaj; images are at fixed color scale and represent the same production zone at different time gates (TDEMI decay rates).

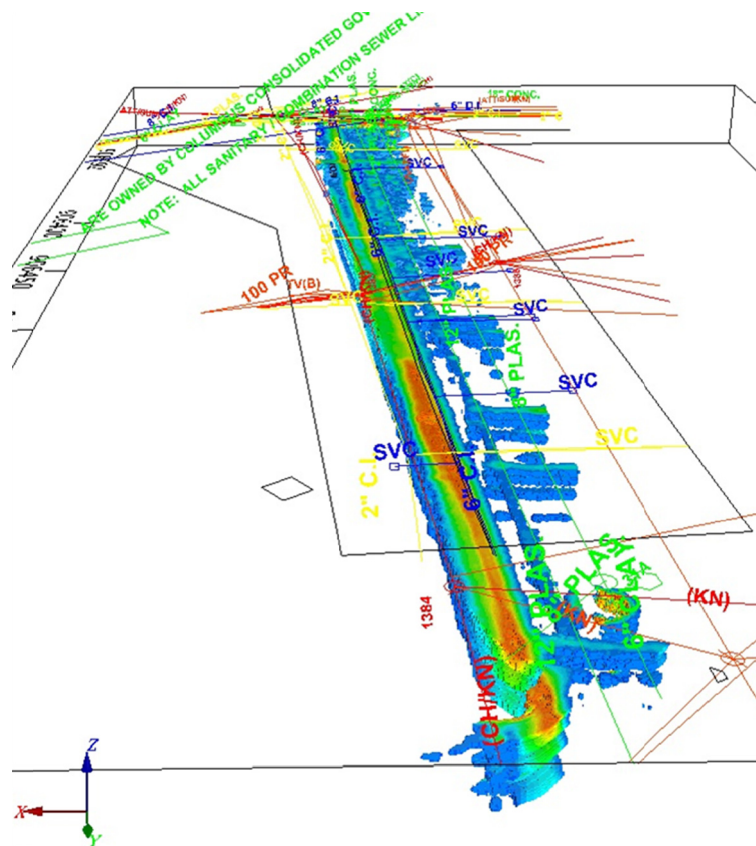


**Figure 3.89. Viewing TDEMI prototype data with 3-D visualization and in conjunction with geo-referenced utility records data.**

technology first spawned by SAIC and NRL's 5-by-5 TDEMI sensor array. The construction and development of the R01B prototype was incremental, as several first efforts were thwarted due to resource constraints and unforeseeable hardware malfunctions early in the project. Ultimately, a 5-by-1 TDEMI sensor array was assembled on a metal-free cart and thoroughly tested at UIT's New York office location as well as the two in-service testing sites. Testing involved the use of a variety of acquisition parameters and careful analysis of the acquired TDEMI data sets. UIT successfully worked with Geosoft to design and create an import template to manage the input and organization of the rich TDEMI prototype data sets produced. Initial results suggest that the system provides improved sensitivity in detecting targets but no significant improvements to horizontal target resolution compared with current TDEMI systems.

Advanced processing of the TDEMI prototype data is ongoing in an attempt to make better sense of the acquired data. This effort involves building on existing interpretative processes, possibly by modifying and implementing target utility characterization and depth estimation techniques that use a combination of modeling and inversion routines created by

SAIC for the munitions response industry. First attempts have been marginally successful with the sample data sets tested. Although the data clearly indicate the presence of buried utilities, it is not yet possible to accurately invert for target parameters. This is primarily due to two factors. First, the SNR is low; it is high enough for detection purposes, but larger signals are needed for stable inversions. Second, the prototype's timing is not disciplined enough to support continuous data collections. This can be observed in Figure 3.90. The time step between data points—defined as  $\text{BlockT} \times n\text{Transmitters} \times n\text{Stk}$ —is  $1/30 \times 5 \times 1 = 0.16667$ , assuming continuous data collection with all five transmitters firing. If a bit extra is added for calculations, the time step is expected to be  $\sim 0.2$  s. When the CPUms (i.e., milliseconds as counted by the CPU) in the data samples is observed, however, the time step is seen to vary—even within a single data file. This is problematic for inversions, because the data measurements must be positioned accurately relative to each other, and that requires accurately matching up the time stamp of the TDEMI data with a time stamp from the GNSS.

Through discussion with the designer and fabricator of the unit, the project team learned that this system has hardware limitations that result in a variable time step. These limitations

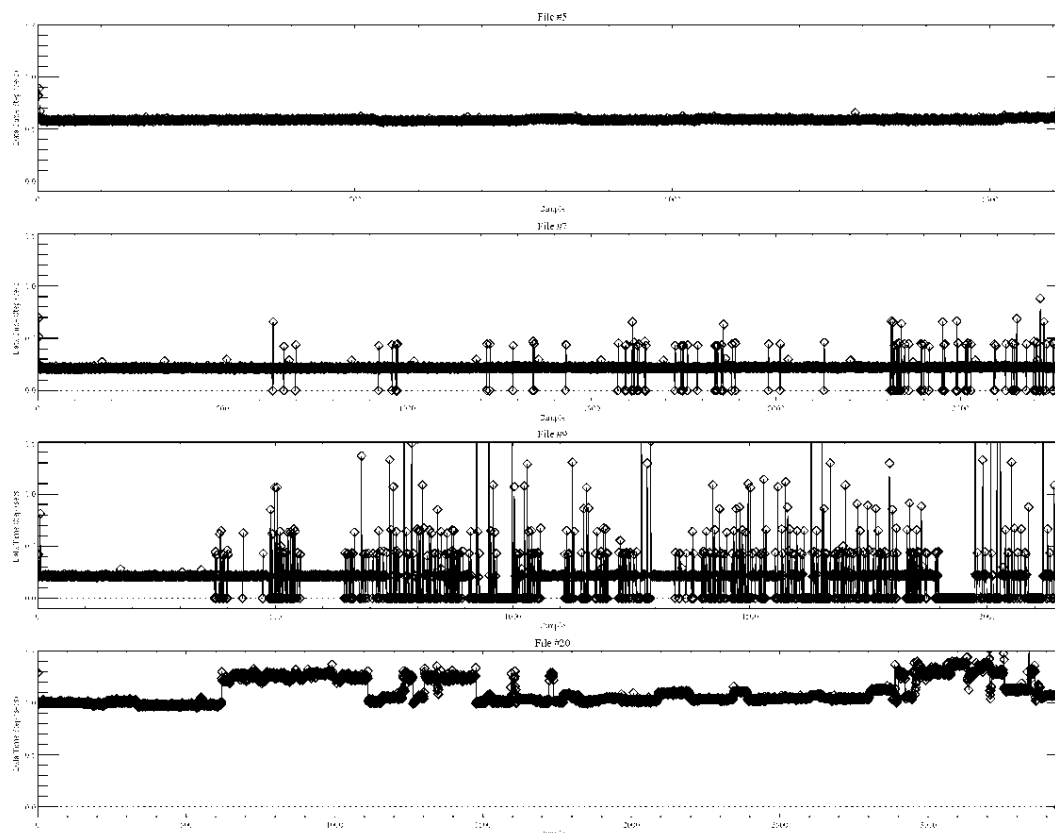


**Figure 3.90.** Example TDEMI prototype data time steps.

were not an issue with the units used for munitions classification because those systems collect data in static mode. Only during the past few years has the TDEMI system's fabricator learned to improve the hardware (and controlling software) such that the units can be used in continuous data collection mode. This problem has been corrected by the system fabricator and will not be a problem in future units.

## In-Service Testing

Two R01B prototypes (TDEMI system and software enhancements for multichannel GPR system) were demonstrated and evaluated during the in-service testing in July 2012. These tools were operated by the research team on actual, current highway projects; and their deployment was observed by an authorized Subsurface Utility Engineering (SUE) firm, So-Deep, Inc., that had previously performed utility mapping at the sites. The data collected by the research team could not be processed in real time, and utilities could not be visualized in the field. All that could be done in the field was confirm that raw data were collected. The data processing and analysis were done in the office, observed by the same SUE firm. The goal of the in-service testing was to determine if the developed tools can image utilities at accurate depths and elevations, detect

utilities that cannot be detected with current methods, reduce the effort needed to find utilities, and confirm the detection capabilities of current methods. On completion of the in-service testing, the SUE firm provided an evaluation report compiling its observations. This report, *Field Evaluation of Tools Developed in the SHRP 2 R01B and R01C Projects* (Anspach and Skahn 2014), is available at <http://www.trb.org/main/blurbs/171470.aspx>.

The selected project sites and SUE firm evaluators for in-service testing were

- Virginia Department of Transportation (DOT) at Stringfellow Road, Fairfax, Virginia; So-Deep, Inc. (see Figure 3.91); and
- Georgia DOT at Talbotton Road, Columbus, Georgia; So-Deep, Inc. (see Figure 3.92).

## In-Service Testing Objectives and Methods

The SHRP 2 R01B and R01C project teams completed the overall in-service testing project at multiple sectors along production routes designated at both the Virginia and Georgia sites. For the Virginia site, data acquisition began at the intersection of Stringfellow Road and Lee Jackson Memorial

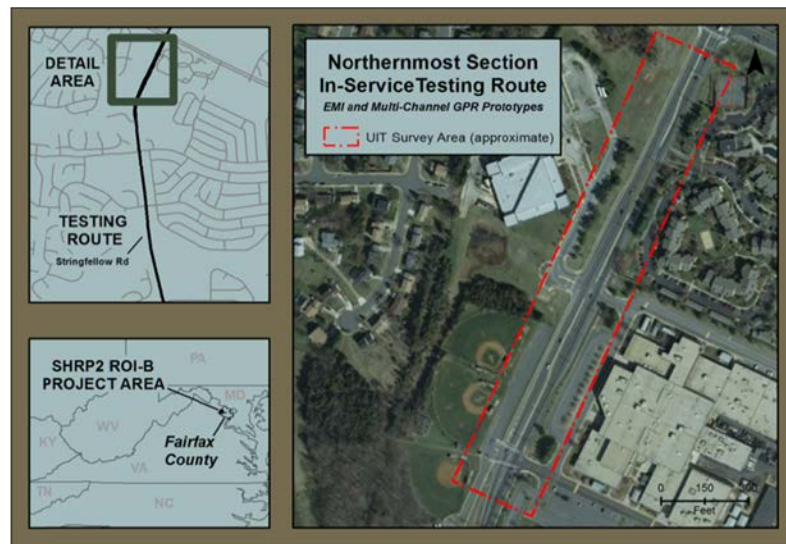


**Figure 3.91.** Stringfellow Road, Fairfax, Virginia, in-service testing site.

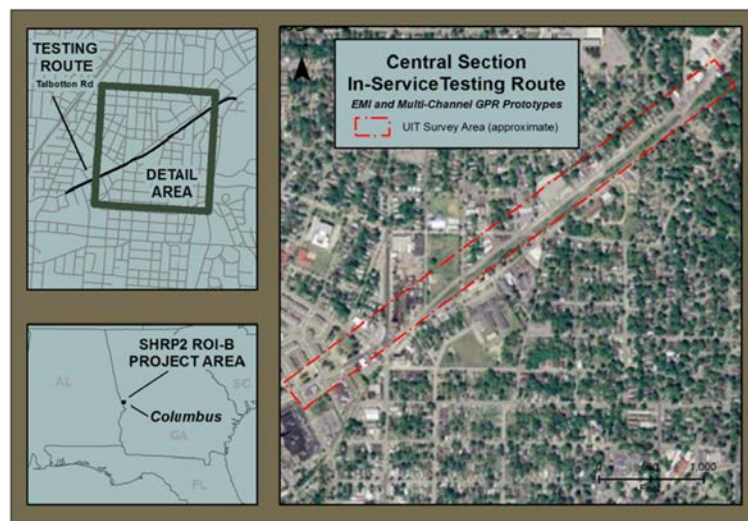


**Figure 3.92.** Talbotton Road, Columbus, Georgia, in-service testing site.

Highway (US-50) and moved south along the production route to specific areas representative of diverse underground utility conditions as determined by the project team, DOT, and SUE firm. For the Georgia site, data acquisition was conducted in a similar manner, beginning at the intersection of Talbotton Road and Hamilton Road and moving eastward and westward along the production route.

At each location, Day 1 required the establishment of survey control (Figure 3.93), a visual site assessment, and thorough review of the existing records of utility quality level validation data. The goal of this activity was to define data collection specifications; identify project logistical support requirements; discuss and validate project staging, access, and

scheduling dependencies; and determine data acquisition strategies at the project areas of interest.

The R01B project team deployed two geophysical systems: the multichannel GPR TerraVision II equipment (Figure 3.94) and the advanced TDEMI system prototype (Figure 3.95). These systems, working together, were considered to offer the greatest likelihood of detecting the subsurface utilities in these localized areas. The primary factors that affected the ability of these geophysical methods to detect subsurface objects include object size, mass, orientation, distance of the object from the sensors, and cultural surface conditions. For GPR detection of utilities, soil conditions need to allow for GPR penetration; for metallic utilities, there needs to be sufficient



**Figure 3.93.** Establishment of survey control before geophysical investigations during in-service testing.



**Figure 3.94.** TerraVision II data acquisition during in-service testing.



**Figure 3.95.** TDEMI prototype data acquisition during in-service testing.

contrast between the metallic utility objects and surrounding materials to distinguish targets within the TDEMI data sets.

The data acquisition software was unique to each prototype evaluated, and the data collected from these geophysical systems were processed in separate specialized analysis software packages. For the TerraVision II, data were acquired with UIT's Data Acquisition Shell (DAS) software. The multichannel GPR data were then processed, analyzed, and interpreted using UIT's SPADE software. For the TDEMI prototype, data were acquired using EM3D software (developed by system fabricator, G&G Sciences). The TDEMI data sets were then processed, analyzed, and interpreted using Geosoft Oasis Montaj software. Both analysis software packages, SPADE and Oasis Montaj, had been recently adapted to improve and enhance the geophysical data processing routines specific to each system.

Data processing and quality control of the production data followed predefined workflows, as defined in the standard operating procedures of Appendices A through D and in UIT's in-service testing report. Daily equipment function tests were performed on all equipment to document that data acquisition was performing as designed. The test regimen included (1) functional checks to ensure the position and geophysical sensor instrumentation was functioning properly before and at the end of each data acquisition session, (2) processing checks to ensure the data collected were of sufficient quality and quantity to meet the project objectives, and (3) interpretation checks to ensure the processed data were representative of the site conditions. Field notes were also reviewed for observations such as cultural features and equipment malfunctions that could influence data quality and interpretation.

### **In-Service Testing Evaluation of Process and Reporting**

The project team and SUE firm monitored and documented observations related to each system tested. Each definable feature of work was evaluated for efficiency, quality, usability, and overall functionality. Data collection was the primary focus from July 9, 2012, to July 20, 2012. Geophysical data processing and interpretation for each system followed in the subsequent weeks. Once data processing was complete, target geophysical anomaly selections were made at predicted utility locations. For TDEMI data, horizontal target selections were made at precise peak instrument response locations (relative to surrounding background) that were believed to be associated with subsurface utilities. For multichannel GPR data, horizontal target selections were made, along with depth estimates, at the interpreted target utility locations. All interpretations were made within the context of supplied resources (labor, existing records, etc.) that a typical SUE contractor might have available for any given project. A qualified UIT

geophysicist reviewed all of the data sets with regard to data quality, coverage, and validity of the target selections.

All the field notes, processing logs, and quality control (QC) test result tables were preserved and made available to the evaluating SUE firm and project sponsor. Daily data were packaged in \*.zip files by the date the data were collected, using the following folder structure:

- Raw data;
- All raw data from the field;
- All raw ASCII files created from the raw data;
- Processed data/daily;
- All QC tests and production data \*.xyz files created after processing in SPADE or Oasis Montaj; and
- All packed QC tests and production data \*.map files created in SPADE or Oasis Montaj.

All raw field data [real-time kinematic (RTK)–GNSS] contained an associated time stamp. Corrections were applied for positioning offsets, instrument bias (including instrument latency), and instrument drift; in addition, final processed data were filtered or normalized. Each data file was named logically and sequentially so that the file name could be easily correlated with the project-specific naming conventions. Data within the files could be delineated into individual fields for each value reported. Values reported in data files included local, geographic, and/or projected coordinates for each measurement (one or more values which were the data associated with each data channel measurement) and the time stamp for each measurement.

The primary goal of the R01B and R01C in-service testing was to have the SUE firm observe the application of the prototype tools (hardware and software) that had been developed to meet actual field conditions. This observation covered not only the deployment of the tools but also the methods and means by which the data gathered were processed and depicted. After this observation, the SUE firm was asked to review interpretation results, compare results with existing records, and generate a report detailing the assessment. The SHRP 2 project team solicited input from the User Group Panel to develop relevant questions and thoughts for the SUE

firm's report. The preferred approach for the in-service testing was the independent SUE provider's active participation in the assessment of the prototype tool(s), working in close coordination with UIT.

### In-Service Testing SUE Firm Summary

The SUE firm report—Observation, Evaluation, and Report on the SHRP 2 R01B and R01C Tools (Anspach and Skahn 2014)—states that the TerraVision II and TDEMI prototype appear to be good tools for certain projects and may enhance, but not replace, traditional utility mapping methods. It was determined that significant further testing was warranted: a comprehensive test hole program would be beneficial going forward, especially for determination of unknowns, reliability of depths, and identification of areas of anomalies.

Also, a concern arose that DOTs may be reluctant to increase their utility mapping budgets to accommodate the costs associated with the new tools. One solution was proposed: some of the utility mapping costs of the new tools could be offset with funds budgeted from other DOT departments that would benefit from the additional data the prototype tools provide. These might include but are not limited to paving and maintenance functions, archeological surveys, environmental surveys, geotechnical base-lining and bore hole placement development, arborist (for historical tree root determinations), septic field mapping, limits of cemeteries, and reduction of unknown or differing site conditions for construction departments.

Tables 3.7 and 3.8 summarize the results of the R01B tools compared with the existing SUE records for each of the in-service testing sites.

### In-Service Testing Results and Experience

The in-service testing for this project was done on a “stand alone” basis: the two main system components (on which development occurred and which were far enough along for testing) were tested on two sites where other work has been carried out by So-Deep. So-Deep used standard pipe and cable locators and test holes to map the utilities at the sites,

**Table 3.7. So-Deep QL-B Versus R01B Tool Utility Footage—Stringfellow Road, Virginia Utility Results (Anspach and Skahn 2014)**

Utility	Water	Gas	Telephone	Electric	Cable TV	Sanitary	Storm	Unknown <sup>a</sup>
<b>So-Deep QL-B footage</b>	1,860 ft	2,795 ft	1,695 ft	75 ft	NA	NA	NA	NA
<b>R01B footage</b>	1,740 ft	825 ft	205 ft	0	NA	NA	NA	210 ft
<b>Percent footage found by R01B</b>	93%	33%	12%	0%	NA	NA	NA	NA

Note: NA = not available.

<sup>a</sup> Out of So-Deep scope or newly installed lines.

**Table 3.8. So-Deep QL-B Versus R01B Tool Utility Footage—Talbotton Road, Georgia Utility Results (Anspach and Skahn 2014)**

Utility	Water	Gas	Telephone	Electric	Cable TV	Sanitary	Storm	Unknown <sup>a</sup>
<b>So-Deep QL-B footage</b>	2,635 ft	1,655 ft	1,405 ft	90 ft	85 ft	1,815 ft	220 ft	880 ft
<b>R01B footage</b>	1,855 ft	860 ft	135 ft	0 ft	0 ft	610 ft	290 ft	775 ft
<b>Percent footage found by R01B</b>	70%	51%	9%	0%	0%	33%	100%+	na

Note: na = not applicable.

<sup>a</sup> Data for Unknown (unknown utility or instrument response) is shown for comparison purposes. The unknown lines found by So-Deep do not necessarily coincide with the unknown lines found by the new tools; therefore, percentages of lines found do not apply.

then the new systems were brought in for a comparison study. Those comparisons are shown in Tables 3.6 and 3.7. The main outcomes from the testing showed that in conditions that were optimal for each system, each system performed reasonably well. In less than optimal conditions, such as clays soils for GPR, the system didn't necessarily perform well. This was the most straightforward method of performing an honest test, but it was not really a test of the "system" approach to performing multisensor utility mapping. Essentially one set of system components were tested against a separate set of system components, which ultimately is nonsensical. The intention of multisensor systems is to perform the mapping by using all available system components in concert with each other, not competitively. In the normal course of conducting projects, the 3-D GPR system would not have been deployed at the Virginia site because of poor GPR soil conditions, but the other system components would have been deployed.

If the costs of the So-Deep part and the R01B parts of these projects were added up, the resulting project costs would

mostly likely be unpalatable to the DOTs involved (this was not done in this case). The reason that multisensor mapping is not more deeply in the market now is that both consultants and DOTs look at the components as separate items. In most cases, the "extra" cost of doing the added geophysical work is not included. If projects are scoped to include the system approach, the benefits of the multisensor geophysical data become evident. The benefits come from finding unknown utilities (which happens much more often in practice than on the two projects studied in R01B), limited but targeted use of test holes, better 3-D information, enhanced project and public safety from having better mapping, less public inconvenience due to road closures, and environmental benefits from fewer test holes and errant digs during construction. Multisensor mapping has been done on numerous projects by UIT before and since the R01B project and has measurable benefits. See Young and Keaton (2014) for a project example as well as a description of how enhanced utility mapping with multisensor systems fits well into sustainable engineering practice.

## CHAPTER 4

# Conclusions and Suggested Research

### Conclusions

The purpose of this research was to bring together and develop credible nondestructive geophysical techniques on a land-based, towed platform capable of detecting and locating underground utilities under all geologic conditions. The R01B research project resulted in the development and improvement of advanced technologies (detection sensors, analysis software, and work procedures). These technologies contribute to a multisensor approach that offers subsurface utility engineers and geophysical service providers the best chance to completely and accurately detect, locate, and characterize subsurface utilities at any location across the United States and the world. However, even with improved technology, the necessary resources and technologies would not likely be deployed to a site without a cost-benefit analysis that considers potential project delays, safety issues, and cost overruns that could occur if utilities are not effectively identified and located. Thus, technological advances in locating and characterizing utilities must be accompanied by complementary improvements in management and procedures to allow this technology to be used effectively. In fact, the management and funding of efforts to locate utilities, the required training, and the prohibitive cost of implementing effective operations are as much factors in preventing the effective use of advanced technologies in the field as the technology's limitations.

### Recommended System Deployment Strategy

Based on the in-service testing and experience outside the R01B program, the recommended deployment of multisensor geophysical systems is as follows:

1. Perform SUE Level D.
2. Perform SUE Level C.
3. Perform SUE Level B, using
  - a. Pipe and cable locators;
  - b. 2-D GPR, as appropriate;
  - c. 3-D GPR, as appropriate over areas of more complex utility networks or where unknowns are expected;
- d. TEM, as appropriate—but cover nearly every site as completely as possible due to low cost, fast coverage, ability to detect “hard to tone” utilities such as cast iron and ductile iron;
- e. Final interpretation of all system data to produce a combined map of all targets; and
- f. Chosen sites for test holes.
4. Perform test holes as in SUE Level A at selected sites:
  - a. Use test hole data to refine depth parameters for GPR, if GPR was performed;
  - b. Refine GPR depth mapping based on test hole data; and
  - c. Produce final mapping.
5. If desired by DOT or engineer, use all data produced to construct 3-D modeling of utilities.

### Multichannel GPR and SPADE Software

Several GPR technologies are available that range in their ability to detect targets. A common technology used for SUE applications today is single-channel GPR. These systems generally use a grid of data collection transects spaced at some interval greater than the detection footprint of the GPR antenna; as a result of the relatively coarse spacing of these transects, very little information about the subsurface is generally obtained using this technique. By contrast, the multichannel 3-D GPR system (TerraVision) used by UIT contains 14 antennas similar in capability to those commonly employed in single-channel systems. These antennas are spaced approximately 4 in. apart, resulting in much higher data density than can be reasonably achieved with a single-channel system (this would require a single-channel operator to perform individual transects at a spacing of 4 in. to obtain equivalent data density). By collecting adjacent swaths of multichannel data, it is possible to obtain coverage over 100% of accessible areas of a project site. These data can generally be collected more rapidly than single-channel data, reducing field time and project costs while also increasing

data density. SPADE is the sophisticated software package designed to assist data analysts in the visualization and interpretation of these GPR data sets. The R01B project resulted in several enhancements, which were applied to SPADE and offer data analysts proven methods to improve the efficiency and accuracy of geophysical analysis.

The segmentation algorithms and threshold methods developed through this R01B research offer a radically different way of analyzing GPR data. The potential improvements from a more intuitive selection process are large—it is thought that presenting data as a set of forms and surfaces will allow rapid identification of features and rejection of noise. The algorithms that were tested are efficient at identifying the majority of features present in the data.

A number of image processing algorithms can be applied to remove ringing artifacts. A good summary of these can be found in the article, *Removal of Ringing Noise in GPR Data by Signal Processing* (Kim et al. 2007). However, in UIT's TerraVision data the ringing can lead to saturation, at which point image data are irretrievably lost. Sagentia has recommended that UIT address the causes of ringing in the sensor hardware.

Sagentia has produced an improved method for quickly assessing the migration parameters for GPR data and an improved version of the 3-D migration algorithm. The developments also include a method for performing operations on a chosen subset of GPR data that allows for faster computer calculations for heuristic parameter selection. Those parameters can then be applied to the whole data set just one time. A new 3-D migration algorithm fixed some older shortcomings and enhanced the processing speed and accuracy of the migration calculation. Figure 4.1 illustrates this newly developed functionality. These changes are already being implemented in SPADE and are proving to be a big help in improving both the speed and quality of GPR data interpretations.

### High-Frequency Seismic Imaging

This component of the R01B research focused on proof-of-concept ideas. The soil seismic properties investigated under a SHRP 2 subcontract (OES/Psi-G Task II.A, Soil Seismic Properties and Testing) showed S-wave and P-wave velocities to be in reasonable agreement with data presented previously (Lew and Campbell 1985). That work was based on soil properties evaluations performed at a large number of California field sites. The SHRP 2 soil properties tests were designed to yield S-wave and P-wave velocity and attenuation profiles at three regional field sites: Manteno, Illinois; Houston, Texas; and Manassas, Virginia. These results show the S-wave velocities to be in the range 200–300 ft/s at 1-ft depth, increasing to the range 800–1,400 ft/s at 12-ft depth (Figure 3.28). The P-wave velocities at these sites were in the range 450–700 ft/s at 1-ft depth, increasing to the range 1,700–3,600 ft/s at 12-ft depth (Figure 3.30). The velocity gradients were found to be

accurately described by fractional power-law regression curves with depth exponents of 0.521 for S-waves and 0.586 for P-waves. The corresponding quality factor (Q) profiles at these three sites were found to be relatively constant at equal mean values of about  $Q_S = Q_P = 20$ , with variations in the range  $Q_S = 10\text{--}27$  and  $Q_P = 12\text{--}28$ . The attenuation rates corresponding to these Q values are  $\alpha\lambda_S = 2.73\text{--}1.01$  dB per wavelength and  $\alpha\lambda_P = 2.27\text{--}0.975$  dB per wavelength, respectively, with approximately equal mean values of 1.36 dB per wavelength.

These summary velocity and attenuation values and ranges are generalized results derived from recorded field data containing noise and spurious resonance effects in the measurement system. For some of the test sites, the measurements were physically limited to shallower depths than planned. Therefore, the indicated values are only approximate; and in some cases, they are only inferential with respect to the deeper depths. While the quantitative accuracy of these results for each specific test site cannot be determined, the similarities in S-wave and P-wave velocity profiles and their depth trends at the five independent borehole test locations tend to validate the analyses and interpretations. For guidance in any further use of these field results, an empirical accuracy bound of  $\pm 10\text{--}15\%$  is assigned to the results presented in this report.

The soil seismic properties at each regional test site were used to predict the SH-wave reflection system pipe detection capability for pipe sizes of 3-in. diameter and larger. The seismic system operating characteristics were specified to be existing state-of-the-art capabilities with an effective system dynamic range of 120 dB. The system performance model was formulated in combination with the soil seismic properties derived from the regional field tests. The absolute receiver detection threshold was determined to be approximately  $-138$  dB below 1 g peak acceleration source radiation, giving the recorded signals a reasonable signal-to-noise ratio at the system threshold signal recording level. The two-way attenuation loss in the regional soils dominated the model-derived detection depth limits.

Table 4.1 summarizes the maximum detection depths for pipes in the range 3-in. to 10-in. diameter using a two-octave seismic vibrator sweep frequency range of 400–1,600 Hz. These results are based on accurate alignment of the incident SH-wave polarization parallel to the pipe axis. The results show that, for the soil conditions at four of the five soil test boreholes, 3-in.-diameter pipes are only detectable at depths of about 6 ft below the ground surface. The soil at Houston Borehole D2 is the exception, with 3-in.-diameter pipes detectable at depths about twice as deep as at the other sites. These detection performance results are qualified by the accuracy of the derived soil seismic properties and the fact that the threshold detection intercepts are at or near the recognizable resolution of the reflected seismic waves (Table 4.1).

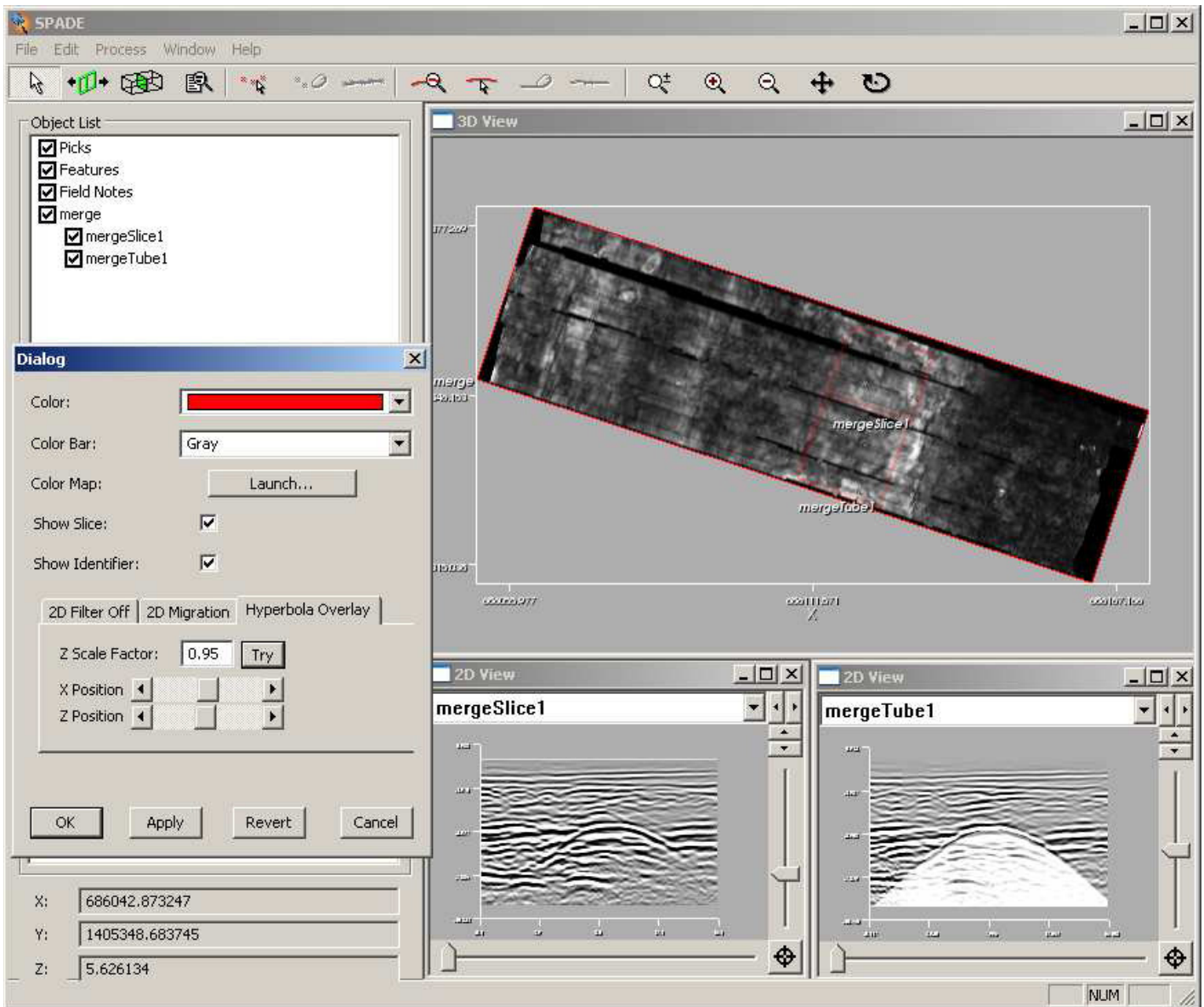


Figure 4.1. Previewing migration with “hyperbola overlay” filter.

Table 4.1. Maximum Detection Depths for Pipes in the Range of 3-in. to 10-in. Diameter

Regional Test Site	Maximum Pipe Detection Depth (ft) for SDR = 120.4 dB					
	3 in. Dia.	4 in. Dia.	5 in. Dia.	6 in. Dia.	8 in. Dia.	10 in. Dia.
Manteno B2	6.5	8.2	10.2	11.5	14.6	17.1
Houston D2	11.7	16.6	>17	>17	>17	>17
Houston E1	6.3	8.4	10.5	12.7	>17	>17
Houston F2	6.0	7.9	10.3	13.0	>17	>17
Manassas H1	6.0	7.4	8.8	10.2	13.4	16.0

In practice, the realizable detection performance will generally be less than that indicated in Table 4.1. For, example, the slopes of the curves in Figures 3.32 through 3.34 for pipes smaller than about 6 in. in diameter are high enough that, when a 10-dB detection margin is allowed, the maximum detection depths decrease by about 0.5–1 ft, depending on the pipe diameter. On this basis, 3-in.-diameter pipes are detectable at depths of about 5.5 ft, and pipes 6 in. in diameter or larger can be expected to be detected at depths down to about 10–12 ft in the tested soils and in soils similar to those at the three regional field sites.

## Seismic Modeling Software

The achieved objectives of the work at Louisiana Tech University related to the R01B research work were (a) to develop finite difference time-domain (FDTD) software capable of simulating propagation of acoustic and elastic waves in a realistic soil, (b) to study the properties of acoustic and elastic wave propagation through a soil and, (c) to analyze the physical consequences of the obtained results. On the basis of the obtained results, Louisiana Tech was supposed to look into the possibility of developing a virtual testing laboratory for the simulation of acoustic and elastic methods of detecting buried pipes and conduits.

Limited resources and time did not allow for full development of the FDTD software. Although LTU developed, tested, and applied several in-house computer models in different situations, the software chosen for simulating the acoustic and elastic wave propagation in soils was the open source Wave Propagation Program (WPP) from the Lawrence Livermore National Laboratory (Center for Applied Scientific Computing 2011). The software is offered “as is,” and users are free to modify it. The WPP software had options for variable wave speeds, attenuation coefficients, and soil densities throughout the computational domain. While the WPP code was used in large-scale seismic cases, it had never been used at the scale of applications of the R01B project. Very detailed studies of the WPP were performed at LTU, including the performance of the code in the high-frequency range, up to the limits allowed by the capabilities of the Louisiana Optical Network Initiative (LONI) system of supercomputers. It was found that the software is adequate for the scope of the R01B project.

Studies of the properties of acoustic and elastic wave propagation through a soil and characteristics of the reflections from the buried pipes were performed using both experimentally obtained data and theoretically possible waves. It was found that there were no limits in applications of the WPP assuming a realistic situation. The physical consequences of the obtained results were analyzed, and some of the results are presented in this report.

LTU is in a position to fully develop a virtual testing laboratory for the simulation of the acoustic and elastic methods for the detection of buried pipes and conduits. Such a virtual lab would be very beneficial in designing the devices for the detection of buried objects by reducing the development cost. While not completely finished, some work was also put into novel methods for signal processing. It was shown that the method would have capabilities of real-time signal analysis.

## TDEMI Technology

The time-domain electromagnetic induction (TDEMI) system prototype has been developed to operate advanced transmit (Tx) and receive (Rx) coil pairs at variable time gate intervals on a towed, nonmetallic instrument platform. The Tx and Rx parameters are fully programmable, which is useful in optimizing the detection and location of underground metallic utilities. The system was designed after SAIC’s current time-domain EMI array, which was developed collaboratively with the U.S. Naval Research Laboratory. During this research the TDEMI array was adapted for data processing and analysis procedures to support data import and manipulation within Geosoft’s Oasis Montaj geophysical software package. Target classification and discrimination of underground utility anomaly sources remain important objectives of the proposed research.

UIT has fully assembled the system and conducted a series of system bench tests, as well as demonstrated the TDEMI prototype’s functionality during in-service testing. This testing has indicated that the TDEMI prototype offers an improvement to detection of small metallic utilities compared with current TDEMI digital geophysical mapping systems. This is a direct result of the early time gate measurements that can be achieved with the prototype system. Several other aspects of the system, however, require further investigation and improvement; these include system ruggedization and the consolidation of hardware components, system integration with laser-based positioning systems, a more detailed assessment of bistatic measurement(s) capabilities for target characterization, and problems associated with the time step variations.

## Suggested Research

### System Deployment Improvements

All of the geophysical systems experience difficulties when working over terrain that is other than flat. First, there are issues with working on uneven surfaces, including over curbs; these sometimes contain metal—such as pipe and cable locators—that can confuse or provide spurious signals to electromagnetic systems. On irregular terrain, GPR systems sometimes experience apparent noise due to air gaps beneath

the antennas. Sometimes obstacles, such as vegetation or engineered structures, exist above the utilities being mapped. On steep slopes, all of the systems produce signatures that must be mapped perpendicular to the surface, not directly (vertically) beneath the spot on the surface where the signature is indicated.

The rough surface issues must be handled in the field, with careful use of the tools by experienced operators; and for the most part, they are straightforward. Obstacles simply provide challenges that must be considered in the project planning; in the case of vegetation, the site can be mowed, which is often done. The steep slope issue can be handled in two ways. First, if a digital terrain model is available, those data can be used to recompute depths to targets—or accurate surface locations in the case of pipe and cable locators. The second way to handle slopes is to include an inclinometer or other method of determining slope on an inch-by-inch basis as data are collected. This solution applies to cart-based systems; it has not been deployed for regular use by anyone as yet but is an area of future development. Currently, consultants and contractors handle these issues on a case-by-case basis, using solutions appropriate for the situation.

An additional issue is the need to provide utility elevations, not just depths. The geophysical systems that provide depth information need to be augmented with a method of measuring current surface elevation so that elevations of utilities can be computed. UIT currently does this by obtaining a digital elevation model from the project engineer's surveyor. When the geophysical cart-based systems use high-quality RTK or laser robotic survey devices, good quality surface elevations are available, but only on those areas surveyed by the geophysical cart. In the future, lidar scans of the surface will be used to obtain elevations over the whole site. That is another area in which development is needed.

### **Multichannel GPR and TDEMI Technology**

UIT's work experience and the results obtained from the in-service testing indicate that the use of both GPR and TDEMI technologies offers a more complete assessment of the subsurface condition. The horizontal locations of subsurface utility targets can be determined with relative ease using these methods. However, depth information on these targets is a more challenging aspect of the geophysical investigation. With some study of the local soils for calibration, the depth to the pipe can be measured to a tolerance of a few inches with the GPR data. Since the TDEMI system's response has amplitude affects that depend on the distance of the sensor from the pipe, it would be valuable to have a technique for finding the depth to the pipe independently. Further study of GPR signals may also yield information about the pipe itself (e.g., the

corrosion state of rebar in bridge decks is estimated on the basis of variation in the amplitude response of GPR signals).

Aside from depth estimation capability, GPR and TDEMI technologies may provide a realistic approach for pipeline assessment from the ground surface. For TDEMI sensors, pipeline detection should give a very consistent instrument response if materials, depth to the pipe, soil type, and pipe condition are the same along the mapping zone. When any of those conditions change at any section of the mapping zone, the geophysical anomalous signature is expected to change as well. As mentioned, the TDEMI prototype developed through this research was built on a TDEMI system designed for finding UXO targets. Theoretical analysis indicates that a system set up differently—to focus on measuring the response that occurs from interaction of the signals with the surface of the pipe—could be used to more accurately examine the pipe's condition. One suggestion would be to begin research with a newer, more programmable TDEMI that may offer clues to subsurface pipe conditions.

### **Seismic Modeling Software**

The ultimate goal is the modeling of multisensor platforms consisting of the electromagnetic technique and the acoustic technique. The project team hopes that acoustic code developed during the R01B project will be used along with electromagnetic code to study the efficacy of multisensor platforms. The data collected individually from both codes may provide target signatures for carrying out the development of data fusion algorithms.

More development of the postprocessing program will occur in future WPP scenarios. Presently, the postprocessing program is hard-coded to deal with specific names of files and would have to be recompiled to be adapted to the output of future WPP scenarios. If the postprocessing program needs to be shared with other users, or if it begins to be applied to many different WPP scenarios, the program could be adapted to use a configuration file to specify tasks and program options. An easy implementation of this feature is possible via boost program options, a library in the Boost C++ libraries.

The code in the postprocessing program is largely procedural and localized to a few functions. Large portions of the procedural code could be unified into more generic sub-routines, and following from that, the code would not be so localized to a small handful of functions. Documentation would be easier to maintain and create if the code were reduced. Doxygen, an automatic documentation generation program, is used for what little documentation presently exists. The present documentation is no better than the weak documentation in WPP's MATLAB postprocessing scripts. As the demand and/or opportunity arises, these deficiencies should be dealt with.

## SPADE Workflows

Three potential workflow options for UIT have been assessed for efficacy and time-efficiency: depth-slice analysis, time-slice analysis, and migration analysis. Further controlled evaluation of these methods could lead to the optimal data analysis procedures used for subsurface utility investigations. The narrative below provides a brief explanation of these methods.

### *Depth-Slice Analysis*

This is the workflow currently used by UIT. An operator scrolls through vertical depth slices, picking the peaks of hyperbolae. Picks are then joined into features, with the assistance of time slices to provide a plan view of the data.

### *Migration Analysis*

Migration analysis is a reorganization of the workflow. An operator uses a small sample of data to identify the correct  $z$ -factor. Then the entire data set is migrated, and horizontal time slices of the migrated image are assessed for features. Areas of uncertainty can be checked using depth-slice analysis. Once a feature is found, the operator's mouse click initiates a tracing algorithm which attempts to locate the entire feature. The operator refines and improves the machine's effort of feature tracing.

### *Time-Slice Analysis*

A workflow oriented around horizontal time slices, but without the need for migration, this option strikes a balance between the two workflows above. Having merged several swaths to provide a broad data set, an operator scans time slices, focusing on subsections of the whole image. Identified features are picked and the picks joined into features. Areas of uncertainty can be checked using depth-slice analysis.

These three workflows will need to be thoroughly assessed against a set of criteria:

- Preprocessing time. This includes the time to choose the correct migration  $z$ -factor and the time to migrate the data set.
- Processing time. This is the speed of the workflow in processing features in a data set.
- Frequency of false positives. The score assigned is a relative assessment, not a probability or frequency of occurrence.
- Frequency of false negatives. The score assigned is a relative assessment, not a probability or frequency of occurrence.

- Clarity of features. Despite overlap with the two previous classifications, this criterion is explicitly included to characterize the visibility of features against the noise background and the ease of identification of a whole feature—its form (linear, point-like) and directionality.
- Facility of process. The final criterion assesses ease of use and the associated drain on the operator.

The initial subjective assessment suggests that geophysical service providers may be able to improve their workflow with a transition to analysis based on time slices, potentially incorporating migration transformations. UIT currently operates a quality-checking method which involves one operator reassessing an entire data set. This provides an ideal environment for thorough testing of alternative workflows—a new workflow can be trialed and assessed against the old workflow during the quality process.

The project team also suggests that a “polarized view” toggle be introduced to SPADE for the manipulation of TerraVision data. While there is no strong need to process images for migration with separate polarizations, being able to toggle unmigrated images between the three states (both polarizations as viewed currently, A only, or B only) may clarify features exhibiting polarization effects.

## High-Frequency Seismic Imaging

A focus of this research was to demonstrate the SH-wave seismic system concept. Practical soil seismic properties investigated and reported on here impose limitations on detecting 3-in.-diameter pipes at depths greater than about 5.5–6.0 ft and 6-in.-diameter pipes at depths of about 10–12 ft. This detection performance is based on using state-of-the-art high-resolution SH-wave reflection technology adapted specifically to underground pipe detection and mapping. Larger-diameter pipes are detectable at depths greater than 12 ft. On the premise that these predicted detection performance capabilities for state-of-the-art SH-wave reflection seismic technology are potentially applicable to detecting and mapping underground utility pipes, the R01B project efforts may require certain technical revisions.

The recommended technical revisions include the following:

1. Retain the SH-wave seismic operating concept and near-vertical illumination and reflection methodology using radiated SH-waves in the frequency range 400–1,600 Hz.
2. Proof test, troubleshoot, and suppress spurious resonances that were found to exist in the OES MicroVib SH-wave vibrator source. Retain this seismic source, with appropriate corrective adjustments, as a principal component of the

prototype seismic system. Note that, as defined in the license agreement between OES and UIT, no SHRP 2 R01B project work shall be performed to modify the proprietary MicroVib for the intended application.

3. Fabricate the recommended OES proprietary accelerometer sensor array as described in the project plan. Note that fabrication costs of the proprietary sensor array are separate from the SHRP 2 R01B project, as defined in the license agreement between OES and UIT.
4. Replace the automated trailer-based ground-scanning system design outlined in the project plan with a much simpler system configured only to test and evaluate SH-wave seismic reflections from underground pipes. In particular, instead of the previously planned prototype transport and ground scan platform, design a manually operated ground scan platform suitable for conducting controlled field tests of the prototype seismic system at sites having known underground pipe targets.
5. Modify the Dewetron Model 3201-8 data logging system used in soil properties testing to serve as the source excitation and data recording component of the prototype SH-wave seismic reflection system. The needed modifications have already been identified as a direct result of using the Dewetron equipment in the soil seismic properties measurements. These modifications pertain to certain changes in the Model 3201-8 software to integrate several source excitation and signal recording functions for efficient seismic data logging under field operating conditions. The software modifications would need to be performed by Dewetron, Inc.

The recommendations listed above represent a shift of the technical efforts from a directed prototype seismic system development and demonstration to a comprehensive applied research and development effort to refine and demonstrate the intended SH-wave reflection technology.

### **Alternate Suggestions for Seismic Development**

The comments here are based on both the SHRP 2 R01B and R01C projects. Since UIT is the entity that joins the two projects, the R01B principal investigator has made the final interpretations jointly and presents the following analysis and recommendations. It appears that the tasks proposed in the R01B and R01C projects of building both 2-D and 3-D imaging systems have proven to be too challenging for the early stages of this new area of technology. It is suggested that the aim be shifted to build a single 2½-D imaging system based on what we have learned from the testing thus far. What 2½-D means is that the final prototype will produce a single cross section (2-D) image by using a swath of sources and receivers (i.e., by making a partial 3-D measurement). It is believed that this approach is warranted and necessary to allow accountability for the complexities in scattering from targets and non-targets and to adequately characterize the velocity variations in the subsurface well enough to make an image. It is also believed that making 3-D images of the subsurface is beyond both the scope of this project and the currently available scientific knowledge of seismic data in the soils and depths of interest.

## References

- Anspach, J. H., and C. Skahn. 2014. Field Evaluation of Tools Developed in the SHRP 2 R01B and R01C Projects. Transportation Research Board of the National Academies, Washington, D.C.
- Center for Applied Scientific Computing. 2011. *Serpentine Wave Propagation: Theory and Applications*. Lawrence Livermore National Laboratory, Livermore, Calif. <https://computation.llnl.gov/casc/serpentine/index.html>.
- Kim, J., S. Cho, and M. Yi. 2007. Removal of Ringing Noise in GPR Data by Signal Processing. *Geosciences Journal*, Vol. 11, No. 1, pp. 75–81.
- Lew, M., and K. W. Campbell. 1985. Relationships Between Shear Wave Velocity and Depth of Overburden. In *Measurement and Use of Shear Wave Velocity for Evaluating Dynamic Soil Properties* (R. D. Woods, ed.), American Society of Civil Engineers, Reston, Va., pp. 63–76.
- Oelze, M. L., W. D. O'Brien, and R. G. Darmody. 2002. Measurement of Attenuation and Speed of Sound in Soils. *Soil Science Society of America Journal*, Vol. 66, No. 3, pp. 788–796.
- Vossiek, M., L. Wiebking, P. Gulden, J. Weighardt, and C. Hoffmann. 2003. Wireless Local Positioning: Concepts, Solutions, Applications. *Proc., IEEE Radio and Wireless Conference, RAWCON 2003*, Boston, Mass., pp. 219–224.
- Young, G. N., and J. R. Keaton. 2014. Enhanced Detection and Mapping of Buried Utilities—A Sustainability Perspective. *Geo-Strata*, Vol. 18, No. 1, pp. 40–44.

## APPENDIX A

# Standard Operating Procedure for Multichannel GPR Digital Geophysical Mapping Data Collection

### A.1 Purpose

The purpose of this Standard Operating Procedure (SOP) is to provide general procedures for geophysical data collection during subsurface utility field investigations using SHRP 2 R01B multichannel ground-penetrating radar (GPR) digital geophysical mapping (DGM) prototype system, also known as the TerraVision II system. This SOP is to be used in conjunction with the SOP for multichannel GPR DGM data processing (see Appendix B).

### A.2 Scope

This SOP applies to the collection of geophysical and associated spatial location coordinate data. A differential global navigation satellite system (GNSS) and/or robotic total station (RTS) will be coupled with the geophysical instrument(s) to record the  $x$  and  $y$  coordinates for the collected geophysical data points. The objective of the geophysical survey is to detect subsurface metallic objects that are utilities and/or other client-defined targets of interest to ASCE 38-02 standard's Quality Level B (QL-B) information. The purpose of the DGM surveys is to provide information that may be used to support the determination of the exact location of the utilities and targets of interest.

### A.3 Maintenance

The Project/Site Geoscientist, in collaboration with the QC Geoscientist, is responsible for the maintenance of this SOP. Approval authority rests with the Project Manager (PM). Approval authority is the power conferred on the PM to commit the geophysical service provider to the procedures, objectives, and data quality standards as set forth in this SOP.

### A.4 Equipment

The following is a list of equipment that will be necessary to complete a multichannel GPR DGM survey with the geophysical instrumentation for the project:

- TerraVision II antenna banks and control unit;
- Instrumentation platform (cart, wheels, GNSS mast, tow vehicle);
- Appropriate signal and power cables for all instruments;
- Real-time kinematic (RTK) GNSS rover/receiver, GNSS base station (if applicable), data logger, antennas;
- RTS instrument, prism, data collector, tripod(s), survey pole(s); and
- Sufficient batteries for daily operation of all instrumentation.

The following additional equipment and forms will be assembled by the Site Geoscientist(s):

- Task-specific field data logbook, QC tests form, survey report form;
- Pin flags, spray paint, traffic cones, tape measures, miscellaneous;
- Digital camera, USB thumb drive; and
- Personal protective equipment (as required by current health and safety plan).

### A.5 Personnel Requirements and Responsibilities

All personnel assigned to the geophysical investigation team must demonstrate the ability to perform assigned tasks associated with the subsurface geophysical investigation, using equipment and associated software at the

designated project location. This equipment and software include

- RTK GNSS;
- RTS;
- TerraVision II multichannel GPR array
  - a. Pair of antenna array banks (L & R);
  - b. All necessary cables;
  - c. Control unit;
  - d. Field acquisition computer;
  - e. Encoder capture module (ECM);
  - f. 12 V deep-cycle battery; and
  - g. Deployment cart apparatus, including frame, antenna bank tub, positioning system mast, wheels, tongue, hitch, and distance measuring instrument (DMI);
- Data Acquisition Shell (DAS) data acquisition software; and
- TerraVision II control software.

Before the initiation of geophysical survey data collection, a project briefing will be held for all personnel responsible for geophysical surveying, the downloading of data, and quality control of data. Survey methodology, data requirements, field note protocol, data naming conventions, and raw data organization will be explained in detail. The briefing will include an overall discussion of the survey approach and how the data collection and field documentation tasks integrate into the overall QC and project management program. The briefing will also include a review of the internal QC procedures listed in this SOP. The Field Lead will be responsible for providing this briefing and any follow-up training deemed necessary.

## A.6 Preparatory Activities

### A.6.1 Survey Layout and Methods

Before conducting the subsurface geophysical investigation, the geophysical investigation team must have accurate knowledge of the precise location(s) of the survey area boundary. Although it is the client's ultimate responsibility to provide the exact survey area boundaries for any given project, the geophysical service provider (PM and/or Project/Site Geoscientist) shall attempt to gather sufficient geo-referenced site information through reasonably ascertainable means before mobilization to the project site. The survey area boundary information shall include geo-referenced points, lines, and/or polygons that are all referenced to a specific and consistent coordinate system. If possible, an electronic geo-referenced base map should be created and loaded into the data acquisition and processing software for assurance purposes. This

base map should include the project coordinate system and correct distance units. On arrival at the project site and before performing DGM data collection activities, the geophysical service provider and/or a land surveyor shall check the points shown on the base map with RTK GNSS and/or RTS equipment (if work area is referenced to a real-world coordinate system), to ensure location accuracy. The field investigation team shall then determine the most appropriate means for the survey area boundary to be identified and recognized by the DGM operator during data acquisition. Either the DGM operator will have a heads-up computer display showing his/her location in relation to the survey boundary, or the survey boundaries shall be delineated by markings (flags, paint, traffic cones, etc.) or permanent reference points in the field (buildings, street boundaries, fence lines, etc.).

Once the project areas that will undergo DGM have been identified and sufficiently delineated, the geophysical investigation team must determine an optimal data acquisition design. Data shall be collected by traversing along equally spaced parallel paths, unless site conditions and/or the project plan call for an alternate data collection scheme. If possible, data should be collected perpendicular to the orientation of suspected utility orientations. If data collection perpendicular to utility orientation cannot be achieved or is not practical, data may be collected in a direction parallel to a suspected utility location with a portion of data ( $\geq 5\%$ ) collected as tie lines or repeat data, where data is collected perpendicular to the main data acquisition orientation.

Any changes to the field plan must be made by the PM (if present) or Field Lead (if PM is not present).

### A.6.2 Data Collection Parameters

Final data collection parameters will be determined on the basis of project requirements, site conditions, and the adaptive detection/positioning capabilities of the geophysical instrumentation system. If possible, an evaluation of a site-specific sample of DGM data will be evaluated by the field team before the commencement of data acquisition to better define optimal parameters. These parameters include

- Lane spacing—determined by detection footprint of the geophysical system and project requirements.
- Comprehensive coverage—complete inclusive coverage offers greatest detection capability.
- Data collection speed ( $\leq 5$  mph)—data are recorded on distance intervals (either six or 12 scans per foot); exceeding 5 mph may overwhelm the input bandwidth of the control unit's storage system and result in dropped scans.
- General settings—requirements for acquisition software.

### A.6.2.1 Lane Spacing

During data collection, TerraVision II parallel transects should be collected with a minimum of two-channel (antenna) overlap to ensure full coverage of the project site over all accessible areas. Keeping track of transect coverage may be achieved by painting dashed marks on the surface during data collection. More than a two-channel overlap is permitted and expected to occur at most project sites. Surface obstructions and confined areas may cause more overlap. Data collection should be weighted toward more overlap rather than less because the latter may produce gaps between adjacent transects.

### A.6.2.2 Coverage

Unless otherwise specified by the client and agreed to by the Project Manager, 100% coverage in all accessible areas within the survey area boundary of the project site is required when collecting GPR data using the TerraVision II. Obstructions within the project site that prevent the collection of data must be documented with photographs and/or a sketch if photographs are not permitted on the project site. Any changes to the field plan must be made by the PM (if present) or Field Lead (if PM is not present).

### A.6.2.3 Speed

Data collection speeds for the TerraVision II GPR array are 3 mph to 5 mph. Maintaining a consistent and constant speed produces better results. Due to the limitations of the instrument, data collection speeds over 5 mph will produce poor and incomplete data sets.

### A.6.2.4 General Settings

General settings for the TerraVision II should be set at the beginning of each data collection day and should be checked for retention after every system restart and shutdown. There are settings for both DAS and the TerraVision II control software.

The general settings for DAS are as follows:

- General
  - Set directory for files collected.
  - Enter session and channel prefixes here or use the default naming conventions of SS and CH.
- Connections
  - Enable Differential Global Positioning System (DGPS), RTS, or both depending on the positioning instruments to be used.
  - Enable Encoder Capture Module (ECM), which is defaulted and must be set at 768 ticks per foot.

- Carts
  - Select land-based platform type.
  - Check positioning equipment offsets.

The general settings for TerraVision acquisition software are as follows:

- Setup
  - Project file name format,
  - Project site name,
  - Operator,
  - Date and time,
  - Notes on the current project,
  - Soil type,
  - Depth, and
  - Initializing of GPR antennas.
- Configuration
  - Scans per unit,
  - Survey wheel,
  - External device,
  - Soil type,
  - Dielectric, and
  - Depth.

A checklist for these settings is provided at the end of this appendix.

## A.7 Geophysical Data Collection Procedures

### A.7.1 Daily Data Collection

The following set of general procedures should be followed for each field day:

1. Hold tailgate safety and daily project objectives meeting; tailgate safety forms will be filled out and signed by all field investigation team members.
2. Set up equipment.
3. Set DAS and TerraVision II control software parameters.
4. Initialize GPR antennas over a representative area.
5. Perform QC checks and checklist as described in Section A.8 of this SOP.
6. Send field team to production area.
7. Activate the geophysical and RTK GNSS/RTS equipment and check that both units are collecting valid data.
8. Proceed with the DGM activities.

One member of the team will be responsible for maintaining the field documentation record. Note, this does not necessarily mean that person is responsible for creating each document; individual documents may be produced by any member of the field investigation team. Field documentation

includes, at a minimum, the checklists and forms included with this SOP and other relevant SOPs. These documents are delivered to the Field Lead at the end of each production day. Each page of the field documentation will be dated, sequentially numbered, and identified by the project name/number; all entries will be signed by the Field Lead.

At a minimum, the following information should be recorded as field documentation:

- Unit area for data set identification;
- Time survey started;
- Time survey completed;
- Names of geophysical investigation team members;
- Equipment and software settings;
- Weather conditions; and
- File names for the digitally recorded data.

At the end of the day,

- All data are downloaded onto transferable media.
- All equipment is returned to storage, and the batteries are placed on charge.
- The completed survey areas are recorded in the tracking log.
- The DGPS/RTS positional track maps and logbook pages are accessible for periodic verification by the QC Geoscientist.

### **A.7.2 Full Coverage (Grid) Geophysical Survey**

One hundred percent of accessible areas within the project site will be geophysically surveyed with the TerraVision II, integrated with RTK GNSS/RTS. If a DGPS/RTS signal is not achievable or of good quality (low number of visible satellites, too many obstructions, etc.), then data will be collected in straight transects using an established local coordinate system and by marking the endpoints on the ground for subsequent surveying. Data collected in straight transects and in a local coordinate system will be positioned on the basis of measurements from existing structures and/or referenced to GNSS static points collected outside the production area where DGPS signal is achievable and of good quality. Data collected using local coordinates will be translated to project coordinates during data processing.

To ensure that 100% of accessible areas are covered during geophysical data collection, those in charge of the data acquisition must employ measures to keep track of coverage. A few methods include (i) establishing markers in the field to delineate data collection lanes using flags, ropes, painted lines, or cones; (ii) using the heads-up data track display on the data acquisition computer; and (iii) using

swath light-bar guidance systems. Employing one or more of these methods allows for comprehensive data coverage and maximum productivity by eliminating data gaps and overlaps.

### **A.7.3 Equipment Initialization**

When transitioning to areas that have significantly different soil conditions during data collection at the project site, the TerraVision II should be reinitialized. Reinitialization should be conducted in an area believed to be free from subsurface metallic objects and where the subsurface conditions are characteristic of the transition. For example, soil conditions could be expected to differ when moving from a paved area to an unpaved area. By doing so, the data will generally be better gained to the particular soil near the point of initialization. The location of the initialization will be recorded in the field documentation and digitally, by collecting a short 5-foot to 10-foot swath of data and logging the positioning information.

### **A.7.4 Inaccessible Areas**

Physical features such as rock outcrops, boulders, trees, buildings, structures, utilities, stationary vehicles, and water may result in inaccessible areas. All inaccessible areas will be photographed, with the position and the orientation of the photograph documented, sketched on the team's grid sheet, and/or noted on a project site aerial. Reasonable attempts are to be made to have parked vehicles and other potentially moveable obstacles moved. If possible, the boundaries of physical features that obstruct data collection will be geo-referenced using RTK GNSS/RTS for later reference during data processing and mapping.

### **A.7.5 Deviation from Lane Orientation and Spacing**

Deviation from geophysical survey lane spacing and orientation will be determined and documented in the field. The Project/Site Geoscientist will be responsible for determining whether an area is considered inaccessible due to site conditions. All inaccessible areas will be photographed and/or sketched in the field documentation and denoted as to their source. Examples of typical obstructions include manmade immovable structures; unsafe terrain/conditions; and cultural objects such as cars, power lines, signs, and fences. Reasonable attempts are to be made to have parked vehicles and other potentially moveable obstacles moved. The Field Lead will designate one member of the field investigation team to document deviation from standard lane setup due to terrain, slope, or other conditions that make the area impassable. The

following steps are recommended for performing lane deviation documentation:

- Deviations will be tied to an individual data set. If deviation is necessary, a sketch and/or photograph of the data set boundary will be denoted with the cause of the deviation. Data gaps caused by deviations from line path and not obstacles should be filled in with a subsequent data collection set if possible.
- Obstacles may cause inaccessibility and result in additional sources of lane orientation and/or spacing deviations that should be documented. Remove obstacles from the investigation area if possible.

### A.7.6 Daily Data Management

Several files are generated by the geophysical and positioning systems for the acquired data at each investigation area of a project site. These data are stored on the data logger(s), field computer, and RTK GNSS receiver during data acquisition activities. At the end of daily field activities, the data collected by the field investigation team will be uploaded to a designated data management computer or included in the project binder, as appropriate. The following file types are generated for each survey:

- Geophysical data files (.dzt and .ind) and RTK GNSS/RTS positioning coordinates;
- Data acquisition software session folders containing individual GPR file positioning and timestamp information;
- Digital photo files (.jpg); and
- TerraVision II field sheet and checklist (see end of this appendix).

## A.8 Quality Control (QC) and Quality Assurance (QA)

This section outlines the quality control function through discussion of generalized field procedures and testing to document the execution and completion of a subsurface target detection project using GPR digital geophysical mapping. The Project/Site Geoscientist, in collaboration with the QC Geoscientist, is responsible for the maintenance of this procedure.

### A.8.1 Response, Detectability, and Interpretability

Utilities and other targets of interest are detectable and interpretable based on differences in the electrical properties of the targets and the electrical properties of the surrounding

soil. The responses received vary based on the site conditions and the target properties. Target properties that determine the magnitude and value of responses include, but are not limited to, depth of burial, size, orientation, and material properties.

### A.8.2 Equipment Functionality and QC Tests

The geophysical service provider will perform QC tests tailored to the project's specifications to ensure both instrument functionality and consistency of measurements from the TerraVision II GPR multichannel array. On a daily basis, all QC tests will be documented by the Project/Site Geoscientist. The suite of tests is instrument specific and may include some or all of the items in Table A.1.

#### A.8.2.1 Bank Testing

##### APPLICABILITY

TerraVision II

##### PROCEDURE

Before mobilization to the project site, the TerraVision II GPR antenna banks that are to be used on site need to be tested, and settings need to be adjusted to ensure quality data are collected. During bank testing, the Project/Site Geoscientist needs to perform the following tasks and adjust the associated settings if necessary:

- Time Zero Calibration—the top reflector of each channel should be aligned.
- Missing Channel Check—ensure all 14 channels are active.
- Channel Alignment Check—ensure that data collected over a test object line up properly without any offsets or other inconsistencies in the location of the test object's data signature.

All of the above calibrations and checks can be completed with the collection of one or more data files. Place a strip of foil tape on the ground within the testing area. Collect one or more GPR transects perpendicular to the orientation of the

**Table A.1. QC Tests**

Test #	Test Description	Frequency
1	Bank testing	By data set
2	Equipment warm-up	Daily
3	RTK GNSS/RTS streaming check	Daily
4	Initialization check	Daily
5	Foil tape	By data set

foil tape. The foil tape is used for the Channel Alignment Check and does not affect the other checks and calibrations.

All of the above checks and calibrations have to be assessed with processing and interpretation software. It is the responsibility of the Project/Site Geoscientist to process and review the collected GPR transects and determine if the TerraVision II GPR antenna banks are ready for transport to the project site.

*FREQUENCY*

Once before mobilization or DGM data collection activities

### **A.8.2.2 Equipment Warm-Up**

*APPLICABILITY*

TerraVision II

*PROCEDURE*

The multichannel array is particularly sensitive to cold weather conditions. This instrument requires several minutes to acclimate to ambient weather conditions (temperature, humidity, etc.) and stabilize before data collection can take place. Equipment is to be turned on and left to rest for 5–10 minutes before collection of DGM data.

*FREQUENCY*

Daily

### **A.8.2.3 DGPS/RTS Streaming Check**

*APPLICABILITY*

TerraVision II

*PROCEDURE*

Before collecting data at the project site, the positioning sensor needs to be configured for data streaming. The project Location Surveyor is responsible for using the Trimble GPS Configurator software to apply the correct settings for streaming National Marine Electronics Association (NMEA) GGA positioning data from the RTK GNSS. The Location Surveyor or the Project/Site Geoscientist is responsible for confirming that during TerraVision II data collection the proper NMEA output is being received. This can be checked by setting up the GPR array with the positioning sensor and collecting a test strip of data. Within the DAS data acquisition software, if the positioning sensors are counting up during collection, then streaming positioning data are being collected. Alternatively, a terminal software program such as HyperTerminal that can

monitor serial data inputs can be used to check that data are streaming correctly.

*FREQUENCY*

Daily and throughout the entirety of DGM activities

### **A.8.2.4 Initialization Check**

*APPLICABILITY*

TerraVision II

*PROCEDURE*

After the configuration of all general settings (as discussed in Section A.6.2.4), initialize the GPR antennas. Collect a test transect to record the location of the initialization and to review the gain that was applied during initialization. To review the gain applied, download the test transect file to the acquisition computer and review the data with GPR processing software. If the gain applied is not acceptable (high enough, too high, cloudy data, etc.), the TerraVision II array may be over buried metal or saturated ion-rich soils. In this case, change the initialization location and collect another test file. Continue until a gain setting is obtained that provides for an evenly gained data file.

*FREQUENCY*

Daily and whenever subsurface soil conditions are reasonably expected to change (e.g., when moving from pavement to grassy area)

### **A.8.2.5 Foil Tape**

*APPLICABILITY*

TerraVision II

*PROCEDURE*

Foil tape will be laid at multiple points within the project site to ensure there are no latency errors within the multichannel GPR data set collected. Foil tape should be laid on the ground perpendicular to the direction in which a majority of the multichannel GPR data transects will be collected. During data collection activity at the project site, GPR transects will be collected over the foil tape, and its position within the GPR will be checked daily during data processing. Foil tape endpoints shall also be geo-referenced by the Location Surveyor. On grassy areas, a metal chain should be laid, using the same parameters as foil tape.

*FREQUENCY*

Daily within each production area



TERRAVISION™ II FIELD SURVEY CHECK LIST					
Date:	Project:		Field Staff:		
PRE-SURVEY					
CART SETUP					
	Cables from L&R banks routed to correct control unit L&R inputs				
	All COM Cables in correct order on USB-Serial Converter				
	All Cables secured to cart & tongue				
	GPS & Prism Firmly attached & Cables secured				
	Tongue approximately horizontal				
	Antennae warmed up for at least 10 minutes				
DAS CONFIGURATION					
	Session Destination Folder Correctly Named and Selected				
CONNECTIONS TAB					
Primary Positioning Sensor					
Sensor Type:	GDM Theodolite	Generic GPS	(Circle One)		
Port:	COM:	Baud Rate:	Parity:	Stop Bits:	
Secondary Positioning Sensor					
Sensor Type:	GDM Theodolite	Generic GPS	(Circle One)		
Port:	COM:	Baud Rate:	Parity:	Stop Bits:	
Encoder Capture Module					
Port:	Ticks Per Unit:	Units:	Feet	Meters	(Circle One)
TERRAVISION SOFTWARE					
CONFIGURATION PAGE IN TV SOFTWARE					
	Scans per unit verified to be 12				
	Survey wheel setting correctly configured				
	Both wheel calibration values checked to match between DAS & TV Software (768 for DAS & ECM use)				
	Soil Matrix correctly configured to achieve desired depth of penetration				
	"None" selected as External Device				
SETUP PAGE IN TV SOFTWARE					
	File & Project Name correct				
	Investigation depth selected appropriately				
	Soil type/dielectric selected properly				
	TV antennas initialized over area assumed free of targets				
	All 14 channels functioning correctly and time-zero adjusted properly as seen by selecting each Channel Display				
	Settings and operator notes are recorded in field notes				
	Site is sketched in field book				
DURING DATA COLLECTION					
	Start and stop button activated in DAS while cart at a complete stand still				
	New file name present in TV window after pushing start in DAS before moving				
	Position/tick number is incrementing properly in DAS on each line				
	Line lengths are a maximum of +/-300 feet				
	3-5 MPH cart speed maintained during data collection				
	After system crash, changing TV battery, restart of Toughbook, or other "glitch" all configurations & settings double checked				
	Detailed Field notes kept indicating file name, DAS session, and sketch of swaths				
AFTER DATA COLLECTION					
	Entire accessible area of interest was collected				
	Several Perpendicular swaths collected where possible for data checking purposes				
	Data was transferred to Toughbook before shutting down control unit - checked on Toughbook				
	Manhole covers removed/Storm Sewers measured depth to top for dielectric calibration				
	Site was extensively photographed and sketched to account for surface features/layout/obstacles				
	Site was thoroughly surveyed with total station to get foil tape, valves, manholes & other surface features of interest				

## APPENDIX B

# Standard Operating Procedure for Multichannel GPR Digital Geophysical Mapping Data Processing

### B.1 Purpose

The purpose of this Standard Operating Procedure (SOP) is to provide general procedures for geophysical data processing and interpretation of TerraVision II multichannel ground-penetrating radar (GPR) during and after field activities. This SOP is to be used in conjunction with the SOP for GPR digital geophysical mapping (DGM) subsurface geophysical investigation data collection (see Appendix A).

### B.2 Scope

This procedure applies to the data collected during DGM surveys using the TerraVision II multichannel GPR geophysical detection sensor integrated with real-time kinematic (RTK) global navigation satellite system (GNSS) and/or robotic total station (RTS) equipment. The major elements of this procedure are electronic data transfer, data processing, data analysis and interpretation, data archiving, and data tracking. The objective is to depict resulting information gained from the geophysical investigation via computer-aided design and drafting (CADD) onto the client's plan sheets, geographic information system (GIS) databases, ASCE 38-02 standard's Quality Level B (QL-B) information, or other appropriate documents.

### B.3 Maintenance

The Project/Site Geoscientist, in collaboration with the quality control (QC) Geoscientist, is responsible for the maintenance of this procedure. Approval authority rests with the Project Manager (PM). Approval authority is the power conferred on the PM to commit the geophysical service provider to the procedures, objectives, and data quality standards as set forth in this SOP.

### B.4 Equipment

The following is a list of equipment and software that will be necessary to complete GPR data processing and interpretation tasks:

- Computer with sufficient hard drive space and RAM (it is recommended that free hard drive space be at least twice the size of the largest merged file and total RAM amounts of 8 GB or greater);
- Appropriate means to receive and transfer large quantities of digital data (network connection, external hard drive, USB flash drive);
- GPR processing/filtering software (e.g., Geophysical Survey System Inc.'s RADAN); and
- Positioning processing software sufficient to merge recorded positioning information with geophysical sensor data resulting in a geo-referenced GPR data set
  - Underground Imaging Technologies, LLC (UIT) Data Processing Engine (DPE), and
  - Geosoft Oasis Montaj; and
- Interpretation software
  - UIT Semi-Automated Process and Detect (SPADE).

### B.5 Personnel Requirements and Responsibilities

Personnel assigned to perform GPR DGM data processing must be proficient in the use of GPR processing and interpretation software, or they should be under supervision of other proficient personnel at the time of processing and interpretation of any results to be included in a DGM deliverable.

Before the initiation of GPR GDM data processing and interpretation, a project briefing will be held for all personnel responsible for GPR GDM data processing and quality control of data. Survey data collection scheme, project

requirements and goals, field documentation review, data naming conventions, and data organization will be explained in detail. The briefing will include an overall discussion of the survey approach and how the data collection, field documentation, and processing and interpretation tasks integrate into the overall QC and project management program. The briefing will also include review of the internal QC procedures listed in this SOP. The Project Manager will be responsible for providing this briefing and any follow-up training deemed necessary.

## B.6 Data Processing Procedures

The data processing, data interpretation, quality control reprocessing, and quality assurance process steps must flow smoothly, and clear communication must occur. The steps required for this are as follows.

### B.6.1 Transfer of Field Data and Data Tracking

Several files are generated by the geophysical and GNSS systems during DGM data collection. These data are stored on various data loggers or field computers. The following file types may be generated for each survey:

- Raw GPR files generated by both single-channel and multi-channel GPR sensors.
- Raw RTS data containing position track data of the prism affixed to the GPR cart. These files may be generated using provided project site control information or in a local coordinate system. For TerraVision II data collected with Data Acquisition Shell (DAS) data acquisition software, the National Marine Electronics Association [NMEA\_pos(\_1)] files are the raw RTS positioning logs.
- Raw GNSS data containing position track data of the GPS rover affixed to the GPR cart. These files are generated with a real-world coordinate system (usually latitude/longitude or UTM). For TerraVision II data collected with DAS data acquisition software the NMEA\_raw(\_1) files are the raw DGPS positioning logs.
- Encoder Capture Module (ECM) time marker files (.tmf). The ECM is a device that outputs the number of GPR data scans acquired in each transect with the TerraVision II GPR array. The scan count data are stored in a time marker file. The ECM increases the positional accuracy of the GPR data collected (especially in curved transects).
- Survey files are generated by the select positioning instruments used on the project site and are generally in comma-

or tab-delimited format, containing headers such as ID, Northing, Easting, Elevation, and Code.

- Digital photo files (.jpg) are recorded in the field to represent site characteristics and definable field work operations. They may identify type of terrain, cultural conditions, survey obstacles, elements of the field work, or any other visual depiction relevant to the collection of geophysical data.

The above files are to be placed into appropriate folders on the geophysical service providers file storage system drive(s) by the end of the next business day following the return of the field investigation team.

### B.6.2 In-Field Data Processing

In-field data processing is performed so that data acquisition errors, file naming inconsistencies, and/or insufficient data coverage issues can be addressed before a field investigation team's demobilization from the project site. The information gathered here also facilitates a more thorough understanding by the data analyst/interpreter of the project details. Therefore, the in-field data processing should be performed while at the project site or immediately following data collection if possible. It is the responsibility of the Project/Site Geoscientist to keep track of the information gathered during this in-field data processing phase, including performance of the processing. Preliminary data processing may also be performed by office staff while the field investigation team remains in the field, in consultation with the Project Manager and/or QC Geoscientist.

In-field data processing and preliminary QC review consists of a review of the following:

- Ensuring general project information is recorded
  - Site ID, date(s) of data collection, coordinate system; and
  - Acquisition software used, detection instrument settings used, positioning instrument and settings used;
- File naming consistency;
- Production of data coverage maps indicating those areas over which data were collected;
- General preliminary assessment of GPR DGM data quality, including depth of penetration and instrument noise; and
- Proper instrument function and positioning accuracy through examination of data sets for foil tape position.

### B.6.3 GPR Data Processing

Data will be processed and geophysical targets will be picked and classified by an experienced data analyst or project geoscientist. An experienced data analyst is one who is proficient

in data analysis from extensive training and supervision under other geoscientists. Data analysis includes positioning, processing, and interpreting the GPR data. The typical data processing steps are outlined below. It is the responsibility of the assigned data analyst to track the progress and settings applied during GPR data processing.

### B.6.3.1 Multichannel GPR Data Processing

1. Download GPR .dzt files, DAS positioning files, and survey files from the appropriate electronic media to personal computer (PC); and review field notes, sketches, and photographs.
2. Locate multichannel GPR positioning files in the DAS sessions collected during data acquisition with DAS software in the field. These files—either NMEA\_raw(\_1) files (DGPS) or NMEA\_pos(\_1) files (RTS)—are imported into the position processing software along with the multichannel GPR .dzt files generated. Before position processing, the settings in DPE must be set. The settings include the input and output coordinate systems and the TerraVision II time delay. Once the correct settings are in place and the geophysical sensor and positioning files are imported into DPE, .map files for each multichannel GPR transect are created by DPE and output into the DZT folder.
3. Bundle .map files with their associated .dzt multichannel GPR files for viewing in SPADE. Create an .xml file using DPE for import into SPADE.
4. Import multichannel GPR .dzt files into SPADE using the .xml file. Import client-defined project site boundaries, aerials, and/or CAD, drawing into SPADE to determine appropriate data coverage and to check the positions and orientations of the GPR transects.
5. Process multichannel GPR .dzt files in Geophysical Survey Systems, Inc.'s (GSSI) RADAN data processing software, using various filters to clean up and enhance the raw data for better viewing during data interpretation. Filtering in RADAN does the following to improve the quality of the GPR data:
  - Correct time;
  - Remove flat-lying ringing system noise;
  - Remove high-frequency noise (i.e., snow);
  - Remove ringing multiples;
  - Remove diffraction (compress hyperbolas) and correct dipping layers;
  - Increase visibility of low-amplitude features;
  - Detect subtle features; and
  - Generate clearer data displays for reports.
6. Import multichannel GPR .dzt files (now filtered) back into SPADE with supporting files for interpretation. Before interpretation and to improve the efficiency of the workflow,

individual multichannel GPR files are bundled together into merged files for ease of use in data handling and interpretation. The steps for merging files are as follows:

- a. Using the .xml file created in DPE, import individual multichannel GPR .dzt files into SPADE.
  - b. Section off groups of GPR files into areas of contiguous coverage. Keep files of the same orientation together; do not merge perpendicular files.
  - c. Remove significant overlap between files that are to be merged by creating regions (.dzt) and new region .map files. Keep track of the regions to be merged.
  - d. Create merge files by selecting files and region files created from removing overlap, and stitch them together. This creates a merged .dzt file with the positioning embedded within the file, and therefore it does not have an associated .map file.
  - e. Import all merge files into SPADE and take a screenshot. Create a “Merge Map” in Microsoft PowerPoint, Paint, or any other graphics program using the screenshot. Label each merge file on the screenshot as you labeled the file during merging. This “Merge Map” helps other data analysts and the QC Geoscientist quickly access merge files during interpretation and QC review of the results. Save as a PDF or PPT and put the document in the same folder as the merge files.
7. Import multichannel GPR merged .dzt files into SPADE with supporting files for interpretation. Supporting files include utility information CAD files, survey data, and project site aerials. Targets are picked during interpretation based on the scope of the project. The targets interpreted from the data are exported as points, lines, and polygons (.csv and .dxf files) for later results mapping. During interpretation, targets are classified based on existing records and/or field utility delineation from other methods, such as radio frequency pipe and cable locators.

## B.7 Target Selection

Data will be interpreted and targets will be picked and classified by an experienced data analyst using SPADE software. All GPR data are imported via an .xml file or by loading merged files. TerraVision II multichannel GPR data typically represent 100% coverage of accessible areas and are interpreted from a combination of vertical cross-section profiles and horizontal plan-view time slices. The following procedure describes targets interpreted from GPR data in SPADE:

- A point target is a feature that is not extensive enough to be considered a contiguous, subsurface horizontal structure or large enough to be designated as an area of interest.

Generally, these features would be on the order of approximately 1 square foot or less in extent. The shape of features determined to be point targets ranges from round to sub-round. Point targets must be well pronounced within the data set to warrant inclusion in the interpreted results.

- A GPR linear feature is designated as such if the response is contiguous for a predetermined length and well defined by a linear morphology. The origins of these targets are unknown other than that they express a distinct linear expression in the data.
- A GPR utility feature exhibits geophysical characteristics consistent with a utility signature such as a similarly sized and depth-consistent hyperbola, in addition to corresponding to a known mapped utility at the site.
- A GPR planar feature is designated as such if the response constitutes a defined contiguous area over a horizontal or sloping plane within the subsurface, as visible in a plan-view horizontal “slice” of constant approximate depth. These features are of a greater areal extent than point targets.
- A GPR area of interest is defined as an area of unknown origin where a sufficiently distinct geophysical response is seen in plan view and/or cross section that differentiates it from the background geophysical signature.

Data analysts will also use all pertinent information available [field documentation, aerial and site photos, Quality Level C and D subsurface utility engineering (SUE) data, documentation on the location survey of surface features and utility appurtenances, personal communications with site personnel, other geophysical site investigations] to aid the interpretation effort and to discriminate between targets seen in both plan view and cross-sectional GPR data. When possible, this additional information can be used to

attribute utility type to individual targets and otherwise assist in identifying the origins of certain geophysical targets.

## B.8 Quality Control Review

On completion of the GPR target selections, the QC Geoscientist will review the interpretation files with the data analyst responsible for making the interpretation. The QC Geoscientist will conduct the review in the context of all available georeferenced data. If applicable, the QC Geoscientist will compare the selected target locations with the known locations of seed items. These seed items can either be emplaced by the field team or may be preexisting seeds (such as manholes, surface valves, metal grating). In either case, the precise center position and diameter of the surface seed item should be recorded during the field effort with the appropriate positioning system. The QC Geoscientist will evaluate the effectiveness of all data processing and corrections performed (latency, leveling, gridding, etc.). If the QC Geoscientist identifies deficiencies in any data sets (production or QC), the Project/Site Geophysicist will perform a root cause analysis and propose/implement corrective actions, including reprocessing of positioning data, and refiltering the GPR data.

## B.9 Geophysical Data Archiving

All geophysical data including pick and feature files will be archived daily following the geophysical service provider’s project file structure protocol. Files will be copied to alternate digital media. It is the data analyst’s responsibility to ensure all geophysical data are placed in the appropriate folders. Data filing is to be verified by the Project Manager.

## APPENDIX C

# Standard Operating Procedure for TDEMI Digital Geophysical Mapping Data Collection

### C.1 Purpose

The purpose of this Standard Operating Procedure (SOP) is to provide general procedures for geophysical data collection during subsurface utility field investigations using the SHRP 2 R01B time domain electromagnetic induction (TDEMI) digital geophysical mapping (DGM) prototype system, also known as the transient electromagnetic method (TEM) system. This SOP is to be used in conjunction with the SOP for TDEMI DGM data processing (see Appendix D).

### C.2 Scope

This SOP applies to the collection of TDEMI geophysical and associated spatial location coordinate data. A real-time kinematic (RTK) global navigation satellite system (GNSS) will be coupled with the geophysical instrument(s) to record the  $x$  and  $y$  coordinates for the collected geophysical data points. The SHRP 2 R01B TEM  $5 \times 1$  sensor array will be the detection platform to be tested and calibrated in an area that represents specific site conditions. The objective of the geophysical survey is to detect subsurface metallic objects that are utilities and/or other client-defined targets of interest to ASCE 38-02 standard's Quality Level B (QL-B) information. The purpose of the DGM surveys is to provide information which may be used to support the determination of exactly where the utilities and targets of interest are located.

### C.3 Maintenance

The Project/Site Geoscientist, in collaboration with the quality control (QC) Geoscientist, is responsible for the maintenance of this SOP. Approval authority rests with the Project Manager (PM). Approval authority is the power conferred on the PM to commit the geophysical service provider to the

procedures, objectives, and data quality standards as set forth in this SOP.

### C.4 Equipment

The following is a list of equipment that will be necessary to complete a DGM survey with the geophysical instrumentation for the project:

- SHRP 2 R01B TEM geophysical sensor(s) and acquisition computer;
- Appropriate signal and power cables for all instruments;
- RTK GNSS rover/receiver, GPS base station (if applicable), data logger, antennas;
- Sufficient batteries for daily operation of all instrumentation; and
- Instrumentation platform (cart, wheels, GPS mast, tow vehicle).

The following additional equipment and forms will be assembled by the Site Geoscientist(s):

- Task-specific field data logbook, QC tests form, survey report form;
- Pin flags, spray paint, traffic cones, tape measures, 10 ft of metal linked chain, miscellaneous items necessary for data collection;
- Digital camera, USB thumb drive; and
- Personal protective equipment (as required by current health and safety plan).

### C.5 Personnel Requirements and Responsibilities

All personnel assigned to the geophysical investigation team must demonstrate the ability to perform assigned tasks associated with the geophysical investigation with the equipment

at the designated project location. For TDEMI DGM activities this equipment includes

- RTK GNSS; and
- SHRP 2 R01B TEM 5-by-1 sensor array on metal-free platform
  - a. Five coils;
  - b. Five preamps;
  - c. Approximately 20 ft of cabling for five transmit/receive coils;
  - d. National Instruments (NI) electronics box with embedded computer and analog-to-digital (A/D) card;
  - e. G&G Sciences electronics box attached to NI box;
  - f. Power cables for NI box and G&G box;
  - g. Package of NI software and CDs;
  - h. AC power or 18-30 V DC for the NI box, and +12 and -12 volts for G&G box;
  - i. External monitor, mouse, and keyboard (once the networking is configured, a laptop computer and a network cable to “Remote Desktop” onto embedded computer can be used); and
  - j. USB flash drive.

Before the initiation of geophysical survey data collection, a project briefing will be held for all personnel responsible for geophysical surveying, the downloading of data, and quality control of data. Survey methodology, data requirements, field note protocol, data naming conventions, and raw data organization will be explained in detail. The briefing will include an overall discussion of the survey approach and how the data collection and field documentation tasks integrate into the overall QC and project management program. The briefing will also include review of the internal QC procedures listed in this SOP. The Field Lead will be responsible for providing this briefing and any follow-up training deemed necessary.

## C.6 Preparatory Activities

### C.6.1 Survey Layout and Methods

Before conducting the subsurface geophysical investigation, the field investigation team must have accurate knowledge of the precise location(s) of the survey area boundary. Although it is the client’s ultimate responsibility to provide the exact survey area boundaries for any given project, the geophysical service provider (PM and/or Project/Site Geoscientist) shall attempt to gather sufficient geo-referenced site information through reasonably ascertainable means before mobilization to the project site. The survey area boundary information shall include geo-referenced points, lines, and/or polygons that are all referenced to a specific and consistent coordinate system. If possible, an electronic geo-referenced base map should

be created and loaded into the data acquisition and processing software for assurance purposes. This base map should include the project coordinate system and correct distance units. On arrival at the project site and before performing DGM data collection activities, the geophysical service provider and/or a land surveyor shall check the points shown on the base map with RTK GNSS equipment to ensure location accuracy. The field investigation team shall then determine the most appropriate means for the survey area boundary to be identified and recognized by the DGM operator during data acquisition. Either the DGM operator will have a heads-up computer display showing his/her location in relation to the survey boundary, or the survey boundaries shall be delineated by markings (flags, paint, traffic cones, etc.) or permanent reference points in the field (buildings, street boundaries, fence lines, etc.).

Once the project areas that will undergo DGM have been identified and sufficiently delineated, the geophysical investigation team must determine an optimal data acquisition design. Data shall be collected by traversing along equally spaced parallel paths, unless site conditions and/or the project plan call for an alternate data collection scheme. If possible, data should be collected perpendicular to the orientation of suspected utility orientations. If data collection perpendicular to utility-orientation cannot be achieved or is not practical, data may be collected in a direction parallel to suspected utility location with a portion of data ( $\geq 5\%$ ) collected as tie lines or repeat data, where data is collected perpendicular to the main data acquisition orientation.

Any changes to the field plan must be made by the PM (if present) or Field Lead (if PM is not present).

### C.6.2 Data Collection Parameters

Final data collection parameters will be determined on the basis of project requirements, site conditions, and the adaptive detection/positioning capabilities of the geophysical instrumentation system. If possible, an evaluation of a site-specific sample of DGM data will be evaluated by the field team before the commencement of data acquisition to better define optimal parameters. These parameters include

- Lane spacing—determined by detection footprint of the geophysical system and project requirements.
- Sensor height—usually fixed on the basis of the instrument platform; sensors closer to the ground surface offer greatest sensitivity.
- Data collection speed ( $\leq 3$  mph)—because data are usually recorded on set time intervals, slower acquisition speeds offer higher down-line data density.
- Comprehensive coverage—complete inclusive coverage offers greatest detection capability.

- Noise threshold—detection capabilities of electromagnetic induction (EMI) instruments can be adversely affected by natural and/or cultural features (high ambient moisture, surface or near-surface metal, lightning, power lines, etc.).

## C.7 Geophysical Data Collection Procedures

### C.7.1 Daily Data Collection

The following set of general procedures will be followed for each field day:

1. Hold tailgate safety and daily project objectives meeting; tailgate safety forms will be filled out and signed by all field investigation team members.
2. Set up equipment.
3. Perform morning QC tests and checklist as described in Section C.8 of this SOP.
4. Send field team to production area. Remove any metallic debris from the production area if possible.
5. Activate the geophysical and RTK GNSS instrumentation and check that all units are collecting and/or outputting valid data.
6. Proceed with DGM data collection activities.

One member of the team will be responsible for maintaining the field documentation record. Note, this does not necessarily mean that person is responsible for creating each document; individual documents may be produced by any member of the field investigation team. Field documentation includes, at a minimum, the checklists and forms included with this SOP and other relevant SOPs. These documents are delivered to the Field Lead at the end of each production day. Each page of the field documentation will be dated, sequentially numbered, and identified by the project name/number; all entries will be signed by the Field Lead.

At a minimum, the following information should be recorded as field documentation:

- Unit area for data set identification;
- Time survey started;
- Time survey completed;
- Names of geophysical investigation team members;
- All QC and instrument function tests;
- Weather conditions; and
- File names for the digitally recorded data.

At the end of the day,

- All equipment is returned to storage, and the batteries are placed on charge.

- The completed survey areas are recorded in the field documentation.
- The GNSS positional track maps and field documentation are accessible for periodic verification by the QC Geoscientist.

Before any data collection session, the TEM system should be tested in an area free from both surface and subsurface metallic objects. By doing so, the data analyst will be better able to perform drift/leveling corrections on the EMI data and establish true background noise levels, thus enhancing the ability to recognize targets that are only slightly detectable above background (i.e., deeper and/or smaller targets). If possible, each data collection session should begin and end at the same location in the metal-free area. A fewer number of longer time-of-collection data sets are generally more desirable than a greater number of shorter time-of-collection data sets.

### C.7.2 Full Coverage (Grid) Geophysical Survey

One hundred percent of the work scope accessible areas will be geophysically surveyed with the TEM, integrated with RTK GNSS. The field investigation team can use several methods to ensure full coverage. A few methods include (i) establishing markers in the field to delineate data collection lanes using flags, ropes, painted lines, or cones; (ii) using the heads-up data track display on the data acquisition computer; and (iii) using swath light-bar guidance systems. The idea is to gain comprehensive coverage at maximum productivity by eliminating data gaps and overlap. If conditions allow, two or more data collection schemes acquiring data in alternate directions and orientations can be beneficial.

### C.7.3 Real-Time Geophysical Surveys

Real-time geophysical data are collected in either a designed pattern or a meandering path fashion. The geophysical data in this case are interpreted in real time in the investigation area. During this operation it is not necessary to record sensor data. This mode of operation is not currently practical with the TEM system because the DGM operator cannot sufficiently monitor and interpret the TEM sensor readings in real time. Therefore, geophysical data are digitally logged for subsequent analysis; if geophysical anomalies believed to represent buried utilities or other cultural features of interest are encountered during the survey, the geophysical investigation team will document the presence of such features in the project field documentation and record their coordinate position.

### C.7.4 Partial Coverage Geophysical Surveys

For partial coverage DGM, digital geophysical data are collected in either a designed pattern or a meandering path fashion. Data sets are collected in the same manner as for full coverage digital grid surveys with the only exception being that 100% coverage is not required.

### C.7.5 Obstacles and Deviation from Lane Orientation/Spacing

Deviation from geophysical survey lane spacing and orientation will be determined and documented in the field. The Site Geoscientist will be responsible for determining whether an area is considered inaccessible due to site conditions. All inaccessible areas will be photographed and/or sketched in the field documentation and denoted as to their source. Examples of typical obstructions include manmade immovable structures; unsafe terrain/conditions; and cultural objects such as cars, power lines, signs, and fences. Reasonable attempts are to be made to have parked vehicles and other potentially moveable obstacles moved. The Field Lead will designate one member of the field investigation team to document deviation from standard lane setup due to terrain, slope, or other conditions that make the area impassable. The following steps are recommended for performing lane deviation documentation:

- Deviations will be tied to an individual data set. If deviation is necessary, a sketch and/or photograph of the data set boundary will be denoted with the cause of the deviation. Data gaps caused by deviations from line path and not obstacles should be filled in with a subsequent data collection set if possible.
- Obstacles may cause inaccessibility and result in additional sources of lane orientation and/or spacing deviations that should be documented. Remove obstacles from the investigation area if possible.

### C.7.6 Daily Data Management

A few files are generated by the geophysical and positioning systems for the acquired data at each investigation area of a project site. These data are stored on the field computer and are converted to standard importable numerical text files by the operator. At the end of daily field activities, the data collected by the field investigation team will be uploaded to a designated data management computer. The following file types are generated for each survey:

- Geophysical data file with signal intensity and RTK GNSS positioning coordinates (.tem, .Data.csv, and .AcqParams.csv);

- Digital photo files (.jpg) relevant to data acquisition/interpretation; and
- TEM DGM QC checklist at the end of this appendix.

## C.8 Quality Control (QC) and Quality Assurance (QA)

This section outlines the quality control function through discussion of generalized field procedures and testing to document the execution and completion of a subsurface target detection project using TDEMI digital geophysical mapping. The Project/Site Geoscientist, in collaboration with the QC Geoscientist, is responsible for the maintenance of this procedure.

### C.8.1 Response, Detectability, and Interpretability

Utilities and other metallic targets of interest are detectable and interpretable based on the anomalous response (amplitude, shape, size, etc.) exhibited by the source above background levels. The anomalous response of the source varies based on the site conditions and the target's electrical properties. Target properties influencing anomalous responses include, but are not limited to depth of burial, size, orientation, and material properties.

### C.8.2 Equipment Functionality and QC Tests

The geophysical service provider will perform QC tests tailored to the project's specifications to ensure both instrument functionality and consistency of measurements from the instrument in question. A number of QC tests are instrument specific, while others are universal. A daily checklist will be filled out by the field investigation team, and all QC tests will be recorded in the Project/Site Geoscientist's field documentation. The forms are located at the end of this appendix. The suite of tests is instrument specific and may include some or all of the items listed in Table C.1.

**Table C.1. QC Tests**

Test #	Test Description	Equipment	Frequency
1	Equipment warm-up	TEM	Daily
2	Cable/port setup check	TEM/GNSS	Daily
3	Cable shake test	TEM/GNSS	Daily
4	Static repeatability	TEM	Twice daily
5	Latency (chain) test	TEM/GNSS	By data set
6	Geodetic equipment functionality	GNSS	By data set

### C.8.2.1 Equipment Warm-Up

#### APPLICABILITY

TEM

#### PROCEDURE

Minimize sensor drift due to thermal stabilization. Most instruments require several minutes to acclimate to current weather conditions (temperature, humidity, etc.) and stabilize readings before data collection can take place. While the equipment is on and in a static position, monitor readings until the readings stabilize with predictable constant response decay curves (typically 5–15 minutes depending on ambient temperature).

#### FREQUENCY

Beginning of each day and after equipment has been shut down for more than 1 hour if air temperatures are below 50°F

### C.8.2.2 Cable Port Setup Check

#### APPLICABILITY

TEM/GNSS

#### PROCEDURE

Before production mapping or QC testing, data operators ensure accurate cable-to-computer port connections from the geophysical sensors and positioning instrumentation. The field team does this by introducing a piece of metal directly beneath each sensor of the array, one at a time, while viewing the detection response curves for each coil on the acquisition software (EM3D) display monitor.

#### FREQUENCY

Beginning of each day or after the system is disconnected or shut down during a day's operation

### C.8.2.3 Vibration Test (Cable Shake)

#### APPLICABILITY

TEM/GNSS

#### PROCEDURE

Identify and replace shorting cables and broken pins on connectors. With the instrument held in a static position and collecting data, shake all cables to test for shorts and broken pin-outs. An assistant can help by observing any changes in instrument response. If shorts are found, the cable should be immediately repaired or replaced. After repair, cables need to be rigorously tested before use.

#### FREQUENCY

Beginning of each day

### C.8.2.4 Static Repeatability (Instrument Functionality)

#### APPLICABILITY

TEM

#### PROCEDURE

Quantify instrument background readings and electronic drift, locate potential interference spikes in the time domain, and determine response and repeatability of the instrument to a standard test jig designed by the geophysical service provider. Improper instrument function, the presence of local sources of ambient noise (such as electromagnetic transmissions from high-voltage electrical lines), and instability in the earth's magnetic field (as during a magnetic storm) are all potential causes of inconsistent, nonrepeatable readings. To aid in the repeatability of the spike test, the DGM operator will use a spike test jig to ensure the test item is in the same position relative to the sensor(s) for all tests.

For this test, 1 minute of static background data must be collected after instrument warm-up, followed by a 1-minute spike test followed by a second, 1-minute collection of static background data. The DGM operator must review the readings to confirm their stability before continuing with the geophysical survey. To aid in the repeatability of the spike test, the DGM operator will use a spike test jig to ensure the test item is in the same position relative to the sensor(s) for all tests.

#### FREQUENCY

Minimum twice daily

### C.8.2.5 Latency (Chain) Test

#### APPLICABILITY

TEM/GNSS

#### PROCEDURE

Document lag/latency, repeatability of response amplitude, and positional accuracy. This test will be performed at the beginning and/or end of each data set in an area relatively clear of anomalous response. The test line will be well marked, with the chain drawn completely straight to facilitate consistency for each section of the test. The chain should be approximately 10 ft in length so that it can be passed over in nonoverlapping segments. The test requires that the TEM DGM operator traverse over a chain (laid flat and straight) in opposing perpendicular directions at the beginning and/or end of each data session. For chain tests performed twice during the same data collection set, the chain should be placed at differing locations outside of the data session coverage area if possible. Such test(s) will allow the data analyst to monitor instrument latency over a sustained period of time. The endpoints of the chain, at all test locations, should be surveyed

with the site position instrumentation and in the project-specific coordinate system. Those chain endpoint positions should be included in the project location survey file.

*FREQUENCY*

At least once per data set

**C.8.2.6 Geodetic Accuracy and Functionality**

*APPLICABILITY*

GNSS

*PROCEDURE*

At the beginning of each day, a known survey point will have the position recorded and compared to the known position to ensure it is within the tolerance of the navigation system. The position will be checked against the known coordinates in the field before survey activities commence. All surveyed points will be tied into the project network of checkpoints.

*FREQUENCY*

Daily

**TDEMI DGM Field QC Form**

<b>Field Operator TEM QC Tests</b>				
<b><u>Date:</u></b>				
<b><u>Project:</u></b>				
<b><u>Field Team:</u></b>				
<b>Test #</b>	<b>Test Description</b>	<b>Frequency</b>	<b>Completed?</b>	<b>Notes</b>
1	Equipment Warm-up	Daily	yes / no	
2	Cable/Port Setup Check	Daily	yes / no	
3	Cable Shake	Daily	yes / no	
4	Static Repeatability	Minimum: 2 Daily	yes / no	
5	Latency (Chain) Test	Per Data Set	yes / no	
			yes / no	
			yes / no	
			yes / no	
			yes / no	
			yes / no	
			yes / no	
6	Geodetic Accuracy	Daily	yes / no	

## APPENDIX D

# Standard Operating Procedure for TDEMI Digital Geophysical Mapping Data Processing

### D.1 Purpose

The purpose of this Standard Operating Procedure (SOP) is to provide general procedures for geophysical data processing and interpretation of SHRP 2 R01B time domain electromagnetic induction (TDEMI) data sets. This SOP is to be used in conjunction with the SOP for TDEMI digital geophysical mapping (DGM) data collection (see Appendix C).

### D.2 Scope

This SOP applies to the data collected during the DGM activities using TDEMI geophysical detection sensors (SHRP 2 R01B TEM system) integrated with real-time kinematic (RTK) global navigation satellite system (GNSS) equipment. The major elements of this procedure are electronic data transfer, data processing, data analysis and interpretation, data archiving, and data tracking. The objective is to depict resulting information gained from the geophysical investigation via computer-aided design and drafting (CADD) onto the client's plan sheets, geographic information system (GIS) databases, ASCE 38-02 standard's Quality Level B (QL-B) information, or other appropriate documents.

### D.3 Maintenance

The Project/Site Geoscientist, in collaboration with the quality control (QC) Geoscientist, is responsible for the maintenance of this procedure. Approval authority rests with the Project Manager (PM). Approval authority is the power conferred on the PM to commit the geophysical service provider to the procedures, objectives, and data quality standards as set forth in this SOP.

### D.4 Personnel Requirements and Responsibilities

Personnel assigned to perform TEM System DGM data processing require basic understanding of TDEMI data processing concepts and sufficient specific training in Geosoft's Oasis Montaj software with the geophysics extension, Underground Imaging Technology, LLC (UIT) extension, and UX-process menus.

### D.5 Data Processing Procedures

The data processing, data analysis and interpretation, quality control reprocessing, and quality assurance process steps must flow smoothly, and clear communication must occur. The steps required for this are as follows.

#### D.5.1 Transfer of Field Data and Data Tracking

Several files are generated by the geophysical and GNSS systems during a DGM data collection activity. These data are stored on data loggers or field computers. The following file types may be generated for each survey:

- Raw geophysical sensor data files (.tem) represent the signal intensity file in non-ASCII binary format.
- Preliminary processed geophysical sensor data files (.Data.csv and .AcqParams.csv), generated by EM3D software represent the signal intensity file in ASCII format (one file per data collection set). These files may have positioning information embedded within them at regular time intervals.
- Files with the extension .xyz are generated by merging positioning files with sensor signal intensity files in which each detection sensor data point is tagged with an

easting, northing, and time stamp. These files are created with the geophysical data processing software, Geosoft Oasis Montaj.

- Survey files are generated by the select positioning instruments used on the project site and are generally in comma or tab delimited format, containing headers such as ID, Northing, Easting, Elevation, and Code.
- Digital photo files (.jpg) are recorded in the field to represent site characteristics and definable field work operations. They may identify type of terrain, cultural conditions, survey obstacles, elements of the field work, or any other visual depiction relevant to the collection of geophysical data.

All DGM data files will be electronically logged, downloaded from the field computers, and stored on external media (such as flash drives, CD, DVD, PCMCIA card) before the field team's exit from the project site. If possible, all raw recorded TDEMI DGM files will be transferred to an off-site data storage server before the field team's exit from the project site. The following items will be recorded on the field worksheet (notebook) or electronic spreadsheet for each DGM file collected:

- Site ID and location;
- Transect ID, grid (unit of production) ID, static test(s), latency test(s), walk away test(s);
- Geophysical investigation team identifier;
- Date collected; and
- DGM data file name(s).

### D.5.2 TDEMI Initial Data Processing

Initial data processing is performed so that data acquisition operational errors, file naming inconsistencies, and/or insufficient data coverage issues can be addressed before a field team's demobilization. The information gathered here also facilitates a more thorough understanding by the data analyst/interpreter of the project details. Therefore, the initial data processing should be conducted at the project site if possible. The information gathered during this initial processing phase will be tracked on the TDEMI DGM Initial Data Processing form presented at the end of this appendix.

Initial data processing and preliminary QC review consists of the following:

- General project information (site ID, date(s) of data collection, coordinate system, geophysical team identifier);
- Data file completeness, file naming consistency;
- Software used, detection instrument used, positioning instrument used; and
- General assessment and comments on TDEMI DGM data quality (coverage, instrument noise, positional accuracy).

### D.5.3 TDEMI Data Processing

Data will be processed and targets will be picked and classified by an experienced TDEMI data processor/analyst. An experienced data processor is someone who is familiar with the general operations of data acquisition and the entire geophysical system used to acquire the TDEMI data. The experienced data processor has direct experience in the manipulation of input data with the Geosoft Oasis Montaj program to obtain the desired outputs. The experienced data processor understands the basic concepts of Geosoft databases, UX-process menu options, visualization of electromagnetic induction (EMI) data in map and profile view, and the standard data quality issues associated with TDEMI DGM systems. The typical data processing steps are outlined below. Standard EMI data processing information is tracked in the TDEMI DGM Final Processed Data Sheet and QC Review form that is presented at the end of this appendix.

The following is a generalized flow of the TDEMI DGM data evaluation and analysis:

- Download data from the acquisition computer to geophysical service provider server or to personal computer (PC), and review field notes.
- Convert data files to  $x, y, z$  format for import to geophysical data analysis software. For TEM data sets, the raw \*.csv files (converted from \*.tem files with EM3D software) are imported into Geosoft Oasis Montage database(s) using the "Import Advanced EM Sensors . . ." option under the UIT menu tab. At this step, offset positions will be applied to sensors that are not located centerline to the positioning rover device (i.e., GNSS antenna).
- Convert  $x, y$  coordinates to site-specific coordinates as necessary.
- Perform latency corrections (as needed) based on instrument latency determined from transect lines of the latency chain test.
- Review data for completeness, using "graphical window" techniques. This is done by the interpreting geoscientist.
- Remove/smooth detection data dropouts, spikes, and physical interference sources.
- Level/filter the DGM data using a nonlinear filter.
- Grid the sensor reading ( $z$ ) for each time gate acquired.
- Produce an image map of the gridded data. Grids can be stacked to produce a three-dimensional (3-D) representation of decay response.
- Post line path and sample location plots on the map. The data analyst/interpreter reviews the map for down-line and cross-line coverage completeness.
- Import any and all available assisting graphics (aerial photos, CAD drawings, GIS layers, etc.) to act as reference during interpretation and analysis.

- Pick targets at anomaly locations where sensor values are consistently above background levels. Targets are classified based on comparisons to existing records and/or subsurface utility engineering (SUE) utility delineation.
- Produce digital map layers, and their accompanying coordinate lists, as the data interpretation deliverable.

The geophysical service provider will use Geosoft Oasis Montaj to process, interpret, and review the TDEMI DGM data. The QC Geoscientist will review field data to confirm equipment was tested in accordance with QC plans and operated in accordance with specifications. The processing steps mentioned herein are the minimum steps necessary to effectively process the TDEMI data.

#### **D.5.4 Standard TDEMI Data Analysis**

TDEMI DGM data will be postprocessed and analyzed in Geosoft Oasis Montaj software. Standard processing information will be tracked on the TDEMI DGM Final Processed Data Sheet and QC Review form presented at the end of this appendix. The geophysical service provider will perform the following analysis as appropriate:

- Convert easting and northing values to site-specific coordinate system, and apply sensor path and offset correction.
- Sensor bias, background leveling, and/or standardization adjustment for all TDEMI time gate measurements.
- Correct latency. Use the UCELATENCY.GX (for time-based correction) or LAG.GX (for distance-based correction) of Geosoft to perform these latency corrections on the TDEMI DGM data.
- Determine the optimum gridding method, search criteria, and contour-level selection with background shading and analysis based on the data collected.

##### ***D.5.4.1 Sensor Path and Offset Correction***

Sensor path and offset corrections are required when the number of detection sensors is greater than the number of positioning devices or when the detection sensor is not centered in relation to the positioning device during data acquisition. Sensor offset corrections applied within Geosoft Oasis Montaj will be checked as part of the daily QC plan to ensure the offsets do not vary.

##### ***D.5.4.2 Convert Easting and Northing***

Raw positioning measurements are often not recorded in the required site-specific coordinate system. This is the case when TEM data is collected with RTK GNSS integration [latitude and longitude information from GGA National Marine Electronics

Association (NMEA) sentences]. The site-specific northing and easting values can be attained using the “Coordinates” menu option in Geosoft Oasis Montaj.

##### ***D.5.4.3 Filtering of Data***

Each TDEMI channel (TEM time gate measurement) will be leveled independently to remove the effects of instrumental drift. Filtering will also be performed if necessary to remove effects from known surface cultural sources. All TDEMI channels will be viewed by the data analyst in profile view before gridding to ensure proper leveling corrections.

##### ***D.5.4.4 Latency Correction***

Latency will be corrected for on the basis of the results of daily latency chain tests and reviews of the opposing direction, adjacent line paths of the production data. If the data analyst notices misshaped anomalies in areas of adjacent but opposing direction traverses, the latency correction will be reviewed and adjusted as required.

##### ***D.5.4.5 Gridding and Display of Data***

Monostatic channels of the TEM data will be gridded and displayed using Geosoft Oasis Montaj. Profile data will be reviewed and analyzed to ensure quality and that project performance criteria are met. A general rule of thumb for selecting cell size is  $\frac{1}{8}$  to  $\frac{1}{4}$  nominal line spacing and/or  $\frac{1}{2}$  station sample spacing. Blanking distance is set such that color contouring does not exceed  $\frac{1}{3}$  meter from center of sensors' traverse. Grids from the various time gate channels can be stacked to produce a 3-D representation of decay response. Data sample point location plots will also be reviewed to ensure adequate down-line sampling.

#### **D.5.5 Target Selection and Characterization**

The geophysical service provider will use Geosoft Oasis Montaj with the UIT and geophysics extensions to process and analyze target anomalies. Any existing SUE information and/or field observations may provide the geophysical data analyst with a guide for classifying target anomalies into categories. These categories will be organized such that targets will be placed in defined utility-type classes such as gas, electric, water, unknown.

Target selection criteria will be based on contiguous TEM system signals above background response values. Background TDEMI levels will be determined on a site-specific basis and represented through nonspike static tests conducted in the general vicinity of the production zones. Targets may be single points, lines, or polygons. Point targets and line targets

will be made at peak signal locations. Polygon targets will circumscribe an area of elevated signal response. In general, the area where the signal response is highest above the surrounding background values is the point assumed to be directly over the anomaly source. In making the interpretation, the data analyst will also use all pertinent information available (field notes, aerial photos, Quality Level C and D SUE data, documentation on the location of surface features/appurtenances, personal communications with site personnel, other geophysical site investigations, etc.).

It is important that data analysts making target selection interpretation evaluate all aspects of the TEM DGM data. A thorough analysis should be conducted for each time gate measurement in both map view and profile view. Earliest time gates generally represent the highest level of sensor sensitivity and ambient instrument noise, while anomalous responses within the later time gates generally represent those anomaly sources that are most conductive and/or contain the largest metallic mass within the surrounding area.

### **D.5.6 Quantitative Interpretation and Target Map Development**

The data analyst will construct colored contoured maps of the gridded TDEMI data to facilitate the target selection process. Both colored contour maps and profile data will be evaluated to make appropriate picks of potential targets. The data analyst will select targets within the context of all available geo-referenced data (existing utility drawing, UIT utility line designation, and/or other geophysical systems' interpretations). All digital maps will be referenced to at least one consistent coordinate system. Point, line, and area targets are digitized on a Geosoft Oasis Montaj map and are exported as separate layers for inclusion on the electronic mapping

deliverable. Target selections are exported from Geosoft Oasis Montaj in .dxf format and should be of solid-line form (no dashed/dotted lines and no pattern fill; point symbols are to be polygons). Geo-referenced images of the color contoured grid images may also be exported from Geosoft Oasis Montaj in the form of GeoTiffs, including appropriate world files for inclusion into SPADE or other final mapping deliverable.

### **D.5.7 QC Review**

On completion of the EMI target selections, the QC Geoscientist will review the interpretation files with the data analyst responsible for making the interpretation. Again, the QC Geoscientist will conduct the review in the context of all available geo-referenced data. If applicable, the QC Geoscientist will compare the selected target locations with the known locations of seed items. These can be either seed items emplaced by the field team or preexisting seeds (such as manholes, surface valves, metal grating). In either case, the precise center position and diameter of the surface seed item should be recorded during the field effort with the appropriate positioning system. The QC Geoscientist will evaluate the effectiveness of all data processing and corrections performed (latency, leveling, gridding, etc.). If the QC Geoscientist identifies deficiencies in any data sets (production or QC), the Project/Site Geoscientist will perform a root cause analysis and propose/implement corrective actions.

### **D.5.8 Geophysical Data Archiving**

All geophysical data will be archived daily following the geophysical service provider's project file structure protocol. Files will be copied to alternate digital media. Maintenance of the backup data will be verified by the Project Manager or QC Geoscientist.

**TDEMI DGM Initial Data Processing Raw/Preprocessed Data Sheet**

<b>Information Type</b>	
Site name	
Project number	
Project date(s)	
Name of Project/Site Geoscientist	
Geophysical instrument used	
Positioning method used	
Instrument serial number(s)	
Acquisition software	
Coordinate system and unit of measure	
Raw QC data file names	
Raw QC data file names	
Raw Production data file names	
Raw Production data file names	
Data coverage comments	
Data coverage comments	
Instrument latency comments	
Positional accuracy comments	

**TDEMI DGM Final Processed Data Sheet and QC Review**

<b>Information Type</b>	
Site name	
Project number	
Project dates	
Name of Project/Site Geoscientist	
Geophysical instrument used	
Positioning method used	
Instrument serial numbers	
Coordinate system and unit of measure	
Processed data file names	
Name of Data Analyst	
Name of QC Geoscientist	
Data processing software used	
Latency/lag correction and details	
Sensor bias, background leveling, and/or standardization adjustment method and details	
Geophysical noise identification and removal details	
Other filtering/processing performed and details	
Anomaly target selection and decision criteria details	
Geosoft “.map” file for unit of survey	
Target selection file name(s)	
Data image file name(s)	
Other processing comments	
Date data processing is completed	
QC review comments	

## **TRB OVERSIGHT COMMITTEE FOR THE STRATEGIC HIGHWAY RESEARCH PROGRAM 2\***

CHAIR: **Kirk T. Steudle**, *Director, Michigan Department of Transportation*

### **MEMBERS**

**H. Norman Abramson**, *Executive Vice President (retired), Southwest Research Institute*  
**Alan C. Clark**, *MPO Director, Houston–Galveston Area Council*  
**Frank L. Danchetz**, *Vice President, ARCADIS-US, Inc. (deceased January 2015)*  
**Malcolm Dougherty**, *Director, California Department of Transportation*  
**Stanley Gee**, *Executive Deputy Commissioner, New York State Department of Transportation*  
**Mary L. Klein**, *President and CEO, NatureServe*  
**Michael P. Lewis**, *Director, Rhode Island Department of Transportation*  
**John R. Njord**, *Executive Director (retired), Utah Department of Transportation*  
**Charles F. Potts**, *Chief Executive Officer, Heritage Construction and Materials*  
**Ananth K. Prasad**, *Secretary, Florida Department of Transportation*  
**Gerald M. Ross**, *Chief Engineer (retired), Georgia Department of Transportation*  
**George E. Schoener**, *Executive Director, I-95 Corridor Coalition*  
**Kumares C. Sinha**, *Olson Distinguished Professor of Civil Engineering, Purdue University*  
**Paul Trombino III**, *Director, Iowa Department of Transportation*

### **EX OFFICIO MEMBERS**

**Victor M. Mendez**, *Administrator, Federal Highway Administration*  
**David L. Strickland**, *Administrator, National Highway Transportation Safety Administration*  
**Frederick “Bud” Wright**, *Executive Director, American Association of State Highway and Transportation Officials*

### **LIAISONS**

**Ken Jacoby**, *Communications and Outreach Team Director, Office of Corporate Research, Technology, and Innovation Management, Federal Highway Administration*  
**Tony Kane**, *Director, Engineering and Technical Services, American Association of State Highway and Transportation Officials*  
**Jeffrey F. Paniati**, *Executive Director, Federal Highway Administration*  
**John Pearson**, *Program Director, Council of Deputy Ministers Responsible for Transportation and Highway Safety, Canada*  
**Michael F. Trentacoste**, *Associate Administrator, Research, Development, and Technology, Federal Highway Administration*

\* Membership as of January 2015.

## **RENEWAL TECHNICAL COORDINATING COMMITTEE\***

CHAIR: **Daniel D’Angelo**, *Recovery Acting Manager, Director and Deputy Chief Engineer, Office of Design, New York State Department of Transportation*

### **MEMBERS**

**Rachel Arulraj**, *President, InfoInnovation*  
**Michael E. Ayers**, *Consultant, Technology Services, American Concrete Pavement Association*  
**Thomas E. Baker**, *State Materials Engineer, Washington State Department of Transportation*  
**John E. Breen**, *Al-Rashid Chair in Civil Engineering Emeritus, University of Texas at Austin*  
**Steven D. DeWitt**, *Chief Engineer (retired), North Carolina Turnpike Authority*  
**Tom W. Donovan**, *Senior Right of Way Agent (retired), California Department of Transportation*  
**Alan D. Fisher**, *Manager, Construction Structures Group, Cianbro Corporation*  
**Michael Hemmingsen**, *Davison Transportation Service Center Manager (retired), Michigan Department of Transportation*  
**Bruce Johnson**, *State Bridge Engineer, Oregon Department of Transportation, Bridge Engineering Section*  
**Leannie Kavanagh**, *PhD Candidate, Seasonal Lecturer, Civil Engineering Department, University of Manitoba*  
**Cathy Nelson**, *Technical Services Manager/Chief Engineer (retired), Oregon Department of Transportation*  
**John J. Robinson, Jr.**, *Assistant Chief Counsel, Pennsylvania Department of Transportation, Governor’s Office of General Counsel*  
**Ted M. Scott II**, *Director, Engineering, American Trucking Associations, Inc.*  
**Gary D. Taylor**, *Professional Engineer*  
**Gary C. Whited**, *Program Manager, Construction and Materials Support Center, University of Wisconsin–Madison*

### **AASHTO LIAISON**

**James T. McDonnell**, *Program Director for Engineering, American Association of State Highway and Transportation Officials*

### **FHWA LIAISONS**

**Steve Gaj**, *Leader, System Management and Monitoring Team, Office of Asset Management, Federal Highway Administration*  
**Cheryl Allen Richter**, *Assistant Director, Pavement Research and Development, Office of Infrastructure Research and Development, Federal Highway Administration*  
**J. B. “Butch” Wlaschin**, *Director, Office of Asset Management, Federal Highway Administration*

### **CANADA LIAISON**

**Lance Vigfusson**, *Assistant Deputy Minister of Engineering & Operations, Manitoba Infrastructure and Transportation*

\*Membership as of July 2014.

## Related SHRP 2 Research

Encouraging Innovation in Locating and Characterizing Underground Utilities (R01)

Technologies to Support Storage, Retrieval, and Use of 3-D Utility Location Data (R01A)

Innovations to Locate Stacked or Deep Utilities (R01C)

Integrating the Priorities of Transportation Agencies and Utility Companies (R15)

Identification of Utility Conflicts and Solutions (R15B)

Identification of Utility Conflicts and Solutions: Pilot Implementation of the SHRP 2 R15B Products at the Maryland State Highway Administration (R15C)